

Seismic resilience and performance design approach for concrete moment resisting
frame buildings equipped with yielding restrained braces

Ali Naghshineh

A Thesis
In the Department
of
Building, Civil and Environmental Engineering

Presented in Partial Fulfillment of the Requirements
For the Degree of
Doctor of Philosophy (Civil Engineering) at
Concordia University
Montréal, Québec, Canada

October 2021

© Ali Naghshineh, 2021

CONCORDIA UNIVERSITY

School of Graduate Studies

This is to certify that the thesis prepared

By: Ali Naghshineh

Entitled: Seismic resilience and performance design approach for concrete moment resisting frame buildings equipped with yielding restrained braces

and submitted in partial fulfillment of the requirements for the degree of

Doctor of Philosophy (Civil Engineering)

complies with the regulations of the university and meets the accepted standards with respect to originality and quality.

Signed by the final examining committee:

Dr. Arash Mohammadi Chair

Dr. M. Shahria Alam External Examiner

Dr. Muthukumaran Packirisamy External to Program

Dr. Khaled E. Galal Examiner

Dr. Anjan Bhowmick Examiner

Dr. Ashutosh Bagchi Thesis supervisor

Approved by

Dr. Mazdak Nik-Bakht, Graduate Program Director

11/29/2021

Dr. Mourad Debbabi, Dean
Gina Cody School of Engineering and Computer Science

ABSTRACT

Seismic resilience and performance design approach for concrete moment resisting frame buildings equipped with yielding restrained braces

Ali Naghshineh, Ph.D.

Concordia University, 2021

Advanced structural dissipation devices can be classified into three major groups including passive, semi-active and active control energy dissipations. While all of these technologies play an important role in structural design, passive energy dissipation devices are the most common types of control systems which can be classified into six types including Metallic Dampers, Friction Dampers, Viscoelastic Dampers, Viscous Fluid Dampers, Tuned Mass Dampers, and Tuned Liquid Dampers. The primary purpose of this research is to decrease structural damage by minimizing the demand for main structural elements through the use of passive energy dissipation devices, particularly, in the form of Yielding Restrained Braces (YRBs) or Inline Friction Dampers (IFDs). Friction dampers dissipate energy through friction and emerge due to the sliding of two solid elements relative to one another. For instance, solid friction can control earthquake-induced vibration, another example on a smaller scale is automotive brakes which dissipate the kinetic energy of motion. The friction damper (brake) is commonly used to extract kinetic energy from a moving body, when a major earthquake occurs, conventional braces buckle which leads to unsymmetrical hysteretic behaviour and loss of stiffness, while the friction damper slips at a predetermined load before yielding occurs in members of a frame, which dissipate a major part of energy. It saves the initial cost of a new construction or retrofitting of an existing building, where the dampers provide a very high energy dissipation.

Even though damping devices can provide supplemental damping to mitigate vibration in buildings due to wind or earthquake effects, integrating them in the design is not often straightforward. For example, building design with inline friction dampers is not directly provided in the Canadian code. The NBCC 2015 contains recommendations for supplemental energy dissipation in general, but no specific provisions are available for friction dampers. In the National

Building Code of Canada (2015), the minimum earthquake lateral force in a Seismic Force Resisting System(s) (SFRS) is divided by a reduction factor. This factor, known as the response modification factor, can be calculated by multiplying the overstrength factor (R_o) and the ductility-related force modification factor (R_d). As the 2015 NBCC does not provide the overstrength factor (R_o) and the ductility factor (R_d) for friction-damped systems, engineers usually work with the factor for the closest equivalent system, ductile buckling-restrained braced (BRB) frames ($R_d=4$, $R_o=1.2$). This practice is already conservative in nature mainly because the non-damage-based modification factor for a Yielding Restrained Braced (YRB) system has been found to be substantially higher, and because the system can be tested at Maximum Considered Earthquake (MCE) ground motion forces and displacement in contrast to the equivalent systems that cannot avoid uncertainty in their actual behaviour.

The objectives of the present research are to (i) investigate the life safety performance of different concrete moment resisting frames (CMRFs) considering supplemental damping to estimate seismic response factors, (ii) evaluate seismic design parameters of concrete moment resisting frames (CMRFs) equipped with different energy dissipation systems to understand the relative performance of YRBs, (iii) collaborate experimental work with simulation to investigate dynamic performance and reliability of YRBs under real earthquakes, (iv) develop a set of guidelines for the use of yielding restrained braces in concrete frame buildings.

In order to achieve the above goals, a set of buildings with concrete moment resisting frames have been considered. These frames were designed for high seismic locations in Canada and the equivalent locations in the US. The design YRB systems for these frames have been adapted from ASCE/FEMA guidelines and contextualized for Canada. The results show that such an approach could be beneficial for designing buildings with inline friction dampers and could provide not only cost savings but also, enhanced seismic safety and maintainability.

Acknowledgments

First and foremost, I would like to express my gratitude to my supervisor, Professor. Dr. Ashutosh Bagchi for his encouragement, guidance, and help, during this research investigation. His continuous support has given me the confidence to focus and proceed.

Also, our collaborators at the Department of Civil & Geomatics Engineering in California State University of Fresno (USA), Dr. Fariborz M Tehrani, Mr. Logan Couch for their collaborations throughout the experimental part of the thesis. I would like to acknowledge the financial support from Concordia University and the granting agencies such as the Natural Science and Engineering Research Council of Canada (NSERC).

Also, I would like to thank Dr. Farbod Khoshnoud and Dr. Hamid Arabzadeh for their great support during my study. In addition, acknowledge the colleagues of Concordia and those from Quaketek Inc., especially Mr. Oscar Galindo and Mr. Richard Frazao.

Finally, I would like to thank my wife Dr. Leila Farkhondeh Kish, M.D., whose love, patience, continuous inspiration, encouragement, guidance, and support have motivated me to accomplish my academic journey.

Dedication

To my wife; Leila Farkhondeh Kish

Table of Contents

List of Figures	xii
List of Tables	xix
CHAPTER 1 Introduction	1
1.1 Background and Problem Definition.....	1
1.2 Research Significance and Motivation.....	2
1.3 Objectives and Scope of Work.....	4
1.4 Thesis Layout	6
CHAPTER 2 Literature Review and Methodology	8
2.1 Background.....	8
2.2 Performance-based design and evaluation	9
2.3 Control systems for seismic protection of structures	15
2.3.1 Active control systems.....	17
2.3.2 Semi-active control systems	18
2.3.3 Passive Energy Dissipation Devices.....	22
2.3.3.1 Seismic Isolators	24
2.3.3.2 Viscoelastic Dampers.....	26
2.3.3.3 Viscous Fluid Dampers.....	27
2.3.3.4 Tuned Mass and Liquid Dampers	27
2.3.3.5 Metallic yield dampers.....	28
2.3.3.6 Friction Dampers.....	28
2.4 Common types of friction dampers	45
2.4.1 Yielding restrained brace (YRB).....	45
2.4.2 Rotational Friction Damper (FRD).....	46
2.5 Modeling of yielding restrained braces	47
2.5.1 Attached Damping.....	47
2.6 Literature Summary.....	53
2.7 Methodology.....	55
2.7.1 Analysis Procedures	55

2.7.1.1	Linear procedures.....	55
2.7.1.1.1	Linear Static Procedure (LSP).....	55
2.7.1.1.2	Linear Dynamic Procedure (LDP).....	56
2.7.1.2	Nonlinear procedures.....	56
2.7.1.2.1	Nonlinear Static Procedure (NSP).....	56
2.7.1.2.2	Nonlinear Dynamic Procedure (NDP).....	57
2.7.2	Damping devices in a building.....	59
2.8	The structural response modification factor.....	61
2.8.1	Components of response modification factors.....	61
2.8.1.1	Overstrength factor.....	63
2.8.1.2	Ductility factor.....	64
2.8.1.2.2	Krawinkler and Nassar (1992).....	65
2.8.1.2.3	Miranda and Bertero (1994).....	66
2.8.2	Software tools used.....	68
2.8.2.1	Integrated Building Design Software.....	68
2.8.2.2	OpenSees Software.....	69
2.8.3	Details of the tasks.....	69
2.8.3.1	Phase one: study of the effectiveness of supplemental damping systems in CMRFs.....	69
2.8.3.2	Phase two: seismic reduction factors.....	70
2.8.3.3	Phase three: simulation of the experimental work.....	70
2.8.4	Summary.....	70

CHAPTER 3 Seismic Performance Assessment of Reinforced Concrete Moment-Resisting Frames equipped with yielding restrained braces..... 72

3.1	Introduction.....	72
3.2	Performance-Based Design.....	72
3.2.1	Hazard Levels.....	73
3.2.2	Target building performance levels.....	75
3.3	Seismic design provisions.....	78
3.3.1	National Building Code of Canada (NBCC 2015).....	78
3.3.1.1	Uniform Hazard Spectra (UHS) based design.....	78
3.3.1.2	Present methodology-NBCC 2015.....	78

3.3.1.3	Equivalent Lateral Force Procedure (ASCE 7-16)	81
3.3.1.3.1	Design Spectral Acceleration Parameters	81
3.3.1.3.2	Seismic base shear	83
3.4	Design of Structural models	84
3.4.1	Nonlinear Model for structural components.....	88
3.4.2	Modal Analysis.....	90
3.4.3	Nonlinear Static Analysis	91
3.4.4	Inelastic History Analysis.....	94
3.4.5	Roof, inter-story demand results	96
3.4.6	Results and Discussions.....	97
3.5	Enhancing seismic safety of reinforced concrete buildings with friction dampers.....	98
3.5.1	Overview	98
3.5.2	Work to be done by the dampers, the slip load	99
3.5.3	Material quantities and budgets.....	100
3.5.4	Summary.....	101
3.6	Buildings with damping devices	102
3.6.1	The seismic design requirement for structural with damping system	103
3.6.2	Seismic design parameters.....	104
3.6.3	Determination of fundamental period based on the ASCE 7-16 and the NBCC 2015	106
3.6.3.1	Equivalent lateral force procedure for a structure without a damping system.....	108
3.6.3.1.1	Seismic force-resisting system base shear based on the ASCE 7 Procedure 108	
3.6.3.1.2	Seismic force distribution (ASCE).....	109
3.6.3.1.3	Seismic force-resisting system base shear based on the NBCC Procedure 109	
3.6.3.1.4	Seismic force distribution (NBCC)	110
3.6.3.1.5	Structural Irregularities.....	111
3.6.3.1.6	Drift and P-Delta check	112
3.6.3.2	Equivalent lateral force for a structure with a damping system.....	113
3.6.3.2.1	Seismic force-resisting system base shear.....	113

3.6.3.2.2	Steps in the calculation of fundamental mode base shear	114
3.6.3.2.2.1	Effective seismic weight	114
3.6.3.2.2.2	Base mode properties	114
3.6.3.2.2.3	Damping modification factors	115
3.6.3.2.2.4	Fundamental mode base shear.....	116
3.6.3.2.3	Steps in the calculation of residual mode base shear	117
3.6.3.2.3.1	Damping modification factors.....	117
3.6.3.2.3.2	Determination of residual modal properties	118
3.6.3.2.3.3	Residual mode base shear.....	118
3.6.3.2.4	Seismic base shear.....	119
3.6.3.2.5	Control criteria of damping system	119
3.6.3.3	Response Spectrum Procedure (RSP).....	121
3.6.4	Results and discussion.....	123
3.7	Chapter Summary	128

CHAPTER 4 Seismic response characteristics for concrete structures equipped with different dissipation devices **131**

4.1	Introduction	131
4.2	Seismic Performance and Response modification factors of DCMFs with ISFD.....	132
4.3	Design of Structural Models.....	133
4.3.1	Design of Ten-Co Seismic Brake	135
4.3.2	Modal Analysis.....	139
4.3.3	Nonlinear Model for structural components.....	139
4.3.4	Nonlinear Static Pushover Analysis	141
4.3.5	Inelastic Response History Analysis	146
4.3.6	Interpretation of Results	149
4.3.7	Results and Discussions.....	155
4.4	Analysis for multiple levels of earthquakes	157
4.5	Comparative study five different passive energy dissipation systems	160
4.5.1	Design of Structural Models.....	161
4.5.2	Design response spectrum	164
4.5.3	Design of Fluid Viscous Dampers (FVD).....	164

4.5.4	Design of Metallic Yielding Dampers (MYD).....	165
4.5.5	Design of base isolators.....	166
4.5.6	Modal Analysis.....	169
4.5.7	Nonlinear Static Pushover Analysis	169
4.5.8	Inelastic history response Analysis.....	172
4.5.9	Interpretation of Results	175
4.5.10	Results and Discussions.....	181
CHAPTER 5 Experimental test and analytical simulation of yielding restrained brace ..		183
5.1	Introduction	183
5.2	Phase 1: Experimental work.....	183
5.2.1	Recording accelerometer	184
5.3	Loading.....	185
5.3.1	Interim Protocol I- Quasi-Static Cyclic Testing.....	186
5.3.1.1	Loading and load control	186
5.3.1.1.1	Unidirectional testing	188
5.3.1.1.2	Force Controlled loading.....	190
5.3.2	Interim Protocol II-Shake Table Testing.....	190
5.3.2.1	Test Procedures	190
5.3.2.1.1	System Identification Tests	190
5.3.2.1.1.1	White Noise Test	190
5.3.2.1.1.2	Single-Axis Acceleration-Controlled Sinusoidal Sweep Test.....	191
5.3.2.1.1.3	Static pull-back tests.....	191
5.3.2.1.1.4	Resonance Tests and single-axis acceleration.....	191
5.3.2.1.1.5	Performance Evaluation Tests.....	191
5.3.2.1.1.6	Failure Tests	191
5.4	Ground motion scaling	192
5.4.1	History of displacement loading.....	195
5.5	Phase 2: Numerical Work.....	199
5.6	Results and discussions	202
5.6.1	Moment resisting frame with a single leg brace.....	202
5.6.2	Moment resisting frame with yielding restrained brace	208

5.7	Summary and discussions.....	218
CHAPTER 6 Summary, Conclusions, and Recommendations for Future Work.....		224
6.1	Summary.....	224
6.2	Conclusions	227
6.2.1	Conclusions based on the analytical results	227
6.2.2	Conclusions based on the simulated of the experimental model.....	231
6.3	Recommendations for Future Research.....	233
References		234
Appendix A3.1:Beam-column joint.....		250
Appendix A3.2: General important definitions based on ASCE 41-17.....		252
Appendix A4.1: Original and scaled Acceleration.....		253
Appendix A4.2: Original and scaled Velocity		254
Appendix A4.3: Original and scaled Displacement.....		256
Appendix A4.4: Hysteresis Curves of TCSB.....		258
Appendix A4.5: Hysteresis Curves of FVD.....		260
Appendix A4.6: Hysteresis Curves of TMYD.....		261
Appendix A4.7: Hysteresis Curves of LRBI.....		263
Appendix A4.8: Hysteresis Curves of TPI.....		265
Appendix A5.1: Original and scaled Acceleration.....		267
Appendix A5.2: Original and scaled Velocity		272
Appendix A5.3: Original and scaled Displacement.....		278
Appendix A5.4: OpenSees script		284
Appendix A6: Articles authored based on the present work.....		289

List of Figures

Figure 2-1. A schematic view of selecting a performance level (FEMA 273/356, Hamburger and Holmes 1998); Photo Credits: F. M. Tehrani, Buildings in Rasht and Manjil after the 1990 Manjil-Rudbar Earthquake (Tehrani 1990)	10
Figure 2-2. (a) Soft story failure, (b) plastic hinge formation, and (c) ductile detailing problems (EERI, 2020).....	11
Figure 2-3. Externally bonded FRP reinforcement-Flexural strengthening (ISIS 2004).....	13
Figure 2-4. Externally bonded FRP reinforcement- Shear strengthening (ISIS 2004).....	13
Figure 2-5. Externally bonded FRP reinforcement- Axial strengthening (ISIS 2004).....	14
Figure 2-6. Active control system (after Symans et al. 1997)	17
Figure 2-7. Active mass damper (AMD) (Yamamoto and Sone, 2014).....	18
Figure 2-8. Semi-Active control system (after Symans et al. 1997).....	18
Figure 2-9. Stiffness control device (a) installation detail and (b) configurations within full-scale test structure, (after Kobori 1993)	19
Figure 2-10. Schematic of small-scale damper and hysteresis loop for a large-scale damper for two different electric field strengths (after McMahon et al., 1997).....	20
Figure 2-11. Hysteresis loop of idealized Coulomb friction damper (after Feng 1993).....	21
Figure 2-12. Friction controllable bearing (after Feng 1993).....	21
Figure 2-13. Schematic view of damper and hysteresis loops for seven different command voltage levels, subjected to harmonic motion, (after Symans et al. 1997).....	22
Figure 2-14. Passive control system (after Symans et al. 1997).....	23
Figure 2-15. Major types of damper technology (after Kasai et al., 2013).....	24
Figure 2-16. Idealized force-displacement curves (ASCE 41-13).....	25
Figure 2-17. Schematic plots of designated base isolation systems (after Tehrani et.al. 2020, and Su et al. 1989).....	26
Figure 2-18. Schematic view of viscoelastic damper (Soong and Dargush 1999).....	26
Figure 2-19. A typical fluid damper (Taylor devices inc., 2020).....	27
Figure 2-20. Added damping and stiffness (ADAS) element (Dimensions are in inches, Whittaker et. al. 1991)	28
Figure 2-21. The LSB joint: Wall-to-wall joint (left) and Corner Wall-to-wall joint (right), (after Pall 1979).....	30

Figure 2-22. Load-displacement Response of Limited Slip Bolted Joints (Pall 1979)	30
Figure 2-23. Hysteresis Loops of Limited Slip Bolted Joints (Pall 1979).....	31
Figure 2-24. Idealized behaviour of LSB Joint (after Pall et al., 1979).....	31
Figure 2-25. Test specimen on the left is concrete-steel- and on the right is steel-steel-friction-grip connections (after Roik et al.,1988).....	32
Figure 2-26. Hysteresis Loops of a) concrete- steel- and b) steel-steel-friction-grip connections (after Roik et al.,1988).....	33
Figure 2-27. Detail of steel-concrete friction grip by nonlinear disc spring (after Roik et al.,1988)	33
Figure 2-28. a) Principal behaviour of one stiffening element: C_i : stiffness; γ_i : frictional displacement; T_i : frictional force (level of friction), b) Three displacement coupled parallel stiffening elements, c) Three-Stage Stiffening Element, d) Hysteresis loops of a three-stage stiffening element (after Roik et al., 1988)	34
Figure 2-29. Seven story building and with three different versions (after Roik et al., 1988).....	35
Figure 2-30. a) Roof displacement vs time, b) Maximum horizontal displacement and shear force, c) hysteresis loop for the first story of the three systems (after Roik et al., 1988)....	36
Figure 2-31. Specimen setup for a three-stage truss and the simulation of one degree of freedom (Roik et al., 1988)	36
Figure 2-32. Computed measured and calculated (Star symbol) hysteresis response (Roik et al., 1988)	37
Figure 2-33. Schematic view of slotted bolt connections (after Nikoukalam et al. 2017 and Popov et al. 1995)	38
Figure 2-34. SBCs with steel-steel on the right and using brass shims on the left (after Popov et al. 1995).....	38
Figure 2-35. Installation of SSBC (Nikoukalam et al., 2017)	39
Figure 2-36. SSBC applications in EBF, MRF, and CCSW (Nikoukalam et al., 2017)	40
Figure 2-37. a) Friction damper in X-Bracing, b) Friction damper in Chevron-Bracing, and c) Friction damper in Single Diagonal (Pall et al., 1996).....	41
Figure 2-38. Story Displacement and Shear comparison, (Chang et al., 2006).....	42
Figure 2-39. Friction dampers on the left and its test setup used for characterization	43

Figure 2-40. A schematic view of yielding restrained brace (YRB) and its force-displacement relationship (Galindo et al. 2019, Quaketek Inc.).....	46
Figure 2-41. Component and typical action of RFD (Mualla and Belev, 2002)	46
Figure 2-42. Friction characteristics a) free body diagram, b) idealized dynamic friction, C) static friction, d) actual friction (Roberts and Spanos 1990)	47
Figure 2-43. Mass-spring Coulomb damping and hysteresis loop (Roberts and Spanos 1990)...	48
Figure 2-44. Proposed Hysteresis curve with restrains (Lukkunaprasit et al., 2004)	49
Figure 2-45. Different effect of friction model (Makkar et al., 2005).....	50
Figure 2-46. Proposed single degree of freedom and slip lock hysteresis loop (Baber and Noori, 1985).....	51
Figure 2-47. Bouc-Wen Curve (Seismosoft Ltd, 2020).....	52
Figure 2-48. Nonlinear static assessment procedure (FEMA 273/274/356, ATC 58).....	57
Figure 2-49. Nonlinear dynamic process (FEMA 440, 2005)	58
Figure 2-50. Seismic analysis procedures for various structural (FEMA 440, 2005)	59
Figure 2-51. Important parameters for calculating ELFSD	60
Figure 2-52. Important parameters for calculating RSPD	60
Figure 2-53. Important factors in calculating the damping properties.....	61
Figure 2-54. Bilinear approximation (based on ATC-19, 1995).	62
Figure 2-55. Ductility and strength factors (ATC-19).....	63
Figure 2-56. Displacement versus Base shear (based on Alam et al. 2012).....	64
Figure 2-57. Ductility reduction factor, ductility, and period relationship (based on Newmark and hall,1982).	65
Figure 2-58. Ductility and period relationship on the left and modification factors on the right (based on Krawinkler and Nassar,1992).....	66
Figure 2-59. A comparison of ductility factor (based on ATC-19)	67
Figure 2-60. Overview of the analysis framework	67
Figure 2-61. ETABS basic process	68
Figure 3-1. Performance-based earthquake engineering (Hamburger et. al. 1998, ATC 58, 2003)	73
Figure 3-2. Seismic performance objectives for buildings (SEAOC, 1995)	77
Figure 3-3. Design response spectrum (ASCE 7-16).....	82

Figure 3-4. The elevation views and plan of the ductile moment resisting frames (4, 8, 12-.....	86
Figure 3-5. A schematic view of leaning-column concept (12-story)	87
Figure 3-6. Beam-Column idealized elements (Deierlein et al., 2010)	89
Figure 3-7. (a) Idealized flexural element (b) hysteretic response and monotonic backbone curve (c) monotonic backbone curves (PEER/ATC 72-1)	89
Figure 3-8. Backbone curve for 4-story building beam and column based on ATC 72	90
Figure 3-9. Idealized base shear-displacement curve (FEMA 356, 2000)	91
Figure 3-10. Northridge spectral acceleration for 5% damping	91
Figure 3-11. Generalized Component Force-Deformation Relations (FEMA 356, 2000)	92
Figure 3-12. Normalized base shear vs. roof drift ratio for MCE (4,8,12-Story).....	94
Figure 3-13. Formation of plastic hinges for 4-story (DLE &MCE).....	94
Figure 3-14. Matched Accelerograms based on the target response spectrum.....	96
Figure 3-15. Story Drift Ratio for scaled ground motions, SLE, DLE, and MCE (4,8,12-Story) 97	
Figure 3-16. (a) 3-D Models of the building; (b) The positions of friction dampers	99
Figure 3-17. Material quantity and cost percentage of different CMRFs with/without FD (Naghshineh et al., 2018).....	100
Figure 3-18. Inter story drift ratio for bare frame and frame with friction damper (Naghshineh et al., 2018)	101
Figure 3-19. Schematic view of the seismic force-resisting system (SFRS) and Damping system (DS) (FEMA P-2082)	102
Figure 3-20. Site location (SEAOC and OSHPD, 2020).....	104
Figure 3-21. MCE_R and Design response spectrum.....	106
Figure 3-22. Torsional irregularity and amplification factor (ASCE 7, FEMA 451).....	111
Figure 3-23. Seismic response coefficient.....	124
Figure 3-24. Seismic base shear.....	124
Figure 3-25. Calculated different damping properties in percentage based on ELF and RS procedures.....	125
Figure 3-26. Damping Coefficient values based on ELF and RS procedures	126
Figure 3-27. Design demand caused by effective damping.....	127
Figure 3-28. Roof drift ratio versus normalized base shear for SFRS and SFRS with damping system	128

Figure 4-1. Structural models with Single Diagonal Braces (SBD); (a) plan of the buildings, (b) 14-story, (c) 8-story, (d) 4-story	134
Figure 4-2. Wen model parameters for YRB, courtesy of manufacturer (Quaketek Inc., 2016)	136
Figure 4-3. Idealized lateral force-displacement (Ciampi et al., 1995, Tirca et al., 2018)	137
Figure 4-4. MCE_R and DE_R Response Spectrum.....	140
Figure 4-5. Roof drift ratio versus normalized base shear (14-Story)	142
Figure 4-6. Roof drift ratio versus normalized base shear (8-Story)	143
Figure 4-7. Roof drift ratio versus normalized base shear (4-Story)	143
Figure 4-8. Overstrength, ductility, and response modification factors for 14-, 8-, and 4-story	145
Figure 4-9. Matched Accelerograms based on the target response spectrum for 14-, 8-, and 4-story	148
Figure 4-10. Inter-story drift ratio for 14-Story with 8m span (ISDF&BF)	149
Figure 4-11. Inter-story drift ratio for 14-Story with 6m span (ISDF&BF)	150
Figure 4-12. Inter-story drift ratio for 8-Story with 8m span (ISDF&BF)	150
Figure 4-13. Inter-story drift ratio for 8-Story with 6m span (ISDF&BF)	151
Figure 4-14. Inter-story drift ratio for 4-Story with 8m span (ISDF&BF)	151
Figure 4-15. Inter-story drift ratio for 4-Story with 6m span (ISDF&BF)	152
Figure 4-16. Mean and standard deviation values of Inter story drift ratio for 4-, 8-, 14-Story.	153
Figure 4-17. Maximum hysteresis response for 4-, 8-, 14-Story	153
Figure 4-18. Base shear demands for 14-Story.....	154
Figure 4-19. Base shear demands for 8-Story.....	154
Figure 4-20. Base shear demands for 4-Story.....	155
Figure 4-21. Original and multiple levels of DRS.....	157
Figure 4-22. Multiple matched Accelerograms based on DE_R , MCE_R , and 2.5 times DE_R spectrum for 4-story.....	158
Figure 4-23. Multiple matched Accelerograms based on DE_R , MCE_R , and 2.5 times DE_R spectrum for 8-story.....	159
Figure 4-24. Multiple matched Accelerograms based on DE_R , MCE_R , and 2.5 times DE_R spectrum for 14-story.....	159
Figure 4-25. Story Drift profile of 4, 8, and 14-story	160
Figure 4-26. Elevation view of CMRF and TCSB	162

Figure 4-27. Elevation view of dissipation systems	163
Figure 4-28. Constructed design response spectrum based on ASCE 7-16 and NBCC 2015	164
Figure 4-29. Schematic view of yielding damper (Tsai et al., 1993).....	165
Figure 4-30. Idealized bilinear of force-displacement of the isolator (ASCE 7).....	167
Figure 4-31. Pushover results for CMRF, TCSB, TMYD, FVD, LRBI, and TPI.....	170
Figure 4-32. Overstrength factors of dissipating systems.....	171
Figure 4-33. Ductility factors of dissipating systems	171
Figure 4-34. Response modification factors of dissipating systems.....	172
Figure 4-35. Original Accelerograms	174
Figure 4-36. Matched Accelerograms based on the target response spectrum.....	175
Figure 4-37. Comparison of Roof displacement for Fixed, LRBI, and TPI frames	175
Figure 4-38. Inter-story drift ratio for CMRF, TCSB, TMYD, FVD	176
Figure 4-39. Inter-story drift ratio for LRBI, and TPI	177
Figure 4-40. Maximum hysteresis response for TCSB, FVD, TMYD, LRBI, and TPI.....	178
Figure 4-41. Response history of base shear demands for CMRF and TCSB.....	179
Figure 4-42. Response history of base shear demands for TMYD, FVD, and LRBI.....	180
Figure 4-43. Response history of base shear demands for TPI	181
Figure 5-1. 3-D and elevation view of the frame (Couch, 2020).....	184
Figure 5-2. Accelerometer detail GP1-L (SENSRA Monitoring Technologies, 2021).....	185
Figure 5-3. (a) shear drift, and (b) rotation drift (FEMA-461)	186
Figure 5-4. Instrumentation and data acquisition system (FEMA-461)	187
Figure 5-5. ASTM Generic test facility and rack test installations for shear-resistant wall panels (FEMA-461)	187
Figure 5-6. Sketch of deformation-controlled loading history (FEMA-461)	188
Figure 5-7. Example of loading history	189
Figure 5-8. Horizontal plane displacement orbit for drift-controlled bidirectional tests (FEMA- 461)	189
Figure 5-9. DRS and MCE_R response spectrum	192
Figure 5-10. Original ground motions	194
Figure 5-11. Scaled ground motions based on the target response spectrum (MCE_R).....	194
Figure 5-12. Displacement history of multiple ground motions.....	195

Figure 5-13. Individual displacement history of ground motions (Part-a)	196
Figure 5-14. Individual displacement history of ground motions (Part-b)	197
Figure 5-15. Individual displacement history of ground motions (Part-c)	198
Figure 5-16. Displacement history of artificial motions	199
Figure 5-17. Simulation of the experimental frame using ETABS software (loads are in KN). 200	
Figure 5-18. Simulation of experimental models in OpenSees	201
Figure 5-19. Rayleigh Damping parameters	201
Figure 5-20. MRF with single leg brace (Couch et. al., 2020)	202
Figure 5-21. Comparison of roof acceleration of OSLBF subjected to different motions	203
Figure 5-22. Comparison of roof history acceleration of OSLBF (Baseline Correction-Part-a) 203	
Figure 5-23. Comparison of roof history acceleration of OSLBF (Baseline Correction-Part-b) 204	
Figure 5-24. Comparison of roof history acceleration of OSLBF (Baseline Correction-Part-c) 205	
Figure 5-25. Comparison of roof history acceleration of OSLBF (Baseline Correction-Part-d) 206	
Figure 5-26. Comparison of roof history acceleration of OSLBF (Baseline Correction-Part-e) 207	
Figure 5-27. Comparison of damping property of the system in the percentage.....	208
Figure 5-28. Fabricated Ten-Co Seismic brake (Couch et. al., 2020)	209
Figure 5-29. Hysteresis curves for ground/artificial motions (Part-a).....	209
Figure 5-30. Hysteresis curves for ground/artificial motions (Part-b).....	210
Figure 5-31. Hysteresis curves for ground/artificial motions (Part-c).....	211
Figure 5-32. Hysteresis curves for ground/artificial motions (Part-d).....	212
Figure 5-33. Comparison of roof acceleration of YRB subjected to different motions.....	213
Figure 5-34. Comparison of roof history acceleration of YRB (Baseline Correction- Part-a)...	213
Figure 5-35. Comparison of roof history acceleration of YRB (Baseline Correction- Part-b)...	214
Figure 5-36. Comparison of roof history acceleration of YRB (Baseline Correction- Part-c)...	215
Figure 5-37. Comparison of roof history acceleration of YRB (Baseline Correction- Part-d)...	216
Figure 5-38. Comparison of roof history acceleration of YRB (Baseline Correction- Part-e)...	217
Figure 5-39. Comparison of damping properties of MRF with IFD.....	218
Figure 5-40. Average and standard deviation of roof acceleration of SMRF with OSLBF	220
Figure 5-41. Average and standard deviation of roof acceleration of SMRF with YRB	220
Figure 5-42. Damping percentage of MRF with OSLB	221
Figure 5-43. Damping percentage of MRF with IFD	221

Figure 5-44. Maximum displacement of SMRF with YRB.....	222
Figure 5-45. Maximum drift ratio of SMRF with YRB.....	222

List of Tables

Table 2-1. Ductility reduction factor (Newmark and hall,1982)	65
Table 3-1. Hazard levels (ASCE 41-17, 2017).....	74
Table 3-2. Vision 2000 Earthquake Design Levels (SEAOC, 1995)	74
Table 3-3. Structural performance level (Krawinkler, 1997)	76
Table 3-4. Performance level damage descriptions (SEAOC, 1995)	77
Table 3-5. Site classification (ASCE 7-16).....	81
Table 3-6. Approximate period parameters C_t and x (ASCE 7-16).....	84
Table 3-7. Design details for different models	88
Table 3-8. Fundamental period of the structures	90
Table 3-9. Target displacements	93
Table 3-10. Summary of Metadata of Selected Records	95
Table 3-11. SFRSs' design coefficients.....	104
Table 3-12. Seismic design parameters (ASCE 7-16)	106
Table 3-13.The approximate, upper limit and analytical fundamental period of the structure ..	107
Table 3-14. Analytical modal period and frequencies	108
Table 3-15. Seismic base shear.....	108
Table 3-16. Equivalent lateral forces	109
Table 3-17. Seismic base shear.....	110
Table 3-18. Equivalent lateral forces	110
Table 3-19. Torsion irregularities	112
Table 3-20. Equivalent lateral force procedure drift calculation for BF.....	112
Table 3-21. Stability coefficient	113
Table 3-22. First mode for effective seismic weight and modal participation factor	114
Table 3-23.Fundamental mode properties	115
Table 3-24.Supplemental damping parameters.....	116
Table 3-25. Damping modification factors.....	116
Table 3-26. Summary of different fundamental mode base shear parameters	117
Table 3-27. Properties of residual mode and supplemental damping parameters	118
Table 3-28. Summary of residual mode base shear parameters.....	119
Table 3-29. Summary of seismic base shear parameters	119

Table 3-30. Damping properties and modification factors	120
Table 3-31. Roof displacement	120
Table 3-32. Design and maximum earthquake story drift	120
Table 3-33. Design and maximum earthquake story velocity	121
Table 3-34. Summary of seismic base shear parameters	122
Table 3-35. Properties of lateral force	122
Table 3-36. Roof displacement	122
Table 3-37. Design and maximum earthquake story drift and velocity.....	123
Table 4-1. Design details for different models	135
Table 4-2. ISFDs design parameters for different types of structures	137
Table 4-3. Seismic analysis results, slip loads, and calculated mass per damper.....	138
Table 4-4. The fundamental period of the structures	139
Table 4-5. Spectral acceleration parameters for different hazard levels.....	140
Table 4-6. Target displacements parameters	141
Table 4-7. Nonlinear static analysis results	142
Table 4-8. Response modification factor for 4-, 8-, 14-Story.....	144
Table 4-9. Summary of Metadata of Selected Records	147
Table 4-10. Summary of Selected Records.....	158
Table 4-11. Material quantities	162
Table 4-12. Damping coefficient	165
Table 4-13. TMYD design parameters	166
Table 4-14. Preliminary design of LRI and TPI	168
Table 4-15. Empirical Equations (Metric)	169
Table 4-16. The fundamental period of the structures	169
Table 4-17. Pushover analysis results.....	170
Table 4-18. Response modification factor	171
Table 4-19. Summary of selected ground motions	173
Table 4-20. Calculated ground motions parameters pre/post-matching	173
Table 4-21. Calculated ground motions parameters pre/post-matching	174
Table 5-1. Seismic design parameters (ASCE 7-16)	192
Table 5-2. Summary of selected ground motions	193

Table 5-3. Detail of the experimental frame sections	200
Table 5-4. Detail of the bracing system	200

CHAPTER 1

Introduction

1.1 Background and Problem Definition

Performance-Based Seismic Design (PBSD) is increasingly being adopted in various jurisdictions around the world. Based on the owner's expectations, the acceptable levels of dynamic loadings and performance objectives for structural and non-structural elements can be determined. Seismic design codes presently in use are prescription-based and they focus on the strength and capacity of structural members, but the structure's overall performance during a given seismic event cannot be clearly described. Performance-based design differs from this in that it is objective-based with a specific level of structural behaviour during a seismic event. With this approach, different methods of analysis were used here depending on the performance level chosen. Structural and non-structural damages were computed to determine the structure's overall performance. Because of this, the structural engineer, architect, owner, and contractor can all provide input in the determination of the performance level required as well as the achievement of that level. Steel concentrically braced frames have been widely used to protect buildings against lateral loads as they are simple both in design and fabrication. They dissipate energy by yielding in tension and by bending/buckling in compression. However, their performance during past earthquakes has been adversely impacted by several factors including limited ductility, buckling failure, fracture of connections, and unsymmetrical behaviour in tension and compression. In recent years, the fundamental of dissipation systems has been evolving and used within the structural elements. In general, the damage energy can be reduced by supplemental damping, which can be added by incorporating passive/active/semi-active energy dissipaters. In this regard, the passive control system can be more reliable than the active system and they do not need sophisticated sensing equipment or external power. Base isolation tuned mass dampers, friction dampers, viscous dampers, viscoelastic dampers, and hysteretic dampers shall be categorized as this group. Understanding the system and dynamic characteristics and ensuring the stability of the

structures with supplemental dampers may require the application of the concept of the control theory. The thesis will focus on these aspects, particularly in the context of buildings with concrete moment-resisting frames.

1.2 Research Significance and Motivation

A comparison of structural control systems by Soong and Spencer (2002) showed that semi-active control systems are a better option without the limitations associated with the passive and active control systems. Experimentally tested semi-active control systems include stiffness control devices, electrorheological dampers, magnetorheological dampers, friction control devices, fluid viscous dampers, and tuned liquid dampers were explained, and it was observed from the experimental testing that the semi-active control method can improve the seismic behaviour of structures. Similar results were obtained (Soong and Spencer 2002; Fisco and Adeli 2011; Yanik, and Aldemir 2019), these researchers study the active and semi-active control systems from 1997 to 2018. Moreover, Yanik and Aldemir (2019) did not find any study on the review of the new active and semi-active control approaches. This entire technology is still evolving, further experimental and analytical studies are required to understand these systems better, and to include their realistic performance as well as long-term operation as they are integrated into the structural systems.

Different types of devices that dissipate energy through friction are including Limited Slip Bolt Joint (Pall et al., 1979), Three-stage Friction Grip Elements (Roik et al., 1988), Friction-Damper in X-Bracing, Friction-Damper in Chevron-Bracing, and Friction-Damper in Single Diagonal (Pall et al., 1996), Sumitomo Friction Damper (Aiken and Kelly, 1990), Energy Dissipating Restraint (Nims et al., 1993), and Slotted Bolted Connection (Popov et al. 1995). The Idealized behaviour of LSB Joint which was presented by Pall et al. (1979), was further investigated by Roik et al. (1988) for three-stage friction grip elements. It was shown the mechanical properties of the bolts and the limited geometrical of slotted holes play an important role in lateral stiffness, slip force, and the amount of dissipated energy per cycle. Moreover, friction grip connections can reduce

horizontal forces and displacements by their energy dissipation capacity, however, the proposed model was not able to capture additional force-displacement. The effectiveness of slotted bolted connections with steel brass surface was verified by Popov et al. 1995, more investigations are required to investigate the effects of different surface treatments. Galvanic corrosion and the effects of different coating, as well as large-scale tests, need more investigations.

Pall friction dampers consist of treated plates in a series that develop resistance when sliding against one another. Pall and Marsh (1982), Patil et al. (2015), and Tirca et al. (2018) proposed a combination of moment-resisting frames with friction devices. Colajanni et al. (1997) discussed hysteresis characteristics of friction damper and Morgan et al. (2007) presented their effectiveness of friction dampers. Significant savings in the construction cost of friction dampers were discussed by Chang et al. (2006), Vail et al. (2003). Constantinou et al. (1998), Tirca (2009), Haider et al. (2012), Chen et al. (2001), and Kiran et. al., (2016) showed a reduction in seismic demand using friction devices. Nonlinear static pushover and time history analysis analyses were performed to assess the over strength, ductility, and response modification factors for steel buckling restrained braced frame. It was observed the response modification factor decreased when the story height and span length increased (Moni et al. 2016). Sarjou and Shabakhty (2017) showed improved pall friction dampers in concentric steel bracing frames, reduced the base shear, and relative displacement.

Modeling of yielding restrained braces including Coulomb friction and Bouc-Wen models are discussed. The method proposed by Baber and Noori in 1985 and 1986, is discussed in detail, they added a general degradation model to smooth the hysteresis model of Bouc and Barber and Wen 1981, to capture the pinching effect. It was revealed the sliding mechanism was subjected to different parameters including types of loading, friction coefficient, temperature, velocity as well as the contact treatment, material, pressure, and size (Pall 1979; Constantinou et al. 1990; Sextro 2007). Therefore, to avoid discontinuity between stick-slip and slip phases Makkar et al. (2005) proposed a new friction model with a combination of the stribek effect, Coulomb friction, and viscous dissipation.

The critical review of the literature reveals that most of the researchers focused on retrofitting of steel structure by seismic dissipater devices and concrete structure by using fiber-reinforced polymer (FRP) composites materials and very few studies have been conducted in case of the performance-based seismic design for concrete structures utilizing supplementary dampers such as yielding restrained braces. Moreover, yielding restrained braces have been used to improve the dynamic characteristics and stability of structures, the 2015 NBCC recommendation is for supplemental energy dissipation in general, and not for friction dampers in particular. Buildings designed and constructed in accordance with earlier codes and standards often do not meet the life safety criteria based on the current seismic criteria objectives as earthquake requirements changed over time (NBCC 2015 commentary L). There is a need to provide a design guideline, retrofitting, and methodologies to improve the seismic performance of concrete structures and to create a more optimal and economical design by incorporating energy dissipation devices in the seismic force resistance systems. In summary, the seismic performance of different types of concrete moment resisting frames equipped with yielding restrained braces needs more investigation. Moreover, seismic design factors of concrete moment resisting frames equipped with yielding restrained braces are required to be examined. The current study aims to partially address this by using both numerical analyses and simulation of available experimental tests.

1.3 Objectives and Scope of Work

The objectives of the present research are to:

- (i) Investigate the life safety performance of different concrete moment resisting frames (CMRFs) considering supplemental damping to estimate seismic response factors,
- (ii) Evaluate seismic design parameters of concrete moment resisting frames (CMRFs) equipped with different energy dissipation systems to understand the relative performance of YRBs,
- (iii) Collaborate experimental work with simulation to investigate dynamic performance and reliability of YRBs under real earthquakes,

- (iv) Develop a set of guidelines for the use of yielding restrained braces in concrete frame buildings.

In order to achieve the objectives of this research, the scope of research is identified as follows:

- Evaluating the effects of Inline Seismic Friction Dampers (ISFDs) on different concrete moment resisting frames (CMRFs) including ductile, moderately ductile, and elastic frames and comparing them with bare frames as well as the assessment of their economical aspects.
- Conducting a comparison between the effects of conventional and FEMA procedures on the overall response of the structure and evaluating the damping properties.
- Conducting nonlinear static analysis to evaluate the seismic force reduction factors of concrete structures with different heights and span lengths equipped with inline seismic friction dampers including the overstrength, ductility, and response modification factors as well as performing a nonlinear response history analysis to assess the overall structural performances.
- Conducting a comparative study between the design procedures of American and Canadian standards for a fourteen-story ductile concrete moment resisting frames using ETABS software, and investigate the effects of six passive energy systems on the overall response of the structure including Ductile Concrete Moment Resisting Frame (DCMRF), Ten-Co Seismic Brake (TCSB), Fluid Viscous Damper (FVD), Triangular Metallic Yielding Dampers (TMYD), as well as two seismic isolators including Lead Rubber Bearing Isolator (LRBI) and Triple Pendulum Isolator (TPI) to define a proper frame of reference for Ten-Co Seismic Brakes.
- Collaborating, experimental studies (this joint work was performed by an MSc student at the California State University, Fresno Lyles College of Engineering, 2020) on the seismic response of Inline Seismic Friction Dampers (ISFDs).
- Simulation of the experimental test using ETABS, OpenSees software to compare their acceleration, damping ratios, drift, and displacement.

1.4 Thesis Layout

This thesis is structured in a sandwich thesis format, which is divided into various chapters such that except chapters 1, 2, and 6, all other chapters can be converted to manuscripts of articles to peer-reviewed journals. The thesis is divided into six chapters as follows:

- Chapter 1 is an introduction to the proposal which includes background and problem definition, research significance, motivation, objective, and scope of work.
- Chapter 2 is the literature review and covers performance base design and evaluation, common strengthening techniques, various types of seismic protection control systems, history and types of friction dampers, and a background of the Coulomb and the Bouc-Wen models of friction dampers as well as the methodology.
- Chapter 3 is the explanation of seismic performance levels and analysis procedures; Seismic performance of three code designed concrete moment-resisting frame buildings evaluated considering FEMA 356 and ATC 72 procedures; enhancing seismic safety and performance of different Reinforced Concrete moment-resisting frames including ductile, moderately ductile as well as elastic frames equipped with/without yielding restrained braces are discussed, moreover the behaviour of inline seismic friction dampers of reinforced concrete moment-resisting frames as well as the procedures of determining the damping properties are discussed.
- Chapter 4 is the investigation of the seismic design parameters of four-, eight-, and fourteen-story ductile concrete frames with inline friction dampers, designed as per the 2015 national building code of Canada. Moreover, the effects of building height and span length for single diagonal braces (SDB) are discussed. In addition, a comparative study of design procedures of American and Canadian standards is discussed and the effects of five passive energy systems including Ten-Co Seismic Brake (TCSB), Fluid Viscous Damper (FVD), Triangular Metallic Yielding Dampers (TMYD), Lead Rubber Bearing Isolator (LRBI) and Triple Pendulum Isolator (TPI) on the overall response of the structure were evaluated.

- Chapter 5 consists of two phases; the first phase is the collaborating experimental work of a dual system moment resisting frame and a single leg braced frame and an inline friction damper. The second phase is the simulation of experimental work to evaluate the effectiveness of the inline friction damper. The discussion covers a comparison of acceleration, damping ratios, drift, and displacement.
- Chapter 6 includes the summary of the research project, the main contributions and conclusions, limitations, and recommendations for future work.

CHAPTER 2

Literature Review and Methodology

2.1 Background

Recent earthquakes all around the world have provided performance data demonstrating that large losses can result from the inadequate performance of Buildings and bridges moreover building codes in various jurisdictions are moving towards performance-based design approaches where a structure is designed not only to have adequate strength but also for the required performance attributes, such as adequate deformability (Mousavi Azad Kasmaei, 2011). Typical problems that have caused extensive damage and collapse in the previous earthquake may be summarized as underestimation of seismic deflection demands, with possibly catastrophic consequences related to unseating of spans and insufficient rotation capacity in plastic hinges and underestimation of seismic forces and inappropriate application of capacity design principles (Sullivan and Calvi, 2013, Calvi et al., 2013).

In 1988 Uang and Bertero proposed the energy relationship with equation 2.1.

$$E_t = E_h + E_d + E_k + E_s \quad (2.1)$$

In which, E_t , is the total energy input, E_h , is the residual energy, E_d , is the dissipated energy by damping, E_k , is the kinetic energy, and E_s is the elastic strain energy. Seismic load and damage relationship was defined by equilibrium energy in which the total seismic inertia is equal to the summation of elastic vibration energy plus cumulative inelastic strain energy and the energy absorbed by damping, therefore the energy induces to the structural damage is equal to the total seismic inertia minus energy absorbed by damping (Akiyama 2000). In other words, damping and damage of a system have a direct effect on one another.

Understanding the system and dynamic characteristics and stability of structures are the concepts of the control theory. In general, the damage energy can be reduced by supplemental damping, which can be added by incorporating passive/active/semi-active energy dissipaters.

Moreover, dampers have been used to improve the dynamic characteristics and stability of structures. In this regard, the passive control system can be more reliable than the active system and they do not need sophisticated sensing equipment or external power. Base isolation tuned mass dampers, friction dampers, viscous dampers, viscoelastic dampers, and hysteretic dampers shall be categorized as this group. Since most of the buildings in Canada were designed and constructed according to earlier codes, retrofitting techniques are essential to improve seismic performance. Moreover, dampers have been used to improve the dynamic characteristics and stability of structures. There is a need to provide retrofitting and methodologies to improve the seismic performance and to create an optimal design of structures by incorporating dissipater devices in earthquake resistance systems.

The objective of this thesis is to propose methods for the optimal design of supplemental damping in structures subjected to seismic loads and to employ passive energy dissipation devices to control the dynamic response of structures. Hence, the following literature focuses on performance-based seismic design and retrofitting techniques, various types of control systems including advanced friction dampers, as well as structural damage control.

2.2 Performance-based design and evaluation

Performance-Based Seismic Design is deemed a performance method of seismic design in many jurisdictions. Engineers can evaluate realistic seismic motions and performance target criteria for both structural and non-structural elements, as per the owner's expectations. Performance-based seismic design concepts are increasingly being adopted in various codes. While the National Building Code of Canada (NBCC 2015), as well as Euro Code-08, are not fully performance-based, they provide some features of a performance-based code, such as displacement control and objective-based solutions. Performance evaluation is an important part of a performance-based design. Seismic design codes presently in use are prescribed-based and focus on the strength and capacity of structural members, but the structure's overall performance during a given seismic event cannot be clearly described. Performance-based design differs from

this in that, it is objective-based performance is concerned with a specific level of structural behaviour during a seismic event as demonstrated in Figure 2-1 (Lateral deformation a seismic event versus base shear demand).



Figure 2-1. A schematic view of selecting a performance level (FEMA 273/356, Hamburger and Holmes 1998); Photo Credits: F. M. Tehrani, Buildings in Rasht and Manjil after the 1990 Manjil-Rudbar Earthquake (Tehrani 1990)

The results of a series of vibration tests conducted on tall reinforced concrete shear wall buildings located in Downtown Vancouver, British Columbia, Canada with the buildings range in height from 15 to 45 stories and ambient vibration tests were performed on each building to obtain its dynamic characteristics, vibration levels, mode shapes, modal frequency, damping, rocking behaviour, and soil-structure interaction of the raft foundation (Turek et al., 2008). It was observed that the fundamental natural period increased from 0.81 to 3.57 seconds. These results showed that the NBCC 2005 is more conservative for taller buildings and by using the predicted period from FEM, lower design forces can be used for response spectrum analysis. Regarding the micro-tremor and base analyses results, there was a significant correlation between the movement of the foundation and the behaviour of the vibration modes of the structure, which showed a strong potential for soil-structure interaction effects due to foundation rocking. Since modal updating

studies dealt with many parameters and became a mathematical problem, it is limited to translate these changes into a real structure.

The 8.8 magnitude MaueI earthquake in 2010 caused strong ground motion, the majority of the buildings were reinforced concrete structures. It was observed that the majority of structural damages were in multi-story and high-rise buildings due to the poor performance of slender RC shear walls, without confined boundary elements, that caused crushing of concrete and buckling of vertical wall reinforcement at the end and throughout of the entire length of the wall. Since Chilean code didn't provide any restrictions in designing irregular structures, hence, soft and weak stories and discontinued shear walls were created that resulted in an increased force and deformation demand and global and local failures. Moreover, the interaction of nonstructural components with the seismic force-resisting system resulted in damages, such as the presence of masonry walls provided forces on columns around window openings created short columns and

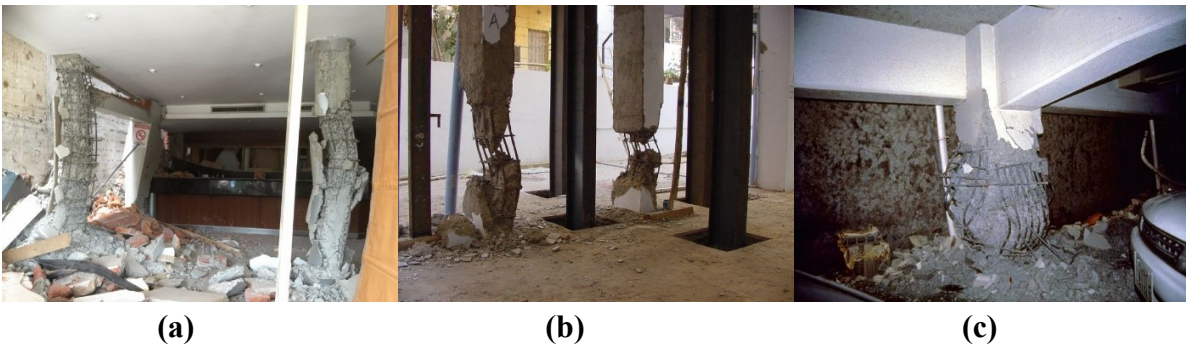


Figure 2-2. (a) Soft story failure, (b) plastic hinge formation, and (c) ductile detailing problems (EERI, 2020)

therefore, resulted in diagonal tension failures, there was also a lack of proper connections in precast structures. More study in seismic detailing practice of RC shear walls and effects of irregularities and a comprehensive study of comparison design of RC buildings according to CSA and Chilean Code are required to find out the weakness of design and RC detailing in CSA (Saatcioglu et al., 2013). Soft story failure, plastic hinge formation, and ductile detailing problems are shown in Figure 2-2 (EERI, 2020).

Four ductile steel moment-resisting frame buildings with heights of 5, 10, 15, and 20 stories, were designed in Vancouver, Canada, and their performances were studied to determine the level of seismic protection implied in the code (Yousuf and Bagchi, 2009). For the seismic load, the equivalent static load (ESL) procedure as provided in NBCC 2005 (NRCC 2005) was used in the preliminary design of the buildings, and this was followed by modal and dynamic analysis. The pushover analysis of the buildings was performed by applying estimated equivalent seismic lateral forces in an inverted triangular shape, as defined in NBCC 2005 (NRCC 2005), and monotonically increasing these forces. Synthesized and scaled real ground motion records were used to evaluate the nonlinear dynamic response of these structures. Both pushover and dynamic analyses indicated that building frames designed according to the seismic provisions of NBCC 2005 achieved the expected performance level of collapse prevention or better. From the pushover analysis, it can also be observed that a building frame's system-level ductility capacity reduces with building height. While the ductility capacities of the 5- and 10-story frames studied were more than five, as was assumed in the calculation of the design lateral forces, the ductility capacities of the 15- and 20-story buildings were much lower. Infill panels were found to reduce dynamic drift demand and damage, while also reducing the ductility capacity of the structural system. In addition, building performance was found to be affected by the presence of the nature of selected ground motion records (Yousuf and Bagchi, 2009).

Strengthening techniques are available in a variety of types such as concrete Jacketing, an integrated shear wall with steel plate, dissipation dampers in the bracing system, seismic isolation, and FRP wrapping. As the most common retrofitting technique, several researchers have investigated the FRP strengthening upgrade in concrete structures. Most of them indicate that the externally bonded FRP improves the deformability and/or strength capacity of members remarkably. The strengthening techniques, depending on the role of the member, upgrade the shear, bending, or confining capacity of the members. There are three main applications for the use of FRPs as external reinforcement of reinforced concrete structures (ISIS 2004):

Flexural Strengthening: In this method, FRP materials are bonded to the tension and/or side faces of a concrete beam to provide additional tensile reinforcement and to increase the strength of the member in bending as is shown in Figure 2-3.

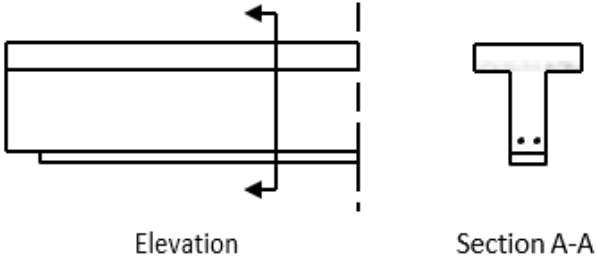


Figure 2-3. Externally bonded FRP reinforcement-Flexural strengthening (ISIS 2004)

Shear Strengthening: In this method as it is presented in Figure 2-4, FRP materials are bonded to the side faces of a concrete beam to provide shear reinforcement which supplements that provided by the internal steel stirrups.

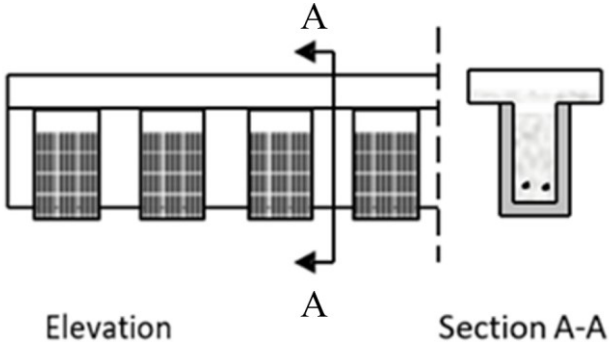


Figure 2-4. Externally bonded FRP reinforcement- Shear strengthening (ISIS 2004)

Confining Reinforcement: In this method, columns are wrapped in the circumferential direction with FRP sheets. Under a compressive axial load, the column expands laterally and the FRP sheets develop a tensile “confining” stress that places the concrete in a state of triaxial stress as shown in Figure 2-5.

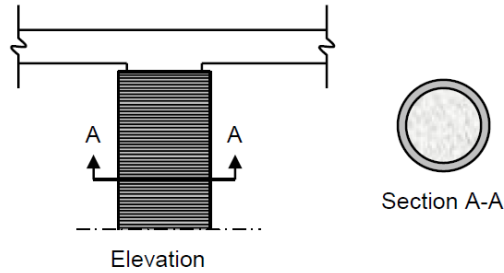


Figure 2-5. Externally bonded FRP reinforcement- Axial strengthening (ISIS 2004)

(Davalos et al., 2012) investigated a “comprehensive study on using externally bonded FRP composites for the rehabilitation of reinforced concrete T-beam bridges”. First concrete T-Beam bridges were classified into three categories for repair with FRP, then two non-destructive tests were performed, the results showed that the quality of some beams was unacceptable, and retrofitting would require major removal and replacement. Moreover, Concrete cylinders were obtained as deck core samples and tested in compression, which was 40 MPa, the cylinders indicating that the deck concrete was not carbonated. Then by applying tandem trucks on one or two lanes, the field test was conducted, also ABAQUS program was used for finite element analysis it was concluded that there is a good correlation between Test and FE under the most critical load case when the rear axle of the truck was at mid-span. After beams were strengthened by FRP according to AASHTO (2002), and a finite element model was built according to as-built drawing and field information and the same test field applied to assess the performance by the verification of the model permitted its confident use in designing FRP reinforcement. Overall, the stiffness of the repaired bridge did not change much which was also verified by the lab-scale studies.

(Hamed et al., 2014) presented Strengthening of Reinforced Concrete Arches with Externally Bonded Composite Materials in this paper an experimental and analytical study that includes testing to failure of fiber-reinforced polymer (FRP) strengthened medium-scaled reinforced concrete shallow arches and the application of a specially tailored high-order finite element for their analysis was presented. The experimental study was included testing to failure of three medium-scaled RC arches, two of them strengthened with FRP and one tested as a control

specimen. All arches had been tested under six nonsymmetric point loads equally spaced along the arch. The theoretical model had been based on a specially tailored multilayered finite element along with modeling the arch as a polygon with inclined segments. The test results had shown that the FRP system can effectively increase the load-carrying capacity of RC arches. In contrast, the application of the FRP had shifted the location of the critical crack to the weakest section that has fewer or no bonded FRP strips. Among the two strengthened arches, the stronger one included FRP-end anchoring and additional FRP strips bonded to the arch sides at two spandrel columns. This structural layout contributes to the continuity of the force taken by the FRP strips. Based on that, the consideration of such overlapping patterns over critical sections was found positive.

2.3 Control systems for seismic protection of structures

The prediction of structural behaviour subjected to seismic excitation is a challenging task for civil engineering. The strength capacity design of a structure is a traditional approach, but newer concepts are including both passive and active control systems. A comprehensive comparison and explanation of passive, active, and semi-active control systems for protecting structures against earthquakes was presented in order to define a reference for semi-active control systems (Symans et. al., 1997).

Supplemental energy dissipation is also presented by (Soong and Spencer 2002), the passive systems which enhance damping, stiffness, and strength of the structure, as well as active structural control systems which include active, hybrid, and semi-active systems, were reviewed, their advantage and limitation were discussed, and their basic concepts are explained. This entire technology is still evolving, further experimental and analytical are required including their realistic performance as well as long-term operation for these devices to be integrated into structural systems.

Active and semi-active control systems were reviewed from 1997 to 2011 by (Fisco and Adeli 2011). Tuned mass dampers, distributed actuators, active tendon systems, and active coupled building systems are included in active control systems, while semi-active control systems are

including, magnetorheological (MR) fluid dampers, semi-active stiffness dampers, semi-active tuned liquid column dampers, and piezoelectric dampers were discussed in this paper. During these years researchers moved from active control to semi-active and hybrid vibration control systems. The state-of-the-art of the new active and semi-active approaches during 2008 and 2018 was evaluated (Yanik, and Aldemir 2019), due to the latest technology and computational advances, there is the numerical evaluation of some developed algorithms. However, there is not any implementation of these control algorithms in the structural system. They did not find any study on the review of the new active and semi-active control approaches. Therefore, there is a need for experimental evaluation and validation of these new active and semi-active control approaches.

The full-scale 5-story building was examined with steel damper, oil damper, viscous damper, and viscoelastic damper using E-Defense three-dimensional shake table (Kasai et al. 2007). Most of the major Japanese buildings were designed and constructed after the Kobe earthquake in 1995 using either base isolator or passive control systems. Since these systems were never tested under a major ground motion, their performance is validated using a full-scale shake table test at the E-Defense. The JR Takatori motion, noise excitation as well as free vibration tests were performed, strain, deformation, displacement, and acceleration were measured. The recorded damper deformation was used for analytical prediction, it was observed damper force is in the same range as the recorded data. Viscous, oil, and viscoelastic dampers were predicted by analysis except the steel damper using a bilinear model. From the vibration periods and damping ratios, the steel dampers showed the shortest period and smallest damping ratio while oil dampers experienced the largest damping ratio of about 17% and viscous and viscoelastic dampers had a damping ratio of about 10%. The reason is the oil dampers were oversized compared with the other dampers. Due to the limitation of budget the building size decreased; and also, the friction dampers performance was not investigated.

Shape memory alloys (SMAs) have the ability to undergo large deformation and recover their initial configuration, this paper investigated the performance of steel moment-resisting frames using shape memory alloys (Sultana and Youssef 2016). Further research is required to examine the optimum use of SMAs in connections as well as bracing elements. This paper examined the

effects of SMAs at identified parts of the frame for reducing the residual inter-story drift as well as the associated costs. Incremental dynamic analysis using five different ground motions was used to identify the floors with severe damage of a ten-story building during earthquake excitations. Then the rigid connections were replaced by SMA connections and nonlinear response history analysis was performed using the same records. It was observed the number of SMA connections influenced the maximum inter-story drift (MID) and its location effect on the maximum residual inter-story drift (MRID). It was also concluded the overall seismic performance of the SMRFs can be improved using SMA with a high reduction in the maximum residual inter-story drift. A large-scale test, as well as a time history analysis of at least seven ground motions, is required to investigate the numbers and locations of SMA in more detail.

There are three major classes of the control system including passive control system, active control system, and semi-active control system. The combination of these control systems is a so-called hybrid control system consisting of combined passive and active devices or passive and semi-active devices.

2.3.1 Active control systems

Active control systems require a large power source for operation, the control forces are generated by electrohydraulic or electromechanical actuators based on feedback information from measured response of the structure or external excitation. These measurements are monitored by a controller which determines the control signal for the operation of actuators presented in Figure 2-6.

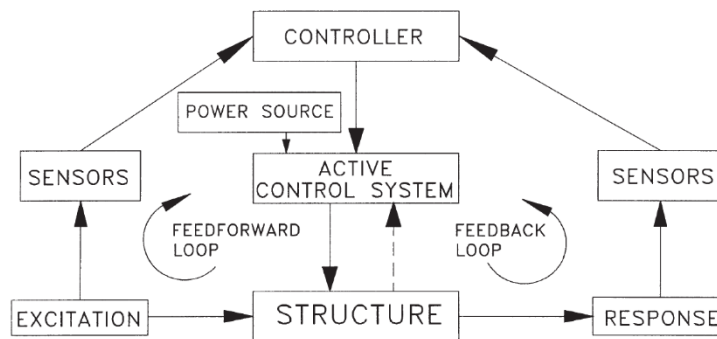


Figure 2-6. Active control system (after Symans et al. 1997)

A common type of active control system is active mass damper (AMD) which is shown in Figure 2-7, which was used to enhance the comfort of people inside the building during strong motions.

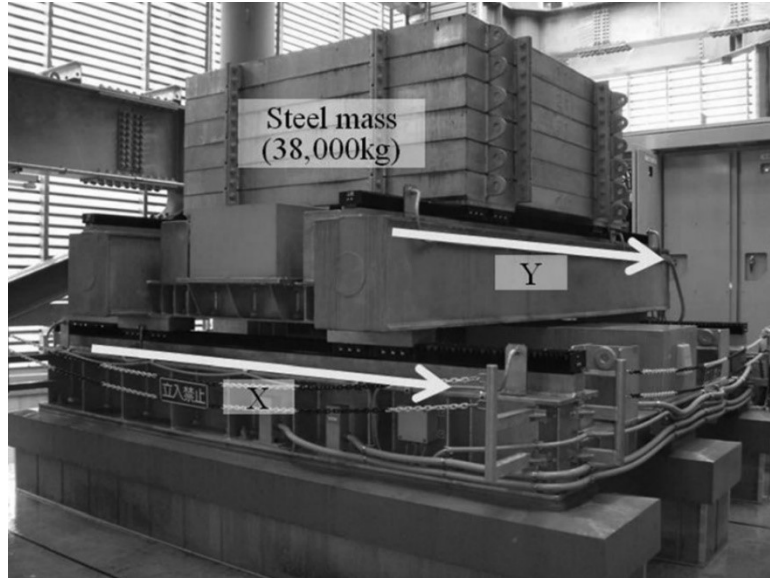


Figure 2-7. Active mass damper (AMD) (Yamamoto and Sone, 2014)

2.3.2 Semi-active control systems

Semi-active control systems require a small external power source for operation and a controller that observes the feedback and produces an essential signal for the devices and utilizes the motion of structure to develop the control forces as demonstrated in Figure 2-8.

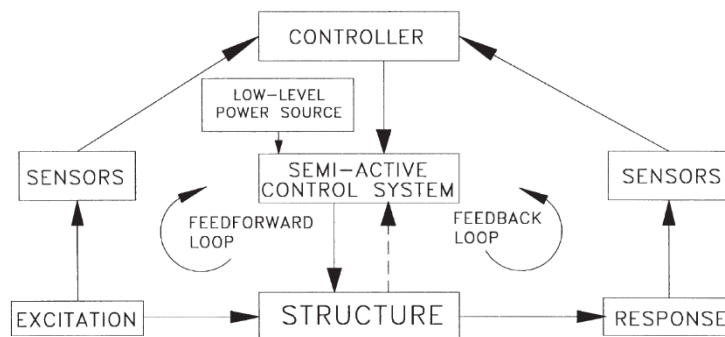


Figure 2-8. Semi-Active control system (after Symans et al. 1997)

In this part, those systems that were experimentally evaluated were reviewed are including stiffness control devices, electrorheological dampers, magnetorheological dampers, friction control devices, fluid viscous dampers, tuned mass dampers, and tuned liquid dampers.

The main function of Stiffness control devices is to modify the stiffness and thus natural vibration characteristics. Figure 2-9 showed the semi-active stiffness device in a chevron bracing arrangement, the device composed of a hydraulic cylinder with solenoid control valve, when the valve is closed the beam locks to braces below and when it is open it disengaged the beam and brace connections, at each time step the stiffness configuration was determined and appropriate command signals were sent to the stiffness control devices. The results showed that the lower magnitude earthquake (4.9) had a 70% reduction of roof acceleration, and the higher magnitude (5.7) had a 40% reduction of roof acceleration, which showed the feasibility of semi-active stiffness control technology.

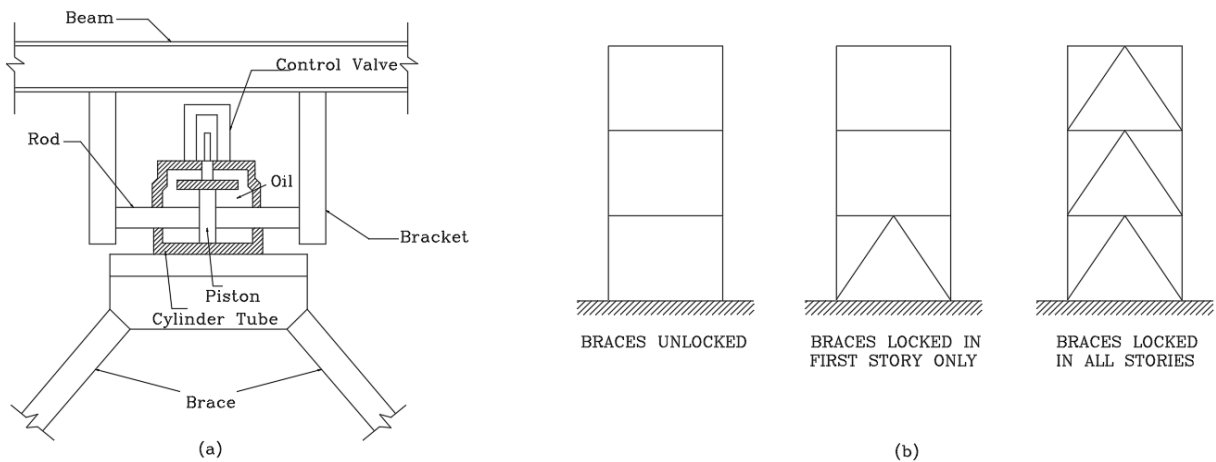


Figure 2-9. Stiffness control device (a) installation detail and (b) configurations within full-scale test structure, (after Kobori 1993)

Electrorheological (ER) dampers consist of a hydraulic cylinder containing micron-sized dielectric particles suspended within a fluid, when a strong electric field happens, the particles polarize and become aligned and increase the resistance to flow. The behaviour of ER dampers

can be modulated by changing the electric field. A large-scale capacity ER was developed (McMahon et al., 1997) as demonstrated in Figure 2-10.

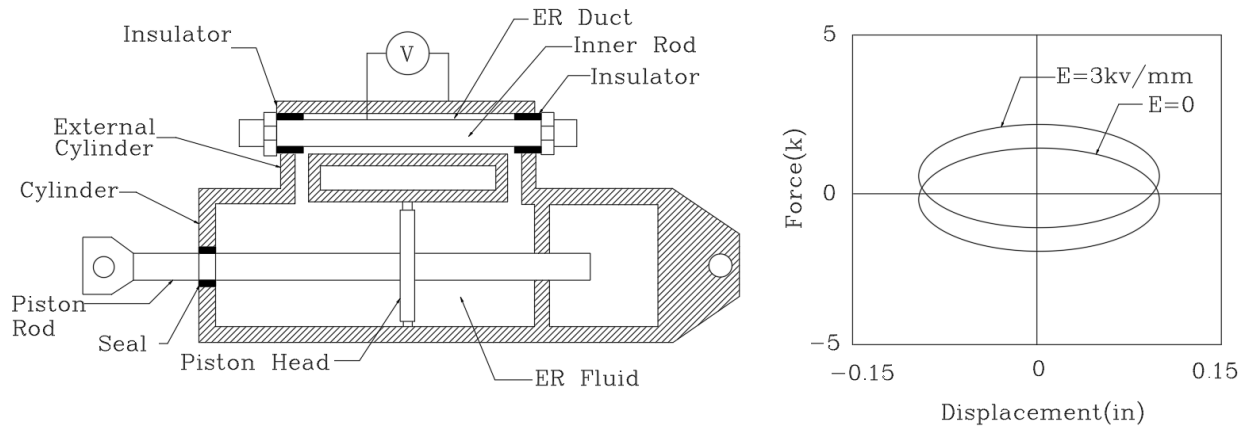


Figure 2-10. Schematic of small-scale damper and hysteresis loop for a large-scale damper for two different electric field strengths (after McMahon et al., 1997)

It was observed that the elliptical shape of the hysteresis loop for the case of no applied electric field may be modeled as a linear viscous dashpot. Similar results reported by Gordaninejad et al. (1994), a hybrid ER damper with two separate compartments, one containing a viscous oil and the other containing an ER fluid was developed and utilized to control the vibration of a simple cantilever beam subjected to sinusoidal excitation, it was shown that increasing the zero-field viscosity may be desirable.

Magnetorheological dampers are the magnetic analogs of ER dampers with similar behaviour but with a control effect of magnetic instead of electric. MR dampers consist of a hydraulic cylinder containing micron-sized, magnetically polarizable particles suspended within the fluid. Its behaviour is controlled by subjecting the fluid to a magnetic field.

Semi-active friction control devices are used as energy dissipaters within the lateral bracing or as components within sliding isolation systems. The idealized hysteresis loop of friction damper is presented in Figure 2-11, as the force is increased, the hysteresis loop expands in the vertical direction, thus the amount of dissipated energy per cycle of the harmonic motion is controlled by the normal force.

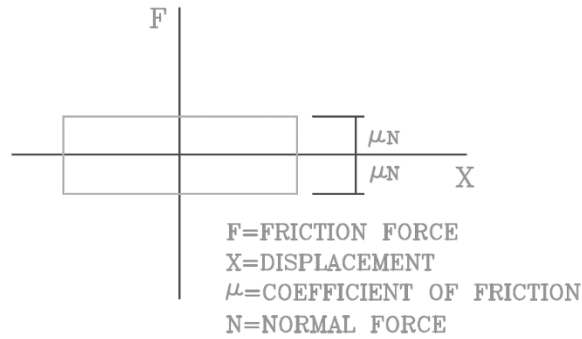


Figure 2-11. Hysteresis loop of idealized Coulomb friction damper (after Feng 1993)

An isolation system was described by Feng et al. (1993), to limit the sliding displacement and minimize the transfer of seismic force to the superstructure, the friction force on the sliding interface between the superstructure and the foundation is controlled. Figure 2-12 demonstrated a cross-sectional and plan view of the semi-active friction control bearing.

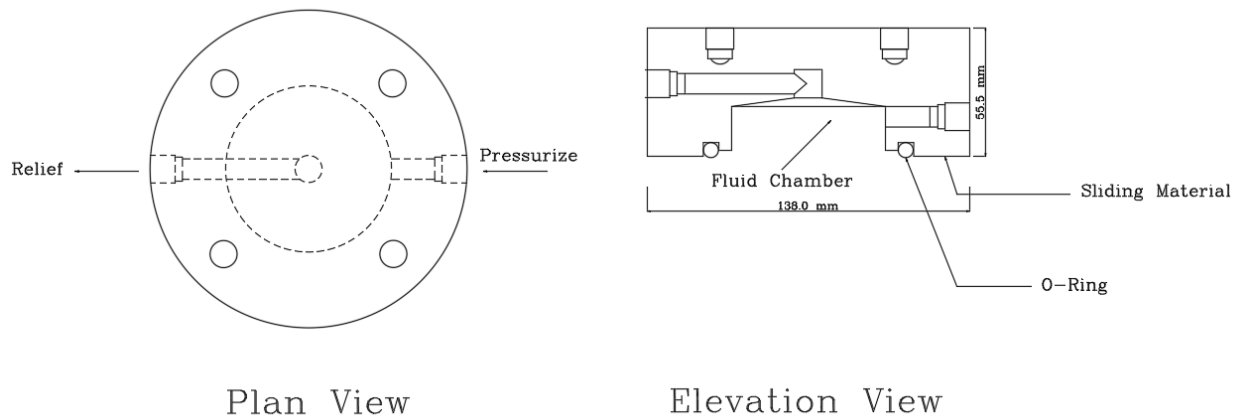


Figure 2-12. Friction controllable bearing (after Feng 1993)

As shown in this Figure, each bearing has a fluid chamber a pressure control system composed of a servo valve, an accumulator, and a computer that is used to modify the pressure.

Semi-fluid viscous dampers consist of a hydraulic cylinder with a piston head to separate the two sides of the cylinder. When the piston is cycled, the fluid is forced to pass through small orifices at high speed and the pressure differential across the piston head, and the output force is modulated by an external control valve, this control valve is in the form of a solenoid valve for on-

off control or a servo valve for variable control. Two different semi-active damper systems were tested by Symans et al. (1997), two-stage and variable dampers utilizing solenoid and servo valve respectively. It consists of a stainless-steel piston rod, a bronze piston head, a piston rod make-up accumulator, and is filled with thin silicone oil as shown in Figure 2-13.

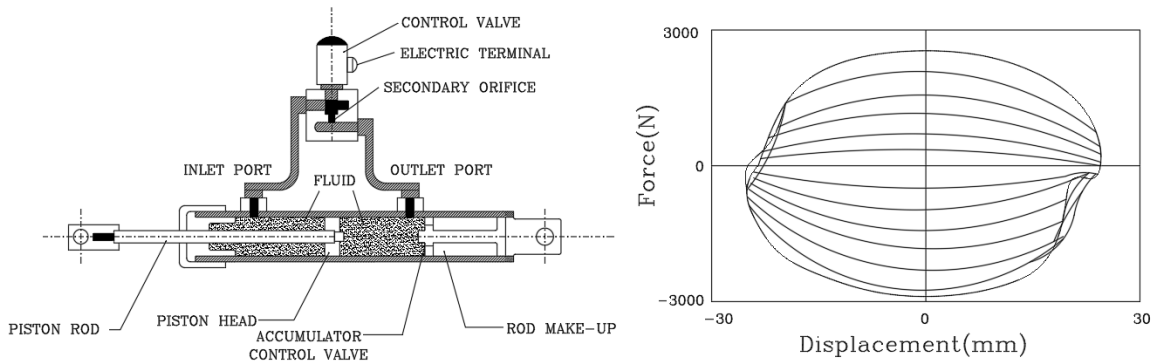


Figure 2-13. Schematic view of damper and hysteresis loops for seven different command voltage levels, subjected to harmonic motion, (after Symans et al. 1997)

The dynamic behaviour of fluid dampers was generated through extensive cyclic testing over a wide range of frequencies. It was observed that the damper behaviour can be described by a linear viscous dashpot with a voltage-dependent damping coefficient. As for a two-stage damper, the damping coefficient can be adjusted between two values of high and low as demonstrated in the above Figure, which also demonstrated that dissipated energy per cycle of motion was very large when voltage is 0V, thus it resulted in fail-safe operation mode.

2.3.3 Passive Energy Dissipation Devices

Passive control systems are a system that does not require an external power source for operation, and it is used to modify the dynamic properties of a structure, thus reducing the demand on the structural system. The response of the structure at the location of the passive control system is used to formulate the control forces as presented in Figure 2-14.

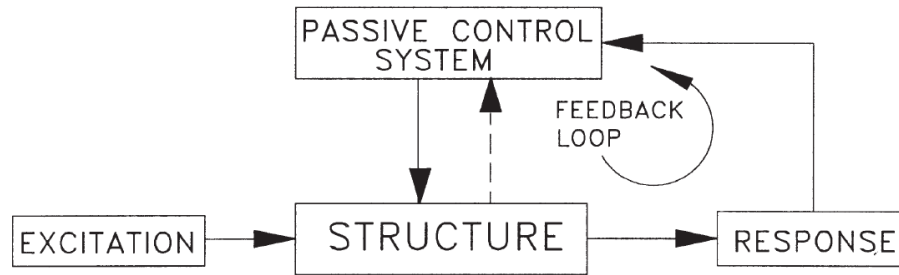


Figure 2-14. Passive control system (after Symans et al. 1997)

Supplemental energy dissipation devices may take many forms and use a different mechanism to dissipate energy including the yielding of mild steel, viscoelastic action in rubber-like materials, shearing of viscous fluid, orificing of fluid, and sliding friction. A specific shape of passive control systems are seismic isolation systems, in which a flexible isolation system is placed between the foundation and superstructure to increase the natural period of the system; this results in reducing acceleration in the superstructure and increasing the displacement in the isolation level. Passive energy dissipation devices minimize the structural damage by reducing demands on the primary structural members.

Passive energy dissipation devices can be divided into six groups which are: Metallic Dampers, Friction Dampers, Viscoelastic Dampers, Viscous Fluid Dampers, Tuned Mass Dampers, and Tuned Liquid Dampers (Soong and Dargush 1998). Figure 2-15 shows major types of dampers. The main function of viscous and oil dampers is to resist the flow of polymer liquid and low viscosity oil. The hysteresis of the Viscous damper is a combination of ellipse and rectangle and can be modeled in a series combination with nonlinear dashpot and elastic spring. While the series combination of linear dashpot and elastic spring is used to model the oil damper. The inclined elliptical shape is developed by a viscoelastic damper which dissipates energy by using the molecular motion of polymer. Energy in steel and friction dampers are dissipated by yielding steel material and through the friction between two solid bodies sliding off next to each other (Kasai et al. 2007).

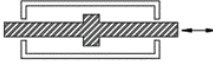
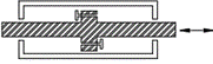
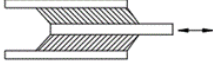
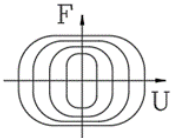
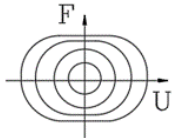
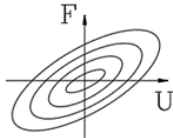
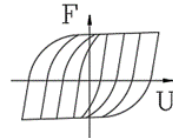
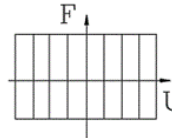
Viscous	Oil	Viscoelastic	Steel	Friction
				
shear/Flow Resist. Panel, Box, Cylinder	Flow Resist. Cylinder	Shear Resist. Brace, Panel, etc.	Axial/Shear Yielding Brace, Panel, etc.	Slip Resist. Brace, Panel
$F=C \cdot \dot{U}^a$	$F=C_1 \cdot \dot{U}$ or $C_2 \cdot \dot{U}$	$F=K(\omega) \cdot \dot{U} + C(\omega) \cdot \dot{U}$	$F=K \cdot f(u)$	$F=K \cdot f(u)$
				

Figure 2-15. Major types of damper technology (after Kasai et al., 2013)

With a comparison of structural control systems (i.e., passive, active, and semi-active), it was observed that semi-active control systems are a better option without passive and active limitations. Experimentally tested semi-active control systems include stiffness control devices, electrorheological dampers, magnetorheological dampers, friction control devices, fluid viscous dampers, and tuned liquid dampers. It was observed from the experimental testing that the semi-active control method can improve the seismic behaviour of structures. However, the large-scale semi-active control systems for seismic response reduction need more investigations. Similar results were obtained (Soong and Spencer 2002; Fisco and Adeli 2011; Yanik, and Aldemir 2019), these researchers study the active and semi-active control systems from 1997 to 2018. Moreover, Yanik and Aldemir (2019) did not find any study on the review of the new active and semi-active control approaches.

2.3.3.1 Seismic Isolators

Seismic isolators are used for decoupling the swimming movement of the structure from horizontal movement of the structure, and they are categorized as either sliding or elastomeric. Elastomeric isolators are including elastomeric bearing consist of natural rubber in the form of thin layers bonded to steel plates with a combination of viscoelastic and hysteresis behaviour; lead-bearing behaviour might be presented as a bilinear hysteretic model, which is constructed of low-

damping rubber with a central hole, in which the lead core deforms in pure shear. In the elastomeric isolator's design, it is important to reduce the height of a bearing when lateral deformation is increased (Kelly, 1993). Sliding isolators including sliding bearing, reduce the transmission force to a desired level of structure, although the peak displacement can be increased due to the absence of critical restoring force. To avoid this phenomenon, the solution would be a combination of a restoring force mechanism with sliding bearings. The sliding bearings idealized hysteresis curves with flat, spherical, and conical surfaces are presented in Figure 2-16.

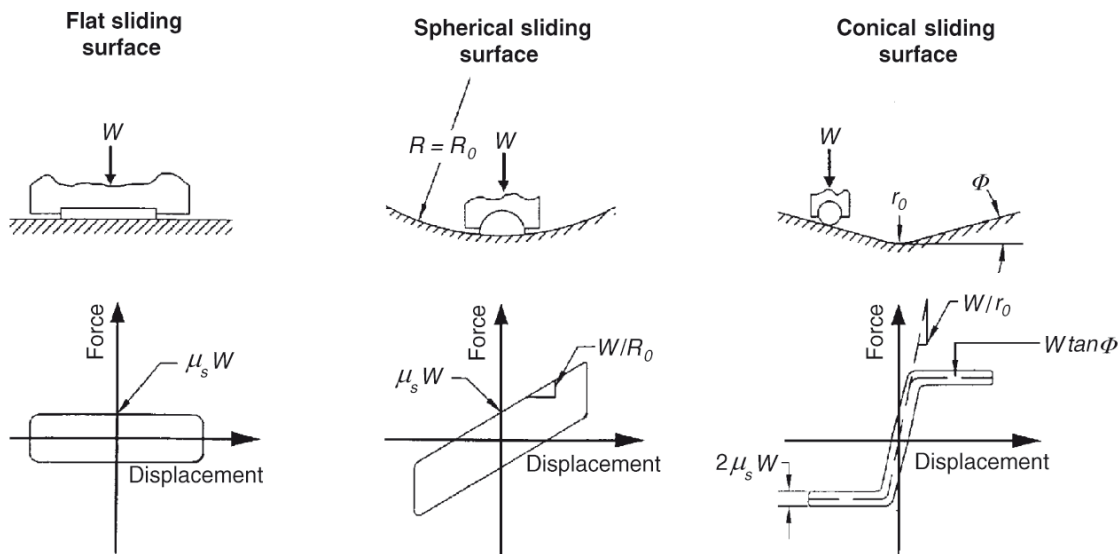


Figure 2-16. Idealized force-displacement curves (ASCE 41-13)

Su et al. 1989, simplified the mathematical models for several isolation systems namely as pure friction (P-F) with friction mechanism, laminated rubber bearing (LRB) with parallel dashpot and spring, resilient friction base isolator (R-FBI) with the parallel mechanism of friction, restoring spring and damping, Electricite de France (EDF) uses elastomeric and friction plate in series, New Zealand (NZ) with hysteretic spring-damper, and sliding resisting friction base isolator (SR-F) in which R-FBI is replaced by a friction plate as shown in Figure 2-17.

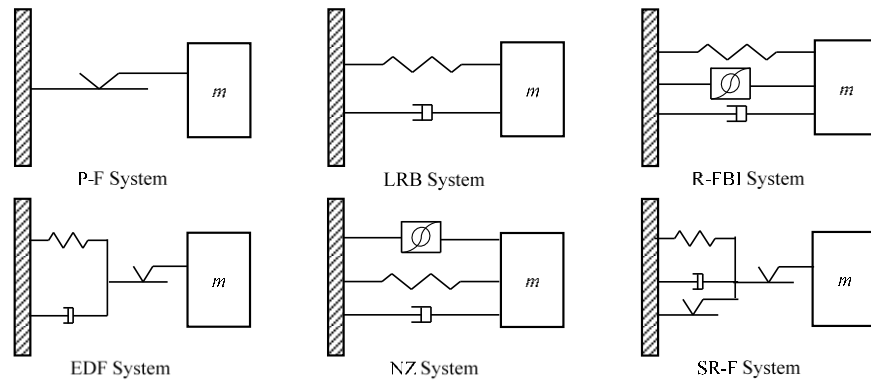


Figure 2-17. Schematic plots of designated base isolation systems (after Tehrani et.al. 2020, and Su et al. 1989)

2.3.3.2 Viscoelastic Dampers

Copolymers or glassy substances are the most common viscoelastic materials, which dissipate energy through shear deformation. Due to the structural movement, the relative motion between steel flanges and the center plate is simulated, which results in shear deformation and energy dissipation. A typical view of a viscoelastic damper is illustrated in Figure 2-18.

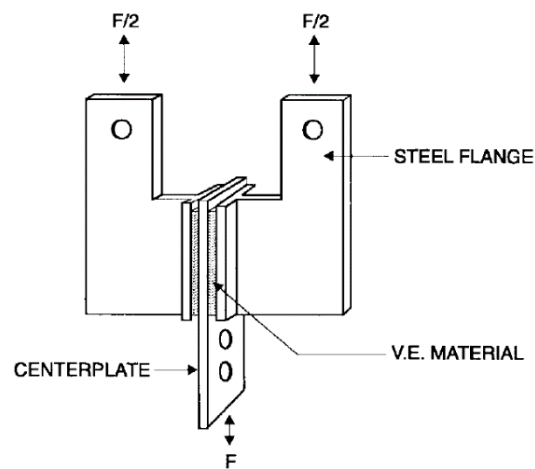


Figure 2-18. Schematic view of viscoelastic damper (Soong and Dargush 1999)

2.3.3.3 Viscous Fluid Dampers

The primary operating system of viscous fluid dampers is based on a high velocity of fluid that flows through orifices, and they have numerous applications in isolation, aerospace, and defense systems. A typical fluid damper is shown in Figure 2-19.

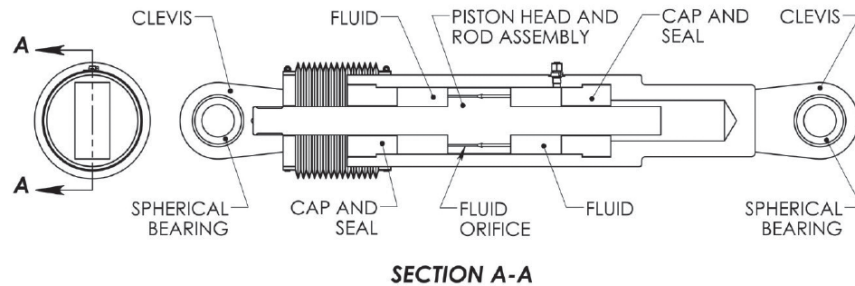


Figure 2-19. A typical fluid damper (Taylor devices inc., 2020)

The fluid damper presented in the figure above consists of two clevises for attachment to the structure, and a cylinder that is full of fluid. This fluid is forced to move through the orifices in the piston head, and to maintain the preservation of the fluid volume, one end of the piston rod moves into the cylinder and another one moves out. The clevis, the piston rod, and the piston head work as a component, while the other parts remain stationary.

2.3.3.4 Tuned Mass and Liquid Dampers

Tuned mass dampers consist of a single degree of freedom (mass-spring-damper) which is mounted on the top floor of a multi-story structure and the dynamic characteristics of the system are tuned to control the motion of the structure. Tuned liquid dampers are similar to tuned mass dampers except that the mass-spring-damper system is replaced by a container filled with fluid. A semi-active tuned liquid damper was proposed by Lou et al. (1994) and the behaviour of the semi-active damper the natural frequency of the sloshing fluid were controlled by the length of a hydraulic tank, and by adjusting the position of rotatable baffles in the tank respectively which demonstrated the effectiveness of different tank lengths for controlling the response of the mass.

2.3.3.5 Metallic yield dampers

The first concept of metallic yield dampers was discovered by (Kelly et al., 1972; Skinner et al., 1975). Metallic yield dampers dissipate energy through the inelastic deformation of metals. Added damping and stiffness (ADAS) elements are other sorts of MYD that improve the stiffness and strength as well the energy dissipation capacity of the system, a typical ASAS device is presented in Figure 2-20. New Zealand and Japan have experienced the first implementation of metallic devices, the seismic upgrade using ADAS energy dissipation was discussed by (Soong and Dargush, 1999; Tena-Colunga, 1997; Whittaker et al., 1999).

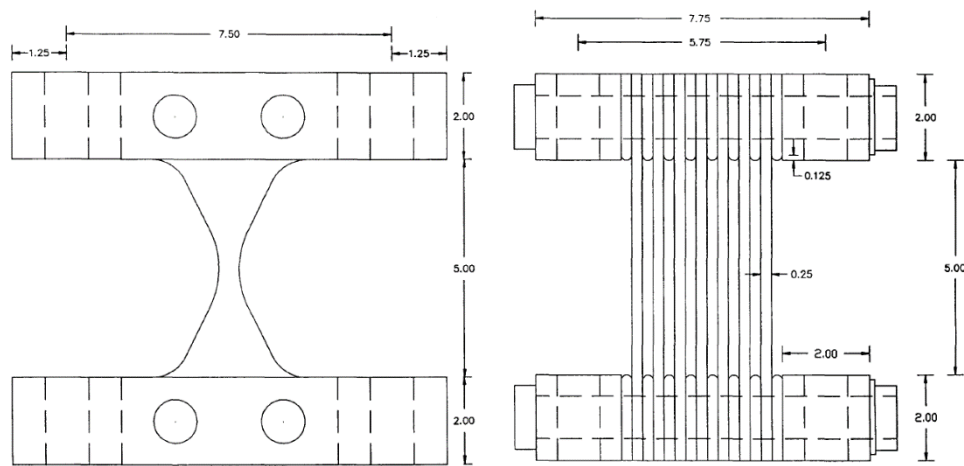


Figure 2-20. Added damping and stiffness (ADAS) element (Dimensions are in inches, Whittaker et. al. 1991)

2.3.3.6 Friction Dampers

Friction dampers dissipate energy through the friction between two sliding solid elements. For instance, solid friction can control tectonic movement and earthquake generation. Another example on a smaller scale is automotive brakes which dissipate the kinetic energy of motion. To extract kinetic energy from a moving body the friction brake is widely used pall et al. (1996). When a major earthquake occurs, the friction damper slip at a predetermined load before yielding occurs in members of a frame, which dissipates a major part of energy. It saves the initial cost of a new construction or retrofitting of existing buildings, with very high energy dissipation. The concept of a semi-active frictional damper as an adjustable frictional damper, using hydraulic

pressure to secure the clamping force was introduced (Samani, Mirtaheri, and Zandi 2015). Hysteresis behaviour of adjustable friction damper was studied using analytical and experimental methods. Dynamic and static loadings were used for the experimental test, the hysteric behaviour of adjustable frictional damper was examined statically using three hydraulic pressure (0.1 Hz) and dynamically using different frequencies (0.5 Hz, 0.7 Hz, 1 Hz). Slippage load, dissipated energy, effective stiffness as well as equivalent viscous damping were calculated and qualified based on the ASCE/SEI 41-06. Close agreement between numerical and analytical was reached for hysteretic force-displacement. Due to the limitation of the testing machine the hydraulic pressure was taken as 70 bars with a 20mm stroke. Large experimental tests and analytical evaluation are required to examine the real performance of the proposed devise as well as its costs compared to other types of friction dampers.

Several devices have been developed to dissipate energy through friction including Limited Slip Bolt Joint (Pall et al., 1980), Three-stage Friction Grip Elements (Roik et al., 1988), Friction-Damper in X-Bracing, Friction-Damper in Chevron-Bracing, and Friction-Damper in Single Diagonal (Pall et al., 1996), Sumitomo Friction Damper (Aiken and Kelly, 1990), Energy Dissipating Restraint (Nims et al., 1993), and Slotted Bolted Connection (Popov et al., 1995). The following literature provides a brief explanation of some friction devices.

2.3.3.6.1 Limited Slip Bolt Joint

In large panel structures, the damage is usually along the joints during an earthquake, therefore the joints are the only locations where dissipate energy and based on the concept of energy dissipation (Pall, 1979) maximized their capacity and developed a dissipated joint for seismic control of large panel structures which is shown in Figure 2-21.

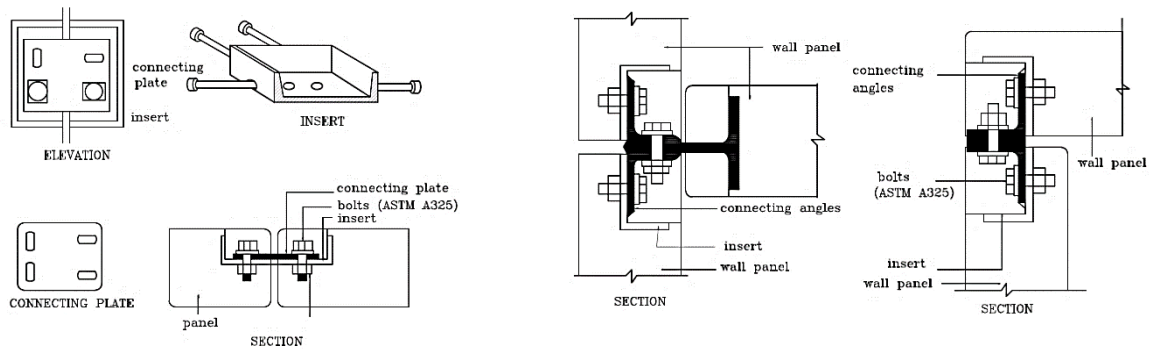


Figure 2-21. The LSB joint: Wall-to-wall joint (left) and Corner Wall-to-wall joint (right), (after Pall 1979)

In order to provide a consistent force-displacement response, the LSB design, the “brake lining pads” was incorporated between steel plates. To obtain basic design data and realistic structural response Pall conducted several experimental tests under static and dynamic cyclic tests on a variety of simple sliding elements having different surface treatments including mill scale, sandblasted, inorganic zinc-rich paint, metalized, brake lining pads, and a polyethylene coating. The resulting load-displacement response under monotonic loading is shown in Figure 2-22, while Figure 2-23 is the hysteresis behaviour under constant amplitude displacement-controlled cyclic loading. Although metalized surfaces showed the highest static slip coefficient and energy dissipation, their performance was far from predictable. The best behaviour was shown by brake lining pads located between steel plates with mill scale surfaces.

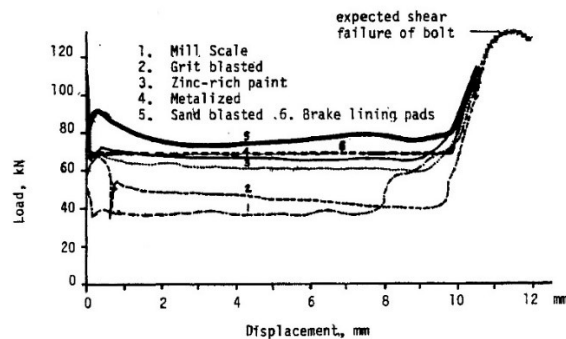


Figure 2-22. Load-displacement Response of Limited Slip Bolted Joints (Pall 1979)

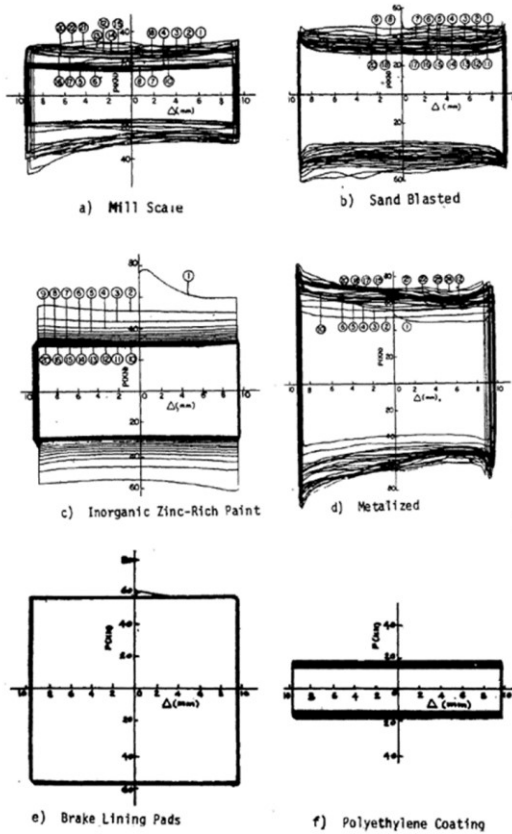


Figure 2-23. Hysteresis Loops of Limited Slip Bolted Joints (Pall 1979)

Based upon the behaviour obtained by Pall et al. (1979), the Idealized behaviour of LSB Joint is shown in Figure 2-24, stage one is the elastic phase, the slipping phase, is shown in stage 2 and simulated by a plateau, bearing phase is stage three and stage four is the failure which depends on the slot length due to shear force. Cyclic tests subjected to reversal load did not perform and SLB ideal “elasto-plastic” behaviour needs more investigation.

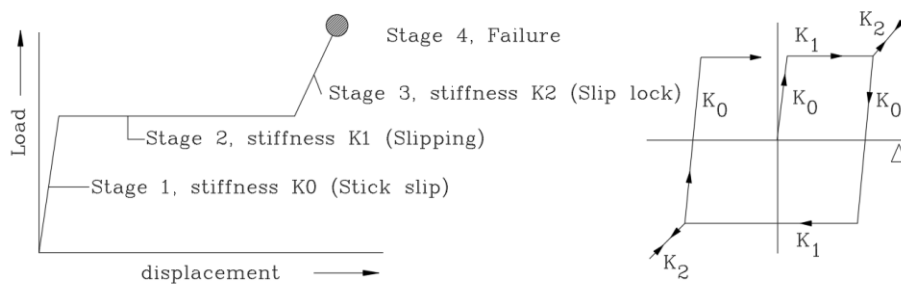


Figure 2-24. Idealized behaviour of LSB Joint (after Pall et al., 1979)

2.3.3.6.2 Three-stage Friction Grip Elements

Roik et al. (1988) discussed seismic control of structures under earthquake loading by three-stage friction-grip elements, the energy dissipation of each story can be designed according to serviceability, medium- and strong-motion earthquake based on the friction joints that was verified by Pall (1982). The idea was created from braking by friction, for instance, to avoid high forces by sudden braking the driver can push on the pedal softly.

Tests were performed on a single joint were investigated for simple concrete-steel-/steel-steel-friction-grip connections in order to show the mechanism of energy dissipation (SFB A51) as demonstrated in Figure 2-25 and Figure 2-26 which shows the behaviour of the hysteresis loops under repeated loading with the same amplitude and period. The durability of this type of connection under high short-term dynamic loading was very satisfactory.

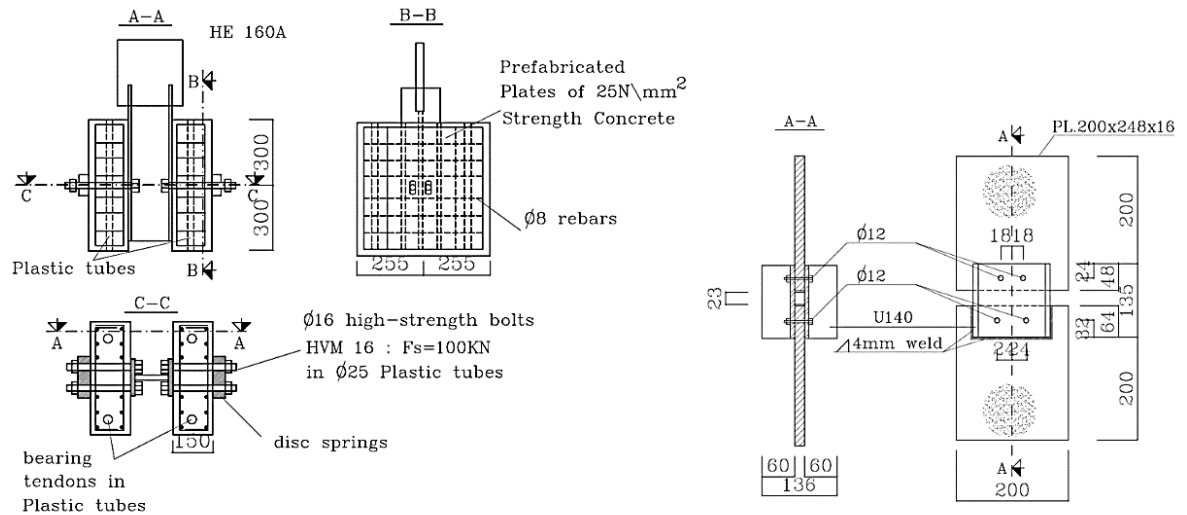


Figure 2-25. Test specimen on the left is concrete-steel- and on the right is steel-steel-friction-grip connections (after Roik et al.,1988)

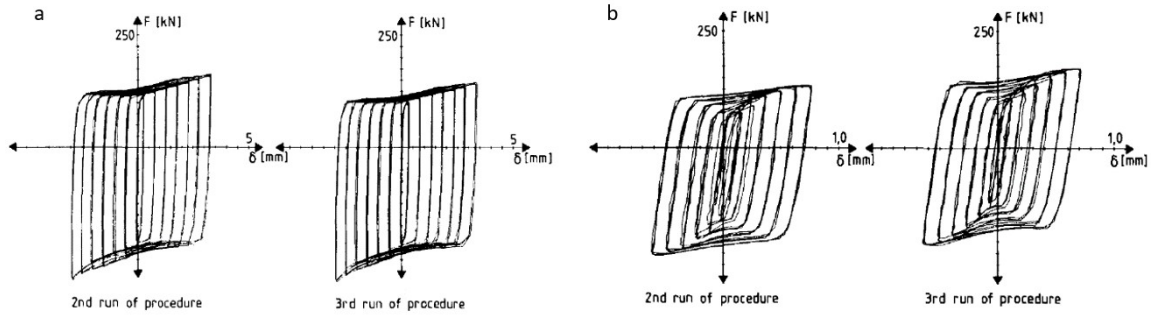


Figure 2-26. Hysteresis Loops of a) concrete- steel- and b) steel-steel-friction-grip connections (after Roik et al.,1988)

Using nonlinear spring elements with the bolts can control the loss of prestressing, therefore friction grip joints can resist high dynamic loading and their hysteresis depends on the prestressing of the bolts as demonstrated in Figure 2-27.

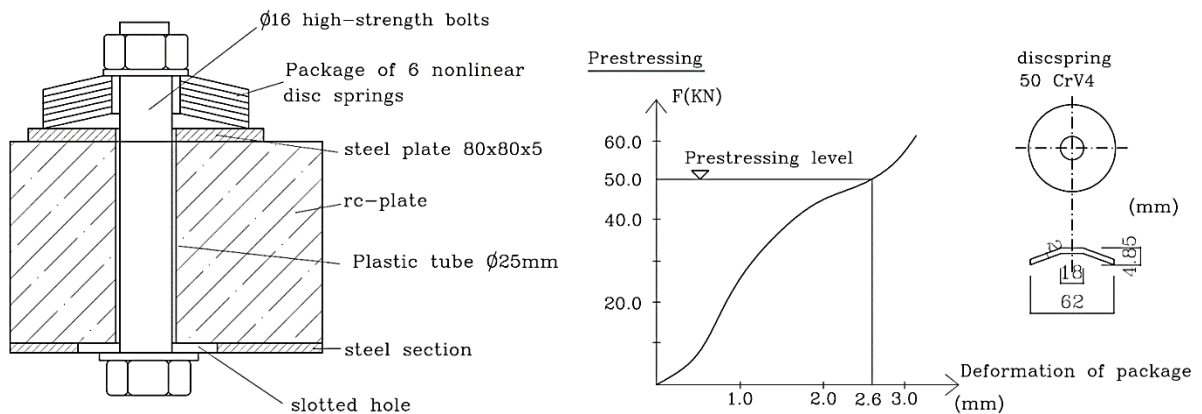


Figure 2-27. Detail of steel-concrete friction grip by nonlinear disc spring (after Roik et al.,1988)

They observed that coupling in parallel as shown in Figure 2-28(a), avoids vibration by transition phase from elastic behaviour to slipping stage. The component behaviour and the predicted performance of a three-Stage Stiffening Element as well as hysteresis loop were presented in Figure 2-28(b, c, d). Stage one is the serviceability limit state for linear structural behaviour and small displacement, stage two is the transition stage with no damage and larger displacement under medium earthquake to obtain the required smooth transition from stage 1 to

stage 3, stage 3 is the ultimate design limit state under the maximum strong motion with minor damage and large displacement.

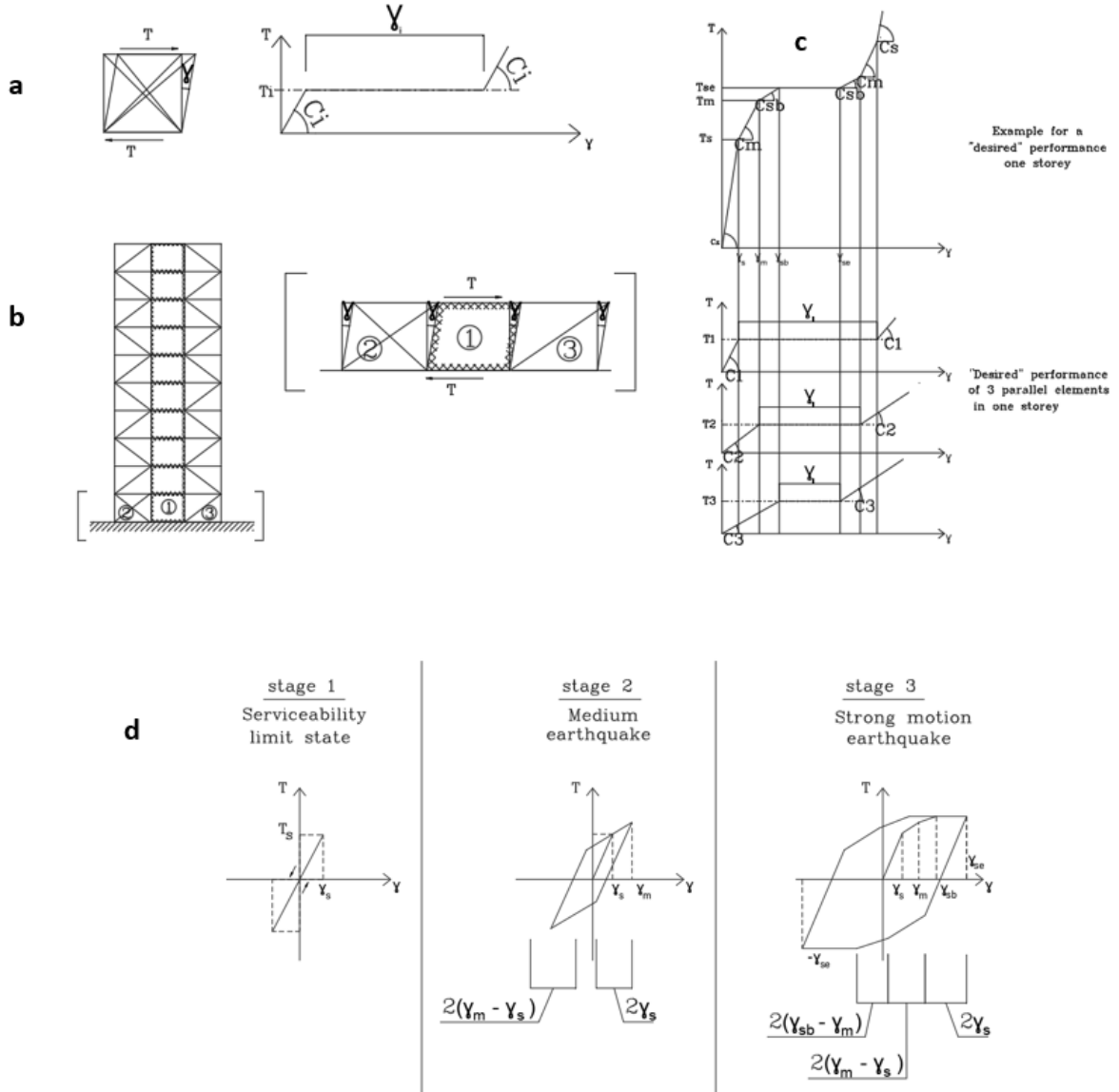


Figure 2-28. a) Principal behaviour of one stiffening element: C_i : stiffness; γ_i : frictional displacement; T_i : frictional force (level of friction), b) Three displacement coupled parallel stiffening elements, c) Three-Stage Stiffening Element, d) Hysteresis loops of a three-stage stiffening element (after Roik et al., 1988)

A seven-story building was chosen for the three-system investigation namely a ductile frame, three-stage truss, and stiff core which is shown in Figure 2-29. The truss system with three-stage elements was modeled by the girders hinged to columns. All three models were calculated by 5 percent damping and the P- Δ effect.

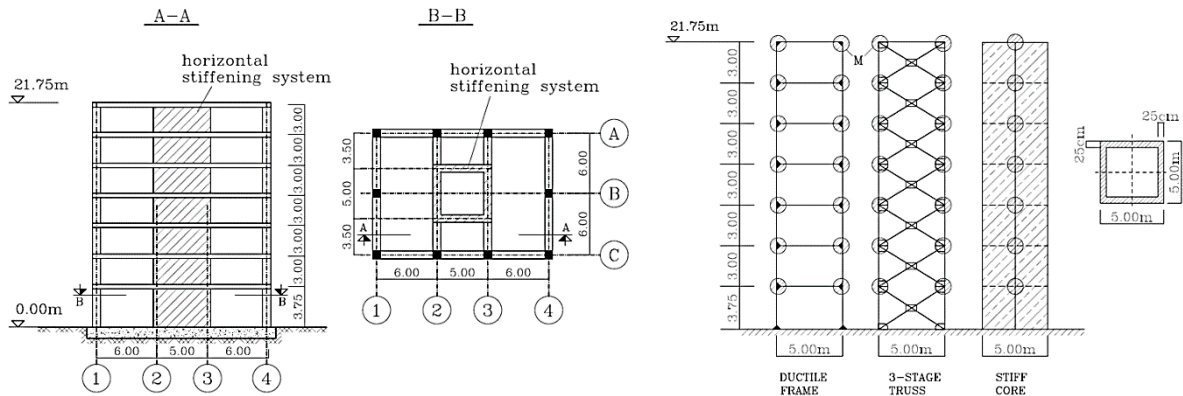


Figure 2-29. Seven story building and with three different versions (after Roik et al., 1988)

As demonstrated in Figure 2-30, the elastic concrete core had a small maximum displacement and the three-stage truss limited both the horizontal displacement and the story shear due to energy balance versus time. Since the internal forces of both the three-stage truss and the ductile frame are similar they showed the same energy balance with the frame having higher kinetic and viscous energy. The three-stage truss showed the highest percentage of energy dissipation which allows economical design.

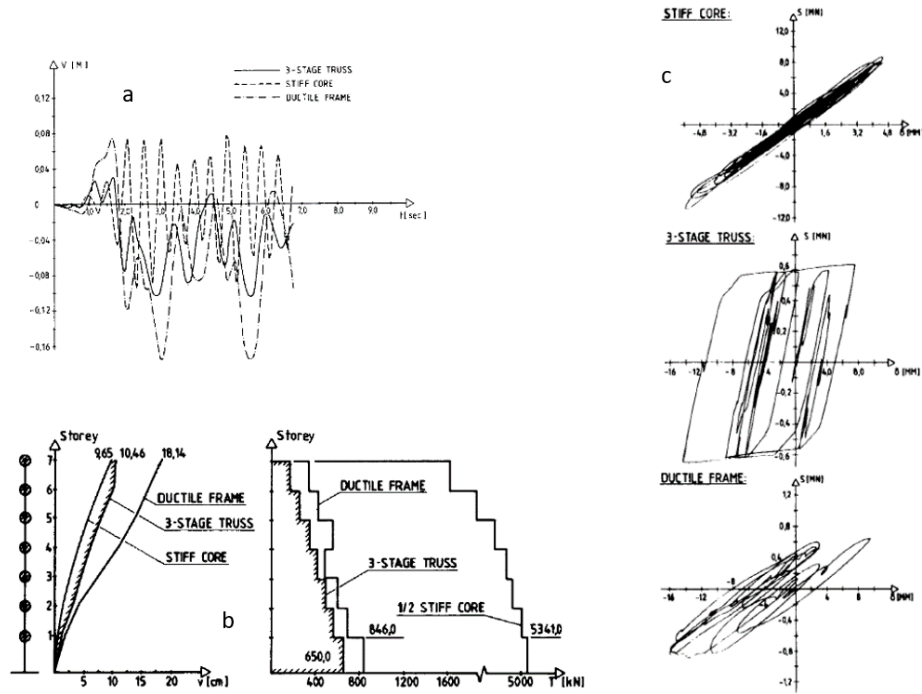


Figure 2-30. a) Roof displacement vs time, b) Maximum horizontal displacement and shear force, c) hysteresis loop for the first story of the three systems (after Roik et al., 1988)

An online earthquake was also simulated to verify the behaviour of a three-stage truss, the specimen was scaled down with the available testing facility as given in Figure 2-31.

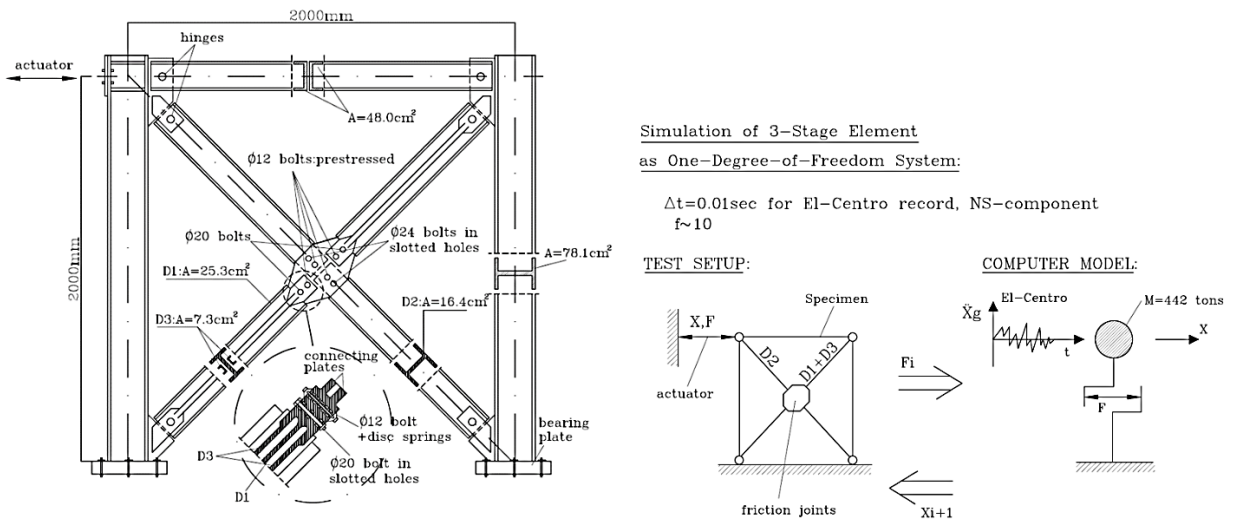


Figure 2-31. Specimen setup for a three-stage truss and the simulation of one degree of freedom (Roik et al., 1988)

The hysteresis loop tested under the N-S component of the Elcentro record revealed the smoothing effect of three-stage elements by a transition from sticking to sliding and the force overshoot was due to the bolt impact, as it was shown the proposed model was unable to capture additional force-displacement Figure 2-32.

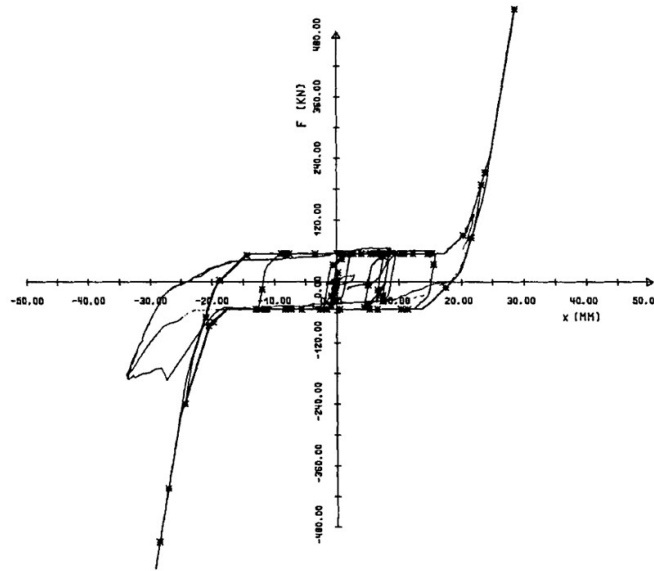


Figure 2-32. Computed measured and calculated (Star symbol) hysteresis response (Roik et al., 1988)

The mechanical properties of the bolts and the limited geometrical of slotted holes play an important role in lateral stiffness, slip force, and the amount of dissipated energy per cycle. It was concluded that friction grip connections can reduce horizontal forces and displacements by their energy dissipation capacity. The experimental test was limited to one story and the effect of the whole structure was not considered, moreover three-stage elements using steel concrete friction grip required further study.

2.3.3.6.3 Slotted Bolted connection (SBC)

Slotted bolted connections dissipate energy by moving two surfaces against one another and through friction mechanism as presented in Figure 2-33. Different slotted bolted connections, as well as their performance in the structure, were examined separately and in a system (Popov et al., 1995). Two different SBCs with steel-steel and steel-brass surfaces were examined individually and subjected to sinusoidal and artificial earthquake displacements.

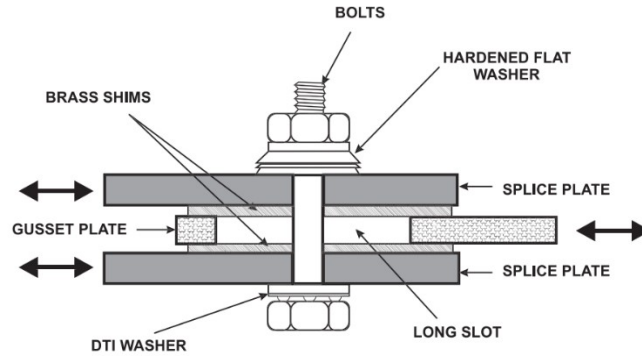


Figure 2-33. Schematic view of slotted bolt connections (after Nikoukalam et al. 2017 and Popov et al. 1995)

Although SBCs with steel-steel showed unacceptable behaviour, this behaviour was modified by brass shim plates. Effects of various A325 bolts were examined for SBCs with steel-brass. Figure 2-34 presents the hysteresis loop of SBCs with steel-steel with one A325 bolt and diameter of ½ inch on the left with higher static slip force which may cause an extra shock, however, when SBCs examined with steel-brass and two A325 bolts on the right the slip force had a plateau with lower static slip force with smaller differences between kinetic and static forces compare with steel-steel SBCs.

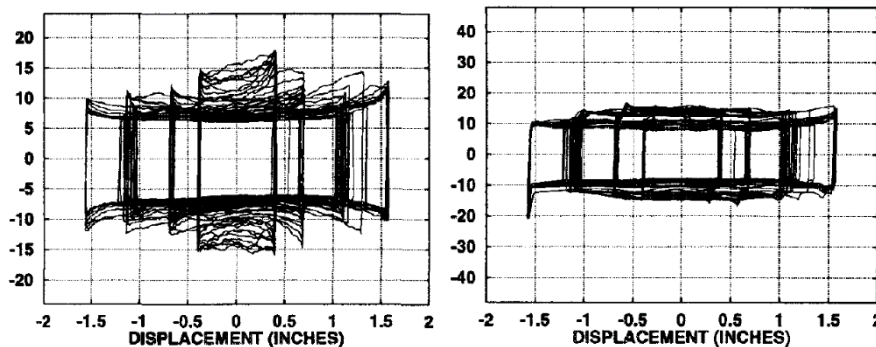


Figure 2-34. SBCs with steel-steel on the right and using brass shims on the left (after Popov et al. 1995)

They found out the use of shims with mill scaled steel surfaces and high strength bolts, resulted in stable behaviour of slip forces. Although the brass shims were insensitive to washers, they were useful in reducing the loss of bolt in tension. The results of SBCs on the chevron braces of the three-story structures on a shake table showed the effectiveness of SBCs in controlling damage as

well as story drifts. This study was limited to SBCs with brass shims as a frictional treatment, more investigations are required for different surface treatments such as shims materials. Galvanic corrosion and the effects of different coating as well as large-scale SBCs to simulate industrial structures and the extra slip force in chevron bracings causes vertical forces at intersections of beams to braces need more investigations. More experimental and analytical works and developing a design method for using SBCs in a practical sector such as nonlinear dynamic analysis as well as non-intensive methods, and considering possible torsional forces caused by braces with not in line SBCs within the stiffness of structure in a specified floor need more studies.

The behaviour of slotted bolted connections under dynamic loads was performed by (Law et al., 2006), the shear deformation was proposed by an analytical model. SBC can be used to shift the natural frequency of a structure by changing initial stiffness and slippage load. Slotted bolted connections with modified bolts have been in the 1980s in the bracing systems. Then rotational slotted bolted connections (RSBCs) were developed by Yang and Popov in 1995 in order to integrate them into the moment-resisting frame system. The behaviour of RSBCs is limited to flexural behaviour, however, in some cases, shear is dominated by flexural behaviour such as eccentrically braced frames (EBFs). Therefore, Nikoukalam et al. 2017, developed Shear slotted bolted connections (SSBC), which dissipate energy through the friction activated by shear force as is presented in Figure 2-35.

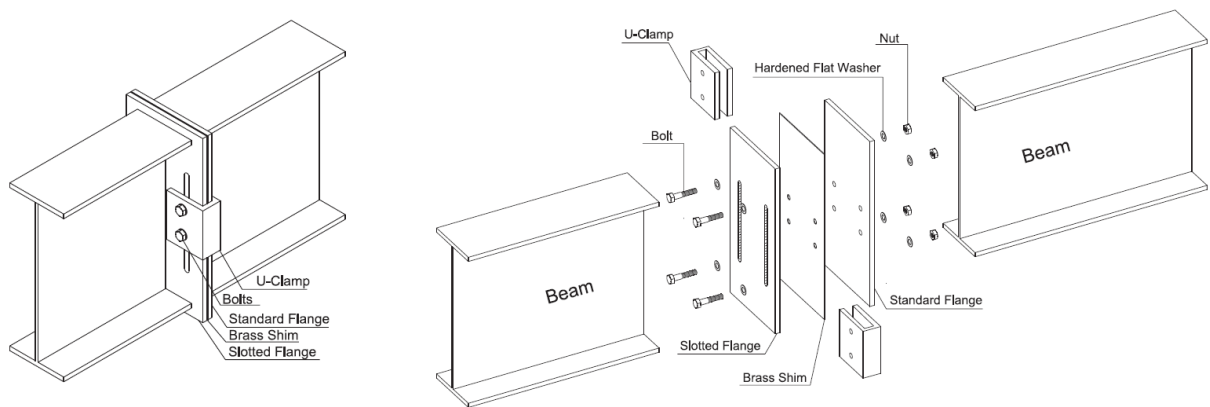


Figure 2-35. Installation of SSBC (Nikoukalam et al., 2017)

The applications of SSBC in eccentricity brace frame, moment-resisting frame, and coupled concrete shear walls are presented in Figure 2-36.

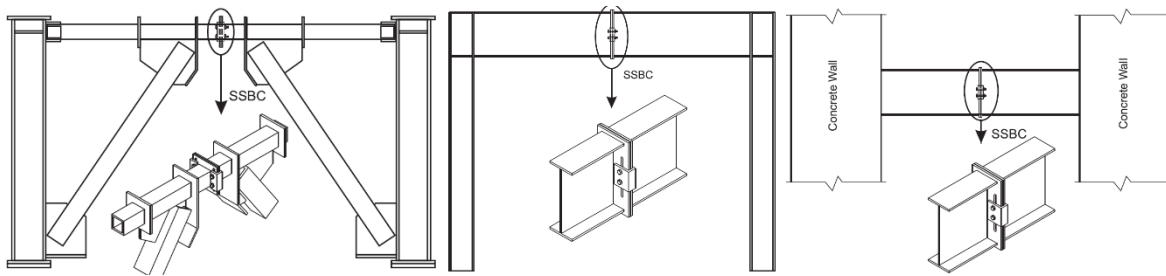


Figure 2-36. SSBC applications in EBF, MRF, and CCSW (Nikoukalam et al., 2017)

The effectiveness of SSBC was examined in an existing eccentricity braced frame using finite element software, and the results were compared with a conventional EBF, additionally, its effect on a one-story moment resisting frame with three different span lengths was studied. It was observed SSBC can improve the energy dissipation capacity of EBF compared to the traditional one. SSBC can be acted as a mechanical shear fuse in MRFs, and its capacity to dissipate energy was better in lower span length. Large scale and component tests and their comparison with simulated work required further studies. Additionally, its effectiveness in different applications, as well as SSBCs' residual displacements, required further investigations.

2.3.3.6.4 Pall Friction Dampers

Based on the development of LSB, Pall and Marsh (1982) proposed a system with a combination of friction dampers in a moment-resisting frame, during severe earthquake excitations, a large portion of the energy is dissipated by the friction when the device slips. Pall friction dampers can be grouped as (Pall et al., 1996): Friction-Damper in X-Bracing, Friction-Damper in Chevron-Bracing, and Friction-Damper in Single Diagonal as shown in Figure 2-37.

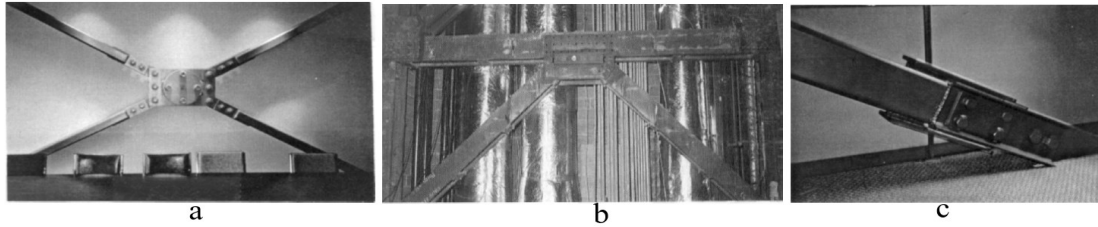


Figure 2-37. a) Friction damper in X-Bracing, b) Friction damper in Chevron-Bracing, and c) Friction damper in Single Diagonal (Pall et al., 1996)

Pall Friction Dampers hysteresis loops are similar to an ideal elasto-plastic behaviour having a wide rectangular shape, and their performance is independent of velocity. The forces on the individual members can be adjusted based on their capacity by an appropriate slip load. The Pall Friction Dampers in line and cross bracing were used to upgrade the Boeing commercial airplane factory, reduced the lateral deflection, the exerted force, and the strengthening of existing members (Vail et al. 2003). Chevron brace with two friction dampers was used in Sharp Memorial Hospital. The results of the nonlinear analysis showed an economical performance-based design (Soli et al. 2004).

Colajanni et al.(1997) examined the hysteresis characteristic of one-story friction damped brace frames in order to evaluate the role of the period of vibration, the lateral stiffness ratio, and the global slip load calibration of the dissipative device. It was observed that the frequency of the slip excursions depends on the period of the system vibration and the average amplitude of the normalized slip excursions is independent of the period and increases by lateral stiffness ratio. The optimization of the response of friction-damped multistory frames can be further studied on the distribution of the global slip load of the devices along with the structure's height.

Friction dampers have been utilized as a practical and cost-effective energy dissipation mechanism in many constructed structures. Chang et al. (2006) examined the application of friction dampers for seismic retrofit of a 3-story steel structure which didn't satisfy the current building code seismic requirement. Since the third floor was used by the court, 48 friction dampers were used at the ground and second levels. The FEMA 351,356 were used in the analysis, the 3-D

model was used by ETABS, the story shear and displacement were reduced by friction dampers as demonstrated in Figure 2-38.

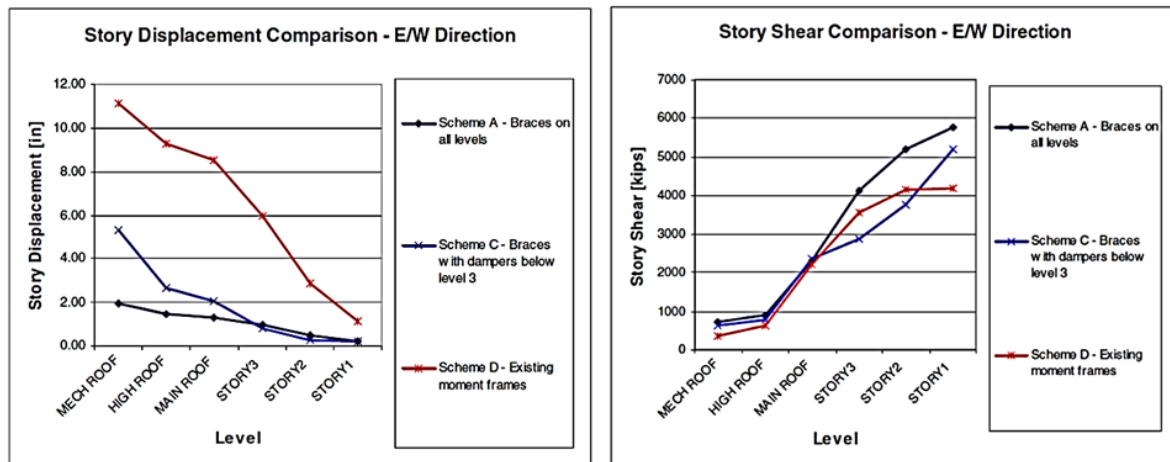


Figure 2-38. Story Displacement and Shear comparison, (Chang et al., 2006)

It was observed that the friction dampers significantly improve the structural performance and with this reduction in story displacement and shear, the seismic force was reduced above the 3rd floor.

A performance-based plastic design for a 21-story steel moment-resisting frame with friction dampers was examined by Patil et al. (2015). In order to achieve a uniform target drift compatible with peak inter-story drift limits, nonlinear static pushover analysis, and nonlinear response history analysis were performed. It was observed using friction dampers can specify a certain inelastic displacement for a given earthquake, moreover, there was a reduction of almost 85% in the peak inter-story ratio and the flexural moment at columns.

The use of friction dampers in the seismic design of unbounded post-tensioned precast concrete frame structures was investigated by Morgan et al. (2007). In order to determine the friction damper slip forces and post-tensioning steel areas and selected damper distribution, a nonlinear reversed cyclic analysis under lateral load was conducted. It was shown that friction-damped precast concrete frames can dissipate energy levels while maintaining a large level of self-centering capability due to the post-tensioning force.

A tall cylindrical tower which is used in industrial processes is called a process column, during its seismic assessment, it was found that anchor bolts were not meeting the code requirement. Therefore, a retrofitting scheme using passive control devices was used (Kiran et. al., 2016). Various passive control devices are including viscoelastic damper, elasto-plastic damper, tuned mass damper, tuned liquid damper, and friction which can be easily replaced after an earthquake. Since viscoelastic dampers are affected by temperature and stiffness degradation and also the limitation of tuned dampers is required the tuning the natural frequency, double sliding friction dampers were used as they don't possess many of these limitations. Figure 2-39 showed the one end of the damper is fixed rigidly through the bracket and another end is connected to the hydraulic actuator.



Figure 2-39. Friction dampers on the left and its test setup used for characterization (Kiran et. al., 2016)

The cyclic load was repeated for ten cycles by considering various torque values, a stable hysteretic behaviour was obtained, and the variation of slip load was linear with respect to the applied torque. After retrofitting the seismic demand was reduced to 15% of the capacity of existing foundation bolts and was qualified for MCE condition.

The damping mechanisms combination of a non-linear Reid damper and a viscous damper showed that the PFD can significantly reduce the response of the structure, Chen et al. (2001). Numerical simulations also showed that the friction dampers driven by the proposed control logic can substantially reduce the peak acceleration and story drift of the building structure under earthquake excitations. The same results were obtained by Haider et al. (2012), the effects of friction dampers were studied subjected to several seismic excitations and it was revealed that the

effectiveness of friction dampers at dissipating the largest amount of energy. A semi-active electromagnetic friction damper and was proposed by Agrawal et al. (2004) and the proposed damper and the control method were investigated for a base-isolated building which showed that the SAEMFD was effective in protecting rubber-bearings of the base-isolated buildings under the strong ground motions. The small scale of one and two-story steel models with a pair of parallel friction devices at each floor was performed on a unidirectional shaking table subjected to artificial and real ground motions as well as the sine-dwells (López-Almansa et al., 2012). There was a good agreement in the experimental and numerical works, reduction in resonance, and response peaks of the structure were observed. The behaviour of steel frames equipped with concentric steel bracing with improved pall friction dampers compared with concentric steel bracing frames with no dampers (Sarjou and Shabakhty, 2017). The study parameters were displacement, capacity percentage to observe energy, and base shear. Two different methods can be used for modeling pall friction dampers including simple which was suggested by pall and used in this study as well as an accurate method. The simple bracing system is considered a damper that yields in pressure and tension with a full elasto-plastic material and rectangular hysteresis curve as the simple method. In this method bracing yields in slip load which is the same as damper slip load. In the accurate method, the stress-strain curve of linear elements is used to define the bracing and damper link. Improved pall friction dampers are similar to pall friction dampers with a central core of the T-shape. It was observed IPFD reduced the base shear and relative displacements, however, the changes in dissipated energy by a damper dependent on the location and the load, and in the absence of dampers, frames experience damages. This study is limited to the simple method, more accurate methods are required to model the friction dampers as well as their verification in experimental tests for practical use. Further study is required to consider the effects of various bracing configurations in structural frames with different heights and the appropriate number of ground motions.

A combination of moment-resisting frames with friction-based frames was used initially to reduce the structural damage since friction brace frames have very limited lateral stiffness when the connection slides, this may result in excessive story drifts and residual displacement, this

behaviour can be lessened by providing secondary lateral resistance (Tirca et al., 2018). Therefore, the application of FBF in 4- and 10-story as secondary steel moment-resisting frames for extra stiffness and recentering capacity were conducted using nonlinear response history analysis. A conventional force-based method was used to design the frame as well as pall friction devices. In addition, harmonic loading signals and real-time seismic displacement histories were used for full-scale testing on brace sub-assemblages and braces equipped with friction dampers. Nonlinear response history analysis confirmed the extra story drift and residual displacement were dissipated by MRFs. The experimental test verified the performance of pall friction dampers with stable slip resistance under displacement demand from analytical simulation. This study was limited to two different steel frames, more parametric studies are required to examine the effectiveness of the proposed method as well as 3-D experimental tests to examine the real capacity of dissipated energy by MRFs as a secondary dissipation system incorporated with pall friction devices.

2.4 Common types of friction dampers

Friction dampers are among the hysteretic systems in which the energy is dissipated within a mechanism that does not depend on the rate of load application (Constantinou et al., 1998). Pall friction dampers consist of treated plates in a series that develop resistance when sliding against one another. Staggered pall friction dampers were proposed by (Tirca, 2009) to optimize the seismic performance of an existing steel moment frame. Staggered pall friction dampers can improve structural performance even for ductile structures. The yielding restrained brace (YRB) and rotational friction damper are among the most popular passive energy dissipation devices currently employed for practical approaches.

2.4.1 Yielding restrained brace (YRB)

A yielding restrained brace is also known as a friction-damped brace. When the axial forces increase the slip load, the energy will be dissipated by an inline tension and compression seismic friction damper. In this yielding mechanism, the force is constant, therefore stiffness and yielding are differentiated. The idea is to equip the structure with a consistent stiffness brace that does not

enter in a ductile mode. YRB consists of a brace attached in-line with a Ten-Co as shown in Figure 2-40 (Galindo et al. 2019, Quaketek Inc.). As it can be seen the hysteretic curve has a rectangular shape, when a force activates an inline tension-compression seismic brake, under dynamic load, tension or compression has the same behaviour.

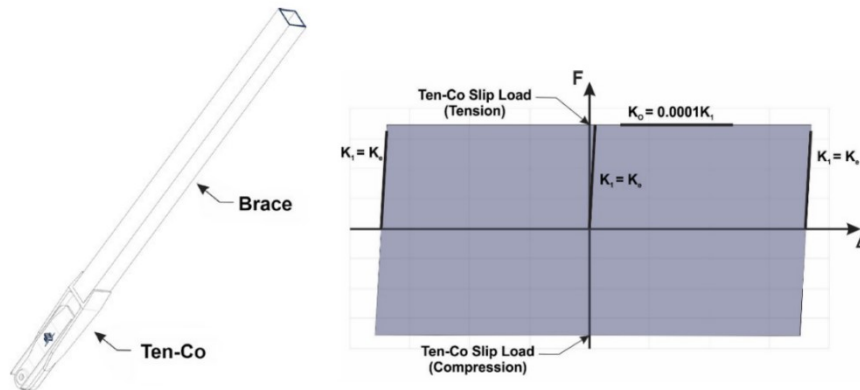


Figure 2-40. A schematic view of yielding restrained brace (YRB) and its force-displacement relationship (Galindo et al. 2019, Quaketek Inc.)

2.4.2 Rotational Friction Damper (FRD)

A rotational friction damper dissipates energy utilizing friction produced by rotating joints' friction and constant torque, they can be in the form of a single or x bracing system. A single friction damper was developed by Mualla and Belev in 2002 and presented in Figure 2-41, when the damper is subjected to a lateral force, it dissipates energy by the frictional forces developed between the steel plates and friction pads.

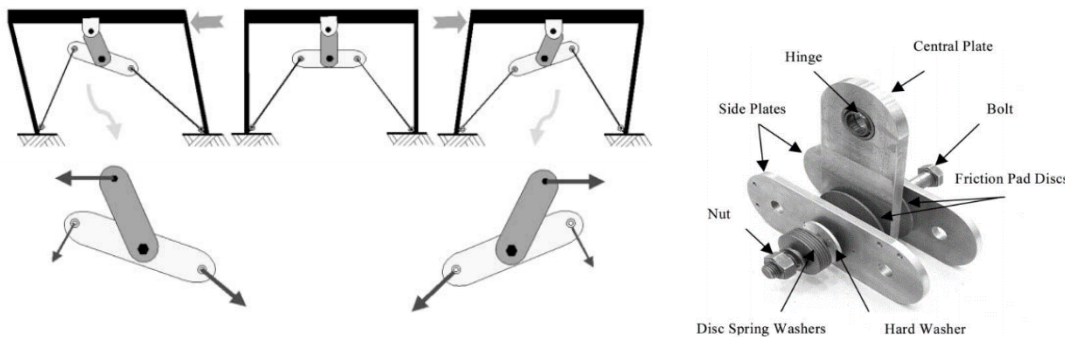


Figure 2-41. Component and typical action of RFD (Mualla and Belev, 2002)

2.5 Modeling of yielding restrained braces

As previously discussed, there are three major stages of energy dissipation through the friction of two surface pall (1979) namely as stage 1 is in the elastic zone or stick-slip and before yielding, stage 2 is when the slipping occurs, and stage 3 is bearing or slip-lock.

2.5.1 Attached Damping

A simple example of attached damping (Coulomb friction) is a block moving on a rough surface in the horizontal direction is presented in Figure 2-42, therefore the created frictional force is proportional to normal force in Equation 2.2.

$$F_{friction} = \mu_k N \quad (2.2)$$

Where μ_k is the dynamic friction coefficient or kinetic energy and N is the normal force.

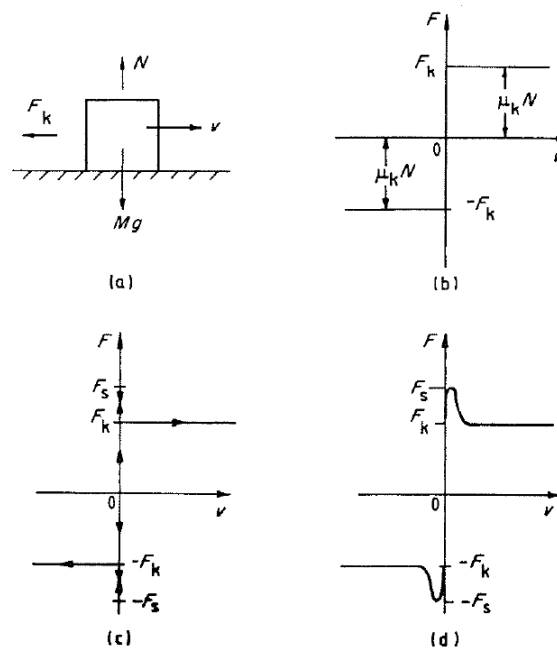


Figure 2-42. Friction characteristics a) free body diagram, b) idealized dynamic friction, C) static friction, d) actual friction (Roberts and Spanos 1990)

Idealized dynamic friction presented in Figure 2-42b frictional force is plotted versus velocity, in which $F_{friction}$ and μ_k remain constant during sliding, this model is named as Coulomb friction.

If static frictional force, F_{static} is greater than kinetic frictional force $F_{friction}$ or F_k , the static force is proportional to normal force in equation 2.3.

$$F_{static} = \mu_s N \quad (2.3)$$

In this equation, μ_s is the static friction coefficient, Figure 2-42c shows two discontinuities, from zero to F_s before the motion and from F_s to F_k after the motion. A more realistic of this transition is presented in Figure 2-42d, however, this demonstrated a sharp peak starting from zero velocity, and slightly beyond critical velocity (Roberts and Spanos 1990). Frictional damping devices subjected to cyclic loading dissipate energy in the form of a non-elliptical hysteretic loop, this can be presented by a single degree of freedom in a simple form of mass, spring, and friction as an ideal Coulomb damper presented in Figure 2-43.

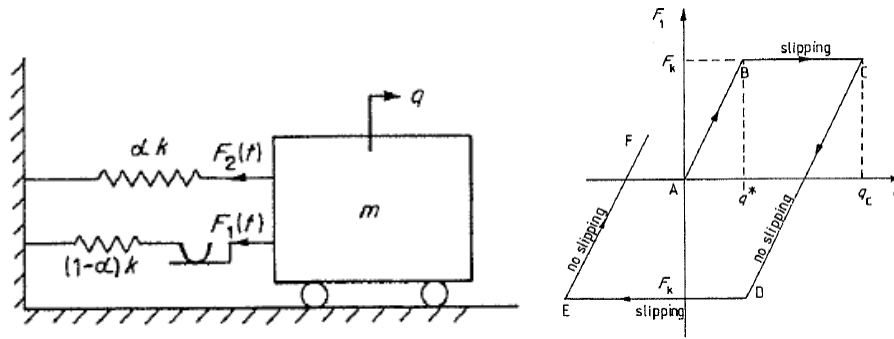


Figure 2-43. Mass-spring Coulomb damping and hysteresis loop (Roberts and Spanos 1990)

If the mass has a displacement of q , and F_t is lower than the Coulomb friction force, F_k , there is no slipping in the system and the characteristics of F_1 - q is shown with the straight line of AB and the slope of $(1-\alpha)k$, when F_t is equal to F_k and displacement passes the critical displacement of q^* then the slipping occurs and the characteristics of the loop is the straight line of BC. When the mass moves in the reverse direction then F_t is lower than F_k , therefore slipping in the system stops and the force decreased along the line CD with the slope of $(1-\alpha)k$. At point D the displacement is $q_c - 2q^*$, and compressive force is equal to F_k , therefore it slips along the line DE. At E the mass moves in the opposite direction therefore the force follows the line EF, and it continues.

Lukkunaprasit et al. 2004, investigated the behaviour of slotted-bolted connections when the slip exceeded the accessible slip length. To avoid severe damage which considerably deteriorates the friction force of the damper, the restraining approach addressed by Roik et al. in 1988 was modified and presented in Figure 2-44. The restrained system will be excited when the activation slip force is greater than the slip distance, therefore the hysteresis loop consists of four major parameters including F_s is the predetermined slip force, Δ_g is the slip distance, F_{max} is the maximum restraining force below the buckling capacity of the brace, and K_r is the restraining stiffness and equal to an axial stiffness of the inline brace.

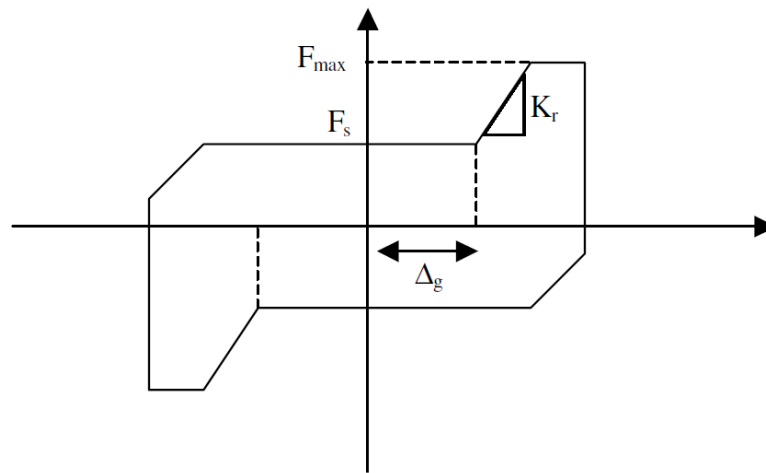


Figure 2-44. Proposed Hysteresis curve with restrains (Lukkunaprasit et al., 2004)

Lukkunaprasit et al. 2004 found that higher base shear is caused by restraining force which has a direct effect on the capacity of foundations. Their investigation was limited to displacement dependent; more parameters are required to study the connections with friction-grip. Moreover, the sliding mechanism is subjected to different parameters including types of loading, friction coefficient, temperature, velocity as well as the contact treatment, material, pressure, and size (Pall 1979; Constantinou et al. 1990; Sextro 2007). Makkar et al. 2005 proposed a new friction model to avoid discontinuity between stick-slip and slip phases based on velocity, this friction model is presented in equation 2.4 and its characteristics are presented in Figure 2-45.

$$F_{\dot{x}} = \gamma_1(\tanh(\gamma_2\dot{x}) - \tanh(\gamma_3\dot{x})) + \gamma_4\tanh(\gamma_5\dot{x}) + \gamma_6\dot{x} \quad (2.4)$$

Where γ is positive slope constants, the first part (I) of the equation captures the stribek effect, the second part (II) describes the Coulomb friction, and the last part (III) is the viscous dissipation condition.

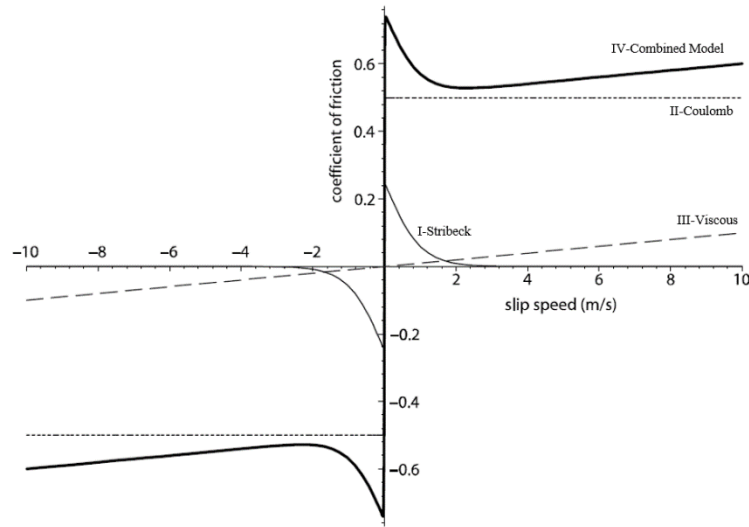


Figure 2-45. Different effect of friction model (Makkar et al., 2005)

2.5.2 BOUC-WEN MODEL

For a smooth hysteresis system under different excitation an equivalent linearization was proposed (Wen, 1980). Various classes of Bouc-Wen models regarding their bounded input/output stability properties as well as physical properties related to true data were investigated by (Ikhouane et al., 2007). Ismail et al. 2009, presented a background of the Bouc-Wen model for hysteresis modeling of nonlinear structures subjected to dynamic loads.

Baber and Noori 1985 and 1986, proposed and added a general degradation model to smooth the hysteresis model of Bouc and Barber and Wen 1981, to capture the pinching effect. A nonlinear single degree of freedom and slip lock hysteresis curve are presented in Figure 2-46.

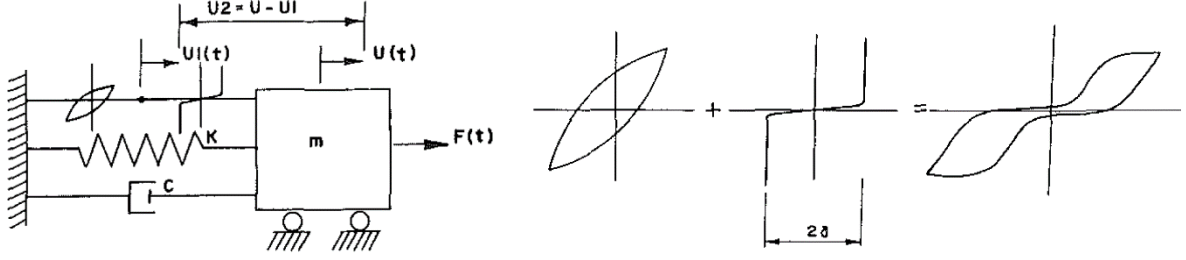


Figure 2-46. Proposed single degree of freedom and slip lock hysteresis loop (Baber and Noori, 1985)

This nonlinear system is presented with the differential equation of motion with equation 2.5.

$$\ddot{x} + 2\zeta\omega_0\dot{x} + \frac{\alpha k_0}{m}x + \frac{(1-\alpha)k_0}{m}z = \frac{1}{m}F(t) \quad (2.5)$$

In which α is the post-/pre-yield stiffness, and z is the hysteresis restoring force which represents the nonlinear hysteresis loop. The modified smooth system is shown with equation 2.6.

$$\dot{z} = \frac{\dot{x}}{\eta} h(z)(A - v(\beta|z|^{n-1}z + \gamma|z|^n)) \quad (2.6)$$

In this equation $h(z)$ is associated with pinching effects, A is the tangent stiffness, β , and n are the shape factors, η , and v represent the strength, and stiffness in the system. These variables can be determined from equations 2.7 to 2.9.

$$A = A_0 - \delta_A \varepsilon(t) \quad (2.7)$$

$$v = 1 - \delta_v \varepsilon(t) \quad (2.8)$$

$$\eta = 1 - \delta_\eta \varepsilon(t) \quad (2.9)$$

Where $\varepsilon(t)$ is the dissipation of energy from equation 2.10, the pinching effect in Figure 2-46 is added by an element with time-dependent slip lock with equation 2.11.

$$\dot{\varepsilon} = \frac{(1-\alpha)k_0}{m} \dot{u}z \quad (2.10)$$

$$\dot{u} = f(z)\dot{z} \quad (2.11)$$

$h(z)$ is equal to one when there is no pinching effect, the other parameters can be defined accordingly, however, if the pinching effect is considered, it can be calculated from equation 2.12.

$$h(z) = 1 - \zeta_1 e^{\left(\frac{-z^2}{\zeta_2^2}\right)} \quad (2.12)$$

In this equation, ζ_1 and ζ_2 control the magnitude and the slope changes and can be determined from equations 2.13 to 2.14 (Foliente 1993).

$$\zeta_1(\epsilon) = \zeta_{ts}(1 - e^{(-pE)}) \quad (2.13)$$

$$\zeta_2(\epsilon) = (\psi_0 + \delta_\psi \epsilon)(\lambda + \zeta_1) \quad (2.14)$$

Where ψ_0 , is the control the amount of pinching, δ_ψ , is the defined change if the slope, p , is the constant value of the drop in initial slope ζ_{ts} , is the total slip, and, λ , is to control the changes in the magnitude and the slope.

A sample of the Bouc-Wen hysteresis loop is presented in Figure 2-47, to construct the model the following parameters shall be defined: initial curve stiffness and hardening ratio, η , the transition from linear to nonlinear, γ and β define the basic hysteresis shape, and A , is the hysteresis amplitude (Seismosoft Ltd, 2020).

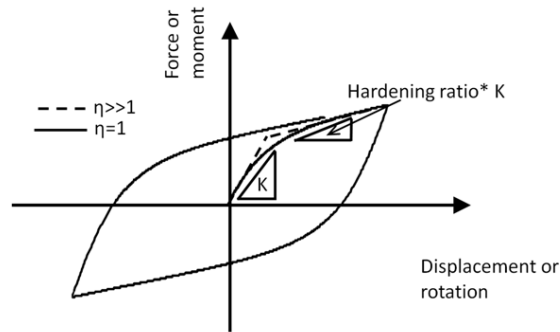


Figure 2-47. Bouc-Wen Curve (Seismosoft Ltd, 2020)

2.6 Literature Summary

In this chapter, performance-based design methods, as well as common FRP-strengthening applications, are explained briefly, different seismic control systems including active, semi-active, and passive as well their different types and some of the previous works of energy dissipaters and their performance are discussed. A comparison of structural control systems showed that semi-active control systems provide a better option without the limitations of the passive and active systems. Experimentally tested semi-active control systems include stiffness control devices, electrorheological dampers, magnetorheological dampers, friction control devices, fluid viscous dampers, and tuned liquid dampers were explained, and it was observed from the experimental testing that the semi-active control method can improve the seismic behaviour of structures.

Different types of devices that dissipate energy through friction are presented. The Idealized behaviour of LSB Joint which was presented by Pall et al. (1979), was further investigated by Roik et al. (1988) for three-stage friction grip elements. It was shown the mechanical properties of the bolts and the limited geometrical of slotted holes play an important role in lateral stiffness, slip force, and the amount of dissipated energy per cycle. Moreover, friction grip connections can reduce horizontal forces and displacements by their energy dissipation capacity, however, the proposed model was not able to capture additional force-displacement.

Modeling of yielding restrained braces including Coulomb friction and Bouc-Wen models are discussed. It was revealed that the sliding mechanism was subjected to different parameters including types of loading, friction coefficient, temperature, velocity as well as the contact treatment, material, pressure, and size (Pall 1979; Constantinou et al. 1990; Sextro 2007). Therefore, to avoid discontinuity between stick-slip and slip phases Makkar et al. 2005 proposed a new friction model with a combination of stribek effect, Coulomb friction, and viscous dissipation. Then, the method proposed by Baber and Noori in 1985 and 1986, are discussed in detail, they added general degradation model to smooth hysteresis model of Bouc and Barber and Wen 1981, to capture the pinching effect.

The critical review of the literature reveals that most of the research focuses on retrofitting of steel structure by seismic dissipater devices and concrete structure by using FRP materials and very few studies have been conducted in case of the based seismic design for concrete structures utilizing supplementary devices i.e. friction dampers, friction dampers are among the passive energy devices, they are reliable and not sensitive to temperature, which makes them suitable for retrofit of existing structures as well as new structures subjected to dynamic loadings. Therefore, the objective of future studies are as follows:

- Most of the tests are on steel frames and the effects of friction dampers on concrete frames and their behaviour are not clear.
- The behaviour of friction dampers under real earthquakes is largely unknown, and their long-term performance and reliability are unclear, which need to be investigated further.
- The effects of different surface treatments of friction dampers need more investigation.
- In some cases, more sophisticated methods are required for performance-based design in that the damage state corresponding to each performance level of the concrete structure utilizing friction dampers must be quantified.
- The development of performance-based seismic design provisions for reinforced concrete structures utilizing friction dampers requires further investigation to develop analytical models and appropriate design methodologies.
- The effects of conventional and FEMA procedures on the overall response of the structure are unclear.
- The response modification factors for concrete structures equipped with friction dampers are unknown.
- Comparative study of different passive energy dissipation systems to place friction devices within a proper frame of reference.

Further studies are required to characterize the capacities of the overall friction damper system in concrete structures, as well as experimental studies to examine their actual behaviour, therefore

numerical and experimental studies need to be conducted to evaluate the long performance and reliability of yielding restrained braces underground motions.

2.7 Methodology

2.7.1 Analysis Procedures

In this study, the following two main types of analysis namely linear procedures including Linear Static procedure (LSP), Linear Dynamic procedure (LDP), and nonlinear procedures including Nonlinear Static procedure (NSP), Nonlinear Dynamic procedure (NDP) are used and described in this section.

FEMA, NEHRP Guidelines for the Seismic Rehabilitation of Buildings (FEMA 1997), and ATC 40 Seismic Evaluation and Retrofit of Concrete Buildings (ATC 1996) were the first guidelines of the nonlinear analysis, with the main focus of nonlinear static analysis. Then, ASCE 41 Seismic Rehabilitation of Existing Buildings (ASCE 2007), FEMA 440 Improvement of Nonlinear Static Seismic Analysis Procedures (FEMA 2005) and FEMA P440A Effects of Strength and Stiffness Degradation on Seismic Response (FEMA 2009a), the ATC 58 Guidelines for Seismic Performance Assessment of Buildings (ATC 2009) is the nonlinear dynamic analyses for seismic performance assessment of new and existing buildings have been introduced (Deierlein et al., 2010).

2.7.1.1 Linear procedures

2.7.1.1.1 Linear Static Procedure (LSP)

In this method, a linearly elastic static analysis should be performed to determine the seismic forces and their distribution over the height of a building, internal forces, and system displacement, in another word the rule of elasticity applies. The fundamental period in this method can be calculated based on the Eigenvalue (dynamic) analysis, Empirical equation, and the approximate methods (ASCE 41-17).

2.7.1.1.2 Linear Dynamic Procedure (LDP)

In this method, a linearly elastic static, dynamic analysis should be performed to determine the seismic forces and their distribution over the height of a building, internal forces, and system displacement. Linearly elastic stiffness and equivalent viscous damping based on the components near or at yield level shall be used to model the building. In linear dynamic procedure or linear response history analysis, the time domain is used to calculate the response of the structure to the seismic events. The linear dynamic analysis shall be performed using the response spectrum method or response history method.

2.7.1.2 Nonlinear procedures

2.7.1.2.1 Nonlinear Static Procedure (NSP)

The nonlinear static procedure of a building is the nonlinear load deformation of individual components of the structure which incorporating directly by a mathematical model and subjected to monotonically increasing lateral loads (ASCE 41-17, 2017). Figure 2-48 represents the nonlinear static procedure, first earthquake hazard is defined by elastic spectrum, then a nonlinear model of structural components is defined into a nonlinear model. When this model is subjected to either monotonically increasing force or displacements, it creates a capacity curve in terms of base shear versus roof displacement. Then ESDOF can be used to calculate the maximum roof displacement. Once component deformation and force action are known, force demands and component deformation shall be checked against the force as well as checking the component deformation based on the acceptance criteria.

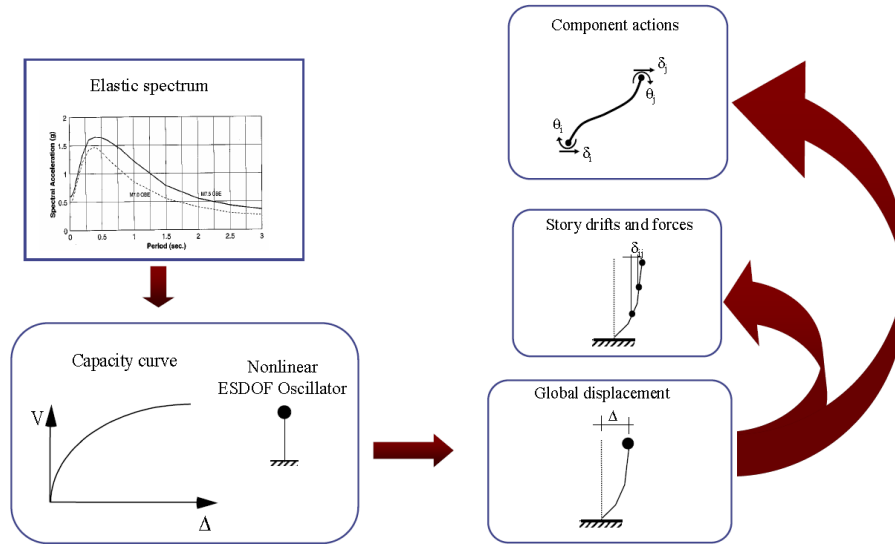


Figure 2-48. Nonlinear static assessment procedure (FEMA 273/274/356, ATC 58)

2.7.1.2.2 Nonlinear Dynamic Procedure (NDP)

Nonlinear dynamic procedure or nonlinear response history analysis of a building is the nonlinear load deformation of individual components of the structure which incorporating directly by a mathematical model and subjected to ground motion acceleration histories (ASCE 41-17, 2017). This method differs from NSP in which ground motions are used instead of response spectra, components force, and deformation shall be calculated based on nonlinear dynamic analysis. Component deformations for each degree of freedom can be estimated with a detailed model subjected to a ground motion, higher-level demands including story drift, roof displacement, and element distortions can be derived from the component action as illustrated in Figure 2-49.

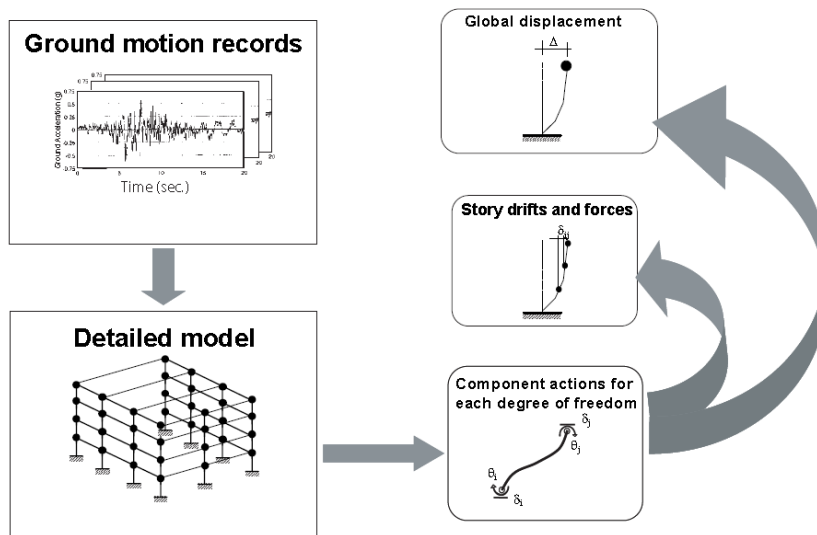


Figure 2-49. Nonlinear dynamic process (FEMA 440, 2005)

The relationship between the type of structural model and the characteristic of ground motion is presented in Figure 2-50. Depending on the parameters of interest some analysis options are better than the others, for instance, a single degree of freedom can represent a good uncertainty associated with global displacement demand when subjected to the variability of ground motions. The maximum global displacement can be calculated by a nonlinear static procedure, a multi-mode pushover analysis can provide inter-story drift that might not be available from SDOF dynamic analysis.

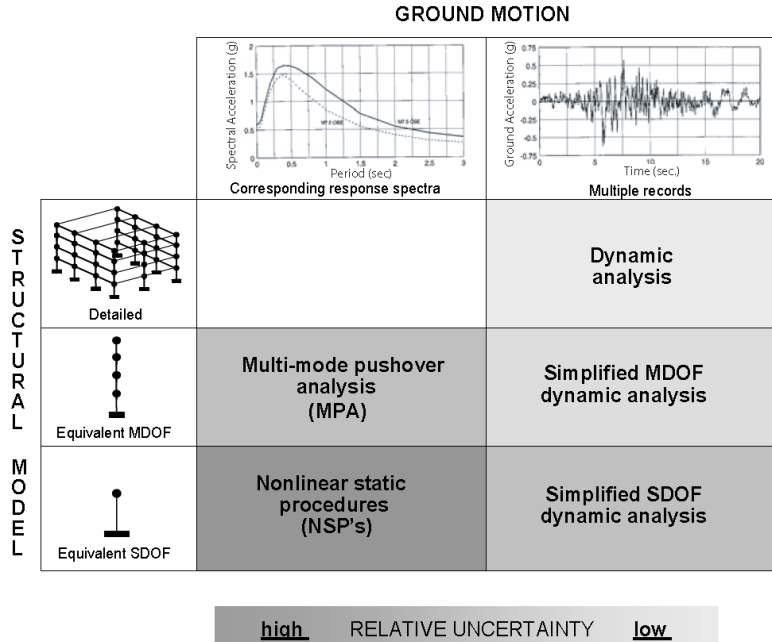


Figure 2-50. Seismic analysis procedures for various structural (FEMA 440, 2005)

2.7.2 Damping devices in a building

The seismic force-resisting system is distinct from the damping system, damping system composes of damping devices combined with structural elements. Damping devices can be categorized into three major groups including displacement-, velocity-dependent and force-controlled elements. For the structures with the damping system, the response of the system can be determined using alternate procedures including response spectrum as well as equivalent lateral force procedures. In these methods design earthquake and maximum considered earthquake should be considered and applied to the system. The seismic base shear for response spectrum procedure is the square root of the sum of squares of modal components, whereas, in the equivalent lateral force procedures, the seismic base shear is the square root of the sum of squares of the fundamental mode and residual base shear. Then the design earthquake displacement and story drift shall be calculated and controlled for both design and maximum credible earthquakes, some of the major parameters for calculating ELFSD and RSPSD are shown in Figure 2-51 and Figure 2-52.

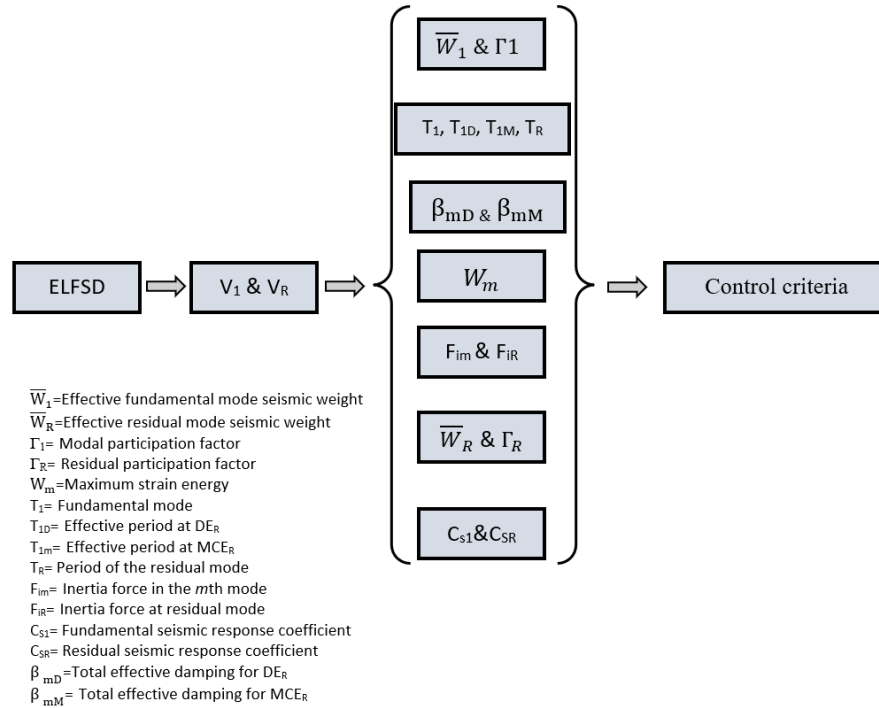


Figure 2-51. Important parameters for calculating ELFSD

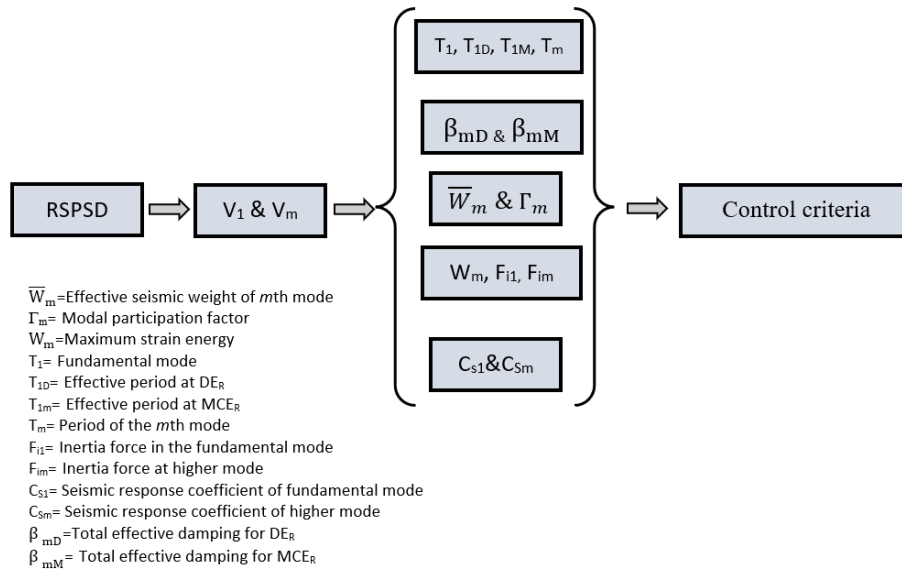


Figure 2-52. Important parameters for calculating RSPD

Next, the effective damping and ductility can be determined (ASCE 7, FEMA P-2082, FEMA 450, FEMA 420), these factors are shown in Figure 2-53. These procedures are explained in detail

in section 3.7. These methods are limited to the height of the structure, therefore, to calculate the seismic parameters following sections are explained.

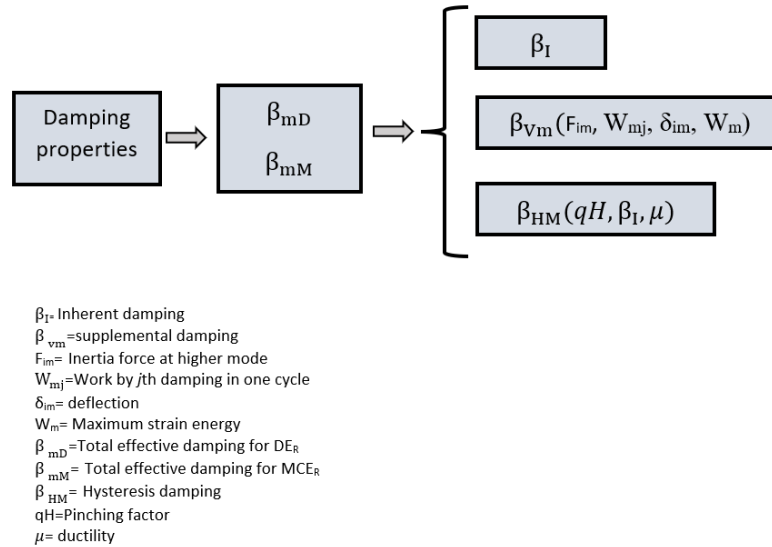


Figure 2-53. Important factors in calculating the damping properties

2.8 The structural response modification factor

The conventional seismic design allows the reduction of forces below the elastic level. This inelastic action occurred in the beams or adjacent to the beam-column joints and is able to dissipate energy (Aiken et. al. 1992). The seismic force values are calculated by forces divided by a response modification factor, symbolized as R. Response modification coefficients including the response modification factor R and the deflection amplification factor C_d were introduced by ATC 3-06 (1978) based on the well detailed seismic framing systems. The general performance of the system types during past earthquakes, toughness, and damping of the system was considered for the selection of R values (ATC 3-06, 1978).

2.8.1 Components of response modification factors

Depending on the performance level of the structure, the component of the response modification factor can be defined in several ways, the focus here is the life safety performance as

recommended in NBCC 2015. There are two bilinear approximation methods that can be used to estimate yield force and yield displacement. The first approximation is the load or strength versus displacement method for reinforced concrete elements (Paulay and Priestley 1992). Hereby, the elastic stiffness is based on the secant stiffness of the frame and can be calculated from the force-displacement curve corresponding to $0.75 V_y$. The second method is the equal energy approach. Utilizing a bilinear approximation of the actual response curve (base shear Vs. displacement), it is assumed that the area enclosed by these curves above the actual curve (i.e. area 1) is equal to the enclosed area below the actual response curve (i.e. area 2), presented in Figure 2-54, where V_y is the yield force, Δ_y is the yield displacement and Δ_m and Δ_u are the displacements corresponding to a limit state and prior to failure. The post-yield stiffness K_1 can be calculated from equation 2.15.

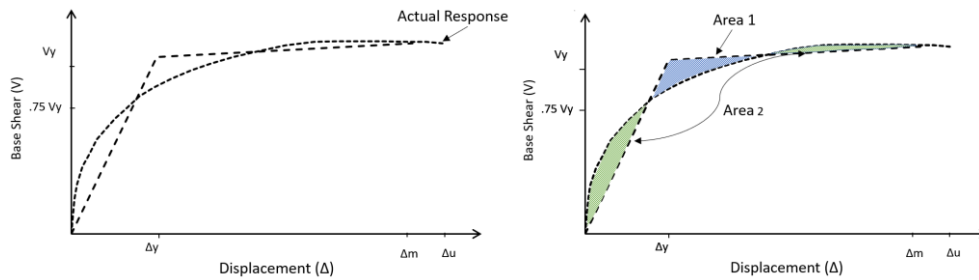


Figure 2-54. Bilinear approximation (based on ATC-19, 1995).

$$K_1 = \frac{V_{max} - V_y}{\Delta_m - \Delta_y} \quad (2.15)$$

Ductility is the ability of a building frame to dissipate energy beyond the elastic level and can be calculated for equation 2.16.

$$\mu_\Delta = \frac{\Delta_m}{\Delta_y} \quad (2.16)$$

Analytical or experimental evaluation can be used to determine the force-displacement relationship. Displacement versus base shear of a braced frame was calculated based on the experimental data in the mid-1980s at the University of California at Berkeley. Using concentrically braced (Uang and Bertero, 1988) and eccentrically braced (Whittaker et. al., 1987),

the Berkeley researchers defined three factors for calculation of R from equation 2.17, namely as reverse strength, R_s , ductility, R_μ , and damping, R_ζ . The calculations of ductility and strength factor are presented in Figure 2-55.

$$R = R_s R_\mu R_\zeta \quad (2.17)$$

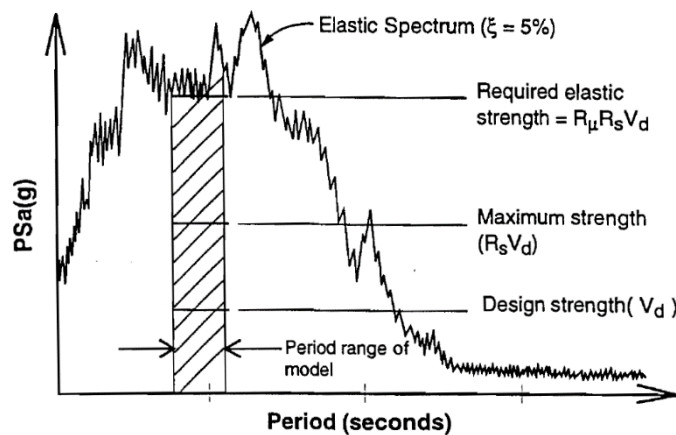


Figure 2-55. Ductility and strength factors (ATC-19)

ATC-34 proposed an updated formula for calculation response modification factor present in equation 2.18. In this equation, R_s and R_μ are “the period-dependent strength and ductility factors”, and R_R is the “redundancy factor”.

$$R = R_s R_\mu R_R \quad (2.18)$$

The only distinction between equations 2.17 and 2.18 is the redundancy factor R_R , which accounts for the quantification of several lines of a building’s vertical seismic frame system. The concept of over strength, and ductility factors are defined in sections 2.8.1.1 and 2.8.1.2.

2.8.1.1 Overstrength factor

Structural analysis under an earthquake in the elastic region can create the reverse strength in the structures, which are bigger than structural response. The seismic codes take advantage of the fact that structures can dissipate a large amount of earthquake energy by their overstrength and ductility (Asgarian et al., 2009 and Moni et al., 2016). The steps in the procedure of calculation

overstrength factor are including nonlinear static analysis and constructing the base shear versus roof displacement, the reserve strength can be calculated from the ratio of the actual lateral strength (V_y) to the design lateral strength (V_d) from equation 2.19 and as shown in Figure 2-56.

$$R_s \text{ or } R_0 = \frac{V_y}{V_d} \quad (2.19)$$

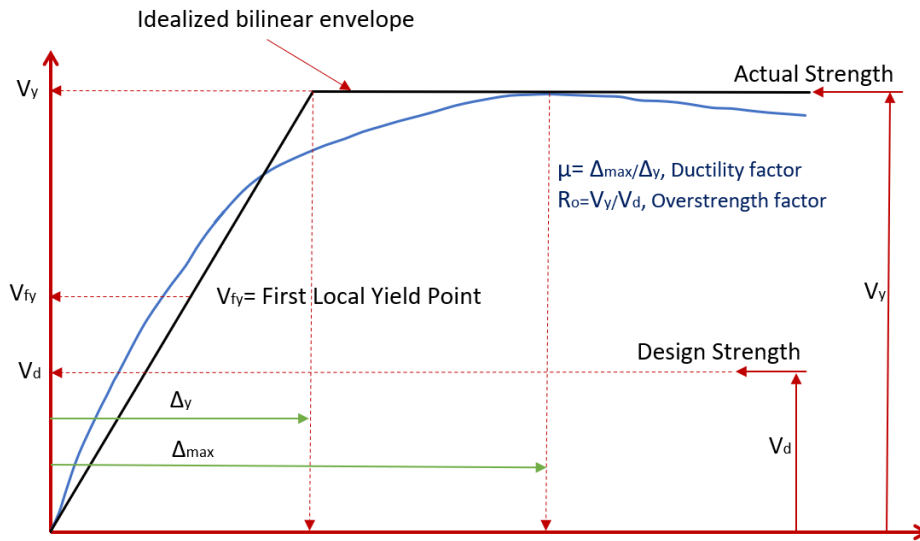


Figure 2-56. Displacement versus Base shear (based on Alam et al. 2012)

2.8.1.2 Ductility factor

R_d is known as the ductility factor which is the capacity of the structure to dissipate energy in inelastic range by considering ductility μ which can be calculated by dividing the maximum displacement over the displacement at the yield point, which depends on the soil type, and the fundamental period of the structure. There are several relationships to estimate the ductility factor (Krawinkler & Seneviratna, 1998; Krawinkler & Nassar, 1992; Miranda & Bertero, 1994; Newmark & Hall, 1982).

2.8.1.2.1 Newmark and Hall (1982)

Newmark and hall (1982) estimated the ductility reduction factor R_μ based on the period of the structure presented in Table 2-1, Figure 2-57 shows the ductility ratios of 2, 4, and 6.

Table 2-1. Ductility reduction factor (Newmark and hall,1982)

Period of Structure T_a (Sec)	Ductility reduction factor R_μ
$T_a < 0.1$	$R_\mu = 1.0$
$0.12 < T_a < 0.5$	$R_\mu = \sqrt{2\mu - 1}$
$T_a > 1$	$R_\mu = \mu$

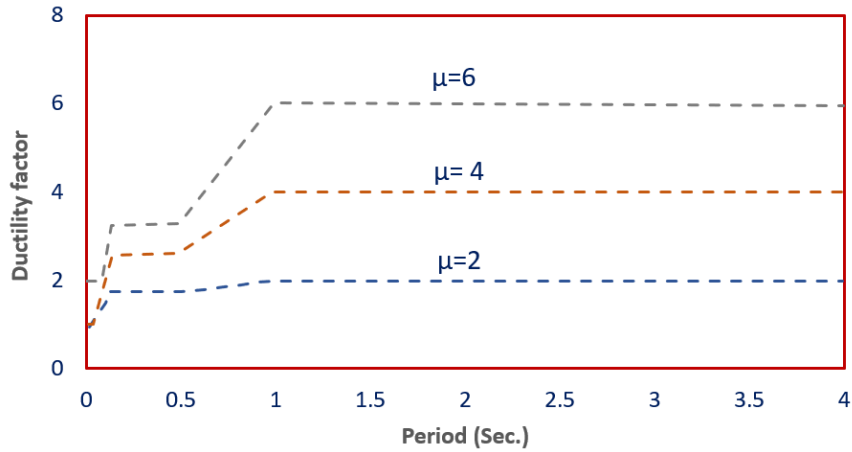


Figure 2-57. Ductility reduction factor, ductility, and period relationship (based on Newmark and hall,1982).

2.8.1.2.2 Krawinkler and Nassar (1992)

Krawinkler and Nassar (1992) developed equation 2.20 based on the statistical study of fifteen ground motions with magnitude ranging from 5.7 to 7.7 assuming 5% damping on rock or stiff soil.

$$R_\mu = \left[\left(\frac{T^a}{(1+T^a)} + \frac{b}{T} \right) (\mu - 1) + 1 \right]^{1 / \left(\frac{T^a}{(1+T^a)} + \frac{b}{T} \right)} \quad (2.20)$$

Herein, a and b are the regression parameters from Figure 2-58.

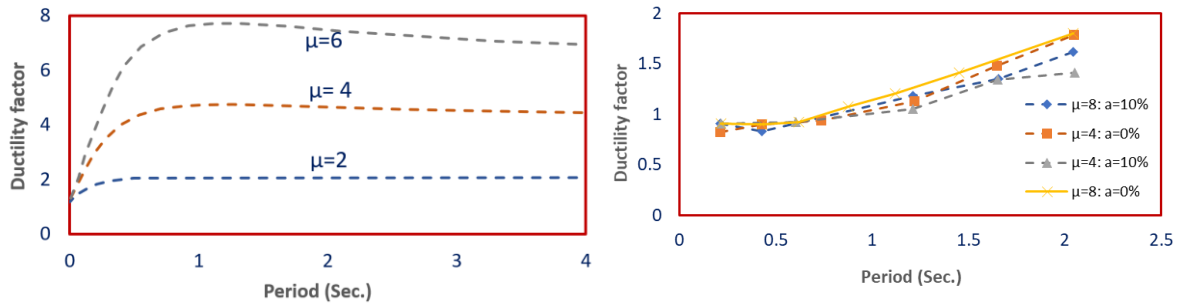


Figure 2-58. Ductility and period relationship on the left and modification factors on the right (based on Krawinkler and Nassar,1992)

2.8.1.2.3 Miranda and Bertero (1994)

Miranda and Bertero (1994) developed ductility reduction factor R_μ in equation 2.21.

$$R_\mu = \frac{\mu - 1}{\phi} + 1 \geq 1 \quad (2.21)$$

Where μ is ductility, T is the natural period of the structures, T_g predominant period of the ground motion, and ϕ is a function of ductility, fundamental period, and soil conditions and can be calculated from equations 2.22 to 2.24.

$$\phi = 1 + \frac{1}{10T - \mu T} - \frac{1}{2T} e^{-1.5|\ln(T) - 0.6|^2} \text{ for rock} \quad (2.22)$$

$$\phi = 1 + \frac{1}{12T - \mu T} - \frac{1}{5T} e^{-2|\ln(T) - 0.2|^2} \text{ for alluvium} \quad (2.23)$$

$$\phi = 1 + \frac{T_g}{3T} - \frac{3T_g}{4T} e^{-3|\ln(T/T_g) - 0.25|^2} \text{ for soft soil} \quad (2.24)$$

Figure 2-59 shows the ductility comparison of ductility factors for Nassar and Krawinkler and Miranda and Bertero, they can be ignored due to small differences.

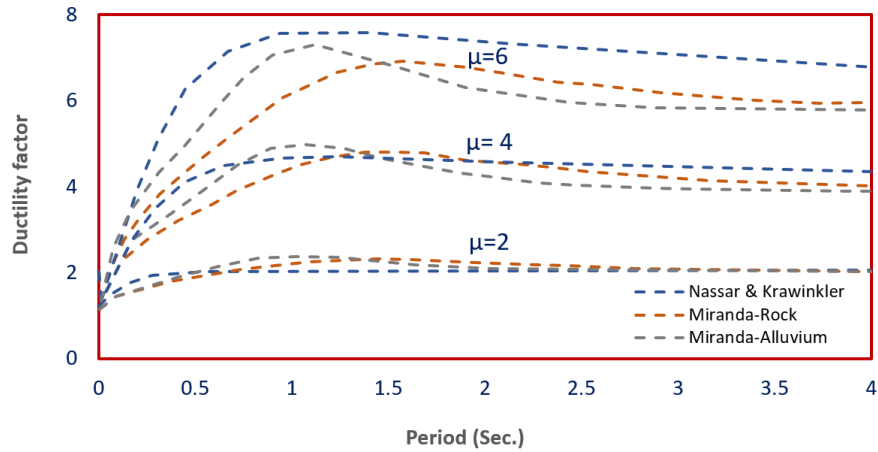


Figure 2-59. A comparison of ductility factor (based on ATC-19)

An overview of the analysis framework is presented in Figure 2-60.

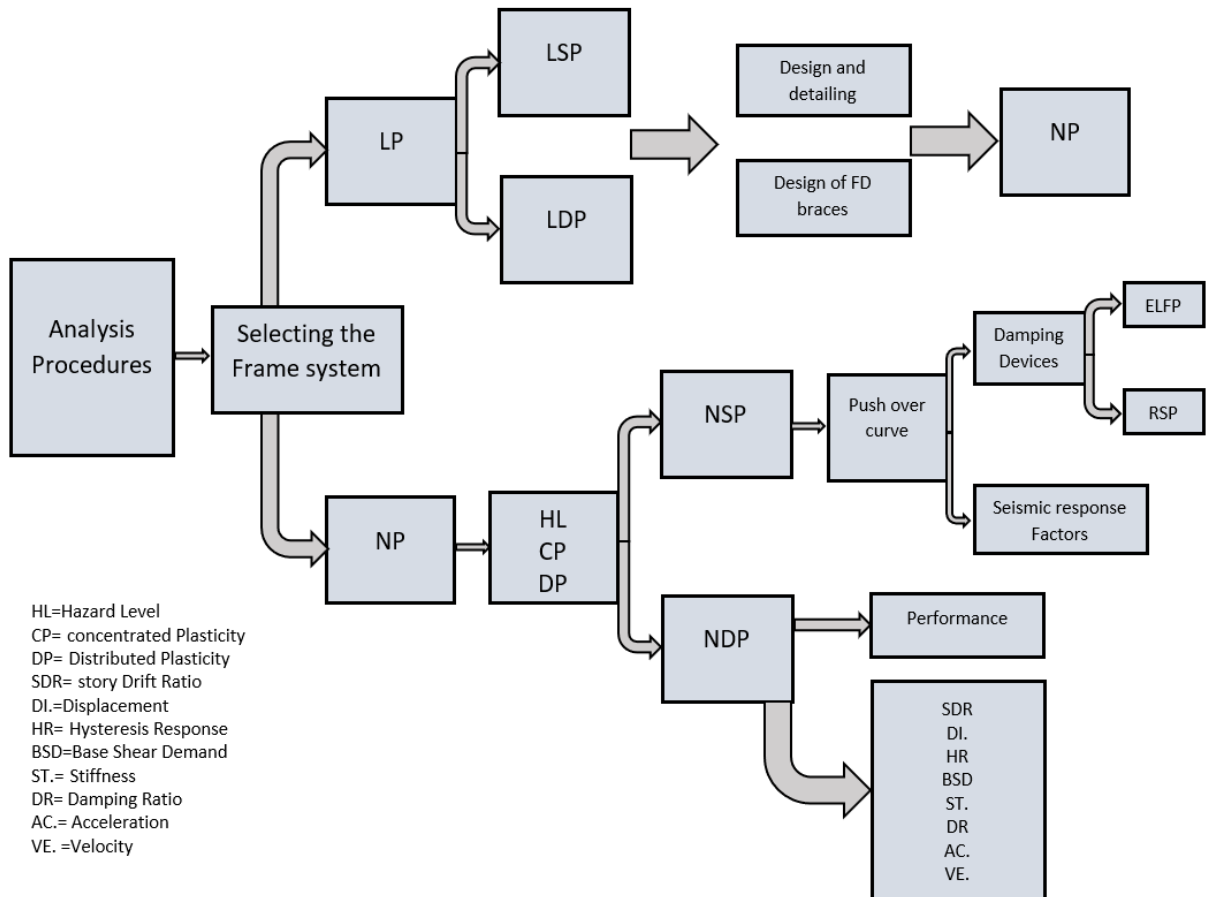


Figure 2-60. Overview of the analysis framework

2.8.2 Software tools used

Following software tools have been used for modeling, analysis, and design. Some of the important features of these software packages are explained below:

2.8.2.1 Integrated Building Design Software

ETABS (CSI, 2016) is a program which is capable of both linear and nonlinear procedures and can be used to solve the most complicated tasks. Some of its basic processes are presented in Figure 2-61. ETABS (CSI, 2016) is user-friendly, a 3D model can be created simple and quick with the maximum precision and different graphical options; however, there is no direct editing of the input file, and the analysis consumes more time and space and it is limited to built-in materials and elements.

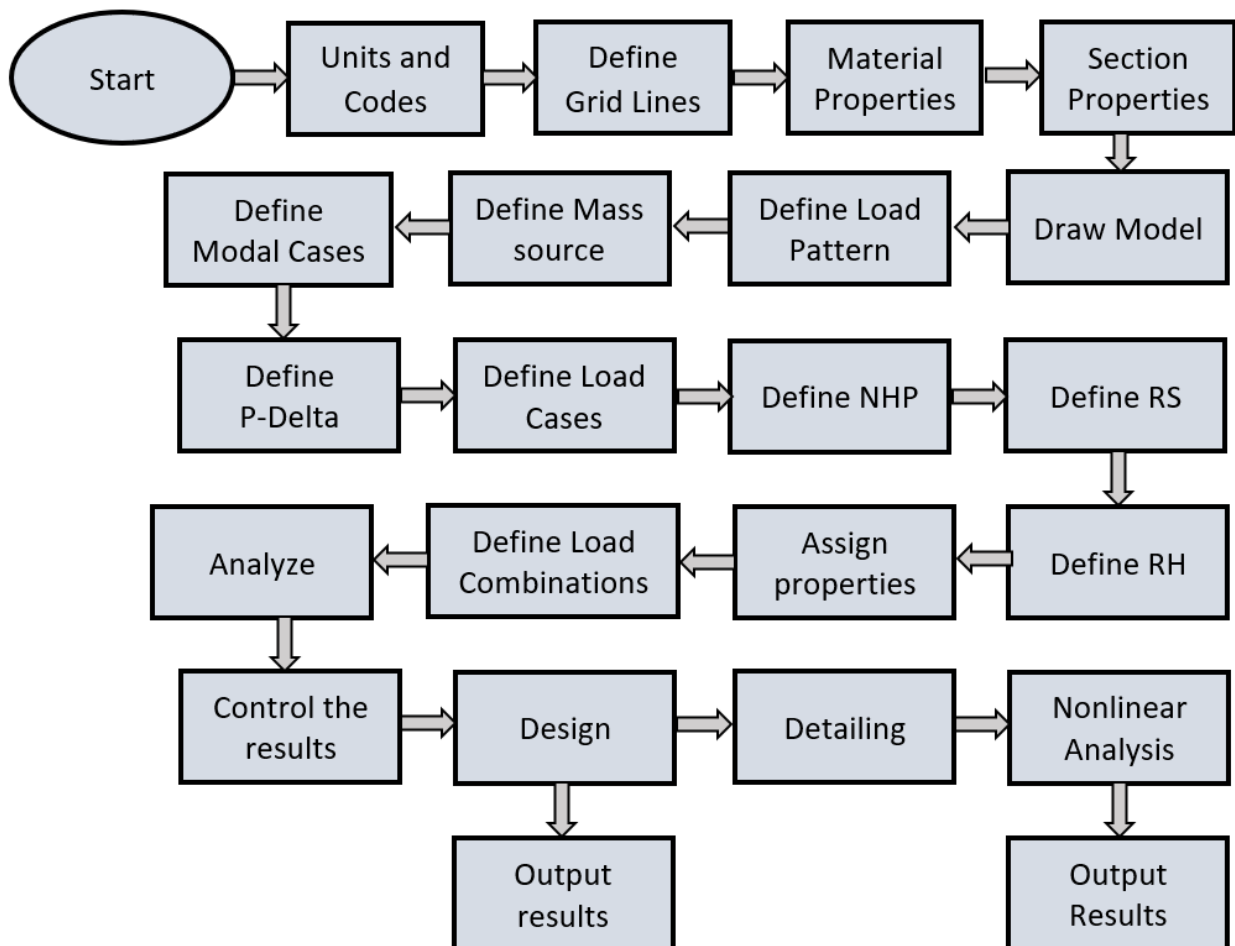


Figure 2-61. ETABS basic process

2.8.2.2 OpenSees Software

OpenSees is an object-oriented finite element software developed by Francis Thomas McKenna at the University of California Berkeley in 1997 (McKenna 1997). It is open-source which allows users to create finite element models in sequential and parallel applications. The program's primary software is C++ and was developed by the contribution of many researchers during the last years and supported by the National Science Foundation (NSF), Network for Earthquake Engineering Simulation (NEES), and the Pacific Earthquake Engineering Research Center (PEER). It is a powerful software for linear and nonlinear numerical simulation as well as geotechnical systems. Analysis with OpenSees (OpenSees Berkeley, 2021) is quick and does not consume computer storage, it is fully programmable with different elements and materials and has different solution methods and algorithms; however, it lacks a user interface, and the input information is typically complex and lengthy.

2.8.3 Details of the tasks

The work of this thesis is performed in three parts to understand the effectiveness of damping systems in concrete moment resisting frames, comparative performance of different supplemental damping systems, and experimental validation of damper models, following subsections provide some details of this work, which are elaborated in subsequent chapters.

2.8.3.1 Phase one: study of the effectiveness of supplemental damping systems in CMRFs

In this phase, ETABS software was used for linear static, Nonlinear dynamic, and static procedures. First, the performance level as well as the nonlinear properties of four-, eight-, and twelve-story ductile CMRF were evaluated using FEMA 356 and ATC 72. The effectiveness of a friction damper was then examined on a fourteen-story CMRF with various framing systems including elastic, ductile, and moderately ductile. Following that, the seismic characteristics for a CMRF structure with a height restriction of a maximum of 30m were computed. Design loads of ASCE 7 and NBCC 2015 procedures for structures without damping systems were used and compared with equivalent lateral force and response spectrum procedures for structures with

damping systems. Damping properties, ductility, displacement, drift, and velocity were calculated and discussed based on ASCE 7, FEMA P-2082, FEMA 450, FEMA 420. Further details along with results and discussion are presented in Chapter 3.

2.8.3.2 Phase two: seismic reduction factors

Seismic performance and reduction factors including overstrength, R_o , and ductility, R_d , of four-, eight-, and fourteen-story ductile CMRF with inline seismic friction dampers were assessed. Next CMRF without dampers and with different dissipation devices such as Ten-Co Seismic Brake, Fluid Viscous Damper, Triangular Metallic Yielding Dampers as well as seismic isolators including Lead Rubber Bearing Isolator and Triple Pendulum Isolator were studied to better understand the performance of Ten-Co Seismic Brake. The aforementioned studies were carried out with the help of the ETABS program. Chapter 4 presents the results and discussion of the findings.

2.8.3.3 Phase three: simulation of the experimental work

In this phase the collaborating experimental test with Quaketek Inc., and Lyles College of Engineering at California State University, Fresno was performed and simulated using ETABS and OpenSees software. The main purpose of this part of the study is to understand the actual behaviour of the inline friction damper under seismic excitation and validate the modeling techniques. The experimental test was conducted by an MSc student at CSU (Couch, 2020), and I was involved in the design of experimental; and the analysis of data including raw data processing. The behaviour of friction dampers and the simulation of the experimental work were validated in Chapter 5.

2.8.4 Summary

The analysis techniques are discussed, including Linear and Nonlinear approaches. Next, the methods for calculating ductility, damping, displacement, drift, and velocity are described, followed by a brief history of seismic design factors and an outline of the methodology utilized in the thesis. Then, the rationale behind software tools and their capabilities are discussed. ETABS

is user-friendly and capable of handling complex problems, which has been used by many engineers for design purposes, whereas OpenSees is more sophisticated but not user-friendly, and it is mostly used for research. As a result, ETABS software is chosen where design and broader analysis were needed. The tasks are divided into three phases, the first phase is the effectiveness of supplemental damping systems in CMRF buildings in Chapter 3. Phase two is the seismic reduction factors, which are discussed in Chapter 4, and phase three, the simulation of the experimental work is explained in chapter 5.

CHAPTER 3

Seismic Performance Assessment of Reinforced Concrete Moment-Resisting Frames equipped with yielding restrained braces

3.1 Introduction

This chapter presents the detailed methodology used for Concrete Moment Resisting Frame (CMRF), the hazard levels, performance levels, and analysis procedures are described here. Then different seismic design procedures including the National Building Code of Canada (NBCC 2015), and equivalent lateral force procedures based on ASCE 7 are discussed.

The effects of the Tension-Compression seismic braces at different types of concrete moment resisting frames including elastic, moderately ductile, and ductile are evaluated. Seismic performance of a set of code-designed 4, 8, and 12 story moment resisting concrete frames at different hazard levels namely, SLE (Service Level Event), DLE (Design Level Event), and MCE (Maximum Considered Event) with and without Ten-Co seismic brake are discussed. Finally, the damping properties design procedures of yielding restrained braces using FEMA 450 are examined.

3.2 Performance-Based Design

Building codes in many jurisdictions are moving away from the traditional prescription procedures towards performance-based seismic design methodology. The performance-based design allows the design teams to evaluate various seismic motions and the performance objectives for a building that is aligned with the owner's expectations (FEMA 349). Resilience-based performance is the next generation of building performance (Risk and Resilience Measurement Committee, 2019).

Seismic design codes presently in use are prescribed-based and focus on the strength and capacity of structural members, but the structure's overall performance during a given seismic

event cannot be clearly described. Performance-based design differs from this in that it is objective-based with a specific level of structural behaviour during a seismic event. With this approach, different methods of analysis were used depending on the performance level chosen. Structural and non-structural damages were computed into the structure's overall performance. Because of this, the structural engineer, architect, owner, and contractor are all a factor in the determination of the performance level required as well as the realization of that level. When a building is subjected to lateral ground motions cause structural components respond nonlinearly, Figure 3-1 the structural response under different performance levels including “Immediate Occupancy” (IO), “Life Safety” (LS), and “Collapse Prevention” (CP).

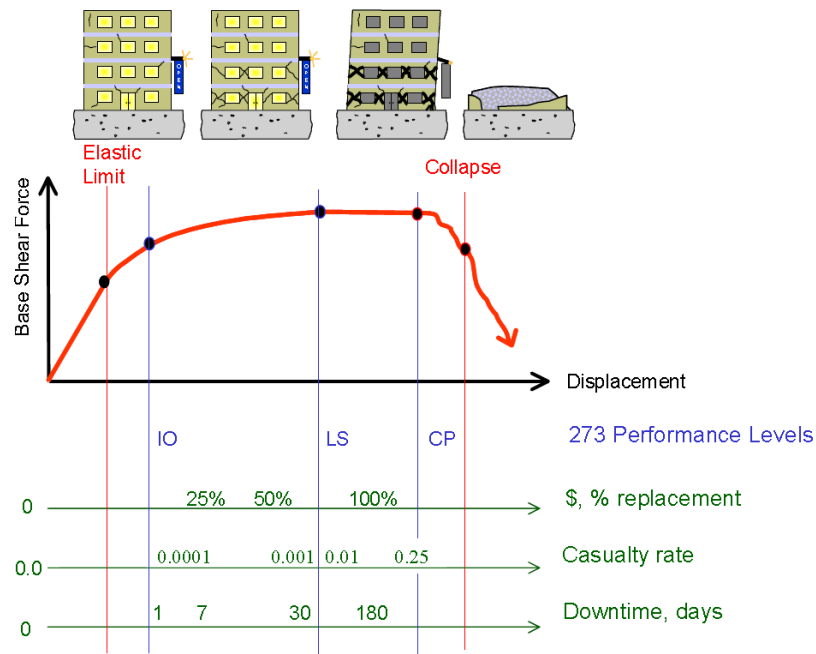


Figure 3-1. Performance-based earthquake engineering (Hamburger et. al. 1998, ATC 58, 2003)

3.2.1 Hazard Levels

Based on the ASCE 41-17, the seismic hazard produced by ground motion shall be defined as acceleration response spectra or ground motion acceleration histories and is based on the distance of the building to the faults, geologic and geotechnical characteristics of the regional and site-specific, and the seismic hazard levels. The ground motion for a seismic hazard level using a 5%

damped response spectrum for short (0.2s) and long (1s) periods in the direction of maximum horizontal response.

This standard categorized earthquake ground motions based on several probabilistic seismic hazard levels as presented in Table 3-1. These ground motions are defined as a probability of exceedance in a specific time-period, for instance, 50% in 50 years, or as a mean return period for exceedance of specific earthquake in 75 years. The four commonly used seismic hazard levels are namely 50%, 20%, 10%, and 2% in 50 years.

Table 3-1. Hazard levels (ASCE 41-17, 2017)

Earthquake probability of exceedance	Mean return period	Spectral Response Acceleration Parameters
50 % in 30 years	43	
50 % in 50 years	75	-
20 % in 50 years	225	BSE-1E
10 % in 50 years	475	BSE-1
5 % in 50 years	975	BSE-2E
2 % in 50 years	2475	BSE-2N

The Vision 2000 report outlined frequent, occasional, rare, and very rare as design levels. Each of these design levels is based on a specific mean recurrence interval or probability of exceedance as presented in Table 3-2. The recurrence interval is expressed as the average number of years between earthquakes with an intensity equal to or greater than the design intensity, for example, 475 years is the average period between the occurrence of earthquakes. The probability of exceedance for example 10% in 50 years is the statistical estimate of the likelihood that a seismic event of that design level will take place within a given period or specified number of years.

Table 3-2. Vision 2000 Earthquake Design Levels (SEAOC, 1995)

Earthquake design level	Recurrence interval (years)	Probability of exceedance
Frequent	43	50% in 30 years
Occasional	72	50% in 50 years
Rare	475	10% in 50 years
Very rare	970	10% in 100 years

3.2.2 Target building performance levels

Performance levels are defined based on the expected building behaviour, or how much damage, economic loss, and disruption may occur. These criteria are considered for both structural and nonstructural elements to define the performance levels, summarized performance levels for both Structural Engineers Association of California (SEAOC) Vision 2000 (1995) and NEHRP guidelines (1997), presented in Table 3-3.

- **Operational Level:** Buildings are expected to sustain minimal or no damage to their structural and nonstructural components. After an earthquake, the building remains safe and suitable for its normal use. Although there might be a slightly impaired mode with power, water, and other utilities provided from emergency sources as well as some nonessential systems
- **Immediate Occupancy:** Buildings are expected to sustain minimal or no damage to their structural components and minor damage to their nonstructural components. Although the building remains safe to occupy immediately after an earthquake, the nonstructural system might not function properly. Therefore, it might be necessary to perform cleanup and repair.
- **Life Safety:** Buildings are expected to experience moderate damage to structural and nonstructural components. Repairs may be required to reoccupy the building; however, it might not be justified from economical aspects.
- **Collapse Prevention:** Buildings are expected to face extensive damage to structural and nonstructural components without total or partial building collapse. Extensive repairs may be required before occupancy; however, they may not be feasible due to extensive damage. and deemed economically impractical.

Table 3-3. Structural performance level (Krawinkler, 1997)

Level of performance		
NEHRP	Vision 2000	Description
Operational	Fully Functional	Both structural and non-structural are in the elastic zone.
Immediate Occupancy	Operational	Structural remains in the elastic zone and non-structural elements are functional.
Life Safety	Life Safe	Structural members experience significant damage, and non-structural elements may not function.
Collapse Prevention	Near Collapse	Substantial damage to both structural and non-structural elements.

Figure 3-2 summarized the recommendation for three different occupancies and uses. Each box is a combination of the earthquake return period and the earthquake performance level represents a performance objective for safety (hazardous), essential, or basic (ordinary) buildings. The philosophy behind these categories is that the safety-critical facilities contain hazardous material and their release would result in an unexpected hazard to a wide range of the public, therefore they should have low-risk damage, their functionality for frequent, occasional, and rare earthquakes should be fully operational and for very rare earthquake should be operational (e.g. nuclear power plants). The essential facilities are critical to post-earthquake operations and their functionality for frequent and occasional earthquakes should be fully operational and for rare and very rare should be operational and life-safe (e.g. hospitals). The basic facilities are not classified as safety or essential buildings and should provide a low risk for life safety, their functionality for frequent, occasional earthquakes, rare and very rare should be fully operational, operational, life-safe, and near collapse. The performance levels are expressed in quantities and presented in Table 3-4.

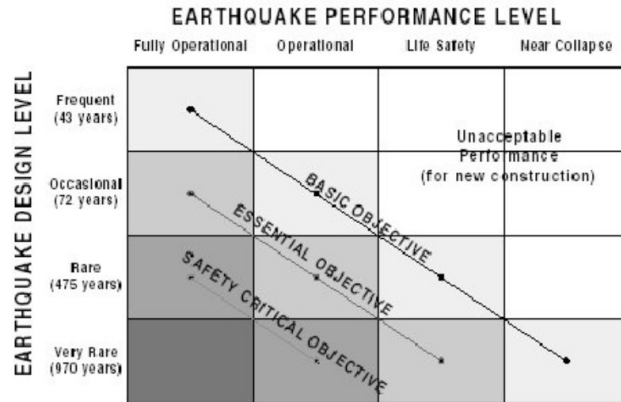


Figure 3-2. Seismic performance objectives for buildings (SEAOC, 1995)

Table 3-4. Performance level damage descriptions (SEAOC, 1995)

Description	Performance level				
	Fully Operational	Operational	Life Safe	Near Collapse	Collapse
Overall building damage	Negligible	Light	Moderate	severe	Complete
Permissible transient drift	< ± 0.2%	< ± 0.5%	< ± 1.5%	< ± 2.5%	< ± 2.5%
Permissible permanent drift	Negligible	Negligible	< ± 0.5%	< ± 2.5%	< ± 2.5%
Vertical load carrying element damage	Negligible	Negligible	Light to moderate, but substantial capacity remains to carry gravity loads.	Moderate to heavy, but element can carry gravity loads.	Partial to total loss of gravity load support.
Lateral load carrying element damage	Negligible, no significant loss.	Light, minor cracking/yielding of structural components.	Moderate, lateral system remains functional, but residual stiffness and strength were reduced.	Negligible residual strength and stiffness, but large permanent drifts.	Partial or total collapse. Primary elements may require demolition.
Damage to architectural systems	Negligible damage to cladding, glazing, partitions, ceiling, finishes, etc.	Light to moderate damage to architectural system.	Moderate to severe damage to architectural system.	Severe damage to architectural system.	Destruction of elements.
Egress systems	Not impaired.	No major obstruction in exit corridors, elevators are functional.	No major obstruction in exit corridors, elevators may be out of service.	Egress may be obstructed.	Egress may be highly or completely obstructed.

3.3 Seismic design provisions

In this section, seismic design provisions based on NBCC 2015, and ASCE 7-14 are explained.

3.3.1 National Building Code of Canada (NBCC 2015)

3.3.1.1 Uniform Hazard Spectra (UHS) based design

In the NBCC 2015, six spectral acceleration parameters for periods of 0.2, 1.0, 2.0, 5.0, and 10 seconds are presented to define spectra matching based on the uniform hazard spectrum. The horizontal Peak Ground Acceleration (PGA) and the horizontal Peak Ground Velocity (PGV) as explained earlier given a 2% probability of being exceeded in 50 years. These six spectral accelerations define spectra to match the shape of the Uniform Hazard Spectra (UHS). Ground Motion Prediction Equations (GMPEs) are revised and can be used for site-specific values of the spectral acceleration $S_a(T)$ (Atkinson and Adams, 2013).

The design spectral acceleration values of $S(T)$ can be determined with the following expressions $S_a(T)$, and straight-line interpolation can be used for intermediate values of T .

$$\begin{aligned} S(T) &= F(0.2)S_a(0.2) \text{ or } F(0.5)S_a(0.5), \text{ whichever is larger for } T \leq 0.2 \text{ s} \\ &= F(0.5)S_a(0.5) \text{ for } T=0.5 \text{ s} \\ &= F(1.0)S_a(1.0) \text{ for } T=1.0 \text{ s} \\ &= F(2.0)S_a(2.0) \text{ for } T=2.0 \text{ s} \\ &= F(5.0)S_a(5.0) \text{ for } T=5.0 \text{ s} \\ &= F(10.0)S_a(10.0) \text{ for } T \geq 10.0 \text{ s} \end{aligned}$$

3.3.1.2 Present methodology-NBCC 2015

Different soil categories from hard rock, Class A, to soft soil, Class E as well Class F for liquefiable soil and sensitive, organic, and highly plastic clays are defined to characterize the soil effect on the amplitude of seismic waves arriving on the surface. NBCC 2015 allows short period structures to be designed for $2/3$ the calculated base shear to have at least a limited amount of ductility, this accounts for reserve strength which undergoes small displacement in such structures. This can achieve by the greatest value of $2/3 \times S(0.2)$ or $S(0.5)$. To have a better estimation of

equivalent static design base shear, the shear multiply by the higher mode factor, equation 3.1, which is based on the assumptions that the structure responds in its first mode (Humar, 2015).

$$V_e = S(T_a)M_vW \quad (3.1)$$

Where V_e is the elastic shear, design spectral acceleration can be obtained from $S(T) = S(T_a)F(T_a)$, $S(T_a)$ can be obtained from the UHS, M_v is the higher mode factor which depends on the period of the buildings and W is the seismic weight.

$$V_d = \frac{S(T_a)M_vI_EW}{R_dR_o} \quad (3.2)$$

Design base shear V_d can be calculated with equation 3.2, R_d accounts for ductility and capability of a structure to dissipate energy in inelastic behaviour, R_o reflects the reserve strength in a structure and I_E is the importance factor. The weight of the building W can be estimated from equation 3.3.

$$W = \sum_{i=1}^n W_i \quad (3.3)$$

The fundamental lateral period, T_s , can be calculated from equations 3.4 to 3.8 depending on the height and Seismic Force Resisting System (SFRS).

$$T_s = 0.085(h_n)^{\frac{3}{4}} \text{ for steel moment frames} \quad (3.4)$$

$$T_s = 0.075(h_n)^{\frac{3}{4}} \text{ for concrete moment frames} \quad (3.5)$$

$$T_s = 0.1N \text{ for other moment frames} \quad (3.6)$$

$$T_s = 0.025h_n \text{ for braced frames} \quad (3.7)$$

$$T_s = 0.05(h_n)^{\frac{3}{4}} \text{ for shear walls and other structures} \quad (3.8)$$

A portion of base shear is concentrated at the top of the building, which can be calculated from the equation 3.9 to 3.11.

$$F_t = 0 \quad T_a \leq 0.7 \quad (3.9)$$

$$F_t = 0.07 T_a V \quad 0.7 < T_a < 3.6 \quad (3.10)$$

$$F_t = 0.25V \quad T_a \geq 3.6 \quad (3.11)$$

The remaining $V - F_t$ shall be distributed along the height of the building, which is representative of the first mode from equation 3.12.

$$F_x = (V - F_t)W_x h_x / (\sum_{i=1}^n W_i h_i) \quad (3.12)$$

Where F_x is the lateral force at level x , W_x is the seismic weight corresponds to level x , h_x is the height, and n is the number of floors. The overturning M_x can be calculated from equation 3.13. Where $J_x=1.0$ for $h_x \geq 0.6h_n$, and $J_x= J + (1-J)(h_x/0.6h_n)$ for $h_x < 0.6h_n$.

$$M_x = J_x \sum_{i=x}^n F_i (h_i - h_x) \quad (3.13)$$

Since the shear V , and F_x account for higher mode effect, the computed overturning moments produced by such modes are overestimated. Therefore, the code specifies the overturning moment reduction factor J , and J_x is the overturning moment reduction factor at each level. Methodology for estimating the shear adjustment factor M_v was explained by (Humar and Mahgoub, 2003), the structure was assumed to remain elastic, and the adjustment factor, M_v , was calculated from equation 3.14, and by assuming that the entire response is in the first mode.

$$M_v = \frac{\sqrt{\sum [S(T_i)W_i]^2}}{S(T_a)W} \quad (3.14)$$

Where $S(T_i)$ is the site-adjusted spectral acceleration corresponding to the i th modal period, W_i corresponding to the modal weight, and W is the total weight of the building. The shear $S(T_a)M_v W$ is distributed across the height to obtain the lateral forces and to calculate the base overturning moment M_{bc} and the story level moment M_{xc} . The corresponding moments obtained from response spectral analysis are M_{be} , and M_{xe} . Therefore, the overturning moment can be calculated from equation 3.15. It is evident that M_v for a given spectral shape depends on only the modal periods and weights (Humar, 2015).

$$J = \frac{M_{be}}{M_{bc}} \quad \text{and} \quad J_x = \frac{M_{xe}}{M_{xc}} \quad (3.15)$$

3.3.1.3 Equivalent Lateral Force Procedure (ASCE 7-16)

This standard provides the minimum load requirements for the design of buildings, including strength design (load and resistance factor) in which the computed member forces by the factor loads do not exceed the member design strength and allowable stress design (working stress design) in which the elastically computed stresses in members by nominal loads do not exceed allowable stresses elastic zone. The code specifies the site soil properties as site class A, B, C, D, E, or F as presented in Table 3-5.

Table 3-5. Site classification (ASCE 7-16)

Site Class	\bar{v}_z	\bar{N} or \bar{N}_{ch}	\bar{s}_u
A. Hard rock	>5,000 ft/s	NA	NA
B. Rock	2,500 to 5,000 ft/s	NA	NA
C. Very dense soil and soft rock	1,200 to 2,500 ft/s	>50	>2,000 psf
D. Stiff soil	600 to 1,200 ft/s	15 to 50	1,000 to 2,000 psf
E. Soft clay soil	<600 ft/s	<15	<1,000 psf
	Any profile with more than 10 ft of soil having the following characteristics: —Plasticity index $PI > 20$, —Moisture content $w \geq 40\%$, —Undrained shear strength $\bar{s}_u < 500$ psf		
F. Soils requiring site response analysis in accordance with Section 21.1	See Section 20.3.1		

For SI: 1 ft/s = 0.3048 m/s; 1 lb/ft² = 0.0479 kN/m².

3.3.1.3.1 Design Spectral Acceleration Parameters

Based on the site classes, the maximum considered earthquake (MCE_R) spectral response acceleration parameter for a short period, S_{MS} and at 1s period S_{M1} can be determined from equations 3.16 and 3.17.

$$S_{MS} = F_a S_S \quad (3.16)$$

$$S_{M1} = F_v S_1 \quad (3.17)$$

Where S_S and S_1 are the mapped spectral response acceleration at a short period and a period of 1s. F_a and F_v are site coefficients. Design spectral response acceleration is categorized at a short period, S_{DS} , and at one second period S_{D1} , which can be determined from equations 3.18 and 3.19.

$$S_{DS} = \frac{2}{3} S_{MS} \quad (3.18)$$

$$S_{D1} = \frac{2}{3} S_{M1} \quad (3.19)$$

Design response spectrum can be developed where site-specific ground motion procedures are not used as presented in Figure 3-3. The construction of the design response spectrum curve is based on equations 3.20 to 3.22.

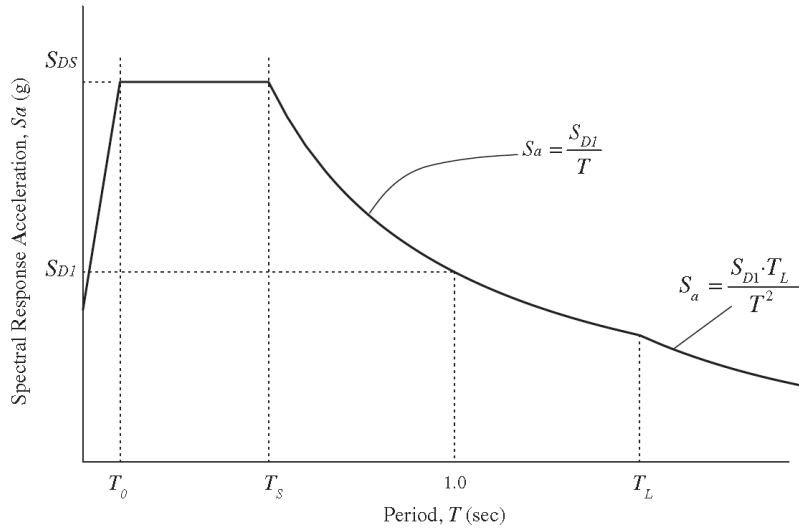


Figure 3-3. Design response spectrum (ASCE 7-16)

$$S_a = S_{DS} \left(0.4 + 0.6 \frac{T}{T_0} \right) \quad (3.20)$$

$$S_a = \frac{S_{D1}}{T} \quad (3.21)$$

$$S_a = \frac{S_{D1} T_L}{T^2} \quad (3.22)$$

Where S_a is the design spectral response acceleration, for $T < T_0$, S_a shall be calculated from equation 3.20, S_a is equal to S_{DS} for $T_0 \leq T \leq T_s$. If $T_s < T \leq T_L$, S_a shall be calculated from equation 3.21, and for $T > T_L$, S_a shall be determined from equation 3.22. S_{DS} is the design spectral response

acceleration at short period, S_{D1} is the design spectral response acceleration at 1 second period, T is the fundamental period, $T_0=0.2(S_{D1}/S_{DS})$, $T_s= S_{D1}/S_{DS}$, and T_L is the long period transition.

3.3.1.3.2 Seismic base shear

The seismic base shear, V , is calculated from equation 3.23. where C_s is the seismic response coefficient shall be determined in accordance with equation 3.24, and W is the seismic weight.

$$V = C_s W \quad (3.23)$$

$$C_s = \frac{S_{DS}}{\left(\frac{R}{I_e}\right)} \quad (3.24)$$

Where S_{DS} is the design spectral acceleration in the short period, R is the response modification factor, and I_e is the importance factor. The seismic response coefficient shall satisfy the equations 3.25 to 3.28.

$$C_s \leq \frac{S_{D1}}{T\left(\frac{R}{I_e}\right)} \text{ for } T \leq T_L \quad (3.25)$$

$$C_s \leq \frac{S_{D1}T_L}{T^2\left(\frac{R}{I_e}\right)} \text{ for } T > T_L \quad (3.26)$$

$$C_s \geq 0.044S_{DS}I_e \geq 0.01 \quad (3.27)$$

$$C_s \geq 0.5S_1/(R/I_e) \text{ for } S_1 \geq 0.6g \quad (3.28)$$

Where S_{D1} is the design spectral response acceleration at a period of 1.0 second, T is the fundamental period, T_L is the long transition period, and S_1 is the maximum considered earthquake spectral response acceleration. The approximate fundamental period, T_a , shall be determined from equation 3.29. where C_t and x are coefficients from Table 3-6, and h_n is the structural height.

$$T_a = C_t h_n^x \quad (3.29)$$

Table 3-6. Approximate period parameters C_t and x (ASCE 7-16)

Structure Type	C_t	x
Moment-resisting frame systems in which the frames resist 100% of the required seismic force and are not enclosed or adjoined by components that are more rigid and will prevent the frames from deflecting where subjected to seismic forces:		
Steel moment-resisting frames	0.028 (0.0724) ^a	0.8
Concrete moment-resisting frames	0.016 (0.0466) ^a	0.9
Steel eccentrically braced frames in accordance with Table 12.2-1 lines B1 or D1	0.03 (0.0731) ^a	0.75
Steel buckling-restrained braced frames	0.03 (0.0731) ^a	0.75
All other structural systems	0.02 (0.0488) ^a	0.75

^aMetric equivalents are shown in parentheses.

The distribution of the seismic force, F_x , along the height of the building can be estimated from equation 3.30. C_{vx} is the vertical distribution factor and can be determined from equation 3.31.

$$F_x = C_{vx}V \quad (3.30)$$

$$C_{vx} = \frac{w_x h_x^k}{\sum_{i=1}^n w_i h_i^k} \quad (3.31)$$

Where V is the total design lateral force, w_i and w_x are the total effective seismic weight, h_i and h_x are the height and relates to the structural period, $K=1$ for $T \leq 0.5s$, $K=2$ for $T \geq 2.5s$, and structure having period between 0.5 and 2.5s, k is 2 or can be determined by linear interpolation.

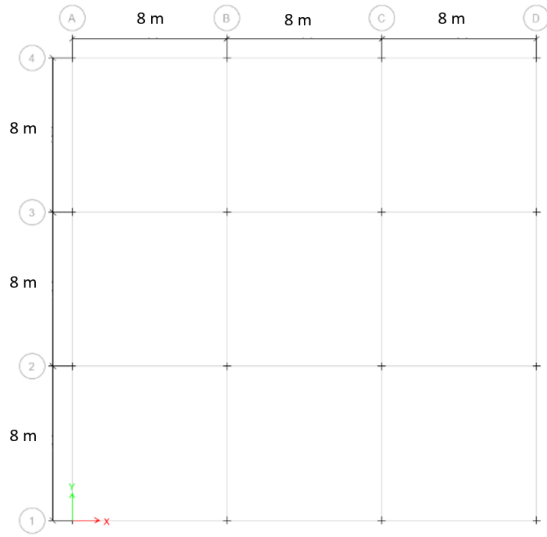
3.4 Design of Structural models

The NBCC 2015 differ from the earlier versions, the life-safety performance based on the drift demand shall be limited to 1%, 2%, and 2.5% for post-disaster, high importance category, and other buildings. In the NBCC 2015, six spectral acceleration parameters for periods of 0.2, 1.0, 2.0, 5.0, and 10 seconds are presented to define spectra matching based on the uniform hazard spectrum with different soil categories from hard rock, Class A, to soft soil, Class E as well Class F for liquefiable soil and sensitive, organic and highly plastic clays are defined to characterize of the soil effect on the amplitude of seismic waves arriving on the surface. The seismic load was calculated based on the equivalent static load procedure in equation 3.32 (NBCC 2015).

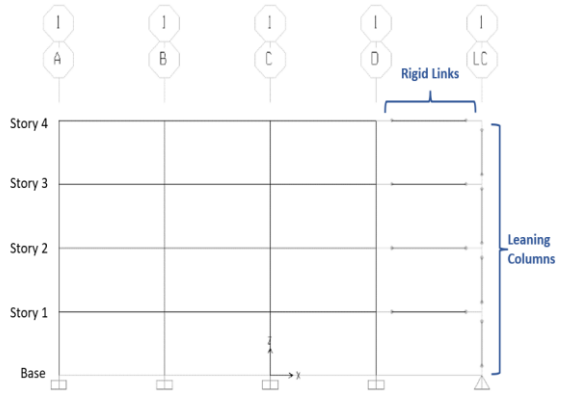
$$V_d = \frac{S(T_a)M_v I_E W}{R_d R_o} \quad (3.32)$$

Where V_d is the design base shear, design spectral acceleration can be obtained from $S(T) = S(T_a)F(T_a)$, $S(T_a)$ can be obtained from the UHS, M_v is the higher mode factor which depends on the period of the buildings, W is the seismic weight, R_d accounts for ductility and capability of a structure to dissipate energy in inelastic behaviour, R_o reflects the reserve strength in a structure, and I_E is the important factor.

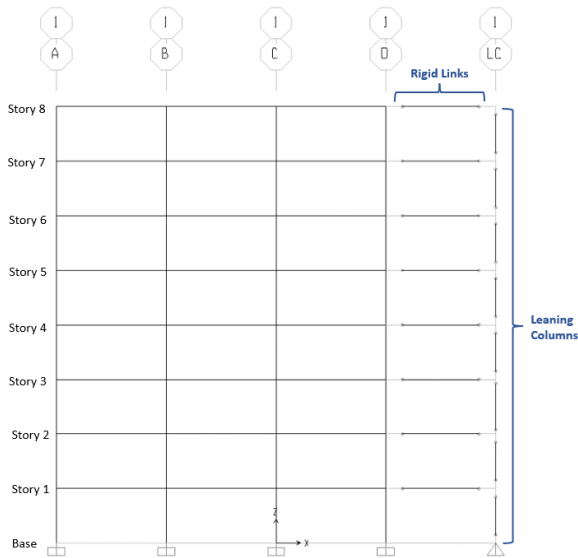
In this section, the 2015 NBCC was used to design four-, eight-, and twelve-story ductile moment resisting concrete frames as presented in Figure 3-4. The buildings consist of 3-bay by 3-bay ductile concrete moment-resisting frames (DCMRF), the height of each level is 4m with a bay length of 8m. Detailing followed the Canadian Standard for reinforced concrete buildings (CSA A23.3). The buildings are assumed to be located in Victoria, BC, in the western part of Canada with site class “C”. The 2015 NBCC prescribes ductility and overstrength factor 4 and 1.7 for ductile concrete moment-resisting frame. The compressive strength f_c' is 30 MPa, modulus of elasticity E_c is 24500 MPa, the design live and dead loads for all models are assumed to be 1.5KN/m² and 2.4 KN/m², and the snow load acting on the roof is 1.64KN/m², P-Δ effect has been considered by leaning column concept.



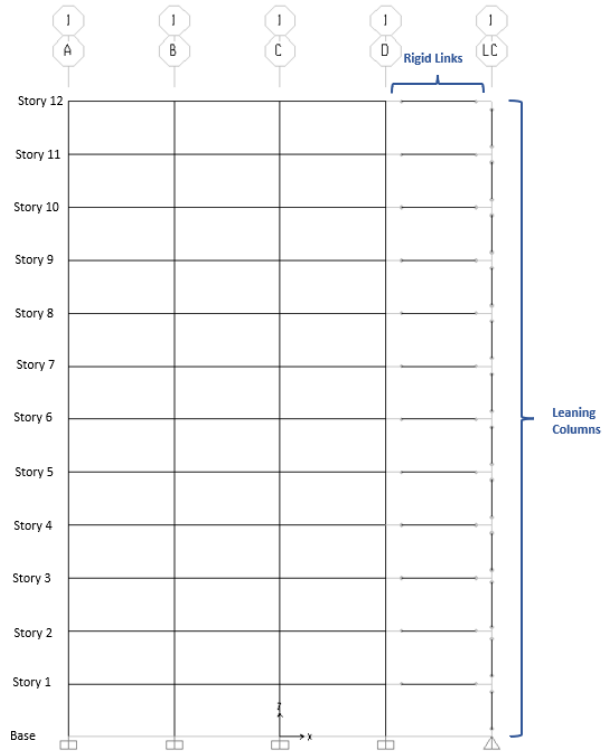
(a) plan of the buildings



(b) 4-story



(c) 8-story



(d) 12-story

Figure 3-4. The elevation views and plan of the ductile moment resisting frames (4, 8, 12-story)

The leaning column concept was utilized to simulate the effect of gravity load (Lignos et al. 2011), the presence of these columns is to capture the $P-\Delta$ correlated with gravity loads, and to ensure that there is no axial deformation along with the component. The leaning column was modeled using an elastic column element with a significantly larger cross-section area (around 100 times the column cross-section area) and a stiff link, as they will not impact the lateral load resistance system as presented in Figure 3-5. The tributary area of the concrete moment resistant frame (P_{tc}) was not taken into account while calculating the gravity loads applied to the leaning column (P_G). The design details of different frames are presented in Table 3-7, the nonlinear model for structural components is calculated and assigned to each column and beam as indicated in section 3.4.1.

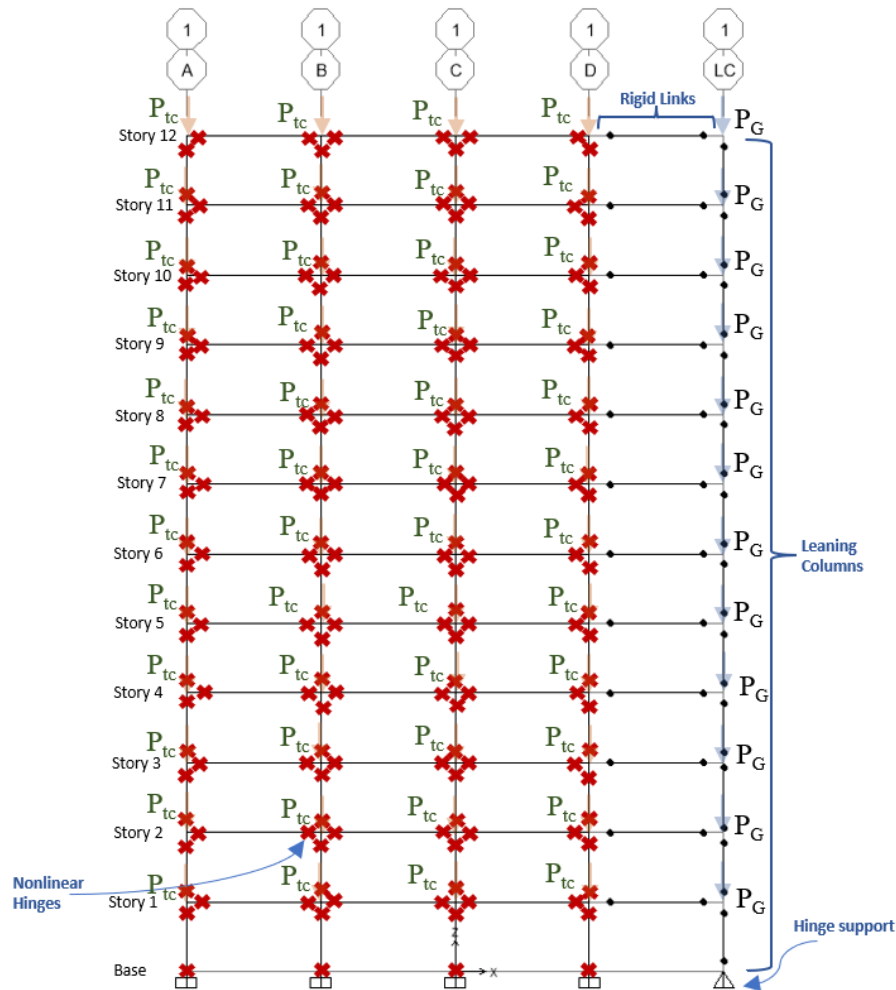


Figure 3-5. A schematic view of leaning-column concept (12-story)

Table 3-7. Design details for different models

Story	Level	Columns		Beams
		Interior (Cm)	Exterior (Cm)	Interior (Cm)
4	4	60×60	55×55	50×45
	3	60×60	55×55	50×45
	2	65×65	60×60	50×50
	1	70×70	65×65	50×50
8	8	70×70	65×65	55×50
	7	70×70	65×65	55×50
	6	75×75	70×70	60×50
	5	75×75	70×70	60×50
	4	80×80	75×75	60×50
	3	80×80	75×75	65×55
	2	80×80	75×75	65×55
	1	80×80	75×75	65×55
12	12	75×75	65×65	55×55
	11	75×75	65×65	55×55
	10	75×75	65×65	55×55
	9	80×80	70×70	60×55
	8	80×80	70×70	60×55
	7	80×80	70×70	60×55
	6	85×85	75×75	65×55
	5	85×85	75×75	65×55
	4	85×85	75×75	65×55
	3	90×90	85×85	70×60
	2	90×90	85×85	70×60
	1	90×90	85×85	70×60

3.4.1 Nonlinear Model for structural components

Plasticity can be distributed through the structural member where the Inelastic component can be identified. Figure 3-6 (a, b) are the simplest form of concentrated inelastic deformation such as plastic hinges and nonlinear spring hinges. The concentrated plasticity with moment-rotation parameters can be used to define hinges at the beginning and end of each element. The distributed plasticity can be presented by the finite length hinge model, fiber section, and finite element shown in Figure 3-6 (c,d,e) (Deierlein et al., 2010). By considering the expected behaviour of the structures, in this study concentrated hinge model was used to have better results in capturing the nonlinear degrading response of members.

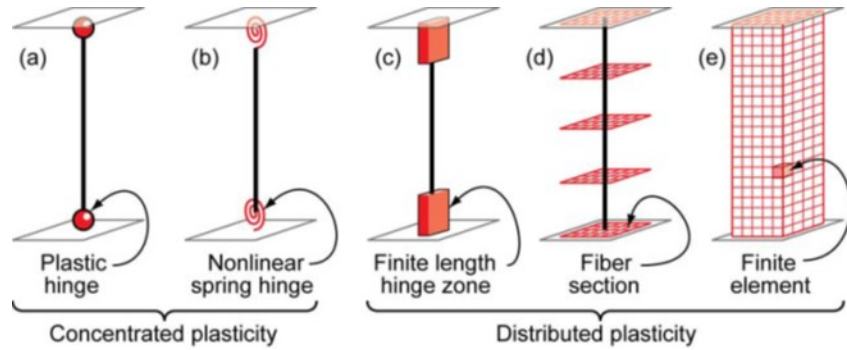


Figure 3-6. Beam-Column idealized elements (Deierlein et al., 2010)

A quasi-static member with inelastic concentrated hinges for a reinforced concrete flexural member is presented in Figure 3-7. These component modeling options are based on the deteriorating hysteretic response and backbone curve. These parameters and acceptance criteria are based on Elwood et al., 2007; Elwood and Eberhard, 2006; Haselton et al., 2007.

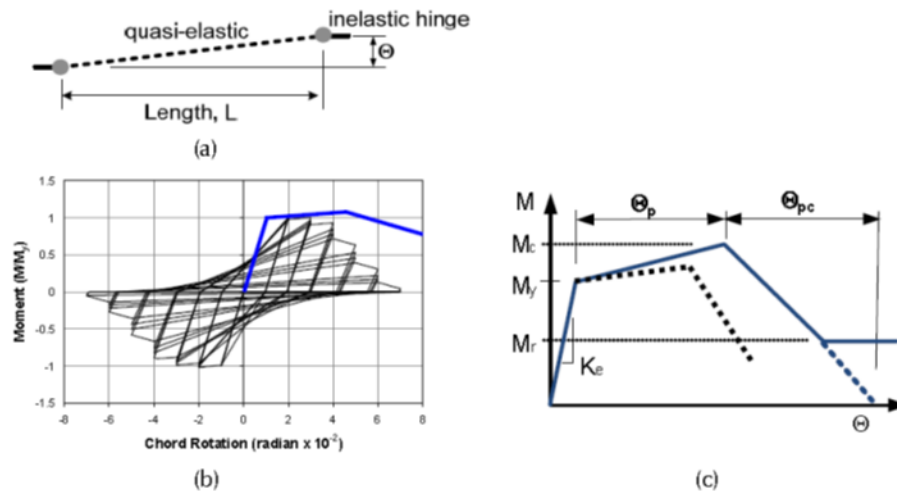


Figure 3-7. (a) Idealized flexural element (b) hysteretic response and monotonic backbone curve (c) monotonic backbone curves (PEER/ATC 72-1)

These component modeling parameters namely pre-capping, θ_p and post capping θ_{pc} plastic rotations as well as the cyclic deterioration λ are calculated based on FEMA 356 and ATC 72, the normalized moment-rotation component models for a sample calculation of beam and column of the 4-story building are presented in Figure 3-8.

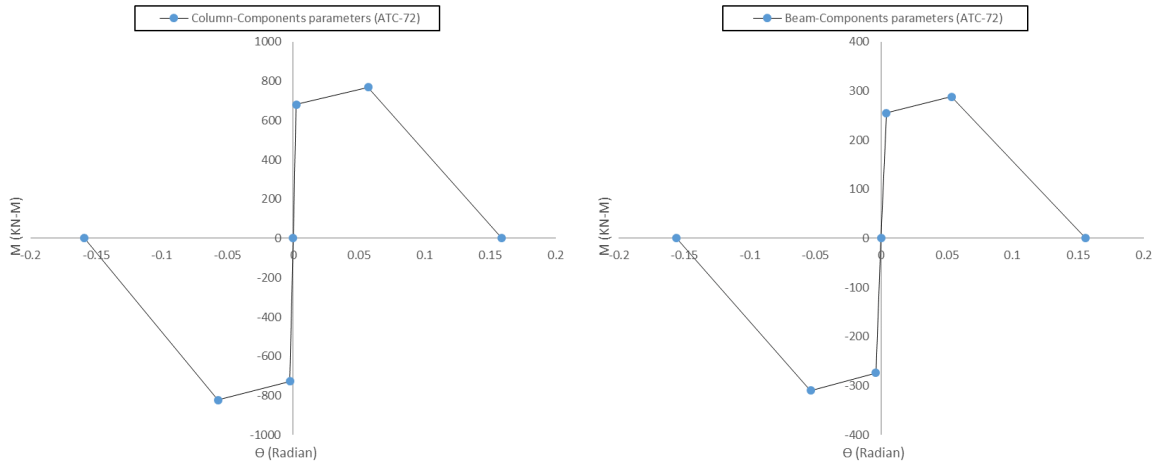


Figure 3-8. Backbone curve for 4-story building beam and column based on ATC 72

3.4.2 Modal Analysis

The calculated natural modes from Eigenvalue analysis which provides the free-vibration mode shapes and frequencies of the system were performed to determine the natural periods of the friction damper frame system. Table 3-8 shows the fundamental period of the structure based on the modal analysis and the results obtained from the 2015 NBCC Empirical equation 3.33.

$$T_a = 0.075h_n^{3/4} \quad (3.33)$$

Where T_a (s) is the fundamental lateral period and h_n is the height of the structure in meters. It can be observed that the empirical equation is more conservative which is about -32% to -45% of the estimated fundamental period.

Table 3-8. Fundamental period of the structures		
Story	Fundamental period	T _a (Empirical)
4	0.888	0.600
8	1.480	1.001
12	1.869	1.367

3.4.3 Nonlinear Static Analysis

Nonlinear static analysis involves pushing the structure under monotonically increasing lateral loads until a target displacement is exceeded. An idealized relationship between base shear and displacement shall be created to calculate the elastic lateral stiffness K_i , effective lateral stiffness K_e as well as effective yield strength V_y as presented in Figure 3-9. Idealized base shear-displacement curve (FEMA 356, 2000).

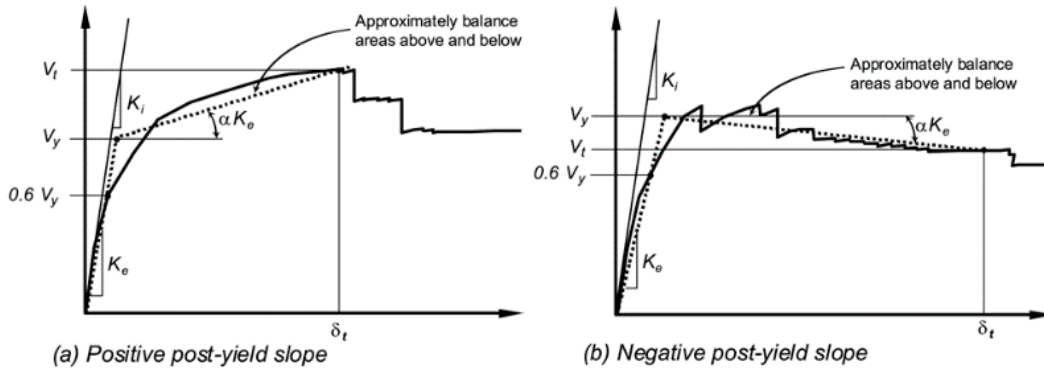


Figure 3-9. Idealized base shear-displacement curve (FEMA 356, 2000)

The mean value of the Northridge spectral acceleration for 101 different stations was calculated based on the Pacific Earthquake Engineering Research Center (PEER) and considered as a design base earthquake as shown in Figure 3-10.

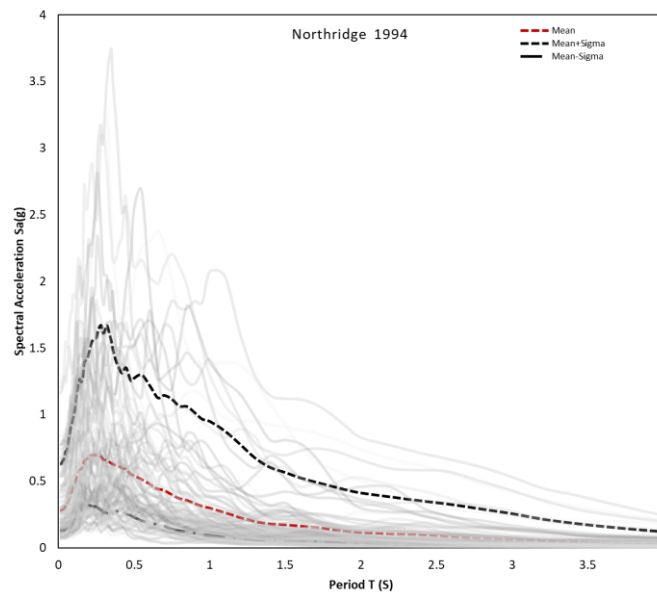


Figure 3-10. Northridge spectral acceleration for 5% damping

Component force versus deformation curves is presented in Figure 3-11. Generalized Component Force-Deformation Relations (FEMA 356, 2000). Linear response is between Points A and yield point B, the slope from B to C represents the strain hardening, line CD shows the component strength at point C and the significant strength degradation. Point E is the reduced strength, and deformation greater than point C is zero. Figure 3-11a and b show the prescribed acceptance criteria in terms of deformation and deformation ratios. Figure 3-11c shows the acceptance criteria for primary and secondary members in accordance with the target performance levels of “Immediate Occupancy” (IO), “Life Safety” (LS), and “Collapse Prevention” (CP).

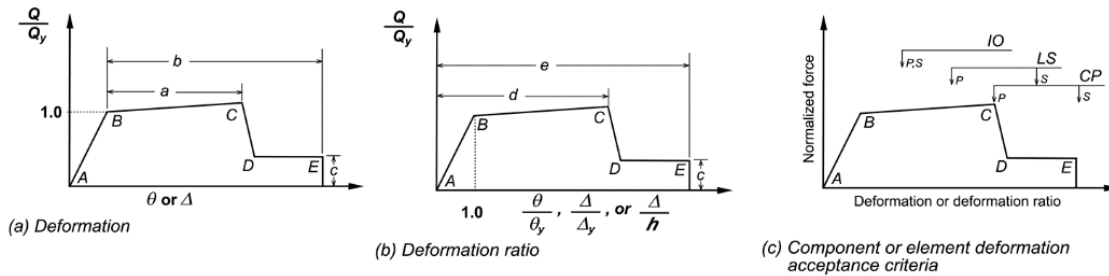


Figure 3-11. Generalized Component Force-Deformation Relations (FEMA 356, 2000)

The target displacement for building with rigid diaphragm was calculated based on FEMA-356/ASCE-41 for SLE, DLE, and MSE from Equation 3.34 and presented in Table 3-9. The effective fundamental period, T_e shall be calculated with Equation 3.35.

$$\delta_T = C_0 C_1 C_2 C_3 S_a \frac{T_e}{4\pi^2} \quad (3.34)$$

$$T_e = T_i \sqrt{\frac{K_i}{K_e}} \quad (3.35)$$

$$C_1 = 1 + \frac{R - 1}{a T_e^2} \quad (3.36)$$

$$R = \frac{S_a}{V_y/W} C_m \quad (3.37)$$

$$C_3 = 1 + \frac{|a|(R - 1)^{3/2}}{T_e} \quad (3.38)$$

Where, C_0 relate roof displacement of MDOF to spectral displacement of an equivalent SDOF, C_1 relate linear elastic response to maximum inelastic displacement, and for a period greater than 0.2 seconds shall be calculated with Equation 3.36, T_i is the elastic fundamental period, a is the site class factor and R is elastic strength demand to yield strength ratio from Equation 3.37, V_y is the yield strength, W is the seismic weight and C_m is the effective mass factor. C_2 considers the effect of pinch hysteretic shape and C_3 represents the increased displacement due to the P-Delta effect in Equation 3.38. An idealized relationship between base shear and displacement was created for all three models and the elastic lateral stiffness K_i , effective lateral stiffness K_e as well as effective yield strength V_y was extracted from the equivalent bilinear envelope.

Table 3-9. Target displacements

Hazard Level (Cm)	Number of Stories		
	4	8	12
$\delta_T(SLE)$	13.387	51.37	73.81
$\delta_T(DLE)$	36.815	141.29	202.97
$\delta_T(MCE)$	60.243	231.20	332.14

Figure 3-12 is the nonlinear static analysis curves for different hazard levels of SLE, DLE, and MCE with and without P- Δ effects. The structure remains in the elastic part in the SLE zone and the P- Δ effect can be ignored, whereas MCE the capacity of the structure was reduced when it accounts for the P- Δ effect.

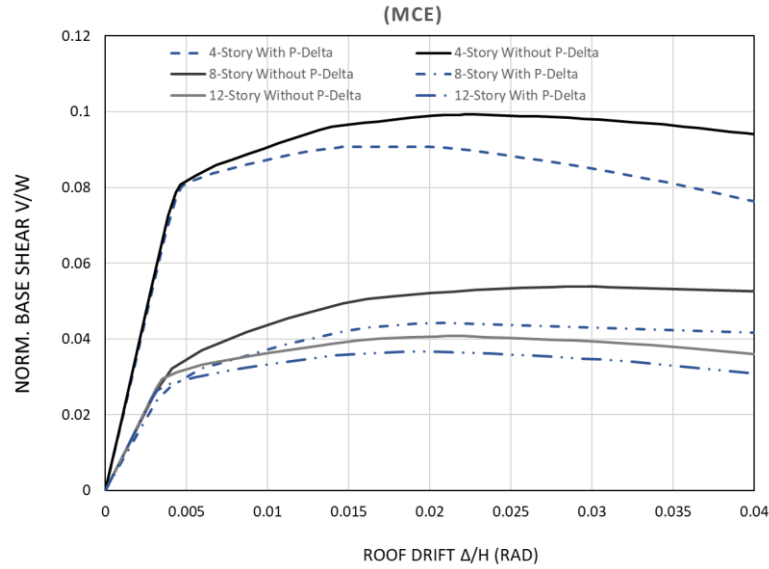


Figure 3-12. Normalized base shear vs. roof drift ratio for MCE (4,8,12-Story)

The sequence of formation of plastic hinges for 4-story in DLE and MCE at step 47 is illustrated in Figure 3-13. The dark blue color represents immediate occupancy, and the turquoise color represents life safety for DLE, which is seismically safe; however, when MCE enters the inelastic zone, the damage mechanisms of the building are formed, as shown in red.

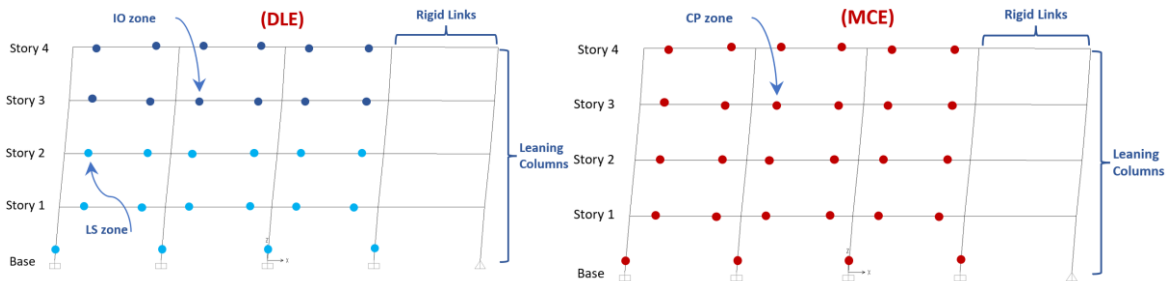


Figure 3-13. Formation of plastic hinges for 4-story (DLE & MCE)

3.4.4 Inelastic History Analysis

The connections between the response of the structure and ground-motion parameters have been explored through different strategies (Gavin et al. 2011, Cordova et al. 2001, Baker 2007). Scaling and spectral matching are two approaches for adjusting time series to be consistent with the design response spectrum.

Scaling includes multiplying the initial time series by scaling factor, then the matched spectrum is equal to or exceeds the design spectrum over a specified period range. Matching the time series frequency content to be consistent with the design spectrum is Spectral matching (Gavin et al. 2011). The higher mode effects are defined based on the NBCC 2015 by considering an additional force applied at the top of the structure, F_t , overturning moment reduction factor, J , as well as M_v , which accounts for higher mode effect on the base shear, and is dependent on the spectral ratio and period of the structure. The corresponding static force approach, however, is not viable for structures with long periods because their responses may be driven by higher modes (NBCC 2015). As a result, dynamic analysis was performed to account for higher mode effects for structures with a long period. In this part, 8 different ground motion records were obtained from the database of the Pacific Earthquake Engineering Research Center (PEER Center) as presented in Table 3-10. The accelerograms were scaled according to the design spectrum using the relevant tool in SeismoMatch 2018 software, as presented in Figure 3-14.

Table 3-10. Summary of Metadata of Selected Records

ID	Scale Factor	Earthquake	Year	Station	Magnitude	Mechanism	PGA(g)
1	1.055	Imperial Valley-02	1940	El Centro Array #9	6.95	strike slip	0.449
2	1.4274	San Fernando	1971	LA - Hollywood Stor FF	6.61	Reverse	0.491
3	1.1281	Imperial Valley-06	1979	Brawley Airport	6.53	strike slip	0.414
4	0.6086	Imperial Valley-06	1979	El Centro Differential Array	6.53	strike slip	0.511
5	0.7353	Irpinia_ Italy-01	1980	Sturno (STN)	6.9	Normal	0.351
6	1.2867	Loma Prieta	1989	Agnews State Hospital	6.93	Reverse Oblique	0.534
7	1.599	Cape Mendocino	1992	Fortuna - Fortuna Blvd	7.01	Reverse	0.385
8		Tohoko	1923		7.9	Subduction	0.453

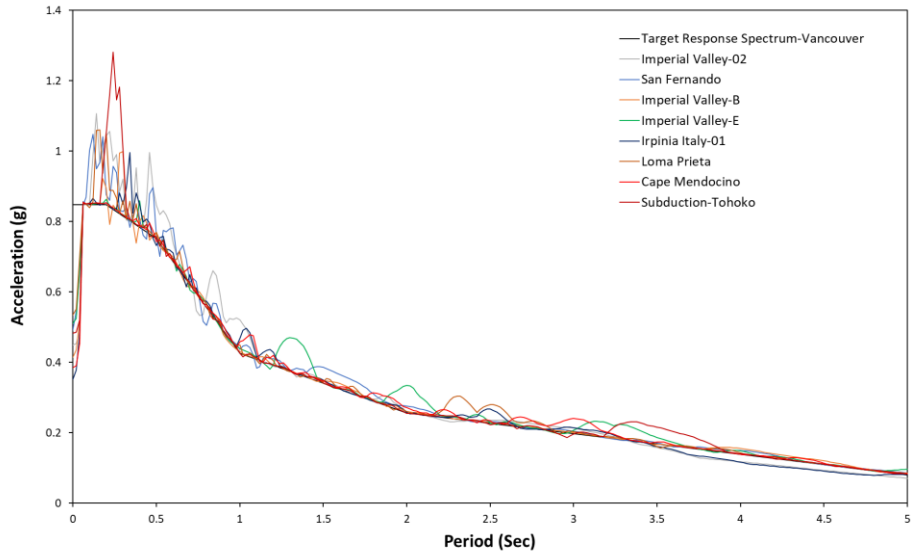


Figure 3-14. Matched Accelerograms based on the target response spectrum

3.4.5 Roof, inter-story demand results

Figure 3-15 shows the story drift ratio for the scaled ground motions as well as SDR for different MCE, DLE, and SLE of pushover analysis. As was expected, the structure remains elastic in the SLE case. Story drift ratios for MCE of all three models are greater than 2.5%, this value for SLE and DLE is below 2.5%. It can be observed from the sum of the standard deviation and the mean values that the inter-story drift is in the range of 1.5% to 2.5% which is the “Life safety” performance of the structure defined in NBCC 2005.

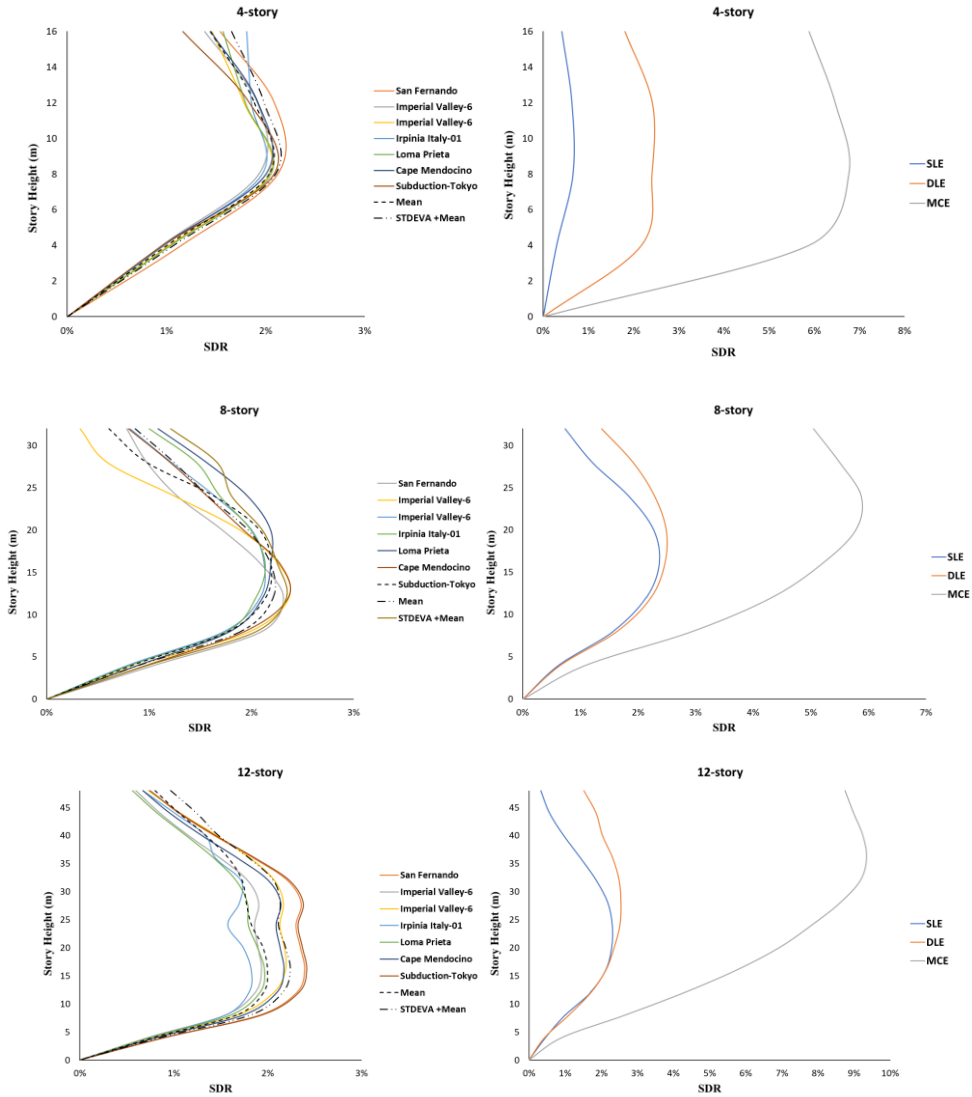


Figure 3-15. Story Drift Ratio for scaled ground motions, SLE, DLE, and MCE (4,8,12-Story)

3.4.6 Results and Discussions

It can be seen that building members can sustain earthquake damage; however, if the P-Delta effect is neglected, they will collapse due to gravity load. Furthermore, second-order effects and geometric nonlinearities have been revealed to have a significant reduction in the flexural capacity of the columns, to consider this phenomenon the strong column-weak beam approach shall be performed. Results obtained from a push-over analysis show that SLE, DLE remains in the elastic zone but MCE due to the second-order elastic analysis the structure enters in the inelastic zone.

The result indicated that there is not a significant difference between FEMA 356 and ATC 72 procedures; however, FEMA 358 is more conservative because it is based on the skeleton curve, and ATC 72 considers many parameters to quantify deterioration at each cycle and is based on the monotonic backbone curve. It is concluded that for buildings with a fundamental period of less than 0.8 second, the higher mode effects can be ignored due to the use of load pattern, which gives reliable results for rigid or short structures; however, a dynamic procedure is required for tall buildings.

3.5 Enhancing seismic safety of reinforced concrete buildings with friction dampers

When there is a significant earthquake, friction dampers absorb energy utilizing friction of two solid bodies sliding against one another, they slip at a specified load before yielding forms in a frame's members. It reduces the primary construction costs of new structures as well as retrofitting of existing structures while providing very high energy dissipation. In this section, the seismic performance of fourteen-story elastic, ductile, and moderately ductile frames using the current version of the National Building Code of Canada (NBCC, 2015) with and without friction dampers are evaluated. The structure is considered to be near Victoria, British Columbia, in the western part of Canada with site class "C". The costs of building frames with and without friction dampers were evaluated and compared. The detailed seismic performance of the structures in both cases was determined by nonlinear response analysis utilizing a set of ground motions. The results indicated the building with dampers has been proven to provide the desired level of performance without any severe damage in the frame (Naghshineh et al., 2018).

3.5.1 Overview

Six models of the selected building were designed in accordance with the broad guidelines of the NBCC (2015) as well as the equivalent lateral static load procedure. The models are including elastic frame, ductile MRF, and moderately ductile MRF, two in each category as they are the typical alternatives for a structural designer, then detailing followed by the Canadian Standard for

reinforced concrete buildings (CSA A23.3). The building consists of 5-bay in both East-west and North-South directions as presented in Figure 3-16 (Naghshineh et al., 2018).

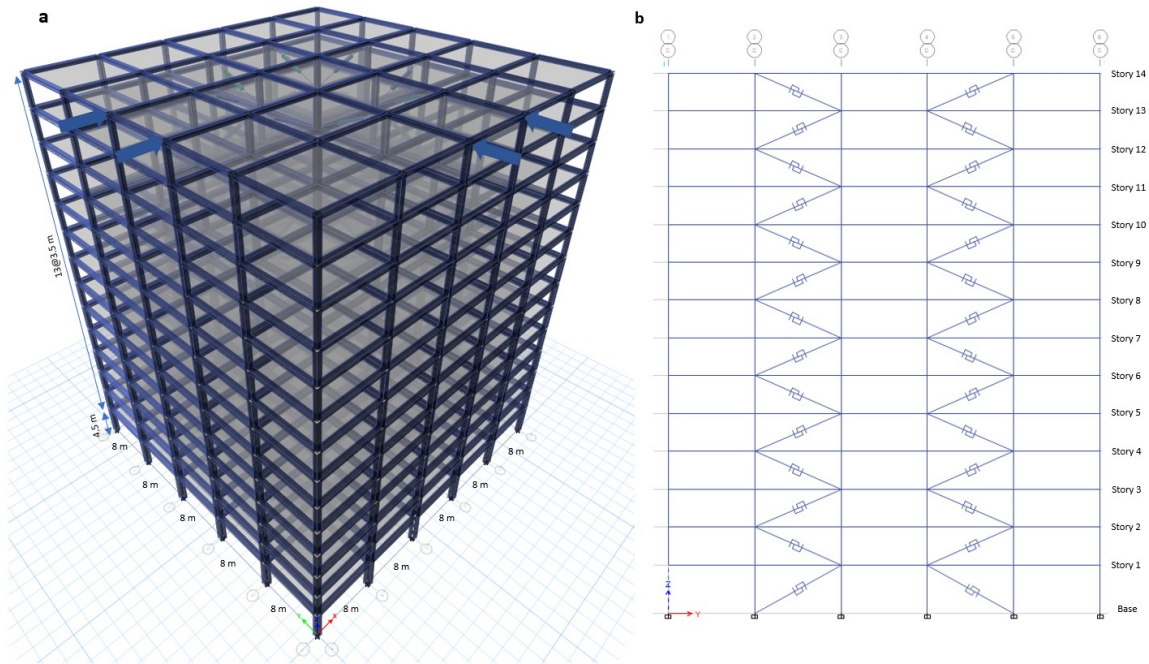


Figure 3-16. (a) 3-D Models of the building; (b) The positions of friction dampers (Naghshineh et al., 2018)

3.5.2 Work to be done by the dampers, the slip load

One of the most significant concerns in friction damper design is the amount of damping the dampers will provide to the structure. Excessive damping will make the structure too stiff, resulting in excessive design forces, and insufficient damping will cause the structure to behave independently of the damping system. As a result, the dampers should have an optimum level of shear forces in order to maximize energy dissipation while transferring the least amount of effort to the frame. This type of calibration is often carried out using nonlinear response history analysis, the purpose of this calibration is to obtain an approximation of forces taken by the dampers using the most common static analysis method. In addition, when significant damping is assigned, the static process in the codes such as FEMA P1050 (2015) tends to attribute a large reduction factor. In this assumption, the consequences of ductility are unclear, as a result, higher degrees of damping increase the stresses in members. Based on the manufacturer report (Quaketek 2016), it is feasible

to have a consistent design with maximum energy dissipation and minimum efforts transmitted to the bare frame by using a value of about 1/3rd of the story shear. This ratio was used in this study and applied to the three damped models (Naghshineh et al., 2018).

3.5.3 Material quantities and budgets

After finalizing the detailing, the steel and concrete quantities were estimated for the elastic, ductile, and moderately ductile models with and without friction dampers including labor costs, as shown in Figure 3-17.

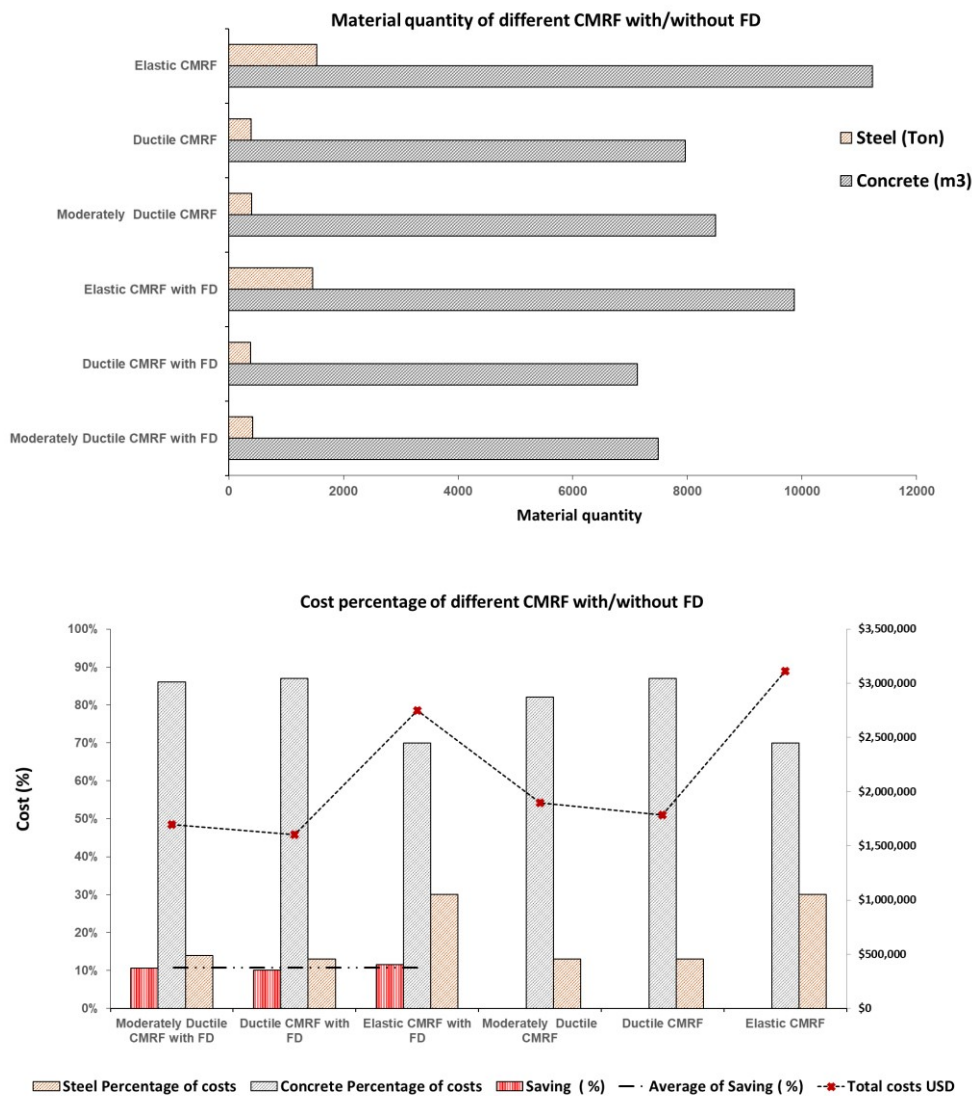


Figure 3-17. Material quantity and cost percentage of different CMRFs with/without FD (Naghshineh et al., 2018)

Different scaled ground motions based on the target response spectrum were used to verify the performance of the structures. Figure 3-18 compares the inter-story drift ratios for both models, according to the sum of the standard deviation and mean values, the friction dampers limited the inter-story drift to 1.6 percent, which is within the range of the structure's "Life safety" performance defined in NBCC 2005 (Naghshineh et al., 2018).

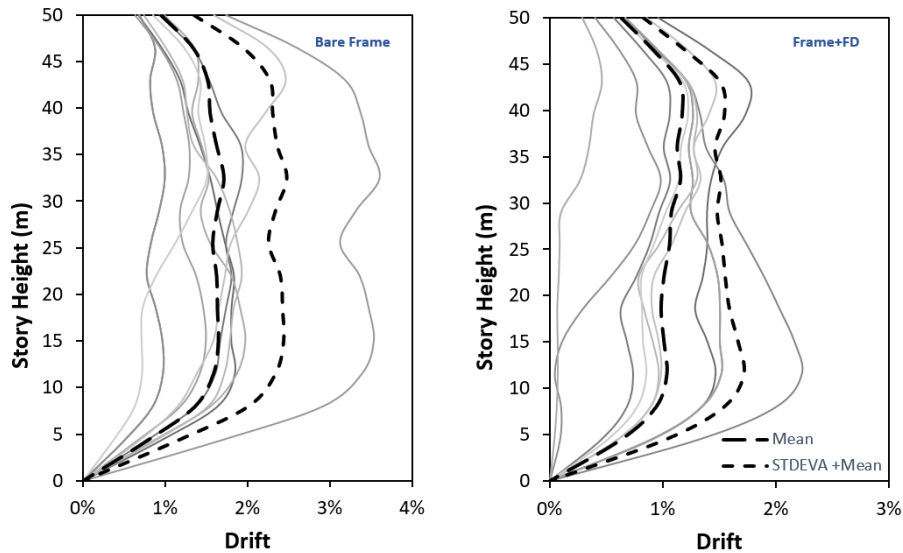


Figure 3-18. Inter story drift ratio for bare frame and frame with friction damper (Naghshineh et al., 2018)

3.5.4 Summary

This investigation provided a static force-based approach for the preliminary design of a fourteen-story reinforced concrete building with and without friction dampers. When the model with integrated friction dampers was compared to the model without friction dampers, the ductile frame's moments and shears were decreased by an average of 75%. For moderately ductile frames these values were dropped by an average of 69%. However, the moments and shears were reduced by an average of 56% in the elastic model. According to the cost analysis employing friction dampers can improve the overall performance of the building at a lower cost. The integration of friction dampers offset the cost of the damping system while enhancing the performance of the building and reducing potential damage to the primary members of the concrete frame by an average cost saving of about 11.5%. Furthermore, the models with friction dampers reduced the

formation of plastic hinges by about 45 percent, which correlates to the life safety performance. All beam-to-column joints in structural frames must satisfy the weak-beam strong-column criteria to ensure that the joint of the concrete moment resisting frames have adequate shear strength due to the maximum expected force in adjoining brace(s) in beam-column joints as stated in Appendix A3.1.

3.6 Buildings with damping devices

It is critical to determine how much damping the dampers will provide to the structure. Excessive damping causes the structure to be too rigid, resulting in excessive design forces, whereas insufficient damping causes the structure to behave independently of the damping system. In addition, the damping system differs from the seismic force-resisting system (SFRS), Figure 3-19 presents different configurations of damping systems with a seismic force-resisting system (FEMA P-2082). The purpose of this section is to determine and compare the seismic properties of eight-story special concrete moment frames (SCFRs) with damping system, using conventional seismic design methods (NBCC 2015 and ASCE 7-16) as well as methods proposed for structure with damping system (FEMA P-2082/1050, FEMA P-2082, FEMA 450, FEMA 420, ASCE 7). The results cover a comparison of the calculated base shear, as well as damping properties and displacement, velocity, and their acceptance criteria.

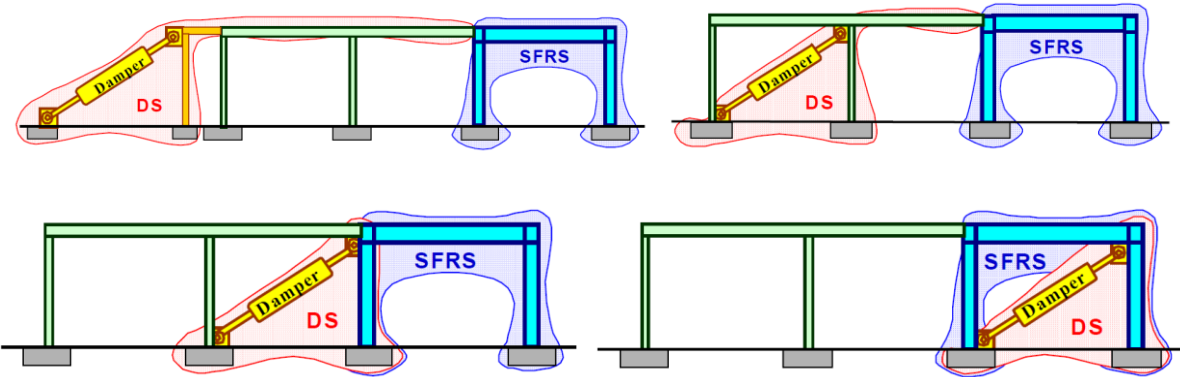


Figure 3-19. Schematic view of the seismic force-resisting system (SFRS) and Damping system (DS) (FEMA P-2082)

The damping system can be external or internal with and without share elements with SFRS. The seismic force-resisting system without a damping system should be designed for at least 75% of the conventional base shear, and the damping system should be designed based on MCE_R (ASCE 7). A damping device is a component which by relative movement at the end of the device dissipates energy and shall be classified into the following groups:

- Displacement-dependent:

The response force is a function of relative displacement between each end of the device and it is independent of the relative velocity.

- Velocity-dependent:

The response force is a function of relative velocity between each end of the device and it may be a function of relative displacement.

The scope of this section is to design structures with a damping system using the equivalent lateral force procedure. The Equivalent lateral force procedure permitted to be used for the design of a structure that all the following criteria apply (FEMA P-2082):

- I. The damping system designed to resist torsion has at least two damping devices in each story.
- II. $\beta_{mD}(m = 1) < 35\%$ of critical and β_{mD} : Total effective damping of the m^{th} mode of vibration of the structure.
- III. The seismic force-resisting system does not have plan irregularity
- IV. Rigid floor diaphragm.
- V. Height of the structure $\leq 30\text{m}$.
- VI. Spectral response acceleration, S_1 , should be below 0.6.

3.6.1 The seismic design requirement for structural with damping system

The important design criteria procedures of an 8-story

- The seismic force-resisting system shall be modeled consistently, and the structure shall be fixed at the base.

- Damping system elements shall be modeled to determine design forces from damping devices to both the ground and seismic force-resisting system.
- The effective stiffens of velocity-dependent damping devices shall be modeled
- Damping devices should not be explicitly modeled
- The stiffness and damping properties shall be based on or verified by prototype tests

The following calculation steps are for an 8-story special reinforced concrete moment frames (SMFs) equipped with friction dampers, which is assumed to be located in Riverside, Los Angeles California, seismic design factors are presented in Table 3-11.

Table 3-11. SFRSs’ design coefficients

Location	Direction	Frame Type	R	R _d	R ₀	C _d	Ω ₀	I _e
Riverside	N-S &E-W	Special reinforced concrete moment frames (ASCE), and Ductile Concrete moment resisting frame (NBCC)	8	4	1.7	5.5	3	1.0

3.6.2 Seismic design parameters

An 8-story medical office building located in Riverside, Los Angeles California, as shown in Figure 3-20, the building has special reinforced concrete moment frames (SMFs) equipped with friction dampers. The risk category is II and the site class is type C with very dense soil.



Figure 3-20. Site location (SEAOC and OSHPD, 2020)

The spectral response acceleration for 5% damped maximum considered earthquake at 1 second, S_{M1} and short period, S_{Ms} , modified based on-site class, can be determined from equations 3.39 and 3.40.

$$S_{Ms} = F_a S_s = 1.20 \times 1.50 = 1.80 \quad (3.39)$$

$$S_{M1} = F_v S_1 = 1.418 \times 0.582 = 0.825 \quad (3.40)$$

Design seismic spectral acceleration at a short period, S_{DS} , and 1 second period, S_{D1} , is about 66% of spectral response acceleration and can be determined from equations 3.41 and 3.42.

$$S_{DS} = \frac{2}{3} S_{Ms} = \frac{2}{3} \times 1.80 = 1.20 \quad (3.41)$$

$$S_{D1} = \frac{2}{3} S_{M1} = \frac{2}{3} \times 0.825 = 0.55 \quad (3.42)$$

T_s and T_0 can be determined from equations 3.43 and 3.44.

$$T_s = \frac{S_{D1}}{S_{DS}} = \frac{0.55}{1.20} = 0.458 \text{ sec} \quad (3.43)$$

$$T_0 = 0.2 \times \frac{S_{D1}}{S_{DS}} = 0.2 \times 0.458 = 0.092 \text{ sec} \quad (3.44)$$

A summary of seismic design parameters is presented in Table 3-12, calculated MCE_R and design response spectrum are presented in Figure 3-21.

Table 3-12. Seismic design parameters (ASCE 7-16)

Type	Value	Description
$S_s(g)$	1.5	MCE_R for 0.2 second
$S_i(g)$	0.582	MCE_R for 1.0 second
$S_{MS}(g)$	1.8	Site modified spectral acceleration
$S_{MI}(g)$	0.825	Site modified spectral acceleration
$S_{DS}(g)$	1.2	Numeric seismic design value at 0.2 second
$S_{DI}(g)$	0.55	Numeric seismic design value at 1.0 second
F_a	1.2	Site amplification factor at 0.2 second
F_v	1.418	Site amplification factor at 1.0 second
PGA(g)	0.5	MCE_G peak ground acceleration
T_s	0.458	S_{DI}/S_{DS}
T_0	0.092	20% of T_s
$T_L(\text{Sec})$	8	Long period

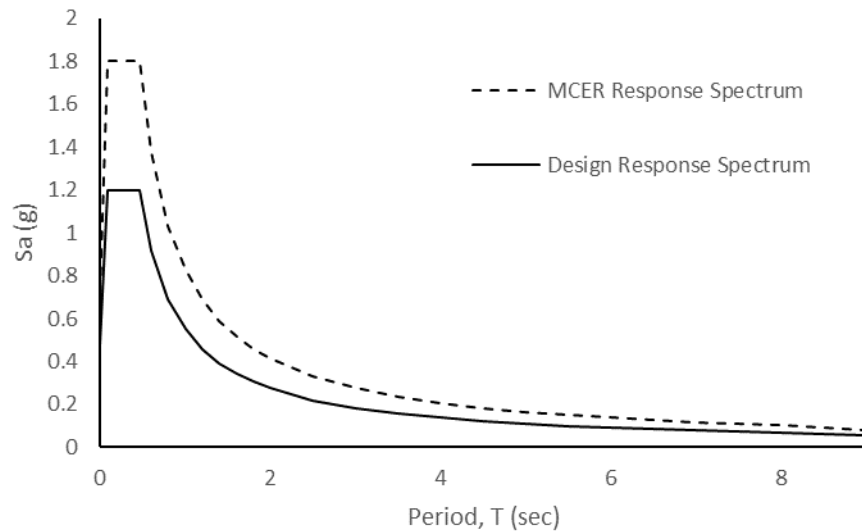


Figure 3-21. MCE_R and Design response spectrum

3.6.3 Determination of fundamental period based on the ASCE 7-16 and the NBCC 2015

In the ASCE 7-16, the approximate fundamental period can be calculated from equation 3.45, where h_n , is the height of the structure, C_t and x are the period parameters and depend on types of

structural systems. The upper limit coefficient, C_u , depends on the design spectral response acceleration.

$$T_a = C_t h_n^x \leq C_u T_a \quad (3.45)$$

The NBCC 2015 recommends equations 3.46 and 3.47 for the fundamental period of concrete moment frame and brace frame. The maximum fundamental period is limited to 150% and 200% of the calculated fundamental period for the moment-resisting frame and braced frame respectively.

$$T_a = 0.075 h_n^{0.75} \leq C_u T_a \quad (3.46)$$

$$T_a = 0.025 h_n \leq C_u T_a \quad (3.47)$$

The calculation of the approximate fundamental period and its upper limit based on the ASCE 7-16 and the NBCC 2015 as well as the analytical period of the structure for both bare frame and the frame equipped with friction dampers are presented in Table 3-13.

Table 3-13. The approximate, upper limit and analytical fundamental period of the structure

Type of system	Period parameters				Empirical equation (Sec)				Analytical	
	C_u ASCE	C_u NBCC	C_t	x	h_n (m)	T_a (ASCE)	T_{au} (ASCE)	T_a (NBCC)	T_{au} (NBCC)	T_a (Sec)
BF	1.4	1.5	0.0466	0.9	29	0.96	1.35	0.94	1.41	1.28
ISFD	1.4	2.0	0.0488	0.75	29	0.61	0.85	0.73	1.45	0.85

Note: BF is the bare frame and ISFDS is inline seismic friction damper

The modal periods and frequencies of the analytical results for the first 12 Modes are presented in Table 3-14.

Table 3-14. Analytical modal period and frequencies

Case	Step Number	Period (Sec)	Frequency (Cyc/sec)	Circ. Freq. (rad/sec)	Eigenvalue rad2/sec2
Modalritz	1	1.287	0.777	4.881	23.829
Modalritz	2	0.451	2.219	13.942	194.366
Modalritz	3	0.249	4.013	25.214	635.741
Modalritz	4	0.190	5.251	32.990	1088.333
Modalritz	5	0.173	5.778	36.301	1317.771
Modalritz	6	0.160	6.256	39.306	1544.929
Modalritz	7	0.150	6.688	42.021	1765.764
Modalritz	8	0.122	8.187	51.444	2646.441
Modalritz	9	0.112	8.955	56.264	3165.596
Modalritz	10	0.110	9.054	56.888	3236.246
Modalritz	11	0.109	9.170	57.620	3320.020
Modalritz	12	0.100	9.989	62.761	3938.983

3.6.3.1 Equivalent lateral force procedure for a structure without a damping system

3.6.3.1.1 Seismic force-resisting system base shear based on the ASCE 7 Procedure

The conventional seismic base shear, V , and its response coefficient, C_s , shall be calculated from equations 3.48 and 3.49, for further information please refer to section 3.4.1.3 of this thesis, these values are presented in Table 3-15.

$$V = C_s W \quad (3.48)$$

$$0.01 \leq 0.044 S_{DS} I_e \leq C_s = \frac{S_{DS}}{(R/I_e)} \leq \frac{S_{D1}}{T(R/I_e)} \quad (3.49)$$

Table 3-15. Seismic base shear

Story	C_s	C_s (Max)	C_s (Min)	C_s (Final)	W(KN)	V (KN)
8	0.15	0.072	0.053	0.072	35658	2554

W is the effective seismic weight should include the following loads:

- The dead loads of all materials as defined in chapter 3 of ASCE 7.
- The 25% of the live load of the storage area, except for the public garage live load and when it is less than 5% of the W.
- The maximum value of the weight of the partition or 0.48 KN/m².

- Equipment load.
- The 20% of the snow load is applicable when it exceeds 1.44 KN/m².
- Weight of the other materials if applicable.

3.6.3.1.2 Seismic force distribution (ASCE)

The seismic lateral force shall be calculated with equations 3.50 and 3.51.

$$F_x = C_{vx}V \quad (3.50)$$

$$C_{vx} = \frac{w_x h_x^k}{\sum_{i=1}^n w_i h_i^k} \quad (3.51)$$

Where C_{vx} is the distribution factor, and K is an exponent depending on the structural period.

The equivalent lateral forces are presented in Table 3-16.

Table 3-16. Equivalent lateral forces

Level	W_x (KN)	h_x (m)	$W_x \cdot h_x$	C_{vx}	F_x (KN)	V_x (KN)	M_x (KN-m)
Roof	3893	29	244939	0.068	174	0	0
7	8155	25.5	437986	0.122	311	174	608
6	12540	22	561649	0.156	398	484	2304
5	16924	18.5	612542	0.170	434	883	5393
4	21374	15	597694	0.166	424	1317	10004
3	25932	11.5	522983	0.145	371	1741	16098
2	30640	8	395452	0.110	281	2112	23491
1	35658	4.5	226779	0.063	161	2393	31866
Base	-	0	3600023	1.000	2554	2554	43357

3.6.3.1.3 Seismic force-resisting system base shear based on the NBCC Procedure

The base shear, V , can be determined from equation 3.52. This value shall not be less than the minimum base shear in Equation 3.53 for moment-resisting frames and shall not be greater than equation 3.54 for all site classes except site class F, as well as ductility reduction factor greater than 1.5.

$$V = \frac{S(T_a)M_v I_E W}{R_d R_o} \quad (3.52)$$

$$V_{min} = \frac{S(2.0)M_v I_E W}{R_d R_o} \quad (3.53)$$

$$V_{max} = Max \left(\frac{2 S(0.2) I_E W}{3 R_d R_o}, \frac{S(0.5) I_E W}{R_d R_o} \right) \quad (3.54)$$

The value of $S(T_a)$ can be determined by linear interpolation between the values of design spectral acceleration, $S(T)$. The seismic base shear, V , and seismic response coefficient, C_N , are presented in Table 3-17.

Table 3-17. Seismic base shear

Story	C_N	C_N (Max)	C_N (Min)	C_N (Final)	W(KN)	V (KN)
8	0.075	0.168	0.041	0.075	35658	2688

3.6.3.1.4 Seismic force distribution (NBCC)

The seismic lateral force shall be calculated with equations 3.55 and 3.56.

$$F_x = C_{vN}(V - F_t) \quad (3.55)$$

$$C_{vN} = \frac{w_x h_x}{\sum_{i=1}^n w_i h_i} \quad (3.56)$$

Where C_{vN} is the distribution factor, F_t is the concentrated lateral force at the roof, which relates to the fundamental period of the structure and shall be less than 25% of the base shear, and the remaining $V-F_t$ shall be distributed along the height of the structure (Section 3.4.1.2 of thesis). The equivalent lateral forces are presented in Table 3-18.

Table 3-18. Equivalent lateral forces

Level	W_x (KN)	h_x (m)	$W_x * h_x$	C_{vN}	F_x (KN)	V_x (KN)	J_x	M_x (KN-m)
Roof	3893	29	244939	0.058	323	0	1.000	0
7	8155	25.5	437986	0.108	270	323	1.000	1132
6	12540	22	561649	0.143	358	593	1.000	3209
5	16924	18.5	612542	0.162	407	952	1.000	6540
4	21374	15	597694	0.166	416	1358	0.996	11274
3	25932	11.5	522983	0.154	387	1775	0.990	17422
2	30640	8	395452	0.127	318	2162	0.984	24865
1	35658	4.5	226779	0.083	208	2480	0.978	33352
Base	-	0	3600023	1.000	2688	2688	0.970	45087

3.6.3.1.5 Structural Irregularities

Two effects shall be considered when using ELF, the structure shall be checked for inertial forces which produce a “critical load effect”, this can be defined by 100/30 rules, this can be used for irregular structures. The other factor accounts for uncertainties for central mass and rigidity, seismic forces’ torsional component, and irregular yielding of structural vertical members (FEMA 451). In ASCE 7-10, where the diaphragm was rigid, accidental torsion was applicable for all types of systems; however, these criteria were changed to the existence of an irregularity or extreme torsional in ASCE 7-16.

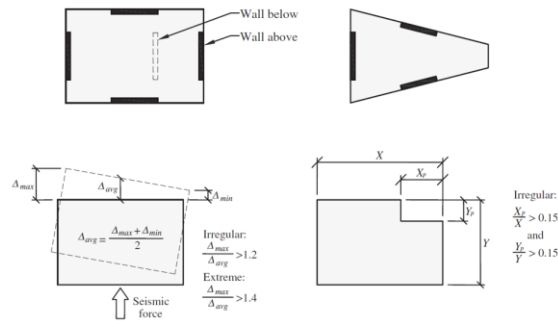


Figure 3-22. Torsional irregularity and amplification factor (ASCE 7, FEMA 451)

Horizontal structural irregularities defined based on seismic define category (ASCE 7), where there is torsional or extreme torsional irregularity, torsional amplification factor, A_x , from equation 3.57, shall be multiplied by accidental torsion moments at each level. Torsional irregularities and torsional amplification factors are presented in Figure 3-22. Table 3-19 presents the determined torsional irregularities, the structure does not have any torsion irregularities and the torsional amplification factor is not applicable.

$$A_x = \left[\frac{\delta_{max}}{1.2\delta_{avg}} \right]^2 \quad (3.57)$$

Table 3-19. Torsion irregularities

Level	δ_1	δ_2	δ_{avg}	δ_{max}	$\delta_{max}/\delta_{avg}$	Irregularities
Roof	0.00061	0.00071	0.00066	0.00071	1.079	Non-Irregular
7	0.00078	0.00092	0.00085	0.00092	1.081	Non-Irregular
6	0.00092	0.00108	0.00100	0.00108	1.081	Non-Irregular
5	0.00097	0.00114	0.00106	0.00114	1.082	Non-Irregular
4	0.00093	0.00109	0.00101	0.00109	1.081	Non-Irregular
3	0.00093	0.00109	0.00101	0.00109	1.081	Non-Irregular
2	0.00080	0.00094	0.00087	0.00094	1.084	Non-Irregular
1	0.00038	0.00045	0.00041	0.00045	1.085	Non-Irregular

3.6.3.1.6 Drift and P-Delta check

Allowable story drift depends on the structural type and the risk categories, in this study the allowable drift ratio is limited to 2% of the story height. The maximum inelastic displacement, δ_M , shall be determined based on equation 3.58, where δ_M is the maximum elastic deformation. The results of the allowable story drift ratio are tabulated in Table 3-20.

$$\delta_M = \frac{C_d \delta_{max}}{I_e} \quad (3.58)$$

Table 3-20. Equivalent lateral force procedure drift calculation for BF

Level	Story Height (mm)	Total Elastic Drift (mm)	Elastic story Drift (mm)	Inelastic story drift (mm)	Drift ratio (%)	Scale factor	Scaled inelastic Drift (mm)	Allowable Drift (mm)
Roof	3500	41.2	3.58	19.69	0.56	1.36	26.75	70
7	3500	37.62	4.87	26.79	0.77	1.36	36.39	70
6	3500	32.75	5.78	31.79	0.91	1.36	43.19	70
5	3500	26.97	6.29	34.60	0.99	1.36	47.00	70
4	3500	20.68	6.36	34.98	1.00	1.36	47.52	70
3	3500	14.32	5.8	31.90	0.91	1.36	43.34	70
2	3500	8.52	5	27.50	0.79	1.36	37.36	70
1	4500	3.52	3.52	19.36	0.43	1.36	26.30	90
Base	0	0	0	0	-	-	-	-

The P-Delta effect shall be ignored when the stability coefficient from equation 3.59 is equal to or less than 0.1. In this equation, P_x is the total gravity loads at story x and above with the load factor one, Δ is the story drift, and β is the shear demand over capacity ratio, calculation of the stability ratio is presented in Table 3-21.

$$\theta = \frac{P_x \Delta I_e}{V_x h_{sx} C_d} \leq \frac{0.5}{\beta C_d} \leq 0.25 \quad (3.59)$$

Table 3-21. Stability coefficient

Level	Story drift (mm)	Story Shear (KN)	Story DL (KN)	Story LL(KN)	Total load (KN)	Accumulative Load (KN)	Stability Ratio
Roof	19.69	174	2560	3840	6400	6400	0.038
7	26.79	484	2560	3840	6400	12800	0.037
6	31.79	883	2560	3840	6400	19200	0.036
5	34.60	1317	2560	3840	6400	25600	0.035
4	34.98	1741	2560	3840	6400	32000	0.033
3	31.90	2112	2560	3840	6400	38400	0.030
2	27.50	2393	2560	3840	6400	44800	0.027
1	19.36	2554	2560	3840	6400	51200	0.016

3.6.3.2 Equivalent lateral force for a structure with a damping system

3.6.3.2.1 Seismic force-resisting system base shear

The seismic base shear shall be determined with equation 3.60.

$$V = \sqrt{V_1^2 + V_R^2} \geq V_{min} \quad (3.60)$$

Where V_1 and V_R are the base shears of the fundamental and residual modes from equations 3.61, and 3.62. V_{min} is the minimum permitted base shear value and can be determined from the maximum value in equation 3.63.

$$V_1 = C_{s1} \bar{W}_1 \quad (3.61)$$

$$V_R = C_{SR} \bar{W}_R \quad (3.62)$$

$$V_{min} = \max\left(\frac{V}{B_{V+1}}, 75\%V\right) \quad (3.63)$$

In the equations above, C_{s1} and C_{SR} are the fundamental and residual mode seismic response coefficients, \bar{W}_1 is the gravity load and a portion of the live load of the effective fundamental mode, and \bar{W}_R is the effective residual gravity load.

3.6.3.2.2 Steps in the calculation of fundamental mode base shear

3.6.3.2.2.1 Effective seismic weight

The effective base mode seismic weight can be determined from equation 3.64. In this equation, w_i , is the portion of the effective seismic weight, and ϕ_{i1} , is the normalized amplitude of displacement for the base mode of vibration. Modal participation factor, Γ_1 , can be calculated from equation 3.65.

$$\overline{W}_1 = \frac{(\sum_{i=1}^n w_i \phi_{i1})^2}{\sum_{i=1}^n w_i \phi_{i1}^2} \quad (3.64)$$

$$\Gamma_1 = \frac{\overline{W}_1}{\sum_{i=1}^n w_i \phi_{i1}} \quad (3.65)$$

The results of calculated effective seismic weight, as well as modal participation factor, are presented in Table 3-22.

Table 3-22. First mode for effective seismic weight and modal participation factor

Level	h_x (m)	Cumulative weight (W_i , KN)	ϕ_{i1}	Cumulative ($W_i \times \phi_{i1}$)	Cumulative ($W_i \times \phi_{i1}^2$)	Cumulative ($W_i \times \phi_{i1}^2$)	W_1 (KN)	Γ_1
Roof	29	3893	1.000	3893	15157162	3893	3893	
7	25.5	12048	0.879	11064	122408891	10198	12003	
6	22	24588	0.759	20577	423399987	17415	24312	
5	18.5	41512	0.638	31373	984284645	24303	40501	1.788
4	15	62886	0.517	42429	1800207225	30021	59965	
3	11.5	88818	0.397	52712	2778561451	34099	81486	
2	8	119458	0.276	61165	3741103864	36430	102692	
1	4.5	155116	0.155	66698	4448574722	37289	119300	

3.6.3.2.2.2 Base mode properties

The Fundamental mode properties are calculated with equation 3.66 and presented in Table 3-23. Where W_i is the effective seismic weight, f_i is the ELF lateral force, and δ_i is the elastic deflection due to the lateral load.

$$T_1 = 2\pi \sqrt{\frac{\sum_{i=1}^n W_i \delta_i^2}{g \sum_{i=1}^n f_i \delta_i}} \quad (3.66)$$

Table 3-23. Fundamental mode properties

Level	h _x (m)	W _i (KN)	δ _i (ELF) (mm)	W _i × δ _{i2} (KN-mm2)	f _i (KN)	f _i × δ _i (KN-mm)	T ₁ (Sec)
Roof	29	3893	41.2	6608507	174	7158	2.012
7	25.5	8155	37.62	11541255	311	11688	
6	22	12540	32.75	13449548	398	13047	
5	18.5	16924	26.97	12310514	434	11718	
4	15	21374	20.68	9140873	424	8768	
3	11.5	25932	14.32	5317592	371	5312	
2	8	30640	8.52	2224193	281	2390	
1	4.5	35658	3.52	441812	161	566	

3.6.3.2.2.3 Damping modification factors

The effects of the damping system shall be applied to the primary structural response, for this purpose the effective damping can be calculated with equation 3.67. The effective damping of the maximum considered earthquake displacement, β_{mM} is a combination of inherent damping β_I, supplemental damping, β_{Vm}, and hysteresis damping, β_{HM}.

$$\beta_{mM} = \beta_I + \beta_{Vm} \sqrt{\mu_M} + \beta_{HM} \quad (3.67)$$

Inherent damping depends on the type of material, structural and nonstructural elements behaviour, the recommended value by the ASCE 7 is below or equal to 3%. Supplemental damping considers the damping devices work in one cycle, W_{mj}, inertial force, F_{im}, deflection, δ_{im}, and maximum strain energy, W_m. Finally, the hysteresis damping is based on the inherent damping, ductility demand, and pinching effect, which is a factor and is considered by 67% of the short period over the first mode of the fundamental period. Therefore, equation 3.67 can be rewritten as equation 3.68.

$$\beta_{mM} = \beta_I + \frac{\sum_j W_{mj}}{4\pi W_m} \sqrt{\mu_M} + 0.41 \left(\frac{T_S}{T_1} \right) \left[1 - \frac{1}{\mu_M} \right] \quad (3.68)$$

Where W_m is the maximum strain energy due to inertia lateral force, which differs from modal weight, and can be calculated with equation 3.69.

$$W_m = \frac{1}{2} \sum_i F_{im} \delta_{im} \quad (3.69)$$

Where δ_{im} , is the deflection at level i , F_{im} is the inertia force from equation 3.70. Viscous damping parameters are calculated and presented in Table 3-24.

$$F_{i1} = w_i \varphi_{i1} \frac{\Gamma_1}{W_1} V_1 \quad (3.70)$$

Table 3-24. Supplemental damping parameters

Level	F_{i1} (KN)	δ_{im} (mm)	W_m (KN-mm)	W_{mj} (KN-mm)
Roof	149	35.35	2634	4215
7	275	33.24	4563	7301
6	364	29.94	5452	8724
5	413	25.66	5303	8485
4	423	20.65	4370	6991
3	394	15.20	2992	4787
2	324	9.83	1590	2545
1	212	4.64	491	786

Damping modification factors including inherent damping β_I , supplemental damping, β_{Vm} , hysteresis damping, β_{HM} and effective damping, β_{mM} , are determined and presented in Table 3-25.

Table 3-25. Damping modification factors

Inherent damping β_I (%)	Supplemental damping β_{Vm} (%)	Hysteresis damping β_{HM} (%)	Effective damping β_1 (%)	Damping coefficient β_{IM}
3	12	19	42	2.18

3.6.3.2.2.4 Fundamental mode base shear

The first step is to calculate the effective ductility demand, μ_M , and effective fundamental period, T_{1M} , based on the maximum considered earthquake using equation 3.71. The short period is less than the design and maximum fundamental period, therefore the seismic response coefficient of the fundamental mode can be determined with equation 3.72.

$$T_{1M} = T_1 \sqrt{\mu_M} \quad (3.71)$$

$$\text{If } T_{1M} \geq T_S, C_{SI} = \left(\frac{R}{C_d} \right) \frac{S_{M1}}{T_{1M}(\Omega_0 B_{1M})} \quad (3.72)$$

Herein, B_{1M} is the numerical coefficient, which depends on the effective damping and the effective fundamental period, this value is calculated in section 3.8.4.2.1.4. The summary results of different fundamental modes, seismic response coefficient, and fundamental mode base shear are presented in Table 3-26.

Table 3-26. Summary of different fundamental mode base shear parameters

Spectral acceleration		20% T_s	Short period	Fundamental period of 1 st mode	Effective fundamental period	Coefficient		Fundamental mode Base shear (KN)	
S_{MS} (g)	S_{MI} (g)	T_0 (Sec)	T_s (Sec)	T_1 (Sec)	T_{1M} (Sec)	C_{SID}	C_{SIM}	V_{1D}	V_{1M}
1.8	0.825	0.092	0.458	2.012	3.28	0.037	0.055	4520	6643

3.6.3.2.3 Steps in the calculation of residual mode base shear

3.6.3.2.3.1 Damping modification factors

The effective damping, β_{mM} , can be determined with equation 3.73. Since the properties of inherent damping, β_I , and hysteresis damping, β_{HM} , are independent of damping, these values are the same as the calculated values in section 3.8.3.2.2.3.

$$\beta_{mM} = \beta_I + \beta_{VR}\sqrt{\mu_M} + \beta_{HM} \quad (3.73)$$

Residual supplemental damping, β_{VR} , can be determined with equation 3.74. In this equation, W_{Rj} , is the residual damping device that work in one cycle, and W_R , is the maximum residual strain energy from equation 3.75.

$$\beta_{vR} = \frac{\sum_j W_{Rj}}{4\pi W_R} \quad (3.74)$$

$$W_R = \frac{1}{2} \sum_i F_{iR} \delta_{iR} \quad (3.75)$$

Where F_{iR} is the residual response from equation 3.76 and δ_{iR} , is the residual mode deflection. The parameters of F_{iR} are explained and determined in section 3.8.3.2.3.2.

$$F_{iR} = w_i \phi_{iR} \frac{\Gamma_R}{\bar{W}_R} V_R \quad (3.76)$$

3.6.3.2.3.2 Determination of residual modal properties

The residual modal shape, ϕ_{iR} , residual participation factor, Γ_1 , and residual seismic weight, \bar{W}_R , can be determined from equations 3.77 to 3.79. The properties of residual modal and supplemental damping properties are presented in Table 3-27.

$$\phi_{iR} = \frac{1 - \Gamma_1 \phi_{i1}}{1 - \Gamma_1} \quad (3.77)$$

$$\Gamma_R = 1 - \Gamma_1 \quad (3.78)$$

$$\bar{W}_R = W - \bar{W}_1 \quad (3.79)$$

Table 3-27. Properties of residual mode and supplemental damping parameters

Level	ϕ_{iR}	Γ_R	W_R (KN)	F_{iR} (KN)	δ_{iR} (mm)	W_R (KN-mm)	W_{Rj} (KN-mm)	F_T (KN)
Roof	1.000		151222	923	219	467146	747433	935
7	0.745		143113	1441	174	581118	929789	1467
6	0.548		130803	1629	134	503951	806321	1669
5	0.410	0.789	114614	1644	102	387953	620725	1696
4	0.314		95151	1592	78	285868	457389	1648
3	0.242		73630	1491	58	198305	317288	1542
2	0.180		52424	1306	40	119677	191484	1345
1	0.114		35816	965	21	47064	75302	988

3.6.3.2.3.3 Residual mode base shear

The coefficient of residual mode can be determined with equation 3.80, B_R is a coefficient and relate to effective damping, and the residual period, T_R , with equation 3.81.

$$C_{SR} = \left(\frac{R}{C_d} \right) \frac{S_{MS}}{\Omega_0 B_R} \quad (3.80)$$

$$T_R = 40\% T_1 \quad (3.81)$$

Residual mode displacement of the maximum considered earthquake can be determined according to equation 3.82.

$$D_{RM} = \left(\frac{g}{4\pi^2} \right) \Gamma_R \frac{S_{M1} T_R}{B_R} \leq \left(\frac{g}{4\pi^2} \right) \Gamma_R \frac{S_{MS} T_R^2}{B_R} \quad (3.82)$$

The parameters values of residual mode base shear are presented in Table 3-28.

Table 3-28. Summary of residual mode base shear parameters

Spectral acceleration (g)		20% T_s (Sec)	Effective Residual period (Sec)	Coefficient		Residual mode Base shear (KN)		Residual displacement (mm)	
S_{MS}	S_{M1}	T_0	T_R	C_{SRD}	$C_{SR-Final}$	V_{RD}	V_{RM}	D_{RM}	D_{RM-Max}
1.8	0.825	0.092	0.804	0.301	0.451	10768	16153	67	118

3.6.3.2.4 Seismic base shear

The seismic base shear can be determined from equation 3.71 as explained in section 3.8.3.2.1.

The results of seismic base shear are tabulated in Table 3-29.

Table 3-29. Summary of seismic base shear parameters

Seismic Coefficient				Fundamental mode Base shear (KN)		Residual mode Base shear (KN)		Seismic base shear (KN)		Minimum seismic base shear (KN)	
C_{SID}	C_{SIM}	C_{SRD}	C_{SRM}	V_{1D}	V_{1M}	V_{RD}	V_{RM}	V_D	V_M	V_{Dmin}	V_{Mmin}
0.037	0.055	0.301	0.451	4520	6643	10768	16153	11679	17466	8759	13099

3.6.3.2.5 Control criteria of damping system

Earthquake design, residual, and maximum roof displacement can be determined with equations 3.83 to 3.85, equations 3.83 and 3.85 depending on the effective period, and the value of S_{D1}/S_{DS} .

$$D_{1D} = \left(\frac{g}{4\pi^2}\right) \Gamma_1 \frac{S_{D1}T_{1D}}{B_{1D}} \geq \left(\frac{g}{4\pi^2}\right) \Gamma_1 \frac{S_{D1}T_1}{B_{1E}}, T_{1D} \geq T_S \quad (3.83)$$

$$D_{RD} = \left(\frac{g}{4\pi^2}\right) \Gamma_R \frac{S_{D1}T_R}{B_R} \leq \left(\frac{g}{4\pi^2}\right) \Gamma_R \frac{S_{DS}T_R^2}{B_R} \quad (3.84)$$

$$D_{1M} = \left(\frac{g}{4\pi^2}\right) \Gamma_1 \frac{S_{M1}T_{1M}}{B_{1M}} \geq \left(\frac{g}{4\pi^2}\right) \Gamma_1 \frac{S_{M1}T_1}{B_{1E}}, T_{1M} \geq T_S \quad (3.85)$$

The summary of damping properties and damping modification factors are presented in Table 3-30. The values of fundamental and residual of earthquake roof displacement corresponding to design and maximum considered earthquake are demonstrated in Table 3-31.

Table 3-30. Damping properties and modification factors

Inherent damping (%)	Supplemental damping (%)		Hysteresis damping (%)		Effective damping (%)					Damping coefficient				
	β_{Vm}	β_{VR}	β_{HD}	β_{HM}	β_{1D}	β_{1M}	β_{RD}	β_{RM}	β_{1E}	B_{1D}	B_{1M}	B_{RD}	B_{RM}	B_{1E}
3	12.73	12.74	18.76	19.06	42.30	42.85	42.31	42.86	15.73	2.16	2.18	2.16	2.18	1.37

Table 3-31. Roof displacement

Roof displacement	Value (mm)	Result
D_{1D}	365	Accepted
$D_{1D(min)}$	358	Minimum
D_{RD}	77	Accepted
$D_{RD(max)}$	78	Maximum
D_{1M}	551	Accepted
$D_{1M(min)}$	538	Minimum
D_{RM}	67	Accepted
$D_{RM(max)}$	118	Maximum

Fundamental, residual of design, and maximum considered earthquake of story drift can be calculated by the square root of the sum of squares of fundamental and residual of design and maximum story drift as presented in Table 3-32.

Table 3-32. Design and maximum earthquake story drift

Level	δ_{i1D} (mm)	δ_{iRD} (mm)	δ_{i1M} (mm)	δ_{iRM} (mm)	Δ_D (mm)	Δ_M (mm)	Result
Roof	366	45	551	67	368	555	Accepted
7	322	33	485	50	323	487	Accepted
6	277	25	418	37	279	420	Accepted
5	233	18	352	28	234	353	Accepted
4	189	14	285	21	190	286	Accepted
3	145	11	219	16	145	219	Accepted
2	101	8	152	12	101	153	Accepted
1	57	5	86	8	57	86	Accepted

The story velocity of design and maximum earthquake can be determined with equations 3.86 and 3.87, the results are presented in Table 3-33.

$$V_D = \sqrt{\left[2\pi \frac{\Delta_{1D}}{T_{1D}}\right]^2 + \left[2\pi \frac{\Delta_{RD}}{T_R}\right]^2} \quad (3.86)$$

$$V_M = \sqrt{\left[2\pi \frac{\Delta_{1M}}{T_{1M}}\right]^2 + \left[2\pi \frac{\Delta_{RM}}{T_R}\right]^2} \quad (3.87)$$

Table 3-33. Design and maximum earthquake story velocity

Level	∇_{1D} (mm/s)	∇_{RD} (mm/s)	∇_{1M} (mm/s)	∇_{RM} (mm/s)	∇_D (mm/s)	∇_M (mm/s)
Roof	708	350	1054	525	790	1178
7	623	261	927	391	675	1006
6	537	192	800	288	570	850
5	452	143	672	215	474	706
4	366	110	545	165	382	570
3	281	85	418	127	293	437
2	195	63	291	94	205	306
1	110	40	164	60	117	174

3.6.3.3 Response Spectrum Procedure (RSP)

In this method, the base shear, V , shall satisfy equation 3.88. The base shear is composed of modal base shear component, V_m , with equation 3.89 using SRSS or CQC mathematical methods.

$$V \geq V_{min} = \max\left(\frac{V}{B_{V+1}}, 75\%V\right) \quad (3.88)$$

$$V_m = C_{sm} \overline{W}_m \quad (3.89)$$

Where C_{Sm} is the seismic coefficient and shall be calculated for the first and greater mode of vibration. The seismic coefficient depends on the effective period of fundamental mode as well as T_s , and the first and greater mode of vibration can be determined with equations 3.90 and 3.91. \overline{W}_m is the effective seismic weight of vibration modes with equation 3.92.

$$\text{If } T_{1D} \geq T_s, C_{S1} = \left(\frac{R}{C_d}\right) \frac{S_{D1}}{T_{1D}(\Omega_0 B_{1D})} \quad (3.90)$$

$$\text{If } T_m \geq T_s, C_{Sm} = \left(\frac{R}{C_d}\right) \frac{S_{D1}}{T_m(\Omega_0 B_{mD})} \quad (3.91)$$

$$\overline{W}_m = \frac{(\sum_{i=1}^n w_i \phi_{im})^2}{\sum_{i=1}^n w_i \phi_{im}^2} \quad (3.92)$$

Herein B_{mD} , is a coefficient based on the effective damping of β_{mD} . T_m is the period of different modal vibrations. The lateral force, F_{im} , is due to vibration mode and shall be calculated with equation 3.93.

$$F_{im} = w_i \phi_{im} \frac{\Gamma_m}{\bar{W}_m} V_m \quad (3.93)$$

Γ_m is the modal participation factor with equation 3.94.

$$\Gamma_m = \frac{\bar{W}_m}{\sum_{i=1}^n w_i \phi_{im}} \quad (3.94)$$

The summary of design base shear, lateral force, acceptance criteria, story drift, and velocity are presented in Table 3-34 to Table 3-37.

Table 3-34. Summary of seismic base shear parameters

Seismic Coefficient				Fundamental mode Base shear (KN)		Higher mode Base shear (KN)		Seismic base shear (KN)		Minimum seismic base shear (KN)	
C _{S1D}	C _{S1M}	C _{SDm}	C _{SMm}	V _{1D}	V _{1M}	V _{mD}	V _{mM}	V _D	V _M	V _{Dmin}	V _{Mmin}
0.037	0.055	0.232	0.344	4520	6643	11785	17524	12622	18741	9466	14056

Table 3-35. Properties of lateral force

Level	W _m (KN)	Γ _m	F _{il} (KN)	F _{im} (KN)	F _T (KN)
Roof	3893		264	990	1024
7	9392		486	1545	1620
6	15787		645	1746	1862
5	22670		732	1763	1909
4	29853	1.097	749	1707	1865
3	37198		697	1599	1744
2	44454		573	1400	1513
1	50866		375	1034	1100

Table 3-36. Roof displacement

Roof displacement	Value (mm)	Result
D _{1D}	365	Accepted
D _{1D(min)}	358	Minimum
D _{1M}	551	Accepted
D _{1M(min)}	538	Minimum
D _{mD}	19	Accepted
D _{mD(max)}	19	Maximum
D _{mM}	28	Accepted
D _{mM(max)}	28	Maximum

Table 3-37. Design and maximum earthquake story drift and velocity

Level	δ_{i1D} (mm)	δ_{imD} (mm)	δ_{i1M} (mm)	δ_{imM} (mm)	Δ_D (mm)	Δ_M (mm)	∇_{1D} (mm/s)	∇_{mD} (mm/s)	∇_{1M} (mm/s)	∇_{mM} (mm/s)	∇_D (mm/s)	∇_M (mm/s)
Roof	366	19	551	28	366	552	708	313	1054	465	774	1152
7	322	14	485	21	322	485	623	233	927	347	665	990
6	278	10	418	15	278	419	537	171	800	255	564	839
5	233	8	352	12	234	352	452	128	672	191	470	699
4	189	6	285	9	189	285	366	98	545	146	379	564
3	145	5	219	7	145	219	281	76	418	113	291	433
2	101	3	152	5	101	152	195	56	291	84	203	303
1	57	2	86	3	57	86	110	36	164	53	116	172

3.6.4 Results and discussion

A summary of seismic response coefficient and the base shear values based on the ASCE 7, NBCC 2015 for structural without damping system and ELFP and RSP for structural with damping system are presented in Figure 3-23 and Figure 3-24. The final seismic response coefficient for ASCE 7 and NBCC 2015 are 7.2% and 7.5%. The fundamental mode seismic response coefficient for design and maximum considered earthquake had a similar value of 0.037 (C_{S1D}) and 0.055 (C_{S1M}) for ELF and RSP procedures. The residual mode and higher mode seismic response coefficient of both design and maximum considered earthquake were 0.301 (C_{SRD}) and 0.451 (C_{SRM}) for ELF and 0.232 (C_{SDm}) and 0.344 (C_{SMm}) for RSP procedures. The base shear values for ASCE 7 and NBCC 2015 were 2554 (KN) and 2688 (KN). The seismic base shear of ELF and RSP procedures are calculated based on fundamental, residual, and higher mode base shears for both design and maximum credible earthquake, these values are 11679 KN (V_D) and 17466 KN (V_M) for ELF and 12622 KN (V_D) and 18741 KN (V_M) for RSP procedures and are greater than the prescribed minimum seismic base shear. It can be observed the seismic base shear based on RSP is about 8% higher compared with the ELF procedure.

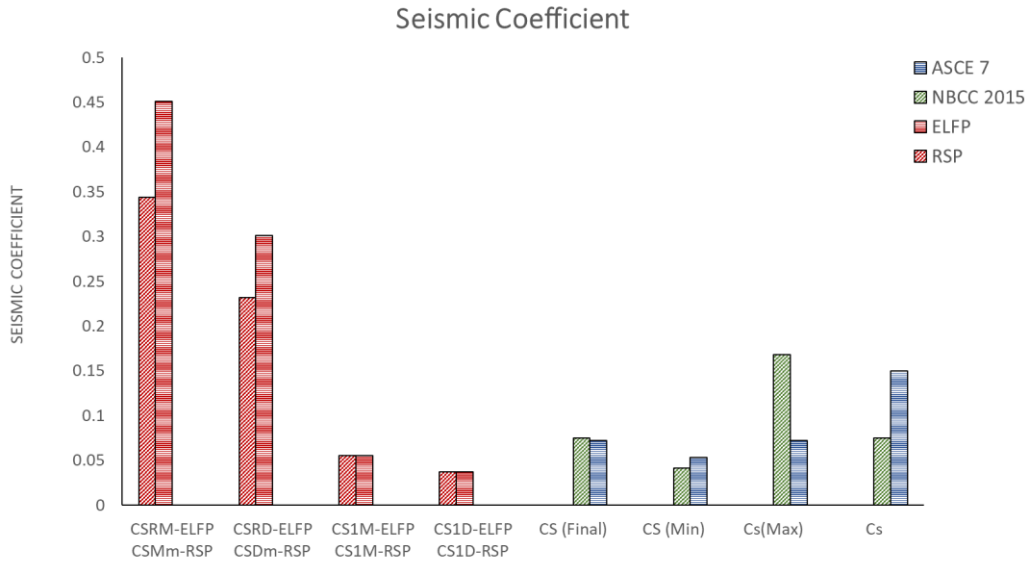


Figure 3-23. Seismic response coefficient

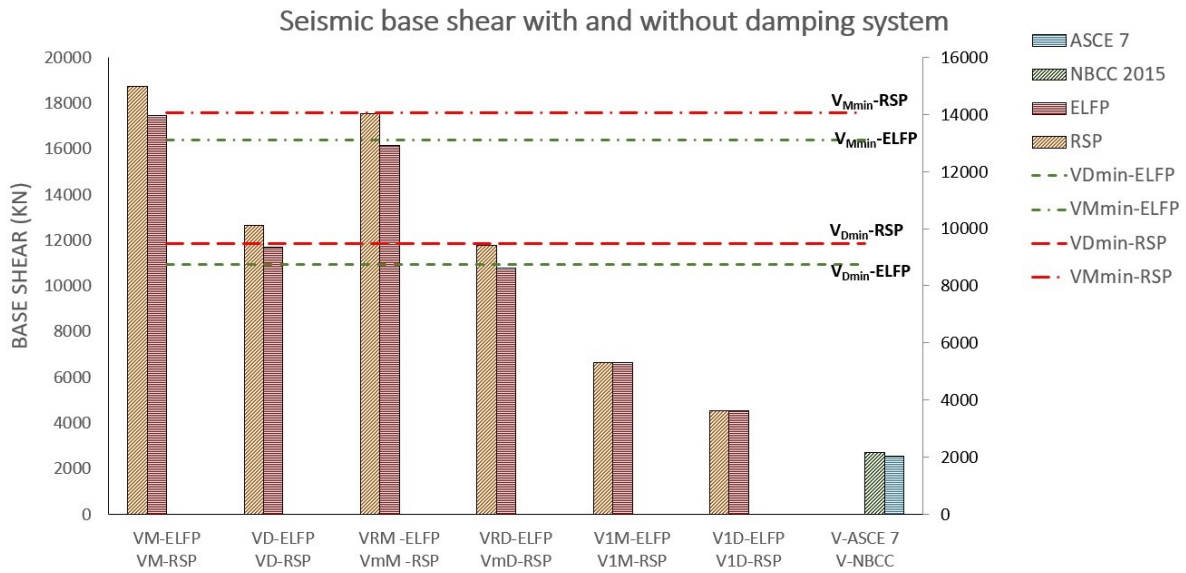


Figure 3-24. Seismic base shear

As explained earlier the effective damping consists of three elements including inherent damping, β_I , with a range of 2% to 5%, hysteretic damping, β_H , and supplemental damping, β_{vm} . Hysteretic damping accounts for 59% to 62% of the hysteretic curve adjustment factor times ductility modification factor, which depends on the effective fundamental period and short period,

the ductility demand value shall be limited to the maximum effective ductility demand value. The pinching and other damping effects which degrade the hysteresis loop are integrated into an adjustment factor of the hysteretic loop. Supplemental damping depends on the dynamic response of work done by each device in one entire cycle, and the maximum strain energy, resulting from inertia lateral force. The calculated damping properties for both ELF and RS procedures are presented in Figure 3-25. The essential importance of supplemental damping including each device's work in one cycle and strain energy due to the lateral force are similar for both methods with the damping percentage of about 13%. The values of hysteretic damping in RS procedure are about 60% higher compared with ELF procedures. The effective damping percentage was in the range of 43% for both design and maximum considered earthquake. These values are increased by about 27% for the RS procedure.

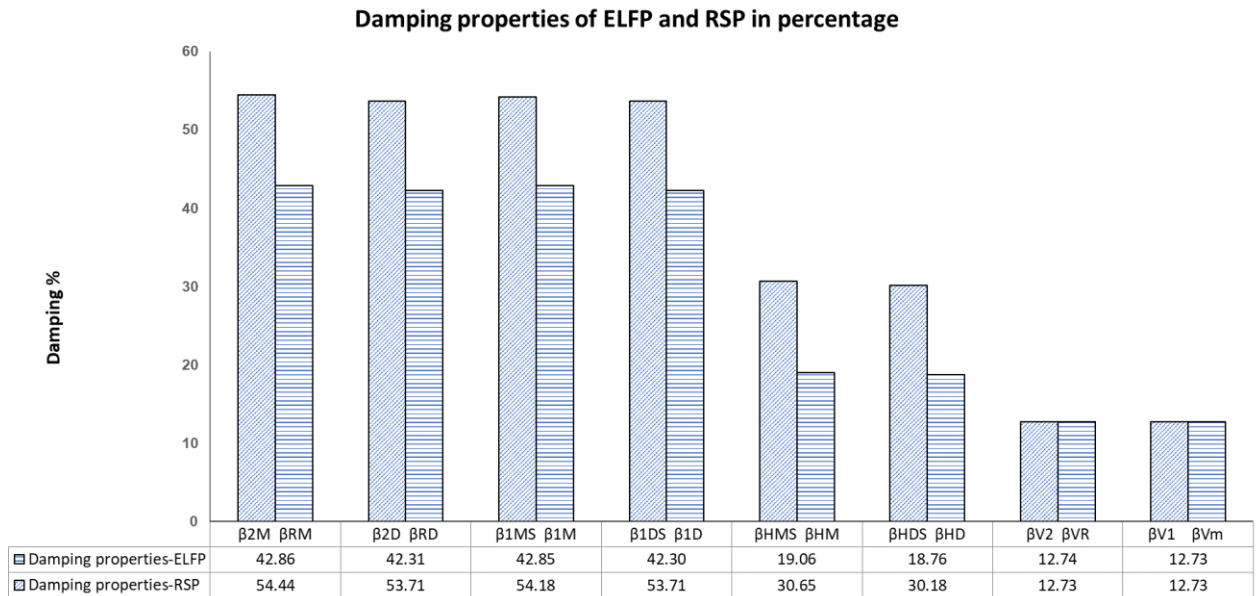


Figure 3-25. Calculated different damping properties in percentage based on ELF and RS procedures

Figure 3-26 presents the values of the damping coefficient for ELF and RS methods. B_{IE} is the numerical coefficient with a combination of inherent damping and supplemental damping, which has the same value of 1.37 for both methods. B_{1D} and B_{1M} are the numerical coefficients based on

the effective damping of design and maximum credible earthquakes, which have values ranging from 2.16 to 2.19 for both procedures. B_{RD} , B_{2D} , B_{RM} , and B_{2M} are the numerical coefficients of the residual and higher mode of effective damping based on the design and maximum considered earthquake with the values ranging from 2.16 to 2.53.

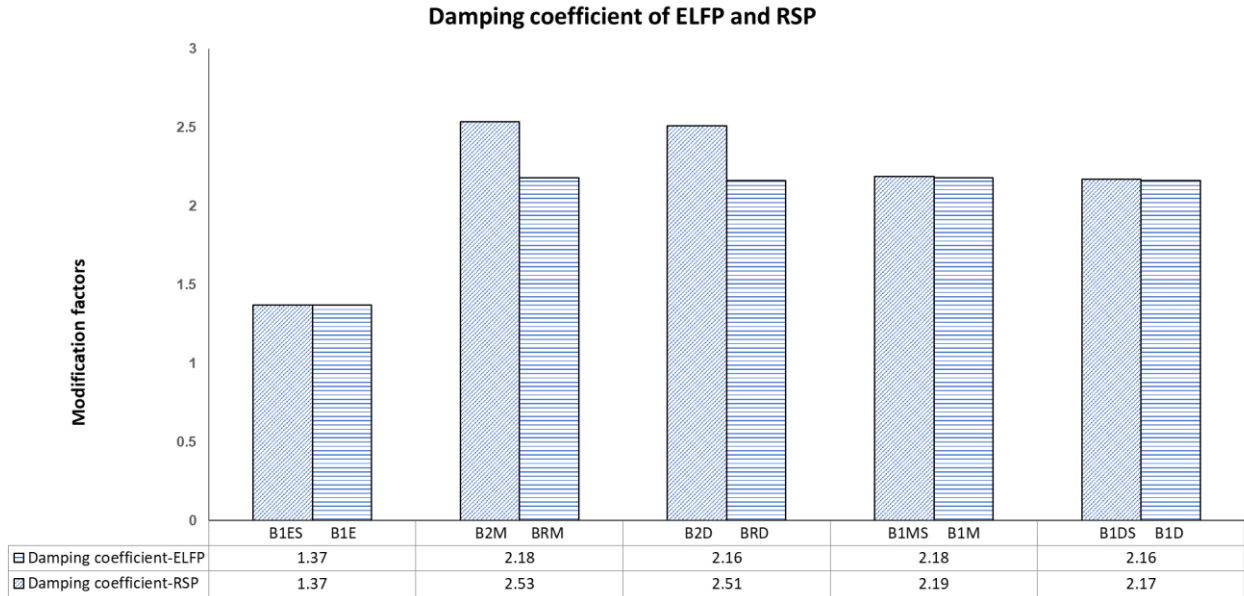


Figure 3-26. Damping Coefficient values based on ELF and RS procedures

Figure 3-27 shows the capacity curve, fundamental period, T_1 , effective period, T_{1D} , different constant periods of 2 and 2.5 seconds, design and maximum earthquake demand spectrum with 5% damping, and the reduced design and maximum earthquake demand spectrum by a combination of inherent damping, β_I , and supplemental damping, β_v . When post-yield displacement reduces by adding dampers the amount of energy dissipated by the seismic force-resisting system decreases in the form of hysteretic damping, this also verified the use of dampers can reduce the damage in the primary members of the structure. If there is no damping system (as in a conventional structure), effective damping simply equals inherent damping. Therefore, ASCE 7-16 considers the inherent damping for conventional structure (Structural without damping system).

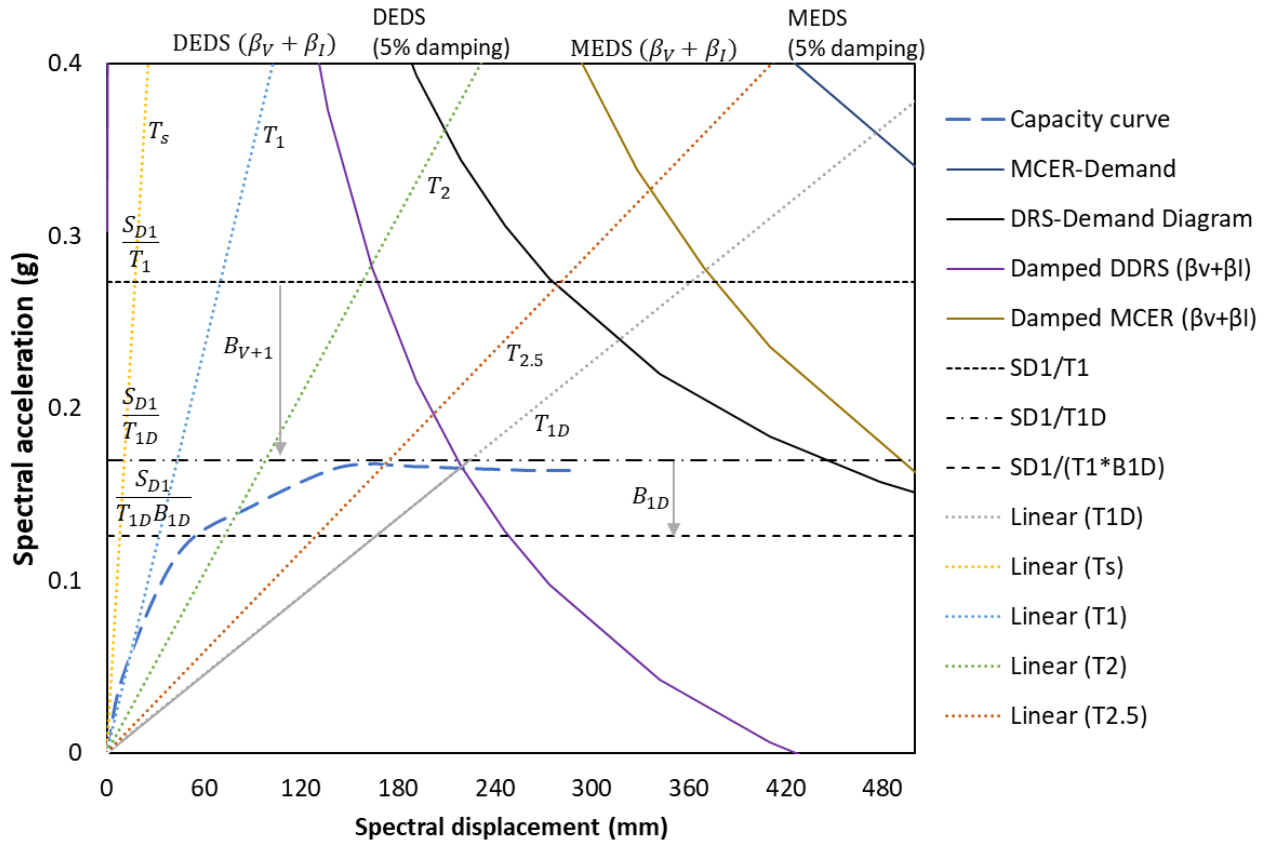


Figure 3-27. Design demand caused by effective damping

In the conventional design procedure, the base shear is determined by multiplying the seismic response coefficient by the effective seismic weight. However, the seismic base shear for the equivalent lateral force procedures is the square root of the sum of squares of the fundamental mode and residual base shear, whereas the response spectrum procedure is the square root of the sum of squares of modal components. Figure 3-28 presents the pushover curve for SFRS and SFERS with damping.

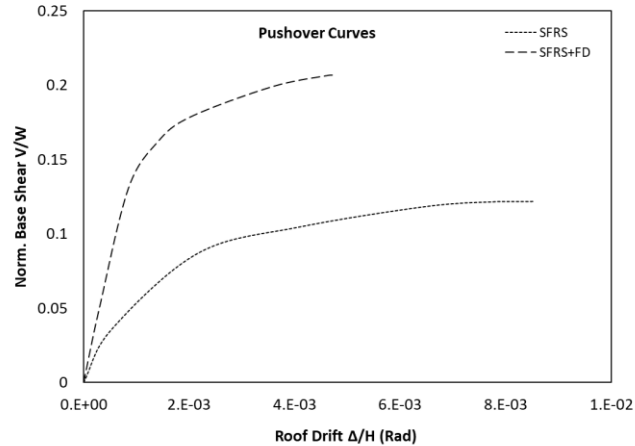


Figure 3-28. Roof drift ratio versus normalized base shear for SFRS and SFRS with damping system

3.7 Chapter Summary

A methodology for evaluating the seismic properties of CMRF building with a damping system, using conventional, equivalent lateral load as well as response spectrum procedures has been presented here. An eight-story CMRF building is used as a case study. The energy dissipation systems can be categorized as displacement-dependent dampers such as yielding dampers, and yielding restrained braces, velocity-dependent dampers such as viscous dampers, and viscous elastic dampers, acceleration-dependent dampers such as tuned mass damper or tuned liquid damper, and base isolators such as rubber or friction isolator. The ASCE 7-16 considers the dissipation system with a combination of the seismic force-resisting system plus damping devices including fluid viscous, viscoelastic, metallic yielding as well as friction devices. Some of the general definitions are provided in Appendix A3.2. A comparison between the calculation of seismic design procedures based on the conventional design for both ASCE 7 and NBCC methods, equivalent lateral force, and response spectrum procedures revealed the following observations:

- ASCE 7-16 defines the maximum and minimum modification factors of damping properties times nominal design properties of each device. These factors are required to be considered for the specification, environment as well as testing. In this study, the minimum and maximum damping properties are assumed to be according to ASCE 7.

- The spectra for both design and maximum considered earthquake are developed as explained in section 3.8.2. Therefore, both spectra need to be used in the analysis and design of ELF and RS procedures for building with damping systems.
- The ELF and RS are based on the yield base shear, whereas the conventional design is based on reduced base shear, this reduction factor depends on types of force-resisting system.
- The initial design loads are calculated based on the ASCE 7 and the NBCC conventional procedures for structural without damping systems. To have a comparison between the two codes, the seismic response coefficient, C_N , is considered for the Canadian standard and compared with the seismic response coefficient, C_S , of the ASCE 7. The base shear value of concrete moment resisting frames is 2688 KN based on the NBCC procedure, which is about 5% higher compared with the 2554 KN based on the ASCE 7 procedure. Since the Canadian code does not recommend any integration of the damping devices. Therefore, it is recommended to select the higher base shear value between the ASCE 7 and the NBCC, which will be followed by ELF or RS procedures. This allows the integration of the damping properties in the NBCC.
- The seismic base shear for ELF and RS procedures should be greater than the maximum of 75% of based shear and base shear divided by effective damping, effective damping is a combination of supplemental and inherent damping. However, in a conventional design, the base shear is adjusted by the seismic response coefficient factor which relates to design spectral response, response modification and importance factors, fundamental period, long period, and spectral acceleration for the design level and maximum considered earthquake.
- The acceptance criteria for ELF and RS procedures are based on the specified design for controlling roof displacement, story drift, and velocity for both design and maximum credible earthquake as well as the general specification of the conventional design.
- The maximum displacement is calculated for displacement-dependent damping systems based on the ELF and RS procedures. The maximum design and maximum credible earthquake story

drift for the ELF procedure are 368mm and 555mm, similar values of 366mm and 552mm are determined based on the RS procedure.

- The maximum velocity is calculated for velocity-dependent damping systems based on the ELF and RS procedures. The maximum calculated values of velocities for design and credible earthquake, based on ELF procedure are 790 mm/s and 1178 mm/s. The values of 774 mm/s and 1152 mm/s, with about a 2% difference, were obtained for the RS procedure.
- The damping redundancy in ASCE 7-16 limits the minimum of four devices of any story in either direction or the minimum of two devices of any story on each side of the middle of stiffness. The devices should endure 1.3 times the maximum displacement calculated under the maximum considered earthquake.
- The ELF and RS procedures are limited to the maximum height of 30m and the spectral acceleration of less than 0.6 when the height of the building is greater than 30m, and S_1 is greater than 0.6 a nonlinear time response analysis is required to determine and validate seismic characteristic, in conventional design, the limitation of the height of the structure depends on the seismic design category. Chapter 4 describes the seismic characteristics of CMRF equipped with inline friction dampers for taller structures and higher spectral acceleration.
- The effective damping percentage consists of inherent damping, supplemental damping, and hysteretic damping. The fundamental mode, and the residual mode for ELF procedure, and the fundamental mode, and the higher mode effects for the RS procedure are used to calculate the effective damping properties. It was concluded that the RS procedure is more conservative with effective damping of about 54% compares with the ELF procedure with effective damping of about 42%.
- The damping coefficient is based on the effective damping, B , which can be determined from Table 18.7-1 of ASCE 7-16, when the period of the structure is greater than 20% of seismic design value at 1 second over seismic design value at 0.2 seconds, T_0 . In case the period is less than, T_0 , linear interpolation shall be used. This method is similar for structural equipped with isolators; however, the damping is limited from below 2% to 20%.

CHAPTER 4

Seismic response characteristics for concrete structures equipped with different dissipation devices

4.1 Introduction

The first section of this chapter describes the process of evaluating the overstrength, ductility, and response modification factors of ductile concrete moment resisting frames with inline seismic friction dampers, considering the effects of different heights and span lengths. The results covered the ductility, force, and response modification factors, which compared with the closest recommended factors in the NBCC 2015. Moreover, the performance of each system with and without inline friction damper including different height and span lengths is determined and compared using twenty-five scaled ground motions. The second section investigates and compares five different passive energy systems in buildings with concrete moment-resisting frames, including, Ten-Co seismic brake, Fluid viscous damper, Triangular Metallic Yielding Dampers, Lead Rubber Bearing Isolator as well as Triple Pendulum Isolator. The seismic characteristic of these devices was assessed and compared by nonlinear static analysis procedure, followed by nonlinear response history analysis using fourteen scaled ground motion records. The impact of the energy dissipaters on the seismic response of concrete moment resisting frames as the lateral load resisting system has been studied, as well as a comparison is made on their response modification factors. Moreover, inter-story drift demand, base shear demand, and different hysteresis behaviour of these systems are compared and discussed to understand the relative performance of Ten-Co seismic brake. Furthermore, the design of structural models is explained based on Canadian and American design codes as well as a comparison of their material quantities.

4.2 Seismic Performance and Response modification factors of DCMFs with ISFD

The philosophy of using the inherent ductility of building to avoid disastrous failure led to the development of seismic design codes and inelastic design response spectra. However, modern structures consider the actual dynamic behaviour of the system which can be categorized as isolation systems, and energy dissipation devices including passive, semi-active, active, and hybrid systems. (Soong et al., 1998; Soong & Dargush, 1999). Friction dampers (seismic brake) are among the passive energy dissipation devices, which dissipate energy by the friction of sliding two solid surfaces moving against each other. When a structure is subjected to a major earthquake, the friction dampers attached to a common brace dissipate a significant part of the energy and slip instead of yielding before the yielding appears in the primary members of structures. Therefore, the initial cost will be reduced significantly with a great high capacity for energy dissipation.

In the national building code of Canada (2015), the minimum earthquake lateral force is divided by Seismic Force Resisting System(s) (SFRS) reduction factor. This factor, known as the response modification factor, can be calculated by multiplying the overstrength factor (R_0) and the ductility-related force modification factor (R_d). In the 2015 NBCC, the overstrength factor (R_0) and the ductility-related force modification factor (R_d) are not yet directly included in table 4.1.8.9, therefore, engineers usually work with the factor of the closest equivalent system, ductile buckling-restrained braced frames ($R_d=4$, $R_0=1.2$). This practice is already conservative in nature mainly because the non-damage based modification factor for ISFD has been found to be substantially higher (Galindo et al., 2019b, 2019a; Naghshineh et al., 2018), and because the system can be tested at MCE ground motion forces and displacement in contrast with the equivalent systems that cannot avoid uncertainty in their actual behaviour. Therefore, this section addresses those issues by evaluating the SFRS reduction factors including the overstrength, ductility, and response modification factors of four-, eight-, and fourteen-story ductile concrete frames with inline seismic friction dampers, using in detail nonlinear static analysis procedures. In addition, the effects of the

building height and the span length are considered. Moreover, the seismic performance of the buildings is assessed using nonlinear response history analysis.

4.3 Design of Structural Models

In the NBCC 2015, six spectral acceleration parameters for periods of 0.2, 1.0, 2.0, 5.0, and 10 seconds are presented to define spectra matching based on the uniform hazard spectrum, these parameters are 5%-damped. The horizontal peak ground acceleration and velocity are based on the 2% probability of exceedance in 50 years. Various soil categories from hard rock, Class A, to soft soil, Class E as well as Class F for liquefiable soil, and sensitive, organic, and highly plastic clays are defined to characterize the soil effect on the amplitude of seismic waves reaching the surface. NBCC 2015 allows the design of short-period structures based on 66% of the calculated base shear to have at least a limited amount of ductility, this accounts for reserve strength, which experiences small displacement in such structures. This can be achieved by the greatest value of $2/3 \times S(0.2)$ or $S(0.5)$. To have a better estimation of equivalent static design base shear, the shear is multiplied by the higher mode factor, equation 4.1, which is based on the assumptions of the structural response in the first mode (Humar, 2015).

$$V_e = S(T_a)M_vW \quad (4.1)$$

Where V_e is the elastic shear, design spectral acceleration can be obtained from $S(T) = S(T_a)F(T_a)$, $S(T_a)$ can be obtained from the UHS, M_v is the higher mode factor, which depends on the period of the buildings, and W is the seismic weight.

$$V_d = \frac{S(T_a)M_vI_EW}{R_dR_o} \quad (4.2)$$

The design base shear, V_d , can be calculated from equation 4.2, R_d accounts for ductility and capability of a structure to dissipate energy in inelastic behaviour, R_o reflects the reserve strength in a structure, and I_E is the importance factor. The 2015 NBCC prescribes ductility and overstrength factors 4 and 1.7 for concrete ductile moment-resisting frames. The buildings are assumed to be located in San Bernardino, California with latitude, and longitude of 34.108, -

117.289 with a high seismic zone and site class “D”. This also represents a similar region of Tofino in Vancouver Island in British Columbia. Diagonal Braces with various span lengths of 6m and 8m are considered in each building. All three models have 5-bay in each direction and are demonstrated in Figure 4-1. The compressive strength f'_c is 30 MPa, the modulus of elasticity E_c is 24500 MPa, the unit weight of reinforced concrete is 24 KN/m³, the design live and dead loads for all models are assumed to be 1.5KN/m² and 2.4 KN/m², and the snow load acting on the roof is 1.64KN/m².

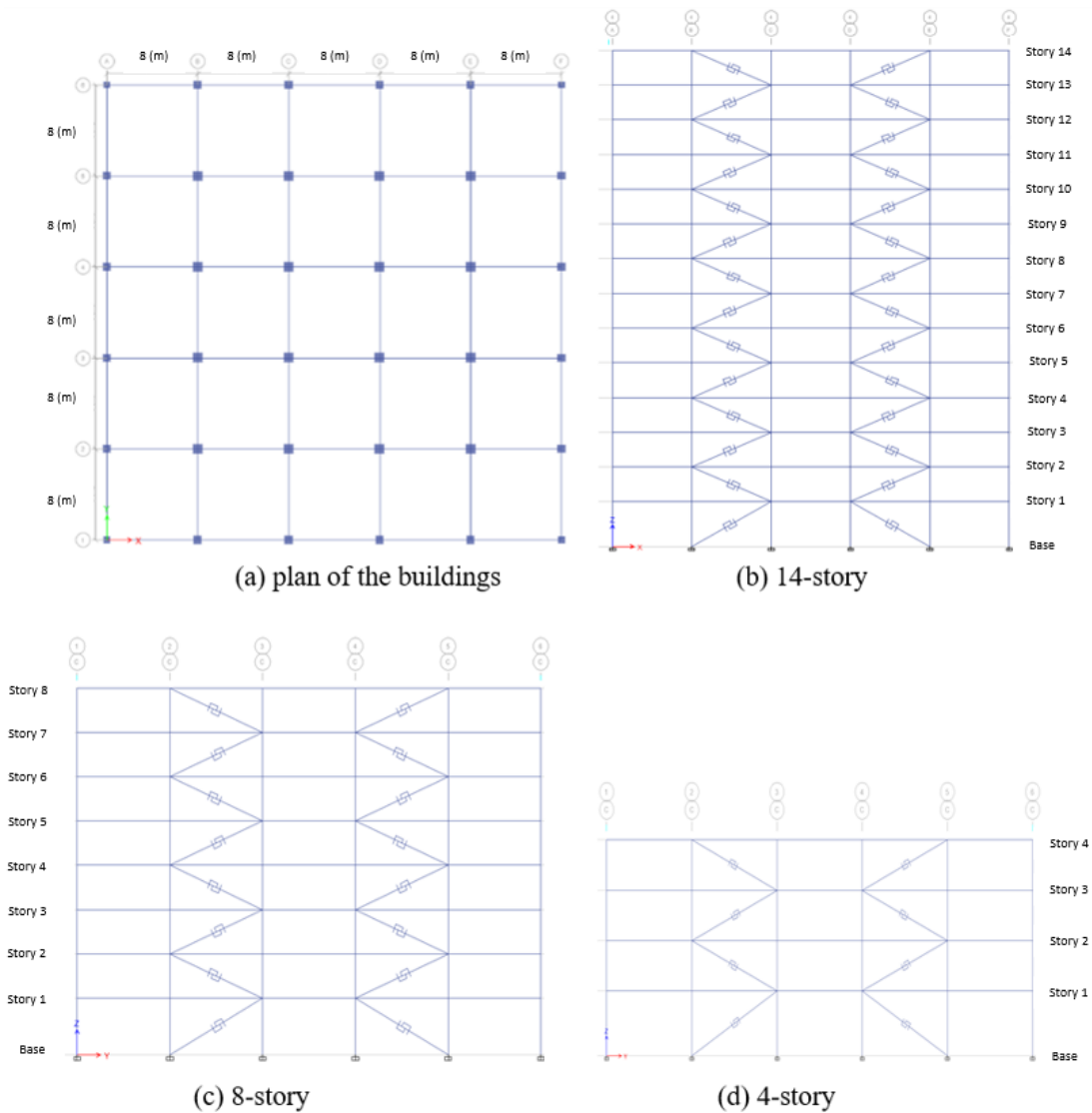


Figure 4-1. Structural models with Single Diagonal Braces (SBD); (a) plan of the buildings, (b) 14-story, (c) 8-story, (d) 4-story

The 2015 NBCC as well as ETABS software (CSI, 2016) was used to design four-, eight-, and fourteen-story ductile concrete frames with inline seismic friction dampers to evaluate the overstrength, ductility, and response modification factors. CSA A23.3-19 was used for detailing the concrete buildings (CSA A23.3-19), the design details, as well as the brace sections, are presented in Table 4-1.

Table 4-1. Design details for different models

Story	Level	Columns		Beams				Brace Section	
		Interior (Cm)		Exterior (Cm)		Interior (Cm)		6m Span	8m Span
		6m Span	8m Span	6m Span	8m Span	6m Span	8m Span		
4	4	45×45	50×50	40×40	45×45	35×35	40×40	W14×34	W14×38
	3	45×45	50×50	40×40	45×45	35×35	40×40	W14×48	W14×53
	2	50×50	55×55	45×45	50×50	40×40	45×45	W14×61	W14×68
	1	55×55	60×60	50×50	55×55	40×40	45×45	W14×90	W14×99
8	8	45×45	50×50	40×40	45×45	40×40	45×45	W14×38	W14×43
	7	45×45	50×50	40×40	45×45	40×40	45×45	W14×53	W14×53
	6	60×60	65×65	55×55	60×60	55×45	55×50	W14×61	W14×68
	5	60×60	65×65	55×55	60×60	55×45	55×50	W14×68	W14×74
	4	65×65	70×70	60×60	65×65	55×45	55×50	W14×74	W14×82
	3	65×65	70×70	60×60	65×65	60×50	65×55	W14×90	W14×99
	2	70×70	75×75	65×65	70×70	60×50	65×55	W14×90	W14×120
	1	70×70	75×75	65×65	70×70	60×50	65×55	W14×159	W14×193
14	14	50×50	55×55	45×45	50×50	45×45	45×45	W14×34	W14×38
	13	50×50	55×55	45×45	50×50	45×45	55×45	W14×43	W14×53
	12	55×55	60×60	50×50	55×55	45×45	55×45	W14×53	W14×68
	11	55×55	60×60	50×50	55×55	55×45	60×50	W14×68	W14×82
	10	55×55	60×60	50×50	55×55	55×45	60×50	W14×74	W14×90
	9	60×60	70×70	55×55	60×60	60×50	65×55	W14×99	W14×120
	8	60×60	70×70	55×55	60×60	60×50	65×55	W14×109	W14×120
	7	60×60	70×70	60×60	65×65	60×50	65×55	W14×109	W14×132
	6	70×70	75×75	60×60	65×65	60×50	65×55	W14×132	W14×159
	5	70×70	75×75	60×60	65×65	65×55	65×55	W14×145	W14×176
	4	70×70	75×75	60×60	65×65	65×55	70×60	W14×145	W14×176
	3	75×75	80×80	65×65	70×70	65×55	70×60	W14×159	W14×176
	2	75×75	80×80	65×65	70×70	65×55	70×60	W14×193	W14×211
	1	75×75	85×85	65×65	70×70	65×55	70×60	W14×193	W14×233

4.3.1 Design of Ten-Co Seismic Brake

The inline seismic friction damper (ISFD) has a better performance and costs compared to concrete shear walls and Buckling Restrained Braces (BRBs). The force-based linear method for seismic friction damper is presented in (Galindo et al., 2019b, 2019a; Naghshineh et al., 2018).

ISFDs shall be utilized accordingly, too many ISFDs make the structure too rigid with excessive design force, fewer ISFDs, however, eliminate their effect in the system. Therefore, it is very crucial to have the most appropriate amount of shear forces to the ISFDs to minimize the demand to the frame and to maximize the energy dissipation. Nonlinear response history analysis shall be used for this type of calibration. The main concept is to perform static analysis and estimate the approximate forces in an inline seismic friction damper. The hysteretic shape of ISFD is characterized by its dynamic friction, throughout the slipping stage. Wen model for elastoplastic materials as presented in Figure 4-2 is recommended to model an inline seismic friction damper ISFD, (Galindo et al., 2019b, 2019a; Naghshineh et al., 2018).

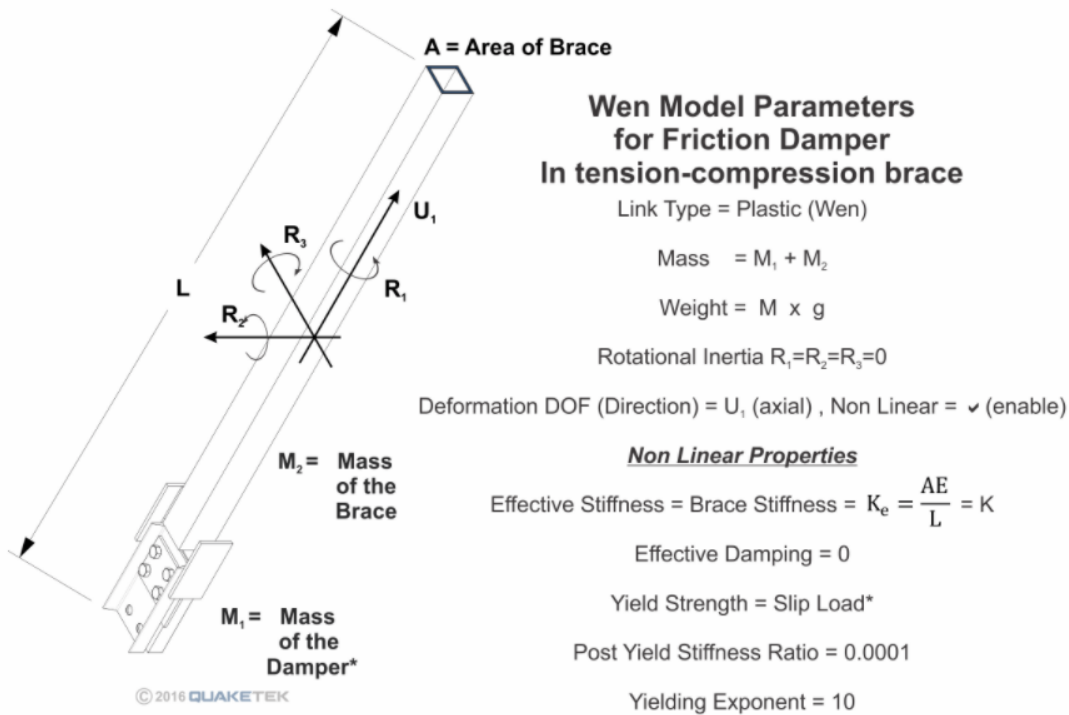


Figure 4-2. Wen model parameters for YRB, courtesy of manufacturer (Quaketek Inc., 2016)

The equivalent lateral static analysis was performed to calculate the base shear and stiffness of each floor as well as the design parameters for each damper, these values are presented in Table 4-2. Based on the manufacturer report (Quaketek 2016), one-third of the story shear can be applied to the ISFDs. 34% of the shear force is assigned to the ISFDs to increase the energy dissipation to

the maximum and have a better consistent design. A minimum of two dissipation devices must be capable of sustaining 130 percent of the maximum estimated displacement, these devices should be located on each side of the center of stiffness (FEMA 356, 2000).

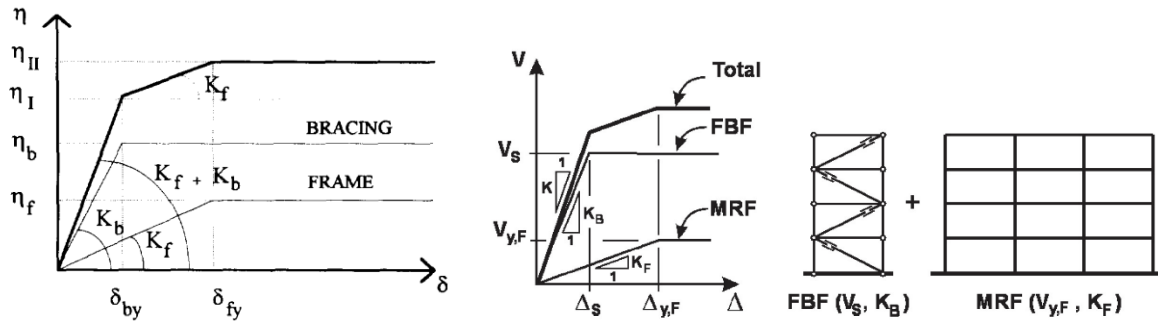


Figure 4-3. Idealized lateral force-displacement (Ciampi et al., 1995, Tirca et al., 2018)

Table 4-2. ISFDs design parameters for different types of structures

Story	Level	K_f (KN/mm)		K_d (KN/mm)		K_{ed} (KN/mm)		Post Yield Stiffness Ratio	Yielding exponent
		6m Span	8m Span	6m Span	8m Span	6m Span	8m Span		
4	4	124	134	136	146	148	165	0.0001	10
	3	182	192	198	210	208	231	0.0001	10
	2	238	262	260	286	265	296	0.0001	10
	1	308	331	353	380	373	409	0.0001	10
8	8	139	143	152	156	165	186	0.0001	10
	7	196	198	214	216	231	231	0.0001	10
	6	233	243	254	265	265	296	0.0001	10
	5	266	275	290	300	296	322	0.0001	10
	4	289	305	315	333	322	355	0.0001	10
	3	335	361	366	394	392	430	0.0001	10
	2	359	461	392	503	392	522	0.0001	10
	1	567	625	650	717	656	798	0.0001	10
14	14	132	147	144	161	148	165	0.0001	10
	13	157	211	171	230	186	231	0.0001	10
	12	209	269	228	293	231	296	0.0001	10
	11	255	314	278	343	296	355	0.0001	10
	10	282	346	307	377	322	392	0.0001	10
	9	390	458	426	499	430	522	0.0001	10
	8	404	472	441	515	473	522	0.0001	10
	7	429	499	468	544	473	573	0.0001	10
	6	510	582	557	635	573	690	0.0001	10
	5	571	647	623	706	631	765	0.0001	10
	4	567	639	619	698	631	765	0.0001	10
	3	622	685	679	748	690	765	0.0001	10
	2	724	801	791	874	839	916	0.0001	10
	1	690	813	792	933	798	963	0.0001	10

The slip loads are calculated based on the method proposed for an equivalent single-degree-of-freedom with idealized lateral load-deformation as presented in Figure 4-3. The ratio of the total braces' stiffness of each floor to the total braces' stiffness plus story stiffness of each floor is calculated based on an iterative procedure and assumed to be 0.8. Nonlinear time history analysis also can be used as an iterative procedure to design the sections of braces and friction dampers (Tirca et al., 2018). Table 4-3 represents the equivalent static force analysis as well as the slip force results for all three models.

Table 4-3. Seismic analysis results, slip loads, and calculated mass per damper

Story	Bracing	Level	Seismic shear forces (KN)		Seismic brake slip forces (KN)		Seismic Weight (KN)		Mass per damper (Kg)	
			6-m Span	8-m Span	6-m Span	8-m Span	6-m Span	8-m Span	6-m Span	8-m Span
4	SBD	4	1314	1364	140	150	12877	16523	80	80
		3	901	949	240	250	12877	16523	115	115
		2	638	676	310	330	12877	16523	115	115
		1	369	387	370	390	12877	16523	115	115
8	SBD	8	1652	1685	180	180	28174	33923	80	80
		7	996	1009	290	290	28174	33923	80	115
		6	857	873	380	390	28174	33923	115	115
		5	753	761	460	470	28174	33923	160	115
		4	615	623	530	540	28174	33923	160	160
		3	472	480	580	590	28174	33923	160	160
		2	332	339	620	630	28174	33923	160	160
		1	190	195	670	680	28174	33923	160	195
14	SBD	14	1579	1773	170	190	49723	65167	80	80
		13	670	781	250	280	49723	65167	115	115
		12	622	727	310	360	49723	65167	115	115
		11	600	706	380	440	49723	65167	115	115
		10	547	644	440	510	49723	65167	115	115
		9	521	616	500	570	49723	65167	160	160
		8	470	556	550	630	49723	65167	160	160
		7	414	490	590	690	49723	65167	160	195
		6	360	425	630	730	49723	65167	160	195
		5	318	378	670	770	49723	65167	160	195
		4	258	306	690	810	49723	65167	160	240
		3	199	236	720	830	49723	65167	195	240
		2	139	166	730	850	49723	65167	195	240
		1	80	95	780	910	49723	65167	195	240

Note: Single Diagonal Braces (SBD)

4.3.2 Modal Analysis

The calculated natural modes from the Eigenvalue analysis provide the free-vibration mode shapes and frequencies of the system, whereas Ritz value analysis finds modes based on a specific loading. Since Ritz value determines a better basis than eigenvalue, especially for analyses that are based on superposition such as response-spectrum or time-history, Ritz value analysis was performed to determine the natural periods of the YRB framed system. Table 4-4 shows the fundamental period of the structure based on the modal analysis and the results obtained from the 2015 NBCC for braced frames can be determined with empirical equation 4.3.

$$T_a = 0.025h_n \quad (4.3)$$

Where $T_a(s)$ is the fundamental lateral period and h_n is the height of the structure in the meter. It can be observed the frame with ISFDs reduced the fundamental period of the structures by an average of about 40% compared with the bare frames. Besides, the empirical equation is about -15% to -60% than those obtained by Ritz analysis.

Table 4-4. The fundamental period of the structures

Story	T (sec)-Analytical ISFD		T (sec)-Analytical Bare frame		T _a (sec)
	6m-Span	8m-Span	6m-Span	8m-Span	
	4	0.56	0.56	0.81	
8	0.89	0.85	1.36	1.33	0.73
14	1.46	1.41	1.85	1.82	1.25

4.3.3 Nonlinear Model for structural components

In this part, the component model parameters are calculated and used based on section 3.6.3. The buildings assumed to be located in San Bernardino, California, which has a seismic design data identical to Tofino in Vancouver Island in British Columbia, a single target response spectrum with 5% damped and maximum considered earthquake (MCE_R) was developed by multiplying the design response spectrum times 1.5 as presented in Figure 4-4, by selecting a comparable location in the United States, allowing MCE_R to be incorporated into Canadian code for performance assessment of the inline friction dampers.

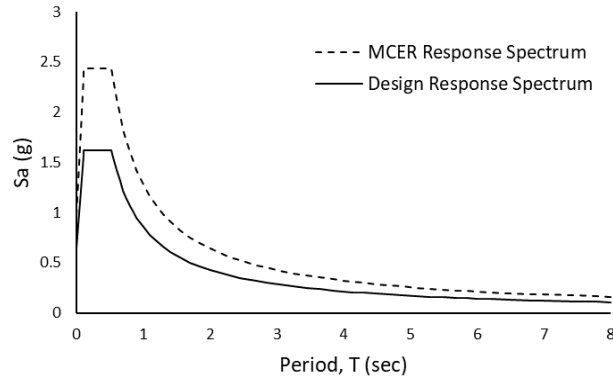


Figure 4-4. MCE_R and DE_R Response Spectrum

Spectral acceleration for a site in San Bernardino in the USA of the basic safety earthquake (BSE) for new building standards and the existing building is presented in Table 4-5. The BSE-1N and BSE-2N match the design earthquake and the maximum considered earthquake in the ASCE 7. S_{XS} and S_{X1} are the spectral response acceleration at short period and 1 second period, T_s can be calculated from S_{XS}/S_{X1} , and T_0 is 20% of the T_s value. Life safety is considered for the basic performance objective for new buildings based on the risk categories I and II. The structural and nonstructural performance levels for life safety are S-3 and N-C. In the S-3 category the structural experienced damage in its components with a margin of safety, nonstructural performance components are not considered, and in the N-C category, the non-structural element does not cause a life safety threat.

Table 4-5. Spectral acceleration parameters for different hazard levels

	DE _R		MCE _R		Not capped at BSE-1E	Not capped at BSE-2E
	BSE-1N	BSE-2N	BSE-1E	BSE-2E	5% in 50 years	20% in 50 years
S_{XS} (g)	1.43	2.14	1.29	2.41	1.29	2.41
S_{X1} (g)	0.97	1.45	0.77	1.45	0.77	1.45
T_s (sec)	0.68	0.68	0.60	0.60	0.60	0.60
T_0 (sec)	0.14	0.14	0.12	0.12	0.12	0.12

Note: DE_R (Design earthquake), MCE_R (Maximum considered earthquake)

BSE1-N and BSE-2N are considered seismic hazard levels, therefore, the target displacement for building with rigid diaphragm was calculated based on ASCE-41 for DLE (Design Level Event) and MCE (Maximum Considered Event) as explained in section 3.6.3. An idealized

relationship between base shear and displacement was created based on an equal displacement approach for all the models and continued until the frame's maximum interstudy drift met the 2.5 percent design limit. The elastic lateral stiffness K_i , effective lateral stiffness K_e as well as effective yield strength V_y were determined. The results of calculated target displacements are presented in Table 4-6.

Table 4-6. Target displacements parameters

Target displacement parameters	4-Story		8-Story		14-Story	
	6m-Span	8m-Span	6m-Span	8m-Span	6m-Span	8m-Span
C_0	1.35	1.35	1.46	1.46	1.50	1.50
C_1	1.22	1.22	1.18	1.21	1	1
C_2	1.08	1.08	1	1	1	1
C_3	1	1	1	1	1	1
T_e (Sec.)	0.59	0.59	0.82	0.85	1.52	1.44
K_i (KN/mm)	245	255	186	208	109	124
K_e (KN/mm)	220	226	174	194	100	117
R	5.86	5.86	10.56	11.03	16.54	18.61
a	60	60	60	60	60	60
V_y (KN)	4436	5437	5148	5934	6448	7509
C_m	0.9	0.9	0.9	0.9	1	1
Hazard Levels (Cm)						
$\delta_T(DLE)$	19	20	49	46	124	112
$\delta_T(MCE)$	33	34	78	74	185	168

4.3.4 Nonlinear Static Pushover Analysis

Nonlinear static pushover analysis is carried out to calculate the structural strength capacities as well as the displacement demand. This procedure involves pushing the structure under a lateral load pattern to the level of displacement expected in the design earthquake. The main goal of this analysis is an evaluation of displacement demands in critical elements with undesirable characteristics such as strength, stiffness discontinuities, extra loads on brittle elements, structural overall stability, and regions exposed to large displacement demand, which require special detailing (Lawsson et al., 1994). The effects of global P-delta can be considered either by non-iterative and iterative based on the mass and load case. The load combinations which are presented the lateral loads shall be concerned for the P-Delta effect. In this study, the factor loads of

1.0D+1.0E+0.5L+0.25S for ultimate limit states based on NBCC 2015 are considered. The buckling load can be reduced due to the local P- δ effect especially in slender columns, and automatically considered in the analysis (Krawinkler et al., 1998).

A pushover analysis may consist of different load cases with different distribution regimes of load on the structure, including acceleration, that is, a lateral force proportional to a specified mode shape, static load pattern, and any combination of acceleration, lateral force, and static load pattern. In this section, a nonlinear static pushover analysis was performed based on the target displacement of MCE_R to calculate the overstrength and ductility factors of each structure. These values are calculated based on the pushover results presented in Figure 4-5 to Figure 4-7 and tabulated in Table 4-7.

Table 4-7. Nonlinear static analysis results

Story	Bracing	Span Length (m)	Yield Strength V_y (KN)	Design Strength V_d (KN)	Overstrength factor R_o	Maximum displacement Δ_{max} (mm)	Yield displacement Δ_y (mm)	Ductility μ
4	SBD	6	4436	2155	2.05	95	20	4.75
		8	5473	2221	2.46	80	22	3.63
8	SBD	6	5148	3362	1.53	140	30	4.66
		8	5934	3481	1.71	133	34	3.92
14	SBD	6	6448	4937	1.30	255	65	3.93
		8	7509	5428	1.38	220	64	3.43

Note: Single Diagonal Braces (SBD)

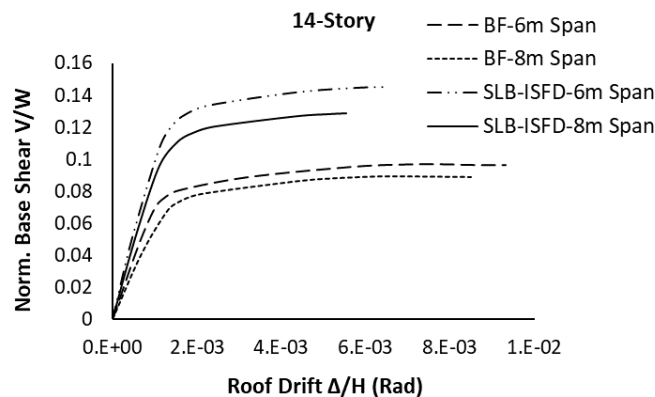


Figure 4-5. Roof drift ratio versus normalized base shear (14-Story)

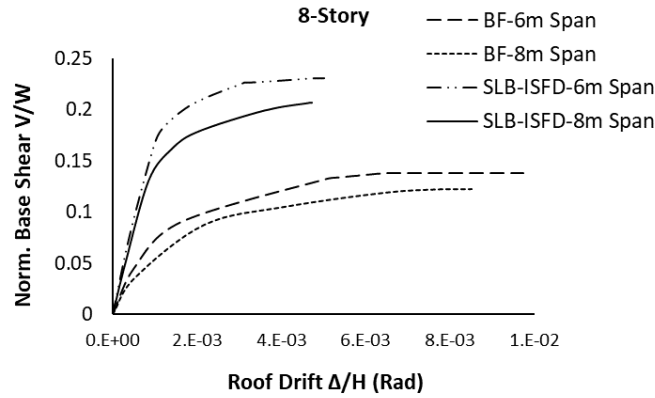


Figure 4-6. Roof drift ratio versus normalized base shear (8-Story)

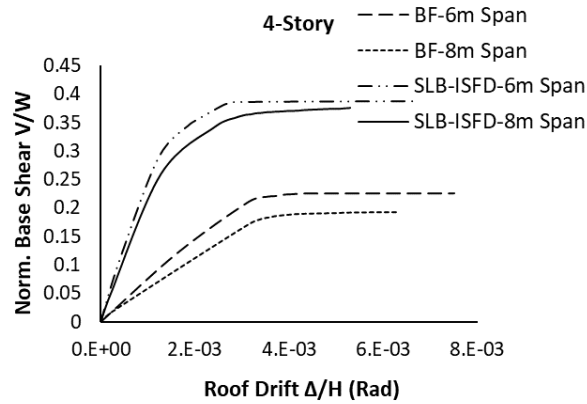


Figure 4-7. Roof drift ratio versus normalized base shear (4-Story)

The 2015 NBCC included force modification factors for several types of Seismic Force Resisting System(s) (SFRS), regardless of building height, span length, or bracing configurations. Furthermore, these aspects are not considered for friction dampers. There are several relationships to estimate the ductility factor (Krawinkler and Seneviratna, 1998; Miranda and Bertero, 1994; Newmark and Hall, 1982). In this research the method proposed by Miranda and Bertero (1994) (Miranda and Bertero, 1994) in equations 4.4 and 4.5 were used for stiff soil to calculate the ductility reduction factor R_μ , where μ is ductility, T is the natural period of the structures and ϕ is a function of ductility, fundamental period, and soil conditions. These results are presented in Table 4-8.

$$R_\mu = \frac{\mu - 1}{\phi} + 1 \geq 1 \tag{4.4}$$

$$\phi = 1 + \frac{1}{10T - \mu T} - \frac{1}{2T} e^{-1.5|\ln(T) - 0.6|^2} \quad (4.5)$$

Table 4-8. Response modification factor for 4-, 8-, 14-Story

Story	Bracing	Span Length	Overstrength factor R_o	Ductility Reduction factor R_μ	Response modification factor
4	SBD	6	3.06	2.61	8.01
		8	2.32	2.55	5.93
8	SBD	6	2.20	3.52	7.74
		8	1.91	2.97	5.64
14	SBD	6	1.47	4.43	6.52
		8	1.41	3.96	5.53

Note: Single Diagonal Braces (SBD)

The results of seismic reduction factors for different types of structures are presented in Figure 4-8. The overstrength factors increased with a decrease in the span length and the height of structures with the average values of 1.88 for 8m span and 2.24 for 6m span different types of buildings. The four-story with 6m span length presented the maximum overstrength factor of 3.06, and the fourteen-story with 8m span length exhibited the minimum value of 1.41. The ductility reduction factors had a minimum value of 2.55 for a four-story 8m span and a maximum value of 4.43 for the fourteen-story 6m span. In general, the ductility factor increased in higher buildings and had average values of 3.16 for 8m span and 3.52 for 6m span length. The closest value of response modification factors for ISFDs can be selected as recommended by the NBCC 2015 ($R=4.8$) and the ASCE 7 ($R=8$) for ductile buckling restrained braced frames are 4.8 and 8. The recommended response modification values are compared with those obtained with the analytical results and shown in Figure 4-8. The highest response modification factor was 8.01 in the four-story building with a 6m span, this value is equal to the prescribed value by the ASCE 7. Generally, all the values were greater than the recommended value by the NBCC 2015 ($R=4.8$), these values decreased with the increase in the height of the structure as well as the span length. Moreover, the average values of response modification factors for all three models are 6.87 and 7.29 for 8m and 6m span length respectively.

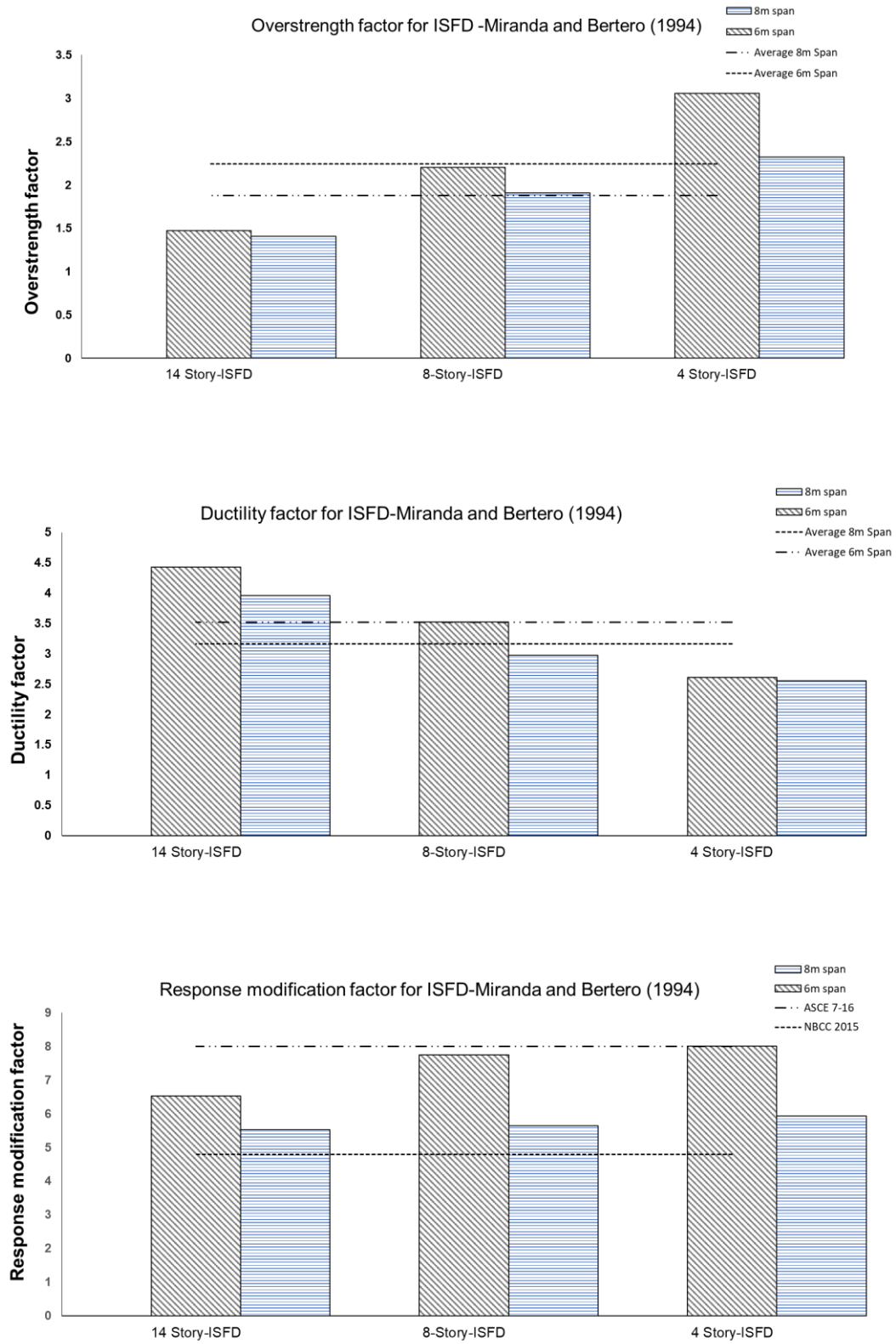


Figure 4-8. Overstrength, ductility, and response modification factors for 14-, 8-, and 4-story

4.3.5 Inelastic Response History Analysis

The connections between the response of the structure and ground-motion parameters have been explored through a different set of strategies (Baker, 2007; Cordova et al., 2000; Gavin and Dickinson, 2011; Gupta, 1990). Scaling and spectral matching are two approaches for adjusting time series to be consistent with the design response spectrum. Ground motions modification includes multiplying the initial time series by scaling factor, then, the matched spectrum is equal to or exceeds the design spectrum over a specified period range. Matching the time series frequency content to be consistent with the design spectrum is Spectral matching (Gavin and Dickinson, 2011; Newmark and Hall, 1982).

Since it is difficult to capture the tolerance over the entire spectrum, the idea is to focus on the period range of interest. The older version of the ASCE (7-05, 7-10) defined this range between $0.2T$ to $1.5T$, in which the lower and higher bounds were to secure higher mode as well as “period elongation” effects. In the ASCE 7-16, nonlinear response history analysis is performed at MCE_R which has a greater inelastic response compared to the design spectrum. Therefore, the upper bound was increased to $2.0T$, where T represents the maximum fundamental period of the building considering the fundamental torsional period as well as transitional directions. In this part, 25 different ground motion records were obtained from the database of the Pacific Earthquake Engineering Research Center (PEER) as presented in Table 4-9. Summary of Metadata of Selected Records, these greater variabilities in the selection of ground motions leads to a better seismic performance result. SeismoMatch 2018 software was used to match the accelerograms spectrally based on the design spectrum, the results are illustrated in Figure 4-9. Appendices A4.2, A4.3, and A4.4 provide the results of original and scaled acceleration, velocity, and displacement.

Table 4-9. Summary of Metadata of Selected Records

ID	Scale Factor	Earthquake	Year	Station	Magnitude	Mechanism	Arias Intensity (cm/sec, OA)	Arias Intensity (cm/sec, MA)	PGA (g)
1	0.8489	San Fernando	1971	Pacoima Dam (upper left abut)	6.61	Reverse	8.94	14.06	1.219
2	1.0261	Gazli USSR	1976	Karakyr	6.8	Reverse	5.28	11.27	0.701
3	0.7926	Tabas Iran	1978	Tabas	7.35	Reverse	11.82	21.08	0.853
4	1.297	Imperial Valley-06	1979	Bonds Corner	6.53	Strike slip	3.98	17.42	0.598
5	1.2494	Nahanni Canada	1985	Site 1	6.76	Reverse	3.88	8.44	1.107
6	1.5274	Superstition Hills-02	1987	Parachute Test Site	6.54	Strike slip	3.74	14.96	0.432
7	1.6425	Loma Prieta	1989	BRAN	6.93	Reverse Oblique	5.35	17.74	0.456
8	1.5415	Erzican Turkey	1992	Erzincan	6.69	Strike slip	1.52	9.12	0.386
9	0.9241	Cape Mendocino	1992	Cape Mendocino	7.01	Strike slip	5.95	8.88	1.491
10	1.1584	Landers	1992	Lucerne	7.28	Strike slip	6.97	10.99	0.725
11	1.6054	Northridge-01	1994	Beverly Hills - 14145 Mulhol	6.69	Reverse	3.08	14.71	0.443
12	1.1671	Kobe Japan	1995	KJMA	6.9	Strike slip	8.39	13.32	0.834
13	1.0745	Chi-Chi Taiwan	1999	CHY028	7.62	Reverse Oblique	5.29	13.71	0.636
14	1.2578	Duzce Turkey	1999	Bolu	7.14	Strike slip	3.72	14.01	0.739
15	1.384	Manjil Iran	1990	Abbar	7.37	Strike slip	4.64	25.29	0.514
16	1.769	Loma Prieta	1989	Los Gatos - Lexington Dam	6.93	Reverse Oblique	1.86	9.96	0.442
17	1.6839	Tottori Japan	2000	SMNH01	6.61	Strike slip	5.29	16.40	0.732
18	1.0737	Bam Iran	2003	Bam	6.6	Strike slip	8.01	16.23	0.807
19	0.7526	Niigata Japan	2004	NIG019	6.63	Reverse	14.49	14.77	1.166
20	1.7991	Chuetsu oki Japan	2007	Joetsu Kakizakiku Kakizaki	6.8	Reverse	1.31	17.23	0.303
21	1.0158	Iwate Japan	2008	AKTH04	6.9	Reverse	11.81	16.44	1.343
22	1.7436	El Mayor Cucapah Mexico	2010	CERRO PRIETO	7.2	Strike slip	2.97	23.58	0.286
23	0.982	Darfield New Zealand	2010	GDLC	7	Strike slip	4.49	11.56	0.764
24	1.5914	Duzce Turkey	1999	IRIGM 496	7.14	Strike slip	13.36	16.21	1.031
25		Tohoku	1923		7.9	Subduction	11.51	59.71	0.427

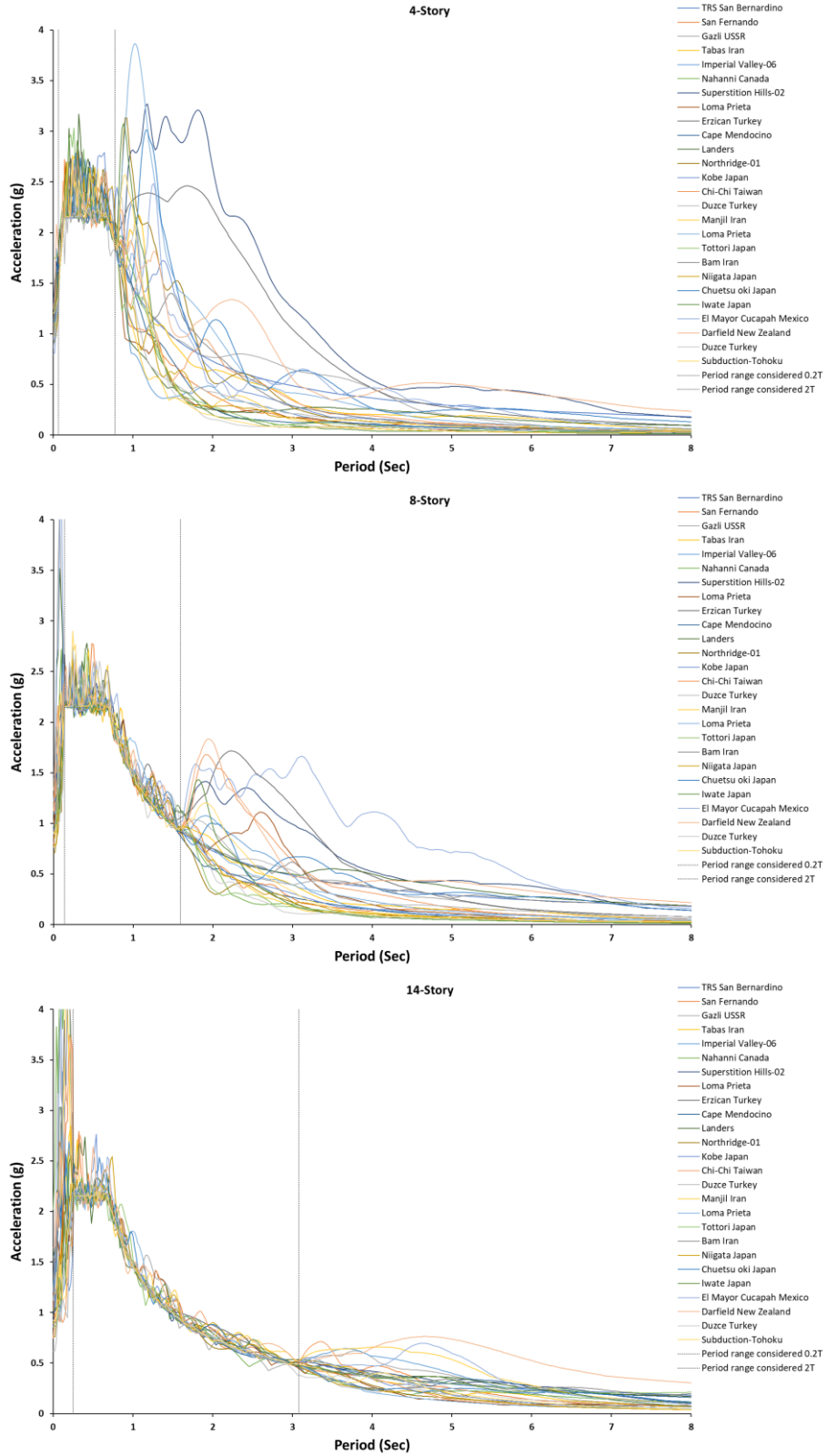


Figure 4-9. Matched Accelerograms based on the target response spectrum for 14-, 8-, and 4-story

4.3.6 Interpretation of Results

Dynamic time history analysis was performed to assess the seismic performance of the ISFDs. Figure 4-10 to Figure 4-15 presents the inter-story drift ratio of different stories with different span lengths subjected to the various ground motions. This figure represents the inter-story drift ratios ranging from 2% and 3.5% for bare frames with 8m and 6m span lengths; however, the inter-story drift ratios shifted below 2.5% when buildings are equipped with ISFDs which is within the range of the “Life safety” performance, according to NBCC 2015 definition. The maximum drift ratio for the fourteen-story with 6m span length occurred at 36m height of the building, this value shifted to a lower level in the 8m span length. In the eight-story model with the 8m span length, the maximum inter-story drift ratio was at 15m height of the building and shifted down to 8m height of the building with lower span length. These values remained the same at the height of 8m for the four-story with both 8m and 6m span lengths.

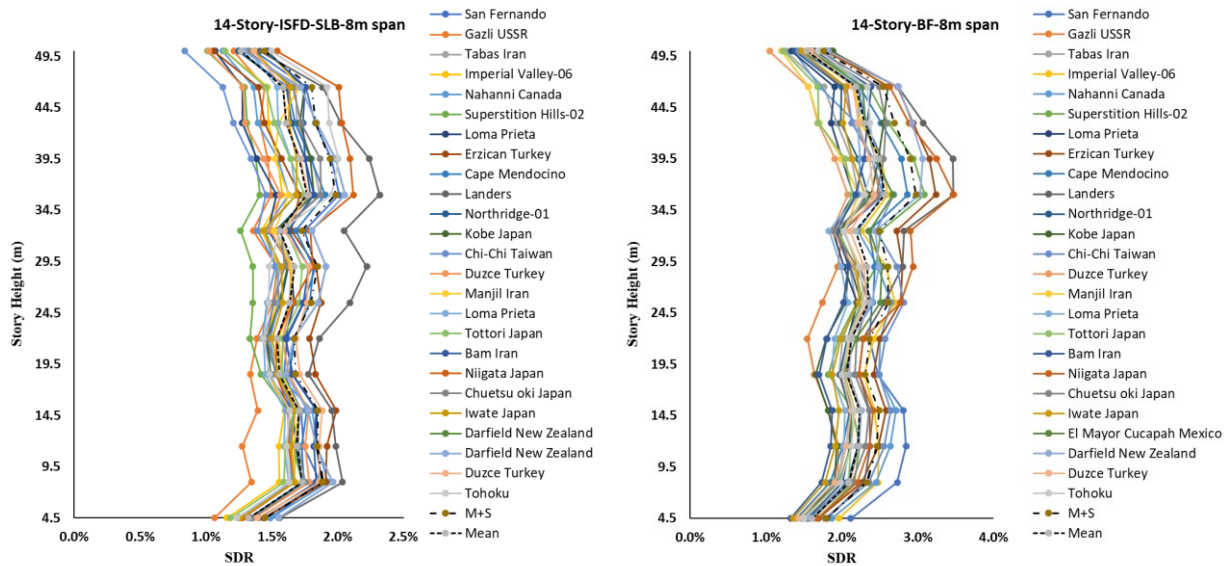


Figure 4-10. Inter-story drift ratio for 14-Story with 8m span (ISDF&BF)

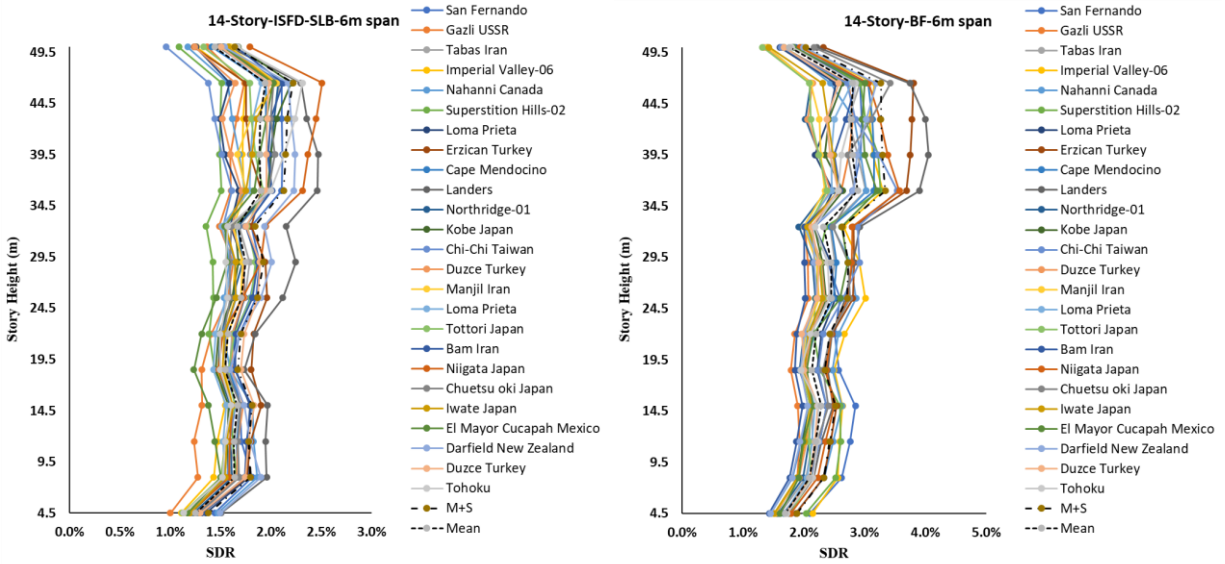


Figure 4-11. Inter-story drift ratio for 14-Story with 6m span (ISDF&BF)

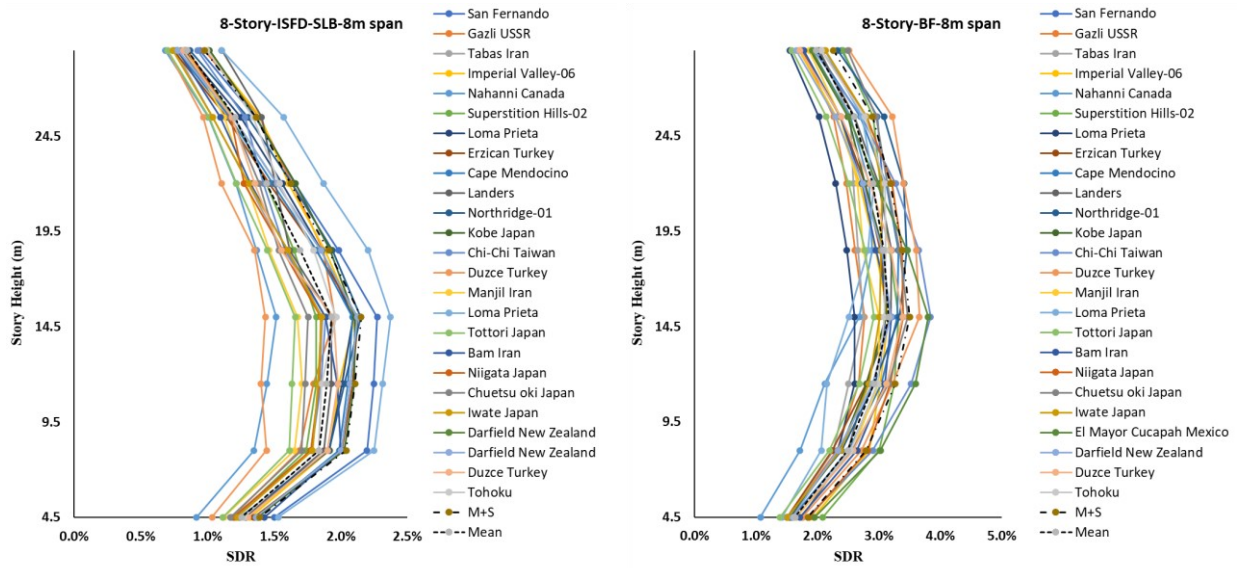


Figure 4-12. Inter-story drift ratio for 8-Story with 8m span (ISDF&BF)

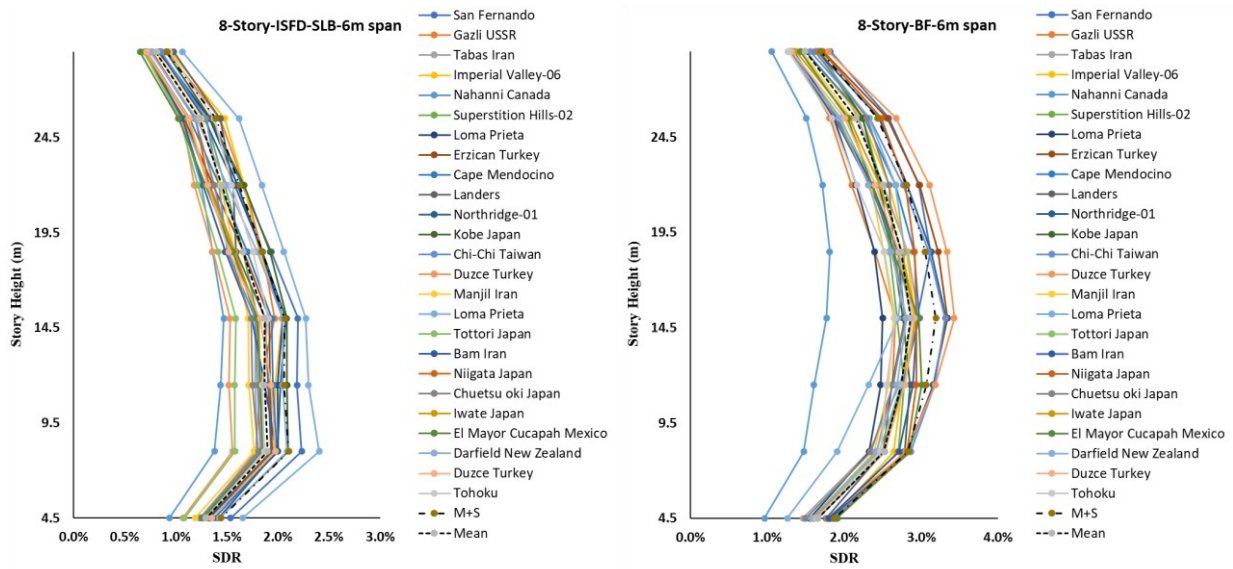


Figure 4-13. Inter-story drift ratio for 8-Story with 6m span (ISDF&BF)

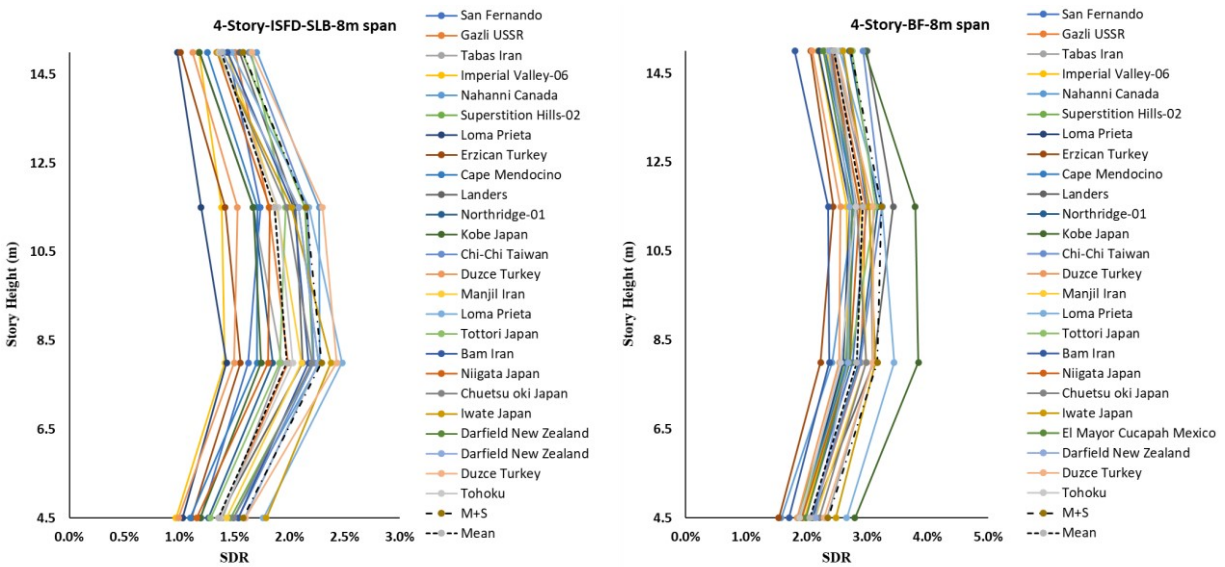


Figure 4-14. Inter-story drift ratio for 4-Story with 8m span (ISDF&BF)

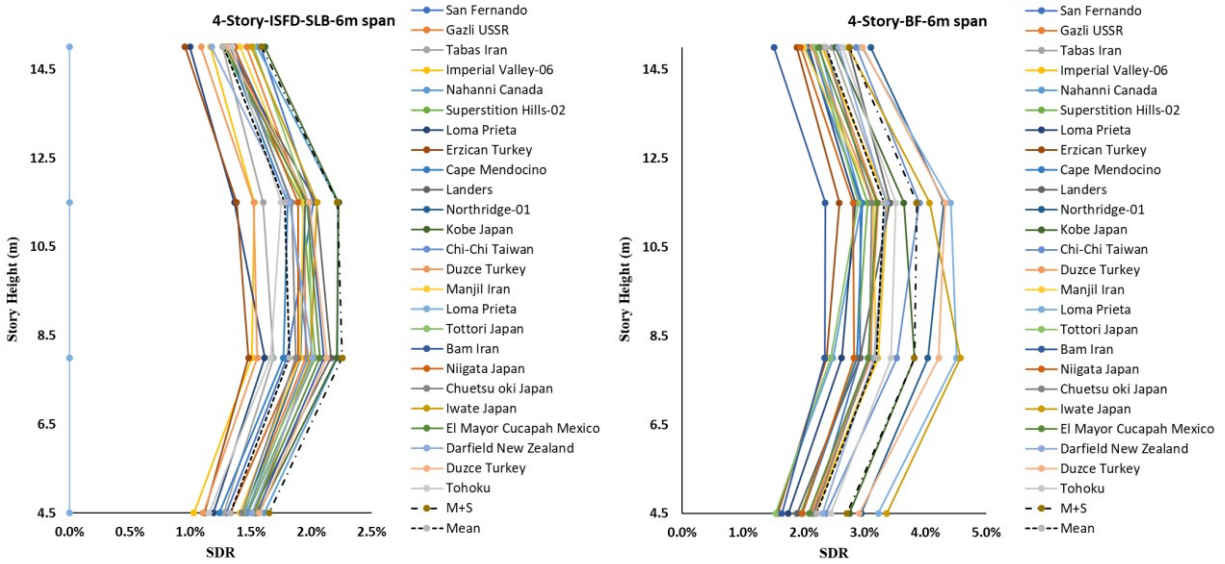


Figure 4-15. Inter-story drift ratio for 4-Story with 6m span (ISDF&BF)

The mean values and sum of standard deviation for all the twelve models are presented in Figure 4-16. The maximum mean values and the sum of standard deviation are 1.98%, 2.20% for the fourteen-story equipped with ISFDs with different span lengths of 8m and 6m respectively, these numbers are increased to 2.90% and 3.33% for the bare frames. The eight-story buildings with ISFDs had the maximum values of 2.10%, and 2.15% for 8m, and 6m span lengths, and the brae frames had the maximum values of 3.20% and 3.50% for 8m, and 6m span lengths. The four-story experienced the same mean and sum of standard deviation values with a maximum of 2.29% for ISFDs with 8m and 6m span lengths and different values of 3.23% and 3.75% for bare frames with different span lengths of 8m and 6m. It can be stated, when the structures were equipped with ISFDs, there was a reduction of about 60% to 70% in the drift ratios, these values moved to a lower level in greater span length. Moreover, the concentration of story drift ratio shifted to higher levels with an increase in the height of the structures.

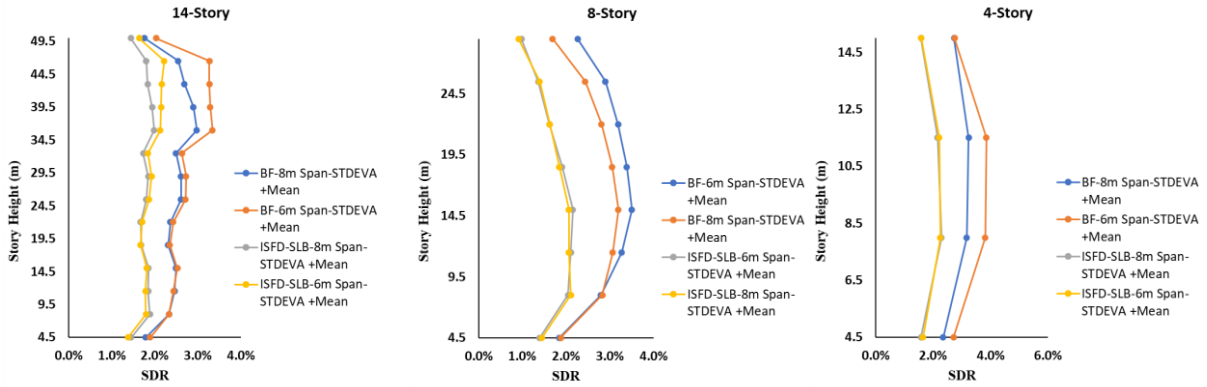


Figure 4-16. Mean and standard deviation values of Inter story drift ratio for 4-, 8-, 14-Story

For the sake of brevity, only the maximum hysteresis curves for these three models are shown in Figure 4-17, which are for 6-m and 8-m spans. The amount of dissipated energy in all models with the 8m span was greater compared with the 6m span length, which is due to the number of axial forces in the bracing.

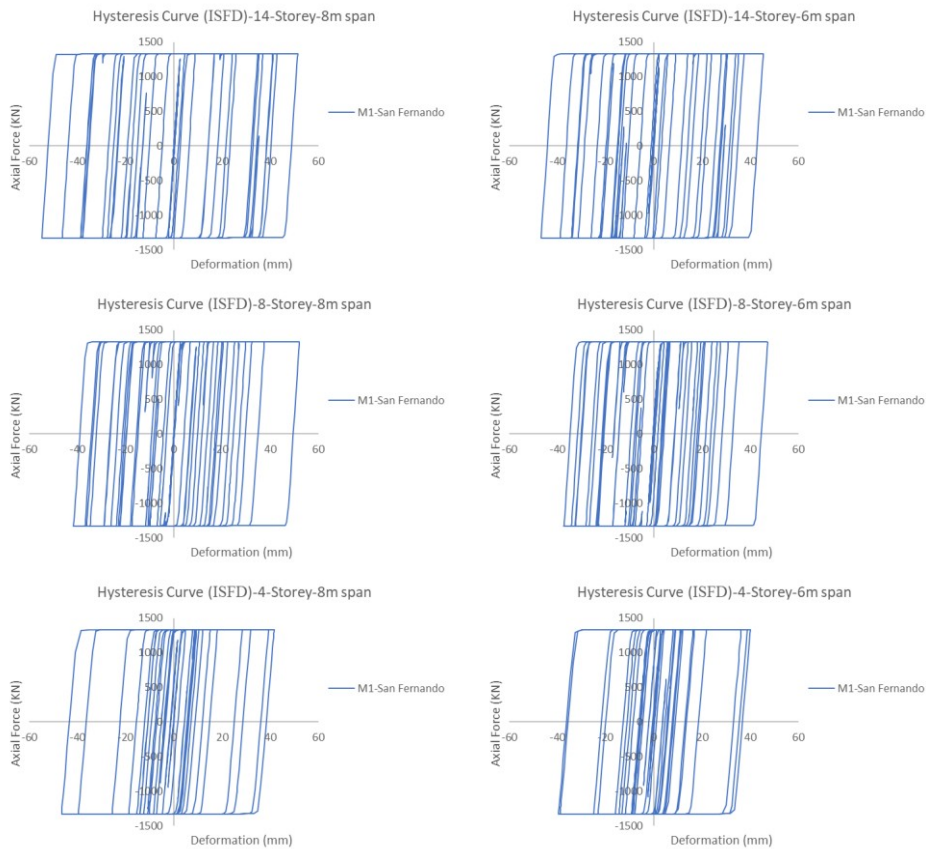


Figure 4-17. Maximum hysteresis response for 4-, 8-, 14-Story

Results from nonlinear response history analysis of the base shear demands are presented in to Figure 4-18 to Figure 4-20. These values were based on the maximum value of base shear for each ground motion, as it can be seen all of these values are below the capacity of each system. In addition, the base shear demands are higher with greater span length and increase in higher buildings.

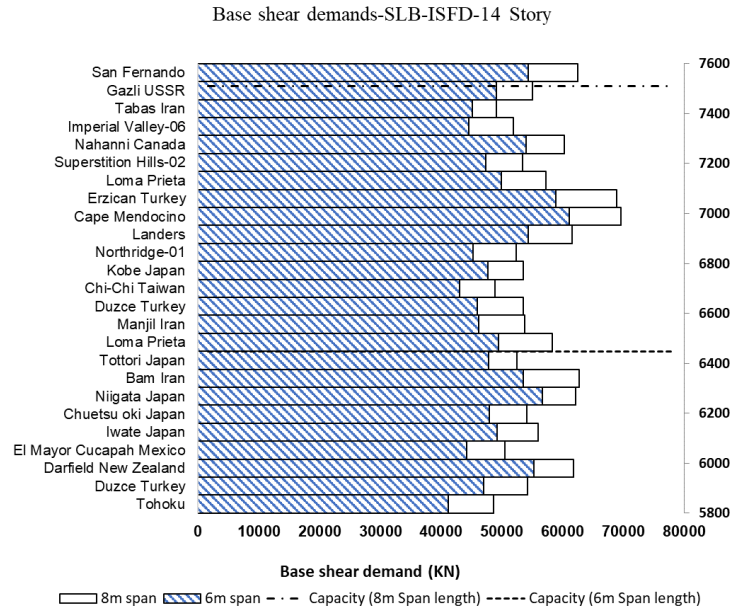


Figure 4-18. Base shear demands for 14-Story

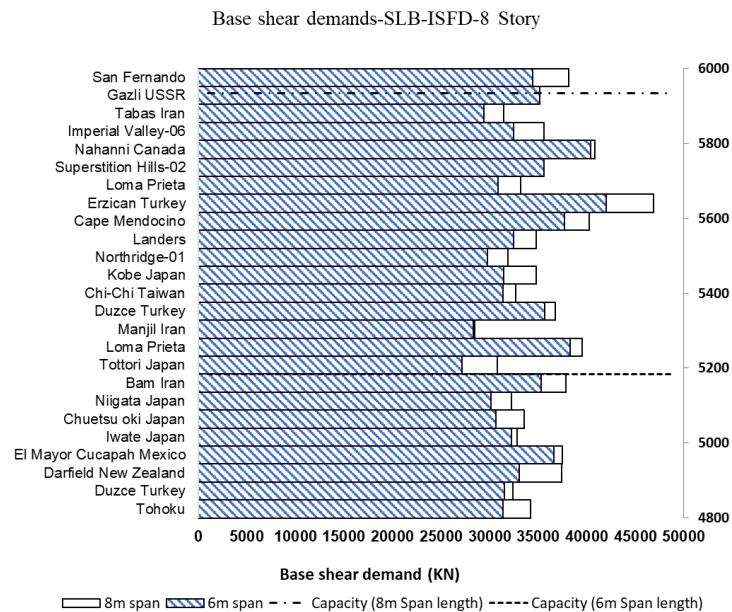


Figure 4-19. Base shear demands for 8-Story

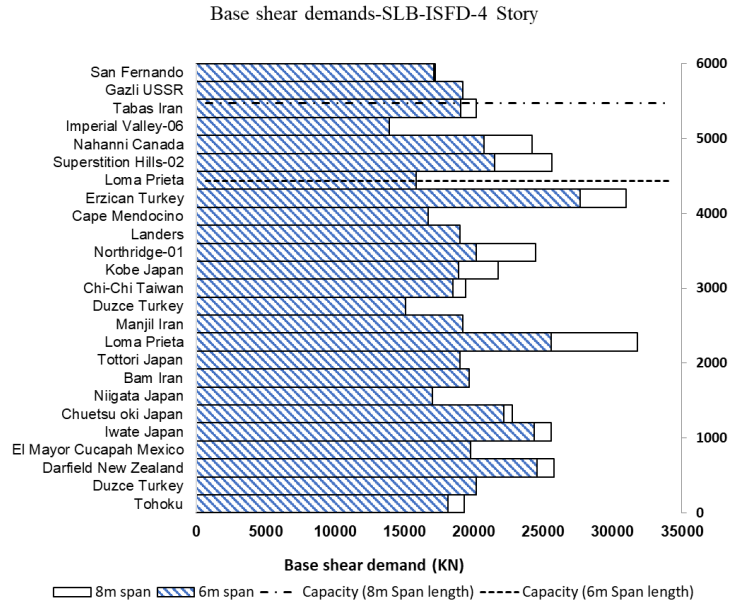


Figure 4-20. Base shear demands for 4-Story

4.3.7 Results and Discussions

This article presents the methodology for overstrength, response modification, and ductility factors of different ISFD's systems. The slip loads are calculated based on the lateral shear forces, shear deflection at each floor, lateral stiffness of braces as well as the lateral stiffness of existing frames and braces. The response modification factors of four- eight- and fourteen-story ductile concrete structures equipped with Inline Seismic Friction Dampers (ISFD) with different span lengths and height are determined based on Miranda and Bertero (1994) method. For this purpose, normalized moment rotation component models are calculated based on ASCE 41 for each beam and column, these component modeling parameters are applied to each member. The target displacement is calculated based on ASCE 41 for DLE, and MSE. Then nonlinear static analysis was performed to assess the seismic characteristics of each system. The performance of each system is evaluated using nonlinear response history analysis. Twenty-five different ground motions were matched based on the target response spectrum and the period of each structure considering the range between 0.2T to 1.5T. The main observations and conclusions are summarized as follows.

- The closest ductility and overstrength factors for an equivalent system are given for a ductile buckling restrained braced frame in the NBCC 2015, the overstrength factors had a range from 1.41 to 3.06 which is higher than the prescribed value ($R_0=1.2$) in the NBCC 2015, these values decreased with increase in height, and are higher in shorter span length. The ductility reduction factors; however, increased when the height increased. The ductility reduction factors ranged from 2.55 to 4.43 compared to the NBCC 2015 ($R_d=4.0$).
- The response modification factors are calculated by multiplying the overstrength by the ductility factors, which had a range from 5.53 to 8.01 in comparison with the recommended value of 4.8 in the NBCC 2015. It was observed the response modification factors decreased when the height increased. Moreover, these values are affected by the span length and are greater in smaller span lengths compare with larger span lengths.
- The slip loads are calculated based on the brace angle, lateral shear forces, shear deflection at each floor, the lateral stiffness of the bare frame as well as the lateral stiffness of braces and their combination. Therefore, for simplicity and practical approach used by engineers, it can be suggested that the system may be modeled as a braced frame, and the axial loads in the braces should be equal or greater than the slip load of friction dampers.
- The STDEVA +Mean values from nonlinear response history analysis indicated the reduction of story drift ratio from 60% to 70% for all three models equipped with ISFDs, as compared to the bare frames. Moreover, the concentration of story drift demands was in higher stories in taller buildings and is about the same or lower when the span length decreased. The results from base shear demand indicated that the increase in the structural height increased the base shear demand. Additionally, a decrease in the span length reduced the base shear demand by about 10%.
- The hysteresis curves showed the dissipated energy was higher in longer span length compared to lower span length. ISFDs system has a direct effect on the reduction of formation of the plastic hinges by about 45% corresponds to the structural performance, which is life safety, or better.

Further investigations can be performed to assess the seismic characteristics of buildings using different bracing configurations, and floor heights with different bracing angles. More details in the modeling of structures equipped with ISFDs shall be considered.

4.4 Analysis for multiple levels of earthquakes

The 2015 NBCC recommended selecting and scaling ground motions based of the design response spectrum (5% damped DRS). The four-, eight-, and fourteen-story ductile concrete moment resisting frames with diagonal inline friction dampers and varied span lengths of 6m and 8m, which were described in section 4.3 are employed in this section and designed based on the design response spectrum shown in Figure 4-21. The structures are considered to be in Victoria, British Columbia, in the western region of Canada, with site class "C" and detailing followed the Canadian Standard for reinforced concrete buildings (CSA A23.3-19). Because the NBCC 2015 does not consider the maximum considered earthquake for dissipation system validation, multiple levels of earthquakes are considered to validate the performance of buildings with inline friction dampers. This method is similar to incremental dynamic analysis (IDA); however, the earthquake levels were kept below the point of failure of the structures, as a very high seismic zone for this location is not reasonable.

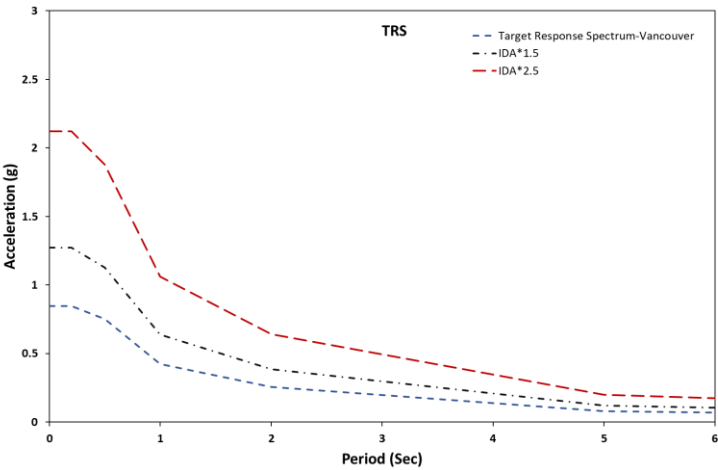


Figure 4-21. Original and multiple levels of DRS

In this part, 12 different ground motion records were obtained from the database of the Pacific Earthquake Engineering Research Center (PEER) as presented in Table 4-10. The accelerograms were scaled according to the multiple levels of design spectrum using the relevant tool in SeismoMatch 2018 software, based of the recommended amplitude scale over the period range of 0.2T to 1.5T (NBCC 2015), as presented in Figure 4-22 to Figure 4-24.

Table 4-10. Summary of Selected Records

ID	Scale Factor	Earthquake	Year	Station	Magnitude	Mechanism	PGA (g)
1	1.055	Imperial Valley-02	1940	El Centro Array #9	6.95	Strike slip	0.449
2	1.4274	San Fernando	1971	LA - Hollywood Stor FF	6.61	Reverse	0.491
3	1.1281	Imperial Valley-06	1979	Brawley Airport	6.53	Strike slip	0.414
4	1.5036	Kobe Japan	1995	Abeno	6.9	Strike slip	
5	0.7353	Irpinia Italy-01	1980	Sturno (STN)	6.9	Normal	0.351
6	1.2867	Loma Prieta	1989	Agnews State Hospital	6.93	Reverse Oblique	0.534
7	1.599	Cape Mendocino	1992	Fortuna - Fortuna Blvd	7.01	Reverse	0.385
8	1.4047	Chi-Chi Taiwan	1999	CHY046	7.62	Reverse Oblique	0.453
9	0.644	Manjil Iran	1990	Abbar	7.37	Strike slip	0.455
10	0.8211	Cape Mendocino	1992	Bunker Hill FAA	7.01	Reverse	0.410
11	1.7422	Chuetsu oki Japan	2007	Joetsu Kita	6.8	Reverse	0.416
12	0.603	El Mayor Cucapah Mexico	2010	MICHOACAN DE OCAMPO	7.2	Strike slip	0.411
13	0.888	Darfield New Zealand	2010	Christchurch Cashmere	7.2	Strike slip	
14		Tohoku	1923		7.9	Subduction	0.453

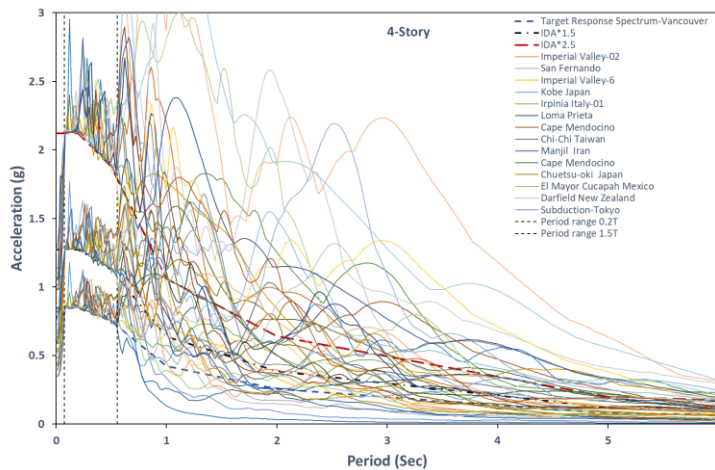


Figure 4-22. Multiple matched Accelerograms based on DER, MCER, and 2.5 times DER spectrum for 4-story

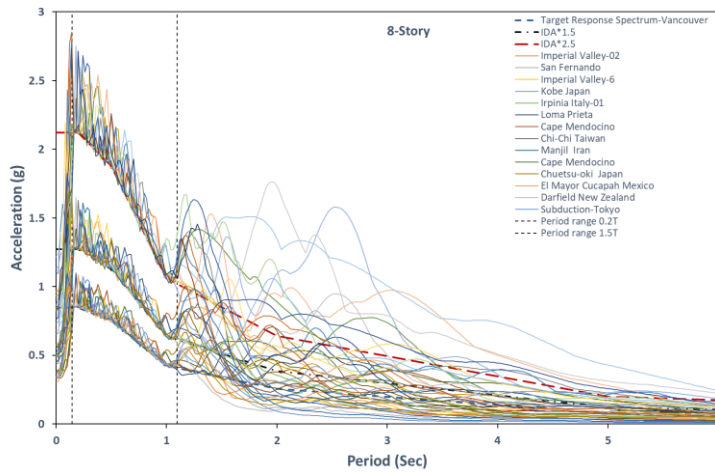


Figure 4-23. Multiple matched Accelerograms based on DER, MCER, and 2.5 times DER spectrum for 8-story

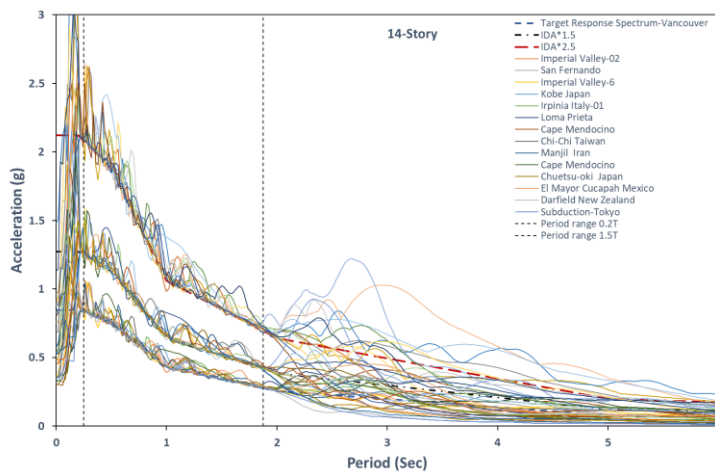


Figure 4-24. Multiple matched Accelerograms based on DER, MCER, and 2.5 times DER spectrum for 14-story

The standard deviation and mean values of drift profiles for all six models are presented in Figure 4-25, as expected, the performance of structures with inline friction dampers falls below the 2.5 percent recommended life safety level based on the NBCC 2015.

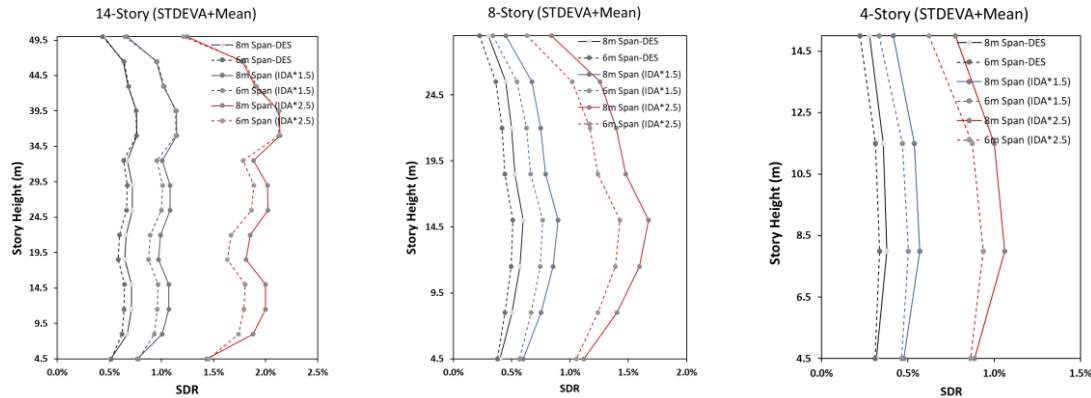


Figure 4-25. Story Drift profile of 4, 8, and 14-story

4.5 Comparative study five different passive energy dissipation systems

The prediction of structural performance subjected to seismic excitation is very important. Stiff structures have higher base shear and acceleration which may cause damage to nonstructural elements, while the flexible structures the damages occur at the primary members. The damage level can be determined when a large amount of kinetic energy caused by an earthquake is dissipated by a structure. Since it is not economically feasible to dissipate this energy within the elastic range of materials, building codes allow that the structure may yield in a controlled location and ductile manner, these designated elements are so-called structural fuses (Ko & Field, 1988). The conventional seismic design allows the reduction of forces below the elastic level. This inelastic action often results in significant damage in the beams or columns. To avoid the formation of plastic hinges in the members of the structure, this study investigates the seismic design factors of five passive energy systems.

The objectives of this study are to compare the design procedures of American and Canadian standards for a fourteen-story moderately ductile concrete moment resisting frames based on ACI 318-19, CSA A23.3-19 and ASCE 7-16, NBCC 2015 Using ETABS software, and to investigate the effects of five passive energy systems including conventional ductile concrete moment resisting frame (CMRF) with no dampers, CMRF with Ten-Co seismic brake, CMRF with Fluid viscous damper, CMRF with Triangular Metallic Yielding Dampers, as well as two seismic

isolators including CMRF with Lead Rubber Bearing Isolator (LRBI) and CMRF with Triple Pendulum Isolator (TPI). Each system is designed individually. Nonlinear static analysis and nonlinear response history analysis were carried out to determine their seismic characteristics and responses and to place friction devices within a proper frame of reference.

4.5.1 Design of Structural Models

In this section, a comparison of design procedures of American and Canadian standards for fourteen-story ductile concrete moment resisting frames using ETABS software is presented. The building is assumed to be located in Vancouver with latitude, the longitude of 49.2827291 and -123.1207375 on a very dense soil and soft rock with site class “C”. The building has a height of 4.5m for the first story and a similar height of 3.5m for all other levels and consists of five bays in both directions. The prescribed design loadings in codes are minimum design loads and related criteria for buildings and other structures (ASCE/SEI 7-16) and the national building code of Canada (NBCC 2015). Design codes are including building code requirements for structural concrete (ACI 318, 2019) and the design of concrete structures CSA A23.3-19 considering the strength design method. The minimum compressive characteristic strength at 28 days on a cylindrical specimen, f'_c , of the reinforced concrete is assumed to be 30 MPa is used for Cast in place concrete. The reinforced concrete unit weight, w_c , is taken as 24 KN/m³ (2400 kg/m³). The initial modulus of elasticity E_c is equal to 27692 MPa (282379 kgf/cm²) and the Poisson ratio, ν , is equal to 0.2, the design live and dead loads for all models are assumed to be 2.4 KN/m² and 1.5 KN/m², and the snow load acting on the roof is 1.64KN/m².

ASCE 7-16 has three categories for concrete moment resisting systems including “special reinforced concrete moment frames” (SMFs), “intermediate reinforced concrete moment frames” (IMFs), “ordinary reinforced concrete moment frames” (OMFs). Whereas the 2015 NBCC defines ductile, moderately ductile, and conventional for moment-resisting frames. In this study, based on the ASCE 7, SMFs have been used in order to reach ductility in high seismic regions, this can be defined by sway special in the program, in this category the response modification factor, R , overstrength factor, Ω_o , and deflection amplification factor, C_d , are 8, 3, and 5.5. The ductility and

overstrength factor of 4 and 1.7 are considered based on the NBCC 2015 for ductile concrete moment-resisting frames. Material quantities for both models are presented in Table 4-11. The design procedures based on American standards can be observed about 10% more material quantities than the Canadian standard.

Table 4-11. Material quantities

System Types	Steel (Tons)		Concrete (m ³)			Total Steel (Tons)	Total Concrete (m ³)
	Column	Beam	Column	Beam	Floor		
DCMFs (NBCC)	131.65	279.35	1322	2637	4701	411	8660
SMFs (ASCE)	145.55	305.32	1466	2875	5161	450	9502

Note: DCMRF: Ductile concrete moment frames, SMFs: Special reinforced concrete moment frames

The bracing configuration and base isolator positions are presented in Figure 4-26 and Figure 4-27.

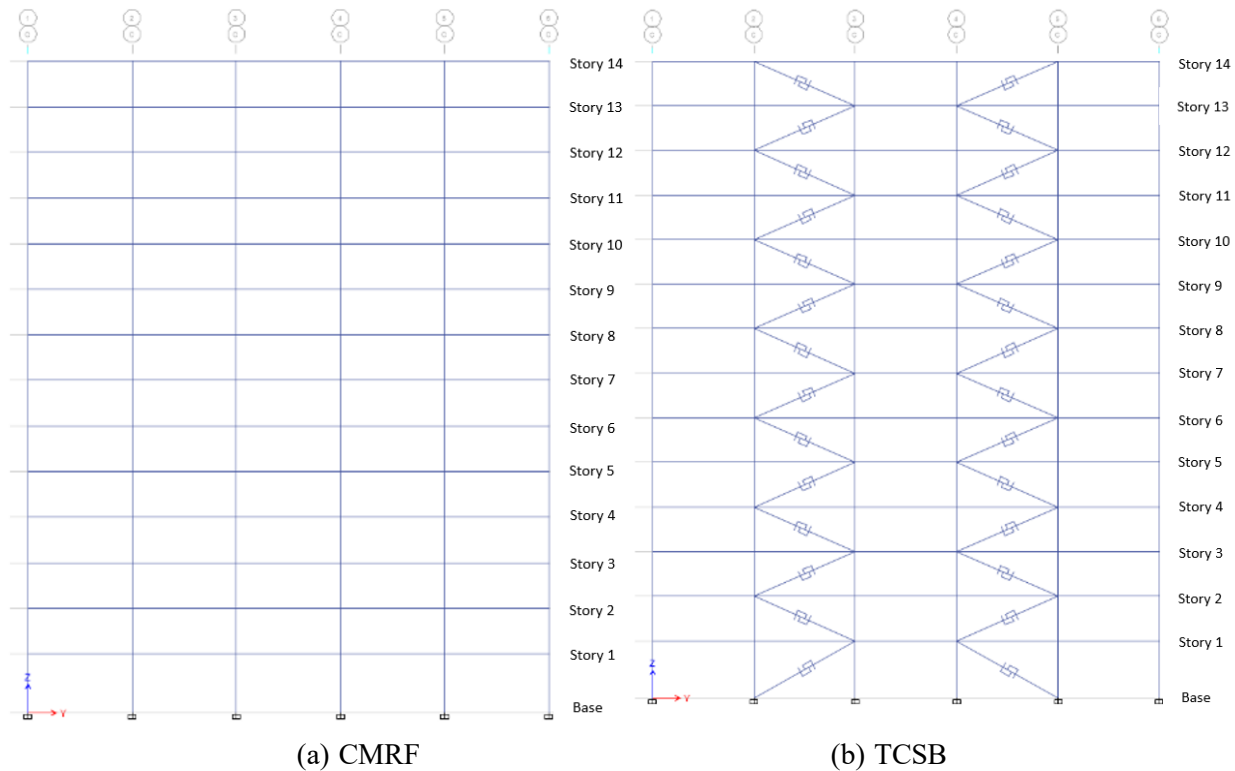
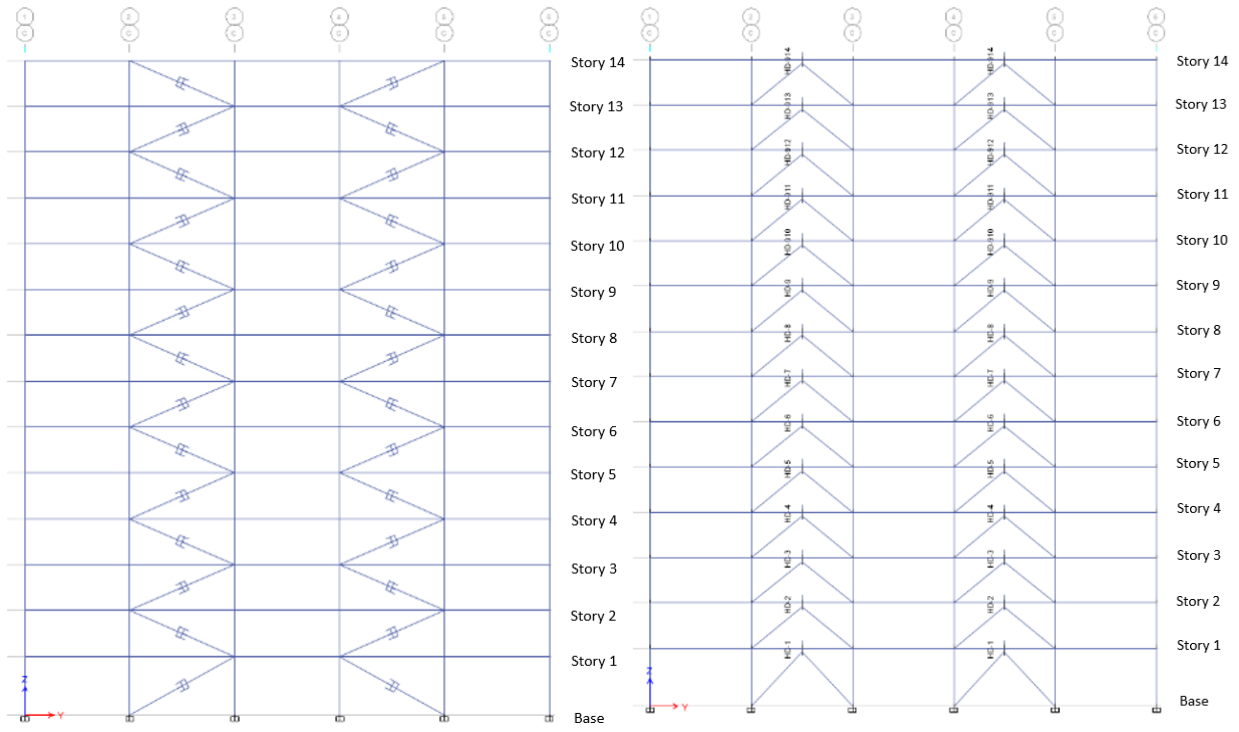
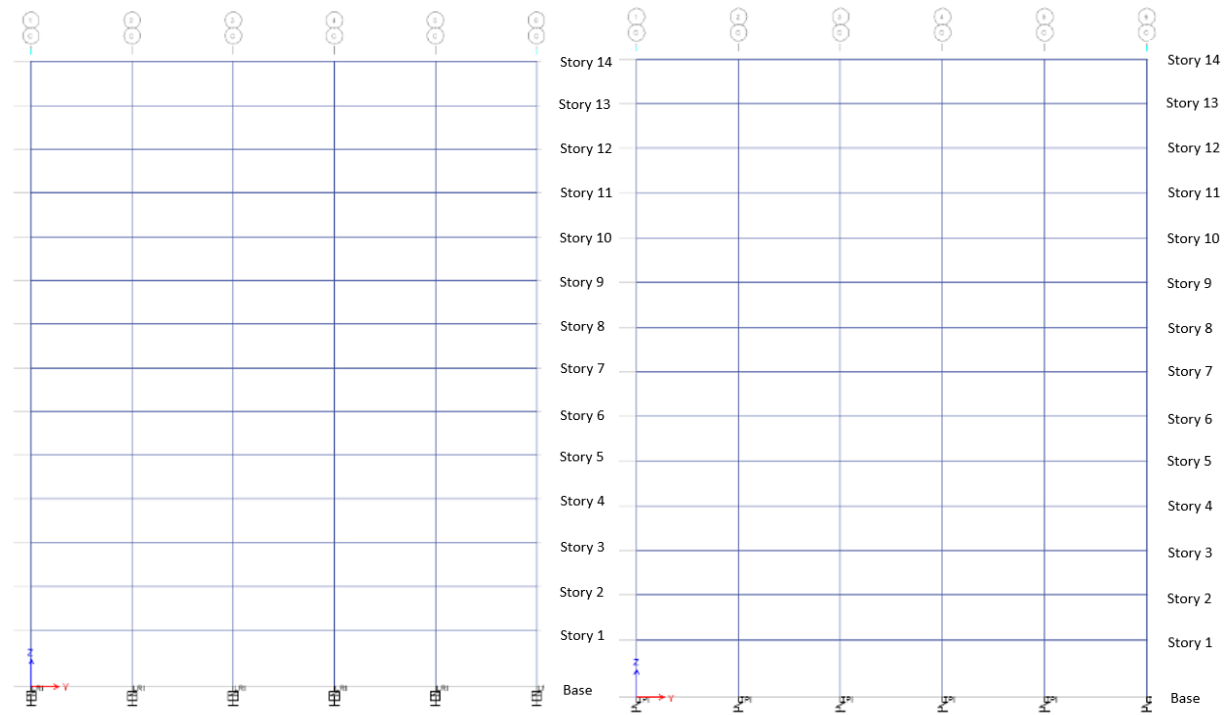


Figure 4-26. Elevation view of CMRF and TCSB



(c) FVD

(d) TMYD



(e) LRBI

(f) TPI

Figure 4-27. Elevation view of dissipation systems

4.5.2 Design response spectrum

In the NBCC 2015, the uniform hazard spectrum can be constructed based on six spectral accelerations for periods of 0.2, 0.5, 1.0, 2.0, 5.0, and 10 seconds considering different soil types from hard rock in class A to class F for liquefiable soil, the horizontal peak ground velocity and acceleration are based on 2% probability of exceedance in 50 years. ASCE 7-16, differs from NBCC 2015, the response spectrum is expected to achieve a 1% probability of collapse in 50 years. In this standard, the design response spectrum can be constructed based on the risk-targeted maximum consider earthquake (MCE_R) as well as site coefficient and fundamental period of the structure. The constructed design response spectrum based on both codes is presented in Figure 4-28.

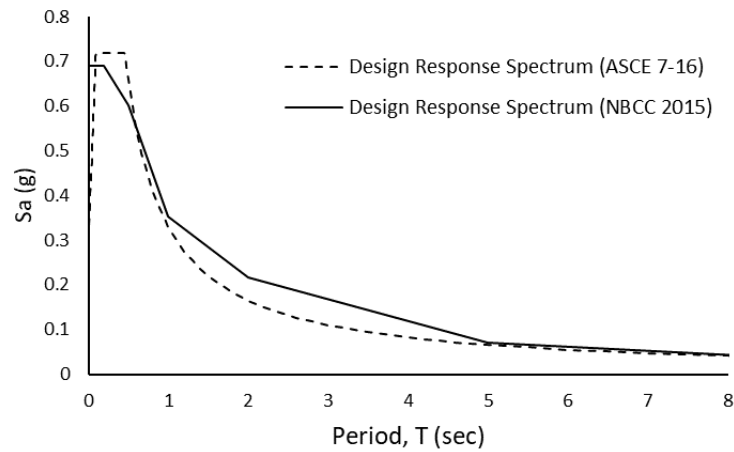


Figure 4-28. Constructed design response spectrum based on ASCE 7-16 and NBCC 2015

4.5.3 Design of Fluid Viscous Dampers (FVD)

The fluid viscous damper force is dependent on the velocity, v , the damping coefficient, C , the velocity exponent, α , and the signum function as presented in equation 4.6.

$$F = C|v|^\alpha \text{sgn}(v) \quad (4.6)$$

In this study modal strain energy method is used to develop the preliminary size of viscous fluid dampers, these values are presented in Table 4-12, where K_i is the story stiffness, θ_i is the damper's angle, η_i is the number of dampers, T is the period of the structure, ζ is the damping ratio and C_i is the damping coefficient.

Table 4-12. Damping coefficient

Story level	K_i (KN/mm)	θ_i (degrees)	η_i	T (Sec.)	ζ	C_i (KN-Sec/mm)
14	206	23	4	1.4	0.22	30.01
13	234	23	4	1.4	0.22	33.99
12	298	23	4	1.4	0.22	43.37
11	335	23	4	1.4	0.22	48.71
10	368	23	4	1.4	0.22	53.57
9	474	23	4	1.4	0.22	68.97
8	485	23	4	1.4	0.22	70.52
7	523	23	4	1.4	0.22	76.15
6	609	23	4	1.4	0.22	88.70
5	669	23	4	1.4	0.22	97.42
4	662	23	4	1.4	0.22	98.83
3	724	23	4	1.4	0.22	105.33
2	804	23	4	1.4	0.22	116.99
1	851	29	4	1.4	0.22	138.56

4.5.4 Design of Metallic Yielding Dampers (MYD)

Metallic yielding dampers dissipate energy through the inelastic behaviour of mild steel plates, which can be in the form of triangular or X shapes. Shear panels, slit and honeycomb dampers, and an unbonded brace are other types of metallic yielding dampers (Soong and Spencer, 2002). Triangular metallic yielding dissipators were initially developed as base isolator's damping elements in New Zealand. TMYD consists of parallel triangular steel plates and can be installed at the end of chevron bracing, when a force is applied to the plate, the energy will be dissipated by yielding metal within the device. To obtain a consistent yielding over the height of the plate the ratio of moment-curvature is to be fixed, this can be achieved by the design of the shape and geometry of the plate. A typical view of Triangular Metallic Yielding Dampers (TMYD) or yielding damper is illustrated in Figure 4-29 (Tsai et al., 1993).

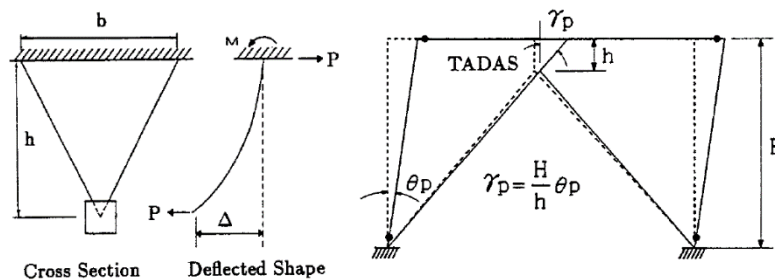


Figure 4-29. Schematic view of yielding damper (Tsai et al., 1993)

The lateral elastic stiffness, K_d , and the yield strength, P_y , of TMYD can be calculated from equations 4.7 and 4.8 (Tsai et al., 1993).

$$K_d = \frac{N \times E \times b \times t^3}{6 \times h^3} \quad (4.7)$$

$$P_y = \frac{F_y \times N \times b \times t^2}{6 \times h} \quad (4.8)$$

Where N is the number of triangular plates, F_y is the tensile yield stress, E is the modulus of elasticity, b , t , and h are the base width, the thickness, and the height of the triangular plate. The design parameters are calculated and presented in Table 4-13.

Table 4-13. TMYD design parameters

Story level	Elevation (m)	K_r (KN/mm)	K_t (KN/mm)	K_d (KN/mm)	P_y (KN)	C_o	PYS ratio
14	50	122	154	32	59	1.3	0.02
13	46.5	175	297	122	287	1.3	0.02
12	43	220	429	209	527	1.3	0.02
11	39.5	259	551	291	792	1.3	0.02
10	36	293	661	368	1053	1.3	0.02
9	32.5	375	760	385	1073	1.3	0.02
8	29	389	848	459	1379	1.3	0.02
7	25.5	444	925	480	1441	1.3	0.02
6	22	429	991	562	1659	1.3	0.02
5	18.5	519	1046	527	1542	1.3	0.02
4	15	529	1090	561	1536	1.3	0.02
3	11.5	515	1123	608	1888	1.3	0.02
2	8	658	1145	487	1443	1.3	0.02
1	4.5	700	1156	456	1302	1.3	0.02

4.5.5 Design of base isolators

In this study Rubber Isolator (RI) and Friction Isolator (FI) are calculated based on FEMA 356 and ASCE 7 seismically isolated structures. The idealized behaviour of the lead rubber isolator is presented in Figure 4-30, K_d is the post-yield stiffness, and f_o or Q_d is the strength characteristic.

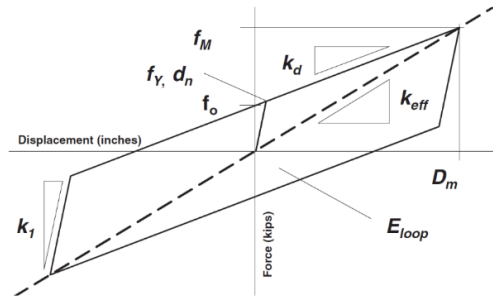


Figure 4-30. Idealized bilinear of force-displacement of the isolator (ASCE 7)

The effective period and the maximum lateral displacement of the isolation system shall be determined by equations 4.9 and 4.10.

$$T_M = 2\pi \sqrt{\frac{W}{gK_M}} \quad (4.9)$$

$$D_M = \frac{gS_{M1}T_M}{4\pi^2 B_M} \quad (4.10)$$

Where g is the acceleration due to gravity, W is the effective seismic weight, K_M is the effective stiffness, S_{M1} is the maximum considered earthquake for 1 second period and B_M is a coefficient based on the effective damping and the maximum displacement. Variation of the design parameters shall be considered using upper and lower bound for each mechanical property of isolators, these property modification factors are in the range of 0.6 to 2.1 and 0.8 to 1.8 for sliding and elastomeric isolators. The properties of lead rubber bearing based on the investigation performed by Constantinou et al. (2011) are calculated for this study and presented in Table 4-14.

Table 4-14. Preliminary design of LRI and TPI

Lead Rubber Isolator (LRI)			Triple Pendulum Isolator (TPI)		
Description	Value	Unit	Description	Value	Unit
Lead yield stress (σ_Y)	12	MPa	Friction coefficient lower bound (μ)	0.072	-
Rubber Shear modulus (G)	0.70	MPa	Friction coefficient upper band (μ)	0.086	-
Lead Shear modulus (G)	5200	MPa	Radius of the concave (R)	2240	mm
Young modulus (E)	2.5	MPa	Height of internal slider (h/2)	120	mm
shear strain (γ_{max})	125	%	Displacement capacity (d)	400	mm
Lead core diameter (DL)	120	mm	Post elastic stiffness (K_d)	14087	N/mm
Bearing diameter (DB)	700	mm	Characteristic strength (F_o, Q_d)	3583908	N
Rubber Thickness (Tr)	200	mm	Assumed (D_M)	400	mm
Yield displacement (Yd)	15	mm	Effective Stiffness	23047	N/mm
Post elastic stiffness (K_d)	19600	N/mm	Effective Period	3.22	Sec
Characteristic strength (F_o, Q_d)	3583908	N	Effective Damping	11	%
Assumed (D_M)	200	mm	Reduction coefficient (B_M)	1.21	-
Effective Stiffness	37520	N/mm	Maximum displacement (D_M)	328	mm
Effective Period	2.53	Sec	Actual displacement ($D > D_M$)	757	mm
Effective Damping	28	%			
Reduction coefficient (B_M)	1.6	-			
Maximum displacement (D_M)	197.43	mm			
DM with torsion (D_{M+T})	234	mm			
1.2DL+0.5L+1.0EQ	67980239	N			
Rubber Thickness	1.20	mm			
Yield strength	135648	N			
Post yield stiffness ratio	0.012	-			

4.5.6 Modal Analysis

Table 4-15 shows the empirical equations based on NBCC 2015 and ASCE 7-16, where T_a (s) is the fundamental lateral period and h_n is the height of the structure.

Table 4-15. Empirical Equations (Metric)

Dissipating systems	T_a-NBCC 2015	T_a -ASCE 7-16
CMRF	$0.075h_n^{0.75}$	$0.0466h_n^{0.9}$
Ten-Co Seismic Brake (TCSB)	$0.025h_n$	$0.0731h_n^{0.75}$
Fluid Viscous Damper (FVD)	$0.025h_n$	$0.0731h_n^{0.75}$
Triangular Metallic Yielding Dampers (TMYD)	$0.025h_n$	$0.0731h_n^{0.75}$
Lead Rubber Bearing Isolator (LRBI)	-	-
Triple Pendulum Isolator (TPI)	-	-

The fundamental period of each system is calculated based on empirical equations and modal analysis and presented in Table 4-16, the values obtained from empirical equations are more conservative compared with the values from modal analysis.

Table 4-16. The fundamental period of the structures

Dissipating systems	Analytical (NBCC 2015)	Empirical (NBCC 2015)	Empirical (ASCE 7-16)
CMRF	1.568	1.411	1.576
CMRF with TCSB	1.540	1.250	1.374
CMRF with FVD	1.819	1.250	1.374
CMRF with TMYD	1.320	1.250	1.374
CMRF with LRBI	2.732	-	-
CMRF with TPI	2.310	-	-

4.5.7 Nonlinear Static Pushover Analysis

The nonlinear static analysis is used to calculate the displacement demand and strength capacity. The steps are using different load cases with varying load distribution, such as any combination of acceleration, static load, and lateral force (Lawson et al. 1994). The distributed plasticity using Fiber section “P-M2-M3” with finite length hinge zone is employed, and the columns are meshed at intermediate joints and intersecting frames to improve the capture of local P-delta effects. The overstrength and ductility factors are calculated based on the idealized behaviour of force versus displacement and are shown in Table 4-17. The normalized base shear against roof drift ratio is presented in Figure 4-31 for each dissipation system. All the dissipation

systems experience almost the same value for ductility except TMYD, which has the lowest ductility value.

Table 4-17. Pushover analysis results

Dissipating systems	Yield Strength V_y (KN)	Design Strength V_d (KN)	Overstrength factor R_o	Maximum displacement Δ_{max} (mm)	Yield displacement Δ_y (mm)	Ductility μ
CMRF	6297	3527	1.785	218	56	3.865
Ten-Co Seismic Brake (TCSB)	6251	3370	1.854	199	59	3.372
Fluid Viscous Damper (FVD)	4840	3361	1.441	236	64	3.683
Triangular Metallic Yielding Dampers (TMYD)	6655	3373	1.973	224	102	2.196
Lead Rubber Bearing Isolator (LRBI)	2400	3361	0.714	330	88	3.743
Triple Pendulum Isolator (TPI)	3066	3361	0.912	245	64	3.781

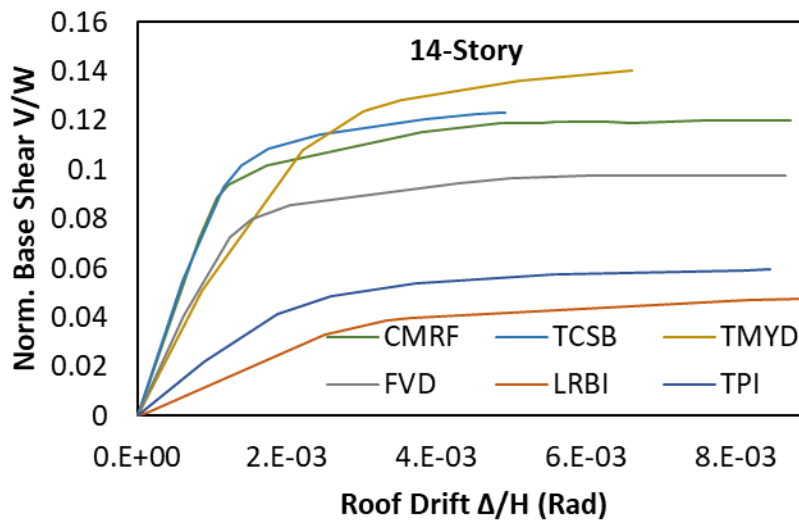


Figure 4-31. Pushover results for CMRF, TCSB, TMYD, FVD, LRBI, and TPI

The proposed method by Miranda and Bertero (1994) is used to determine the ductility reduction factor, R_μ , this parameter depends on ductility, μ , soil condition, ductility coefficient, ϕ , and fundamental period of the structure. The response modification factor is the multiplication of the overstrength factor by the ductility reduction factor. These values are calculated for CMRF, TCSB, FVD, TMYD, LRBI, and TPI and presented in Table 4-18 and Figure 4-32 to Figure 4-34. The CMRF and the LRBI have the highest and lowest response modification factors.

Table 4-18. Response modification factor

Dissipating systems	Overstrength factor R_o	Ductility Reduction factor R_μ	Response modification factor
CMRF	1.785	4.601	8.214
Ten-Co Seismic Brake (TCSB)	1.854	4.015	7.449
Fluid Viscous Damper (FVD)	1.441	4.304	6.199
Triangular Metallic Yielding Dampers (TMYD)	1.973	2.546	5.024
Lead Rubber Bearing Isolator (LRBI)	0.714	3.996	2.854
Triple Pendulum Isolator (TPI)	0.912	4.194	3.826

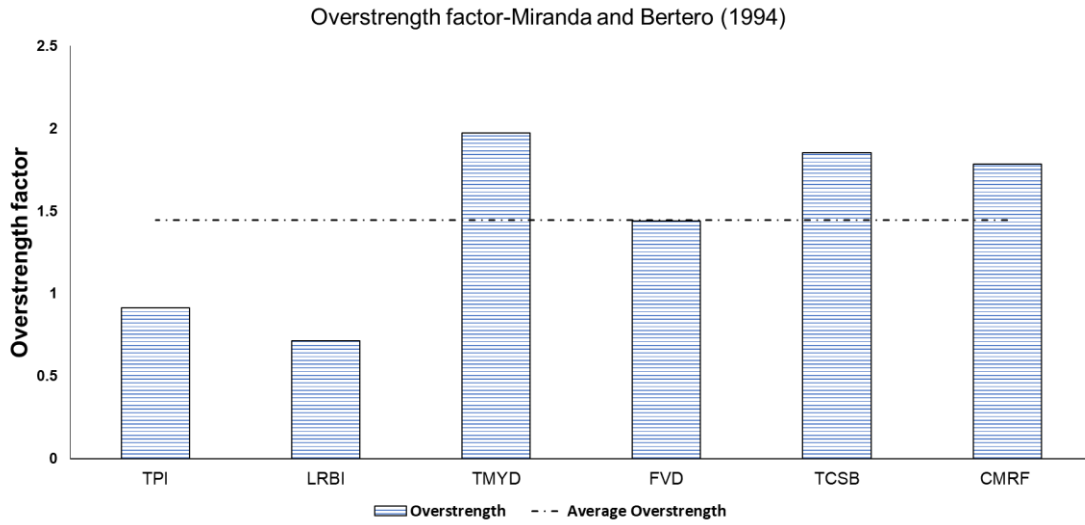


Figure 4-32. Overstrength factors of dissipating systems

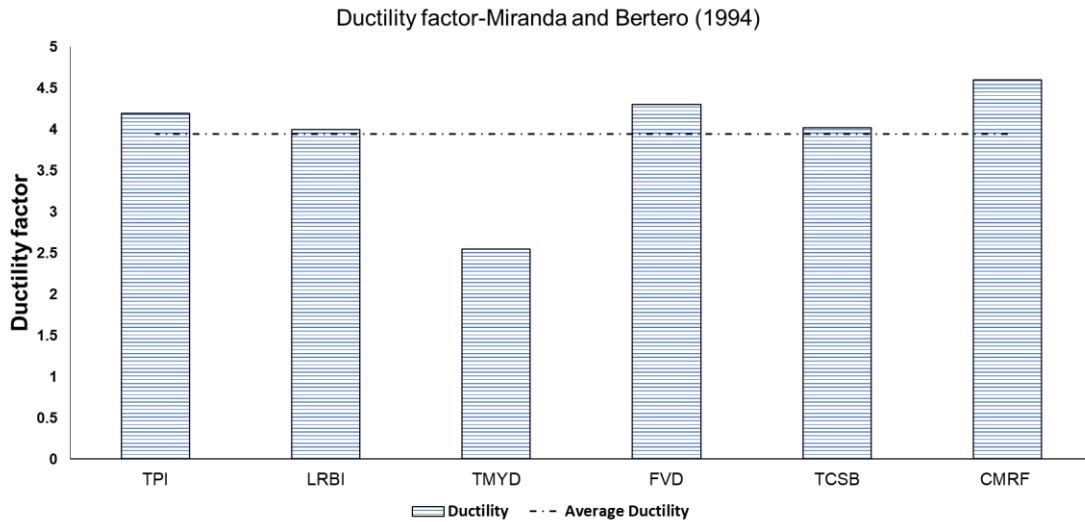


Figure 4-33. Ductility factors of dissipating systems

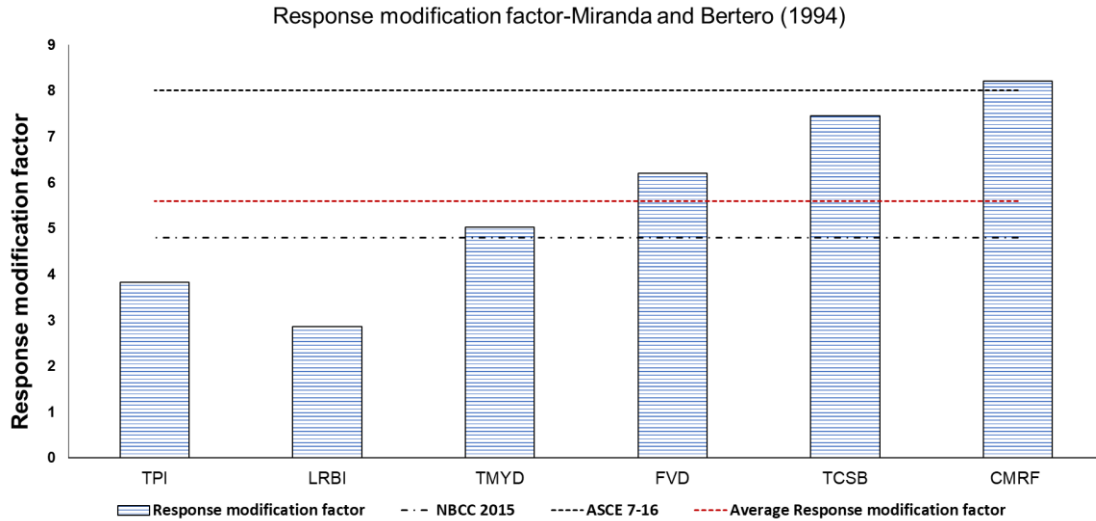


Figure 4-34. Response modification factors of dissipating systems

4.5.8 Inelastic history response Analysis

Dynamic structural analysis can predict the response of the structure under selected different scaled ground motions using spectral acceleration and period of the system (Baker, 2011). The earlier version of ASCE 7 required a minimum of three ground motions to evaluate the structural performance, this number was increased to 11 in the 2016 edition to characterize precisely the mean or variability response. The MCE_R is used for nonlinear response analysis, therefore the upper bond period was increased from $1.5T$ to $2.0T$, the lower bond, $0.2T$, should cover 90% of the mass participation factor, where T is the fundamental period of the structure. In this part, 14 different ground motion records were obtained from the database of the Pacific Earthquake Engineering Research Center (PEER) as presented in Table 4-19, ground motion parameters are presented in Table 4-20 and Table 4-21. The original accelerograms presented in Figure 4-35 were scaled according to the design response spectrum using the relevant tool in SeismoMatch 2018 software, as shown in Figure 4-36.

Table 4-19. Summary of selected ground motions

ID	Scale Factor	Earthquake	Year	Station	Magnitude	Mechanism	PGA (g)	TS (Sec)
1	0.758	Imperial Valley-02	1940	El Centro Array #9	6.95	Strike slip	0.274	0.010
2	1.3112	Kern County	1952	Taft Lincoln School	7.36	Reverse	0.411	0.010
3	1.9001	San Fernando	1971	Pasadena - CIT Athenaeum	6.61	Reverse	0.354	0.010
4	0.8685	Corinth_Greece	1981	Corinth	6.6	Normal Oblique	0.346	0.010
5	1.8829	Superstition Hills-02	1987	Brawley Airport	6.54	strike slip	0.349	0.010
6	1.571	Loma Prieta	1989	Fremont - Emerson Court	6.93	Reverse Oblique	0.348	0.050
7	0.7116	Northridge-01	1994	Arleta - Nordhoff Fire Sta	6.69	Reverse	0.296	0.020
8	1.234	Kobe_Japan	1995	Abeno	6.9	strike slip	0.296	0.010
9	0.8133	Chi-Chi_Taiwan	1999	TCU049	7.62	Reverse Oblique	0.318	0.005
10	0.5322	Niigata_Japan	2004	NIGH11	6.63	Reverse	0.355	0.005
11	1.556	Chuetsu-oki_Japan	2007	Nadachiku Joetsu City	6.8	Reverse	0.362	0.010
12	0.9505	El Mayor-Cucapah_Mexico	2010	Bonds Corner	7.2	strike slip	0.267	0.005
13	0.7605	Darfield_New Zealand	2010	DSLCL	7	strike slip	0.348	0.005
14		Tohoku	1923		7.9	Subduction	0.281	0.010

Table 4-20. Calculated ground motions parameters pre/post-matching

ID Accelerogram		Selected Seismic motions													
		Imperial Valley-02		Kern County		San Fernando		Corinth_Greece		Superstition Hills-02		Loma Prieta		Northridge-01	
		Pre-Mat.	post-Mat.	Pre-Mat.	post-Mat.	Pre-Mat.	post-Mat.	Pre-Mat.	post-Mat.	Pre-Mat.	post-Mat.	Pre-Mat.	post-Mat.	Pre-Mat.	post-Mat.
1	PGA (g)	0.21	0.27	0.18	0.41	0.10	0.35	0.29	0.34	0.11	0.34	0.14	0.34	0.30	0.29
2	PGV (cm/sec)	31.32	51.96	18.62	40.56	10.98	26.48	23.81	34.21	15.99	42.99	14.37	38.38	22.99	34.16
3	PGD (cm)	24.16	144.56	9.35	39.55	2.56	10.40	5.65	9.27	6.89	18.25	11.53	35.24	8.86	15.28
4	v _{max} /a _{max} (sec)	0.15	0.19	0.10	0.10	0.10	0.07	0.08	0.10	0.14	0.12	0.10	0.11	0.07	0.11
5	Arias Intensity (cm/sec)	1.16	3.70	0.59	3.40	0.20	1.82	0.85	1.87	0.25	1.44	0.32	2.30	1.17	1.98
6	CAV (cm/sec)	1251	2389	889	2315	382	1271	820	1377	424	941	558	1607	954	1380
7	Housner Intensity (cm)	114	123	65	124	48	121	96	122	49	118	45	124	106	119
8	Predominant Period (sec)	0.58	0.16	0.44	0.44	0.42	0.46	0.26	0.30	0.10	0.44	0.18	0.32	0.24	0.24
9	Significant Duration (sec)	24.15	26.94	28.78	32.48	12.31	20.69	13.94	16.99	14.34	15.01	17.93	21.76	13.46	17.98

Table 4-21. Calculated ground motions parameters pre/post-matching

ID Accelerogram		Selected Seismic motions													
		Kobe_Japan		Chi-Chi_Taiwan		Niigata_Japan		Chuetsu-oki_Japan		El Mayor-Cuapah_Mexico		Darfield_New Zealand		Tohoku	
		Pre-Mat.	post-Mat.	Pre-Mat.	post-Mat.	Pre-Mat.	post-Mat.	Pre-Mat.	post-Mat.	Pre-Mat.	post-Mat.	Pre-Mat.	post-Mat.	Pre-Mat.	post-Mat.
1	PGA (g)	0.23	0.29	0.24	0.31	0.59	0.35	0.18	0.36	0.27	0.26	0.23	0.34	0.42	0.28
2	PGV (cm/sec)	24.77	38.62	61.66	83.79	58.12	34.01	13.46	26.15	19.54	28.14	67.25	128.88	22.44	22.79
3	PGD (cm)	9.87	21.10	64.03	137.08	13.10	7.29	6.46	16.35	20.82	19.90	81.28	168.31	10.80	9.47
4	v_{max}/a_{max} (sec)	0.10	0.13	0.25	0.26	0.09	0.09	0.072	0.073	0.07	0.10	0.28	0.37	0.05	0.10
5	Arias Intensity (cm/sec)	0.58	2.55	1.36	4.07	2.24	0.96	0.31	1.73	1.77	2.32	1.64	4.67	12.02	5.66
6	CAV (cm/sec)	1210	2532	1375	2632	1166	802	516	1431	1574	1847	1428	2602	5991	4201
7	Housner Intensity (cm)	72	121	109	119	140	120	53	122	82	122	114	125	81	118
8	Predominant Period (sec)	0.14	0.30	0.24	0.16	0.40	0.08	0.42	0.38	0.12	0.24	0.22	0.22	0.26	0.24
9	Significant Duration (sec)	56.38	55.88	22.67	27.42	8.00	9.25	18.19	24.09	24.21	22.96	18.77	22.09	61.91	63.09

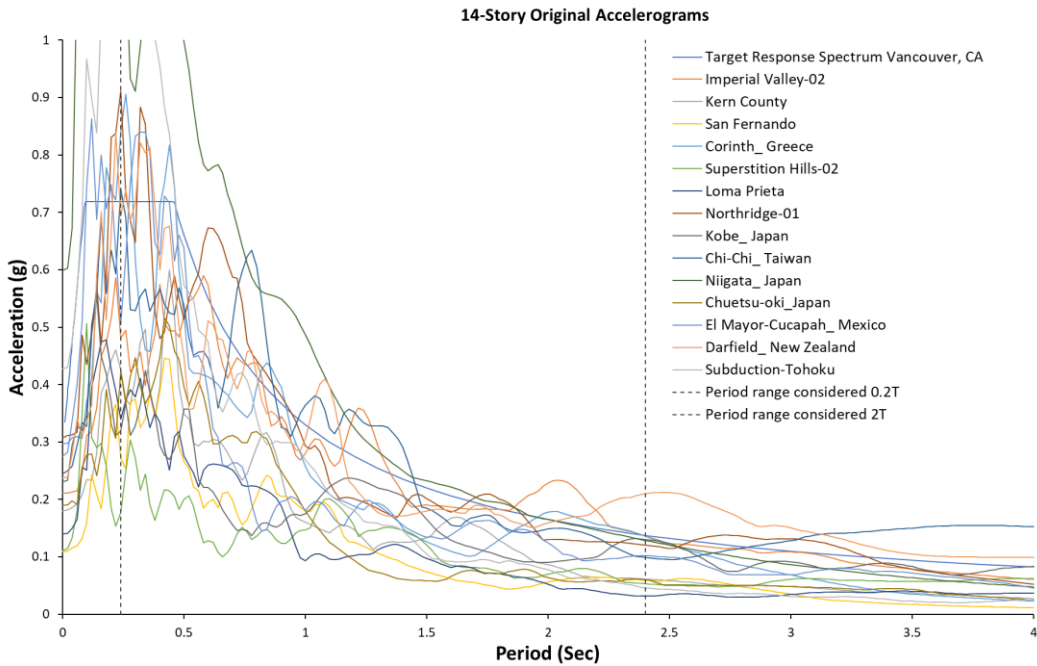


Figure 4-35. Original Accelerograms

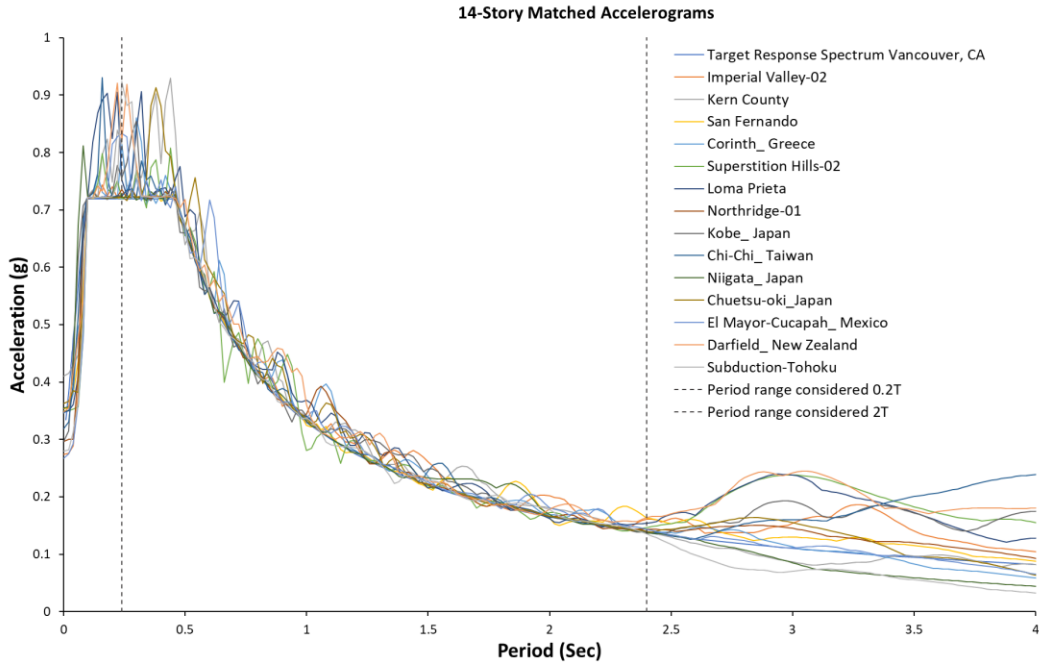


Figure 4-36. Matched Accelerograms based on the target response spectrum

4.5.9 Interpretation of Results

Roof displacement for Lead Rubber Bearing and Triple Pendulum Isolator are presented in Figure 4-37. It can be concluded the roof displacement decreased when equipped with the Lead Rubber Bearing and even more with the Triple Pendulum Isolator compared with the fixed frame.

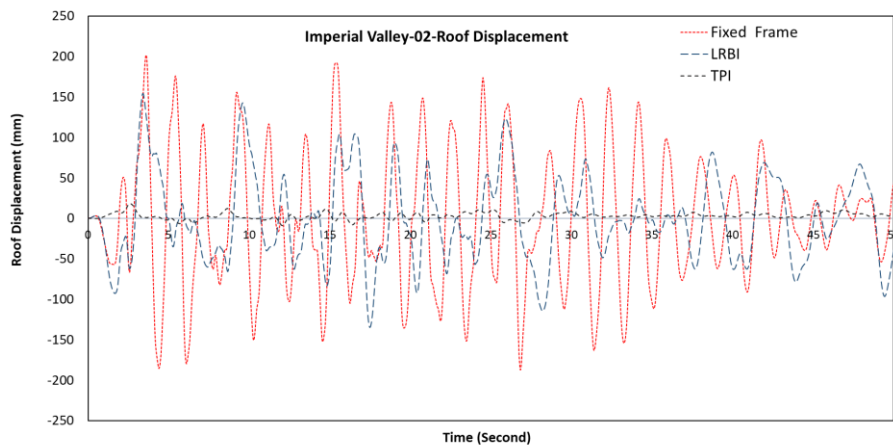


Figure 4-37. Comparison of Roof displacement for Fixed, LRBI, and TPI frames

The seismic behaviour of the dissipation systems is evaluated using dynamic response analysis. The inter-story drift ratios for different scaled ground motions are presented in Figure 4-38 and Figure 4-39. The drift profile is varying due to higher mode effects. The sum of standard deviation and the mean values for CMRF shows the maximum inter-story drift ratio of 0.5% at the 10th story, this value reduced to 0.47% and 0.4% for TCSB, TMYD, and FVD, which is in the range of the “Life safety” performance of the structure defined in NBCC 2005. The LRBI and TPI have the maximum drift ratio of 1.6% and 0.4% at the base due to isolators' movement; these values are close to zero for the rest of the stories.

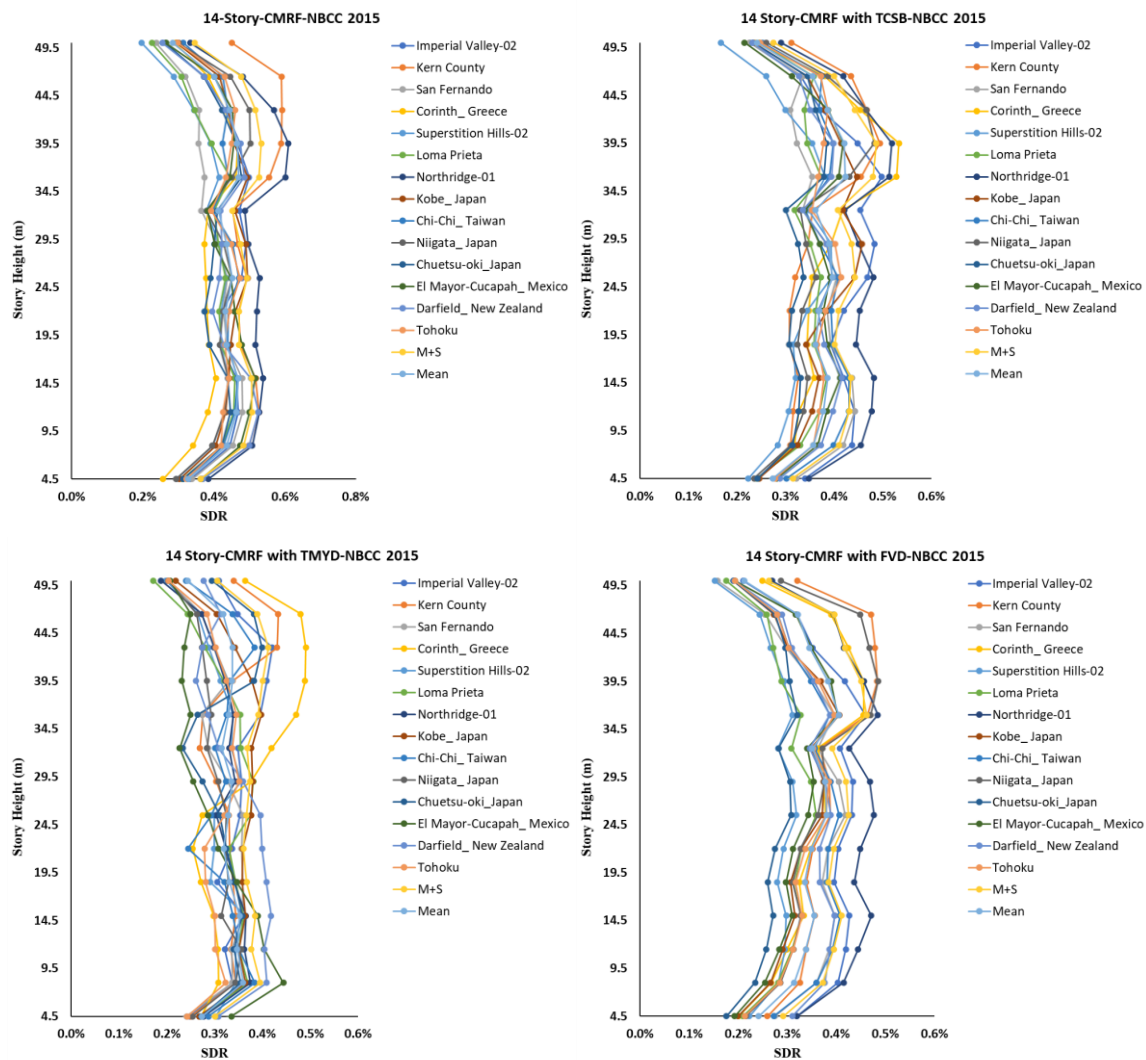


Figure 4-38. Inter-story drift ratio for CMRF, TCSB, TMYD, FVD

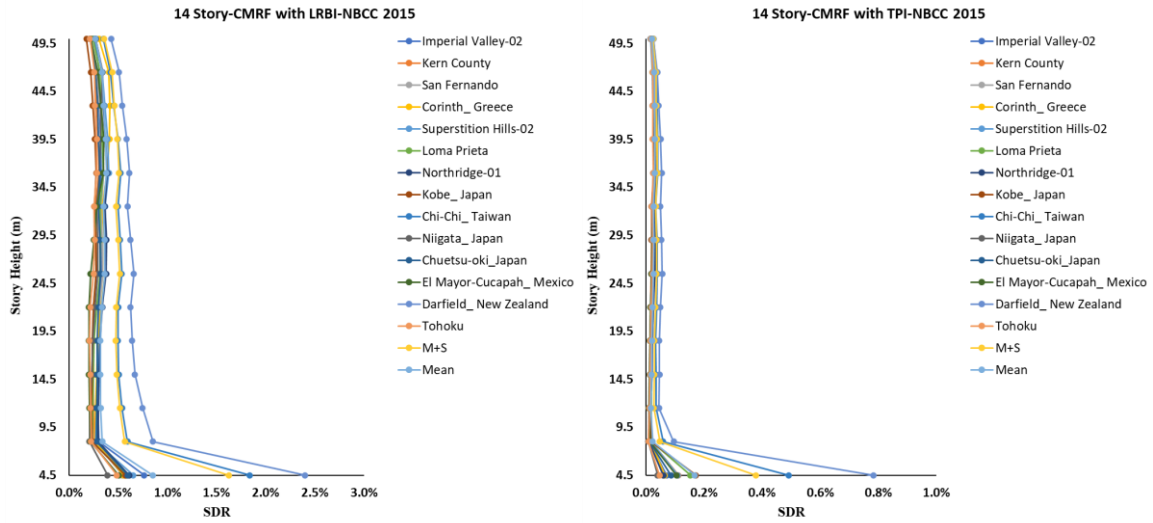


Figure 4-39. Inter-story drift ratio for LRBI, and TPI

In the interest of brevity, the maximum hysteresis behaviour for Imperial valley and Tohoku (subduction) ground motions of TCSB, TMYD, FVD, LRBI, and TPI are presented in Figure 4-40, and Appendices A4.4 to A4.8 show their maximum hysteresis behaviour for the rest of the ground motions.

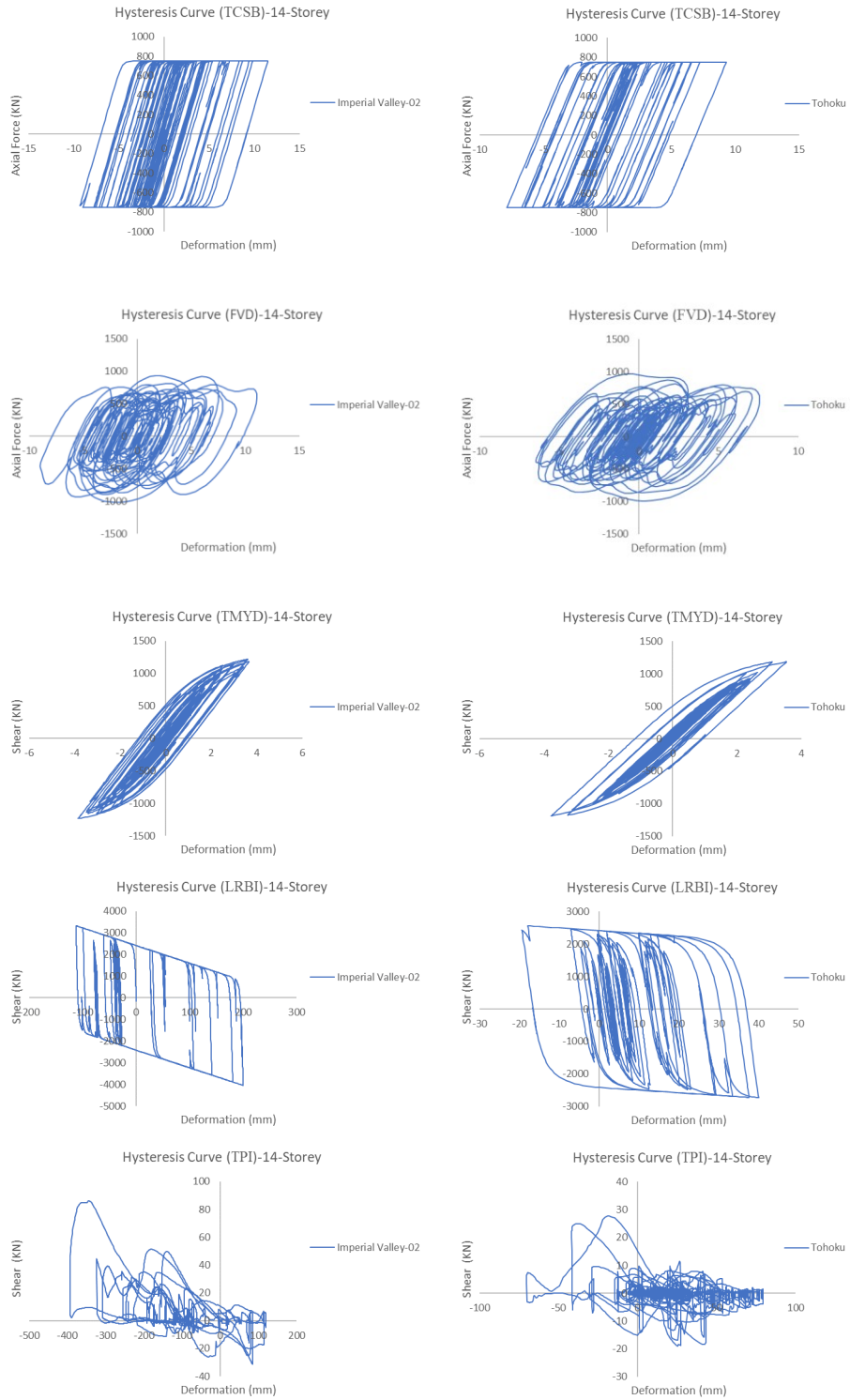


Figure 4-40. Maximum hysteresis response for TCSB, FVD, TMYD, LRBI, and TPI

Response history of base shear demands of 14 ground motions of each dissipation system is shown in Figure 4-41 to Figure 4-43. The CMRF has a maximum value of 19787 KN; this value is reduced from 15760 KN to 13201KN when the frame is equipped with TCSB, TMYD, and FVD. The LRBI and the TPI tremendously decreased the base shear values to 4044 KN and 80KN.

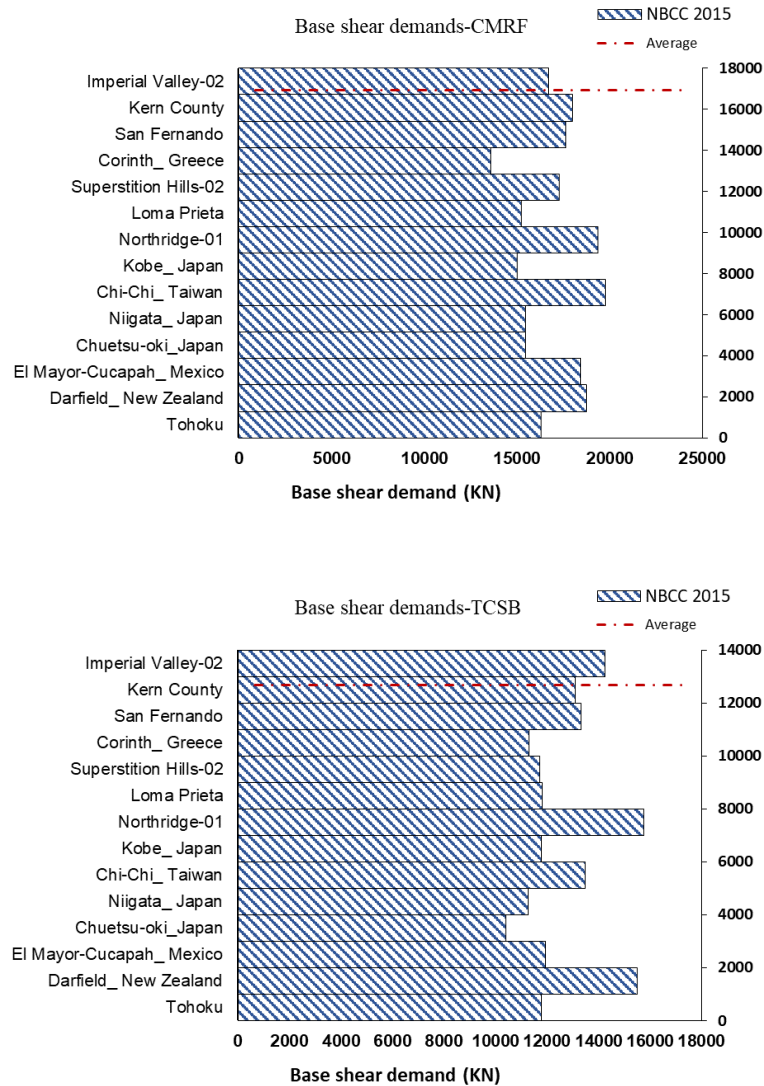


Figure 4-41. Response history of base shear demands for CMRF and TCSB

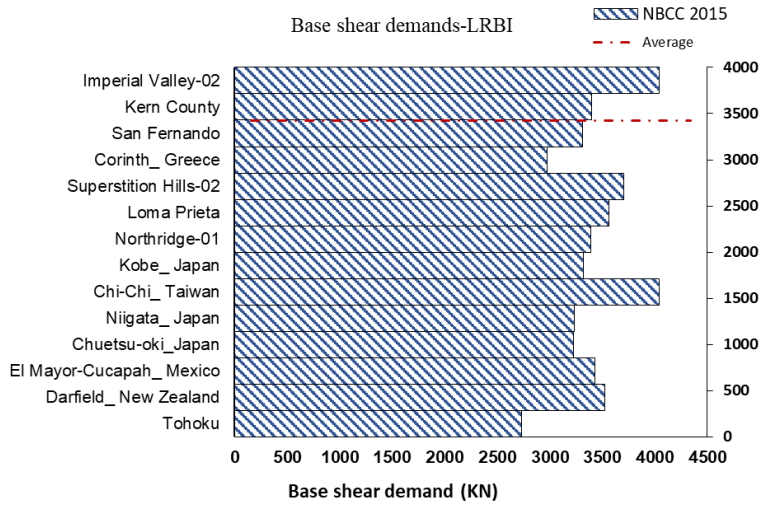
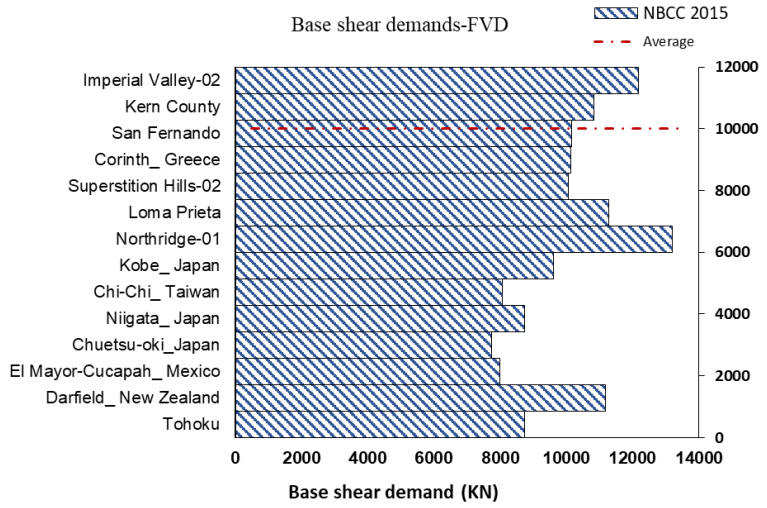
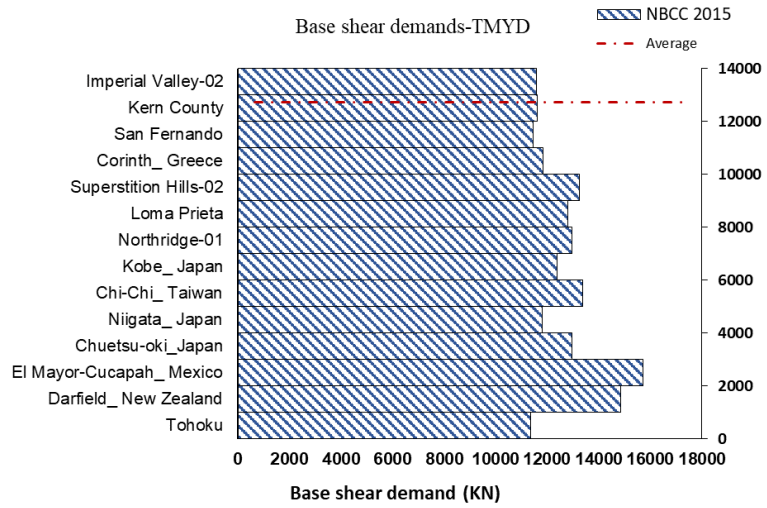


Figure 4-42. Response history of base shear demands for TMYD, FVD, and LRBI

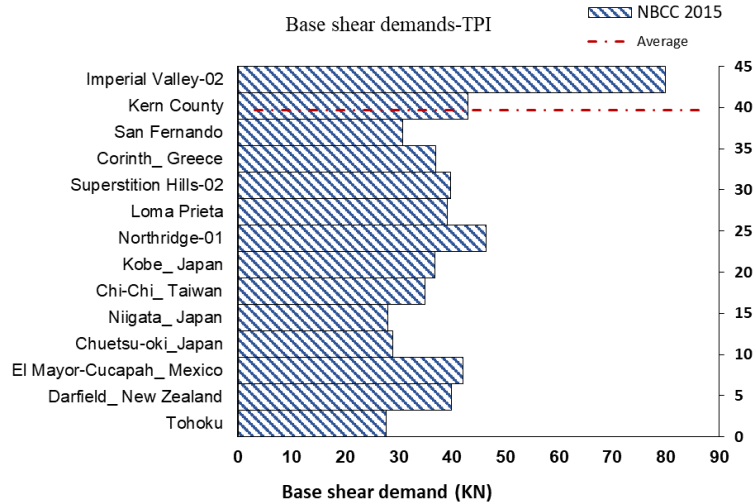


Figure 4-43. Response history of base shear demands for TPI

4.5.10 Results and Discussions

The concrete moment resisting frame is designed based on the NBCC and ASCE, and their material quantities are compared together, each dissipation system designed individually. The design force reduction factors including overstrength, ductility, and reduction factors of CMRF, TCSB, FVD, TMYD, LRBI, and TPI using nonlinear static analysis considering the life safety performance were evaluated against each other. Then the response of each system was determined by conducting nonlinear history analysis in terms of roof displacement, inter-story drift ratios, and base shear demands. The following items are highlighted in this study:

- The design procedures using ASCE/SEI 7-16 and ACI 318, are more conservative than NBCC 2015 and CSA A23.3-19. The calculated material quantity in the ASCE 7 is about 10% higher than the NBCC 2015.
- The fundamental period of CMRF has a value of 1.56 seconds based on the modal analysis, and 1.41 seconds and 1.57 seconds based on the empirical equations defined in the NBCC 2015 and the ASCE 7.
- The overstrength has a range from 1.44 to 1.97 for CMRF, TCSB, FVD, TMYD with an average value of 1.76, the overstrength factor was reduced by about 45% when the structure was equipped with LRBI and TPI.

- The ductility reduction factor, R_{μ} , was calculated based on the proposed method by Miranda and Bertero (1994), TMYD had the lowest ductility factor of 2.54, and CMRF had the highest ductility value of 4.61. The ductility average value of CMRF, TCSB, FVD, and TMYD was 3.86, and 4.09 for LRBI and TPI.
- The response modification factors of CMRF and TMYD had the highest value of 8.21 and the lowest value of 5.02 respectively, the recommended values in the NBCC 2015 and ASCE 7 are 5.25 and 5 for CMRF, and 4.8 and 8 for TCSB, FVD, TMYD. The average response modification factor of TCSB, FVD, and TMYD is 6.22 which is in between the reduction factors proposed by NBCC 2015 and ASCE 7.
- The maximum standard deviation for CMRF was 0.53% at the 10th level, this value was reduced to 0.48%, 0.46%, and 0.41% for TCSB, FVD, TMYD respectively. The maximum standard deviation and mean values for LRBI and TPI were 1.6% and 0.3% at the base due to their movements' function. The inter-story drift shows the performance of life safety for all models.
- The soil types must be taken into account when selecting an isolator considering that the soft soil might magnify seismic demand. Furthermore, LRBI is susceptible to fire, aging, temperature, and torsion. The sliding bearing (TPI) center of mass and stiffness are coincident as stiffness is proportional to axial stresses and they are very rigid in axial direction compared with LRBI.
- The dissipation systems have a reduction of about 15% in material quantity compared with the CMRF. The TCSB had a very regular hysteresis curve compared to the other systems, all the devices reduced the base shear demand, however, the isolators have a significant reduction in base shears as well as the roof displacement.

Further studies are required to determine these devices' seismic characteristics using different heights, span lengths, and bracing configurations. More modeling details and experimental tests are necessary to present the effectiveness of these devices on the response of concrete structures.

CHAPTER 5

Experimental test and analytical simulation of yielding restrained brace

5.1 Introduction

The first phase of the work presented here is concerned with the collaborating of the experimental work of two full-scale dual system moment resisting frames with a conventional single leg brace and with a yielding restrained brace. The experimental frame was analyzed and designed using ASCE 7, AISC-341 and AISC-360, and the uni-axial shake table at the structural laboratory of the Lyles College of Engineering at California State University, Fresno was used to conduct the experimental test as part of the collaborative work, the test was conducted by an MSc student at CSU (Couch, 2020), while the design and further analysis of the results are carried out by the author of the present thesis. Seventeen scaled ground motions, as well as sinusoidal, sweep, and step functions, are applied to the frame. The results cover a comparison of the conventional single leg brace frame and the yielding restrained brace including acceleration, damping, residual drift, system redundancy, and temperature measurement.

The second phase is the simulation of the experimental test using ETABS, and OpenSees, software. The evaluation includes simulation of the experimental frame equipped with a single leg yielding restrain brace frame and a single leg conventional brace frame. The effectiveness of friction damper is presented by comparison of acceleration, damping ratios, drift, and displacement.

5.2 Phase 1: Experimental work

The frame consists of one bay in X direction with 6'-7 1/2" (2.02 m) span length and two bays in Y direction each has a span length of 2'-6 1/4" (0.77m), the height of the frame is 96 inches (2.44m). W6×9 and W6×15 (A992) are used for columns and beams. The shake table was limited

to the minimum and maximum acceleration values of 1.25g and 1.5g. Two concrete blocks were installed on the top of the frame, each block weighed 2200 pounds (9.78 KN). The lateral translation was controlled by two wires with a capacity of 990 pounds (4.4KN), the shake table is 96 in \times 81 in (2.44 m \times 2.06 m) in X and Y directions as presented in Figure 5-1.



Figure 5-1. 3-D and elevation view of the frame (Couch, 2020)

5.2.1 Recording accelerometer

For the accurate response of the frame, three accelerometers were used to measure and record the vibration of the frame in three major axes. The testing direction was set on X direction and Z direction considered for torsional and transverse deformation, and one accelerometer was installed at the base to verify the acceleration data (Couch, 2020). The GP1-L accelerometer uses two AA alkaline batteries which last more than forty years and can be connected to a computer using a USB connector and SENSWARE software, the details, as well as different views of the recording accelerometer, are shown in Figure 5-2. The GP1 has three axes motion to capture, observe, and evaluate different parameters including temperature, movement, impacts. The sampling rate is

100Hz per axis and it has a temperature range of between -20°C to +80°C with a weight of 0.234 kg (SENSRA Monitoring Technologies, 2021).

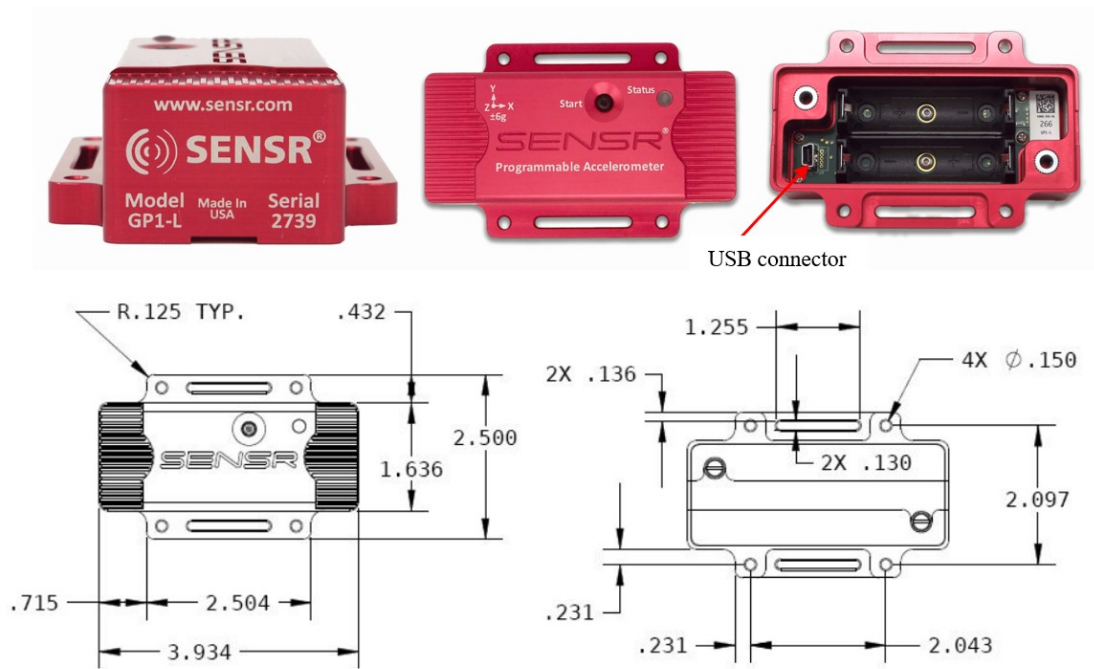


Figure 5-2. Accelerometer detail GP1-L (SENSRA Monitoring Technologies, 2021)

5.3 Loading

A damping device is an element that dissipates energy due to the relative motion of each end of the device. To have a better understanding of the seismic performance of a building including damping devices, interim testing techniques shall be employed to assess the building’s capabilities and components based on their fragility functions. Mathematical interactions define fragility functions and express as probability distributions used to assess the performance of a building and its components under earthquake loadings (FEMA-461, 2007).

Since these loading protocols are needed more evaluation and implementation, they could be used for seismic performance assessment if defined by the local building code. Interim protocols are classified into two groups:

“Interim Protocol I (Quasi-Static Cyclic Testing)”, which can be used for the evaluation of components' performance, and their behaviour is governed by seismic characteristics such as force

and displacement. This protocol is not valid for a component whose behaviour is controlled by its dynamic response or velocity-sensitive.

“Interim Protocol II (Shake Table Testing)”, which can be used for the assessment of components’ performance whose behaviour is controlled by their components dynamic response, velocity-sensitive, or “strain-rate” sensitive.

5.3.1 Interim Protocol I- Quasi-Static Cyclic Testing

In this part, quasi-static cyclic testing procedures are explained for the characteristic assessment of building components (Including Partitions, cladding, pipes, ducts, ...) and substructures (Including shear walls, beam-column, and frame assemblies). If damage is predicted by imposed deformation, Quasi-Static cyclic testing which consists of a slow cyclic load or deformation with a predetermined load pattern, applies to assessment the performance of building parts or components (FEMA-461, 2007). As shown in Figure 5-3 component distortion as a result of inter-story drift in a building is expected, which depends on the loading factor.

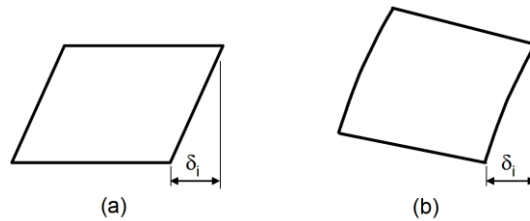


Figure 5-3. (a) shear drift, and (b) rotation drift (FEMA-461)

5.3.1.1 Loading and load control

When accurate force and deformation records are required, a test can be performed within the elastic and inelastic range subjected to force, deformation control, or a combination of force-deformation control. The deformation control parameter must correlate with the deformation parameter of the building, for example, the typical structural analysis provides an inter-story drift parameter of building deformation. The force control which relates to demand quantity can be predicted by structural analysis. Depending on the impact level in the associated fragility function

or the damage state, force or deformation control can be implemented as unidirectional loading in a single degree of freedom or as a bidirectional loading.

Figure 5-4 shows a schematic view of the data acquisition system for the test facility, and the three schematic standard racking test facilities are demonstrated in Figure 5-5 (FEMA-461, 2007).

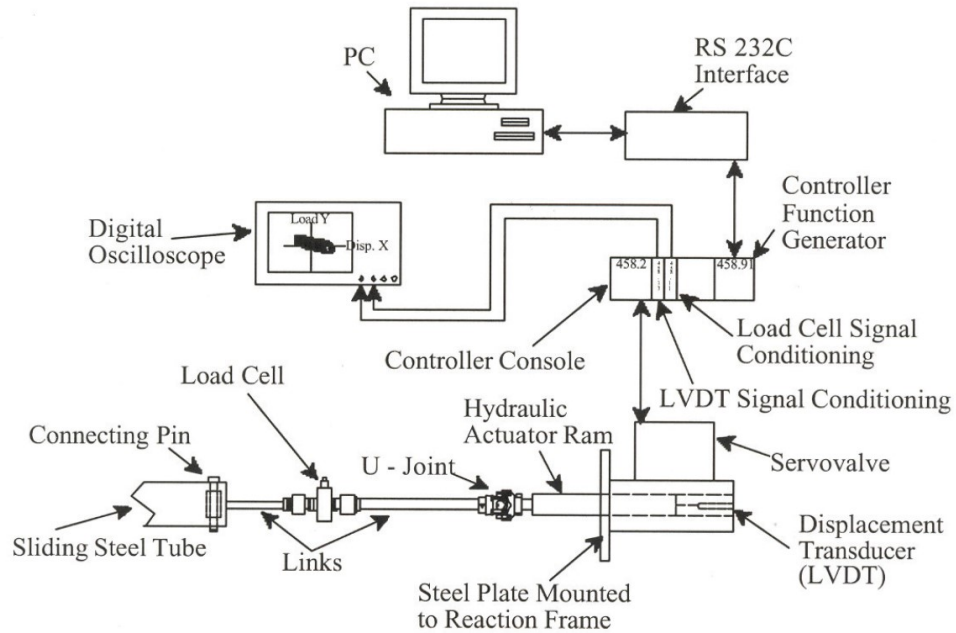


Figure 5-4. Instrumentation and data acquisition system (FEMA-461)

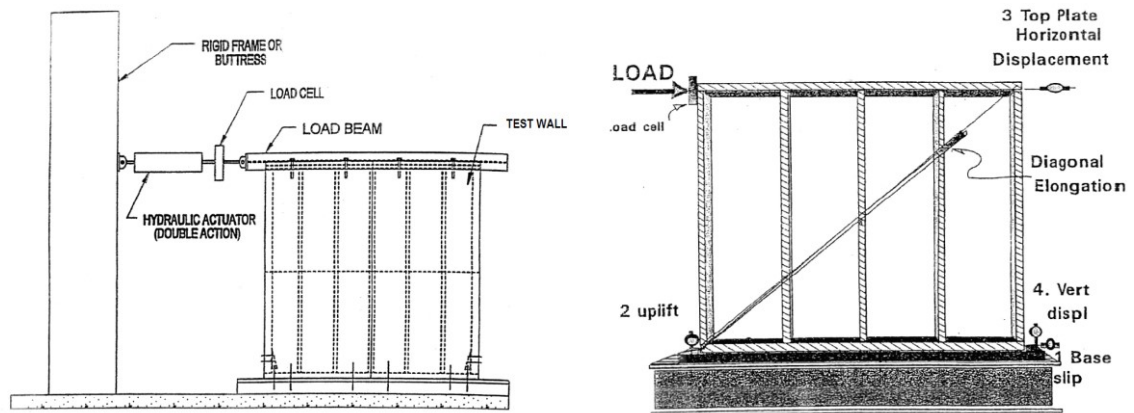


Figure 5-5. ASTM Generic test facility and rack test installations for shear-resistant wall panels (FEMA-461)

5.3.1.1.1 Unidirectional testing

Two types of testing are covered in this part including Racking and Hysteretic Testing. Racking testing can be conducted for components that do not modify the stiffness and strength of a building or do not participate in a structural resisting system, which are excluded in the structural analysis. Hysteretic testing can be carried out on components that alter the rigidity and strength of a structure or contribute to a structural resisting system, which are included in the structural analysis. To quantify all damage states of a single specimen fragility function shall be developed, and one data point for each damage state is obtained. For the cumulative damage estimation, the additional monotonic test is highly recommended. Figure 5-6 is a recommended loading history that consists of repeated cycles of deformation amplitudes increasing gradually. Where Δ_0 is the smallest deformation amplitude, and Δ_m is the maximum deformation amplitude (FEMA-461, 2007).

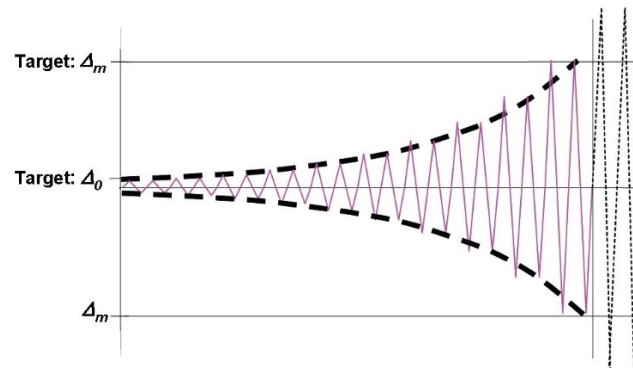


Figure 5-6. Sketch of deformation-controlled loading history (FEMA-461)

Figure 5-7 shows the calculation of loading history for $a_n = \Delta_m$, where a_n is the amplitude of the step exactly equal to maximum deformation amplitude. In this case, the amplitude a_{i+1} of step $i+1$ is calculated according to Equation 5.1 (FEMA-461, 2007).

$$a_{i+1} = 1.4a_i \quad (5.1)$$

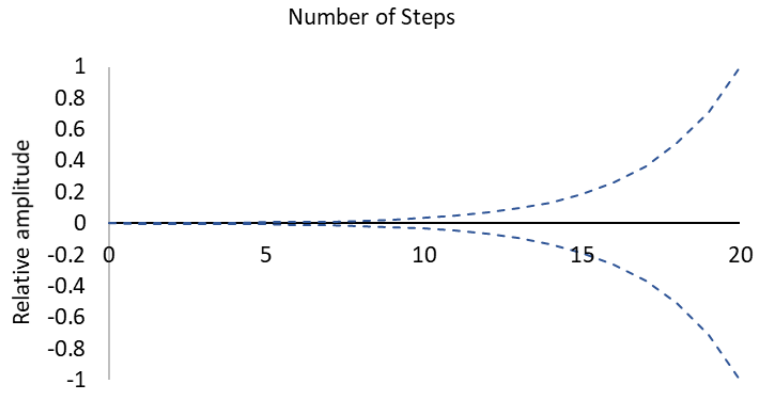


Figure 5-7. Example of loading history

For bidirectional testing, the loading path should follow an orbital pattern in Figure 5-8.

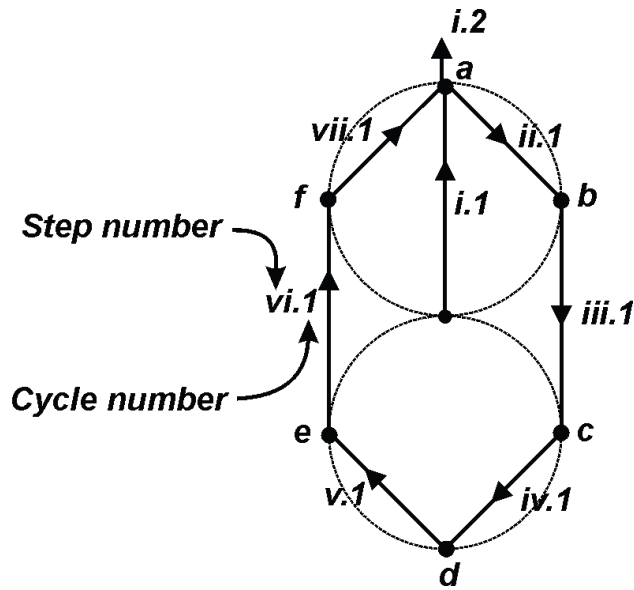


Figure 5-8. Horizontal plane displacement orbit for drift-controlled bidirectional tests (FEMA-461)

5.3.1.1.2 Force Controlled loading

When the component performance is controlled by a force quantity or if an appropriate deformation parameter can not be found, force- controlled testing should be carried out. A general force-based loading protocol can not be developed, as the demands differ depending on the “in-situ” circumstances as well as the type of component. From the analytical or monotonic test, force deformation can be calculated, then a loading history can be constructed utilizing a combination of load-deformation response and cyclic loading history (FEMA-461, 2007).

5.3.2 Interim Protocol II-Shake Table Testing

This section explains the proposed shake table procedures of structural and non-structural building components (FEMA-461, 2007).

5.3.2.1 Test Procedures

The test specimen consists of the following sequential test elements including pretesting inspection and documentation as well as system identification, seismic performance evaluation, and failure tests (FEMA-461, 2007).

5.3.2.1.1 System Identification Tests

To determine the dynamic properties of the test sample as well as their progress during the test, system identification tests should be performed. At least one of the following three methods shall be used to identify the natural frequencies of the test specimen (FEMA-461, 2007).

5.3.2.1.1.1 White Noise Test

In order to simulate the test specimen in every principal mode, a low-intensity white noise of 0.50-30 Hz, “flat”, “clipped-band”, and acceleration control should be employed. The white noise signal root-mean-quarter intensity should be limited to $0.05 \pm 0.01g$ (FEMA-461, 2007).

5.3.2.1.1.2 Single-Axis Acceleration-Controlled Sinusoidal Sweep Test

It should be performed from 0.50 to 30 Hz in each principal axis. To obtain sufficient steady-state response, the sweep rate with the limited peak intensity of $0.05 \pm 0.01g$, should be two octaves (Two frequencies with an interval and frequency ratio of two) per minute (FEMA-461, 2007).

5.3.2.1.1.3 Static pull-back tests

A static pull-back test at the center of gravity of a specimen using a free vibration decay determines the corresponding equivalent modal viscous damping ratio as well as the fundamental frequency. As mentioned above a static pull-back test or the following resonance test should be used to estimate the equivalent fundamental viscous modal damping (FEMA-461, 2007).

5.3.2.1.1.4 Resonance Tests and single-axis acceleration

To simulate the test specimen in each of its main configurations, “a low-intensity acceleration-controlled sinusoidal input” at the predetermined fundamental frequency should be employed, the maximum duration should be 20 times the fundamental period as previously identified (FEMA-461, 2007).

Single-axis system identification tests shall be carried out in each main axis to determine the natural frequencies as an alternative test, it should be noted the input motions parameters should be the peak spectral acceleration at the appropriate natural frequency (FEMA-461, 2007).

5.3.2.1.1.5 Performance Evaluation Tests

It is subjected to increasing intensities of excited input motions, which corresponds to the movement at the single floor of a story structure. “Narrow-Band random sweep acceleration” records that have smooth response spectra are recommended (FEMA-461, 2007).

5.3.2.1.1.6 Failure Tests

To induce damage states with higher intensities of simulated motions used in previous performance assessment tests (FEMA-461, 2007).

5.4 Ground motion scaling

The structure assumed to be located in 16111 Plummer St Los Angeles, California on stiff soil type D with a risk category IV, seismic design parameters are presented in Table 5-1.

Table 5-1. Seismic design parameters (ASCE 7-16)

Type	Value	Description
$S_s(g)$	2.248	MCE_R for 0.2 second
$S_i(g)$	0.718	MCE_R for 1.0 second
$S_{MS}(g)$	2.248	Site modified spectral acceleration
$S_{MI}(g)$	1.078	Site modified spectral acceleration
$S_{DS}(g)$	1.499	Numeric seismic design value at 0.2 second
$S_{DI}(g)$	0.718	Numeric seismic design value at 1.0 second
F_a	1	Site amplification factor at 0.2 second
F_v	1.5	Site amplification factor at 1.0 second
PGA(g)	0.84	MCE_G peak ground acceleration
$T_L(\text{Sec})$	8	Long period

The design response spectrum (DRS) with 5% damped and the maximum considered earthquake (MCE_R) are presented in Figure 5-9.

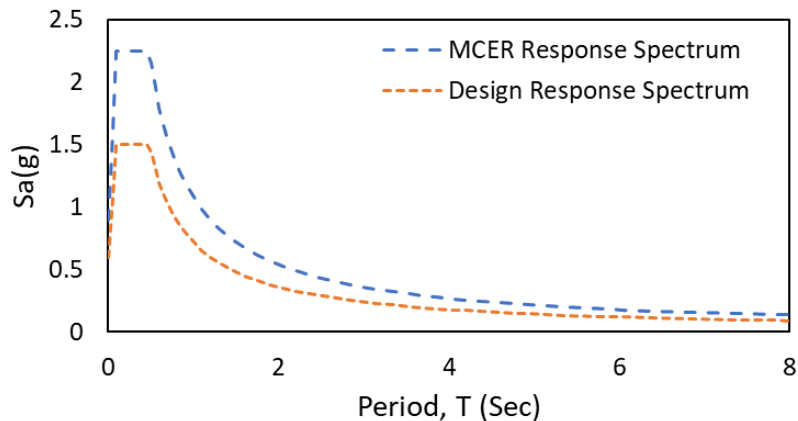


Figure 5-9. DRS and MCE_R response spectrum

The ground motions are selected based on the maximum credible earthquake, which is set as the target response spectrum. Table 5-2 presents a summary of ground motions selected from the “Pacific Earthquake Engineering Research Center (PEER) ground motion database”. Some major

parameters of the search engine are including minimum and maximum range of magnitude, fault types, significant ground motions duration, rupture plane distance (closest), shear wave, and pulse characteristics (PEER, 2010).

Table 5-2. Summary of selected ground motions

ID	Scale Factor	Earthquake	Year	Station	Magnitude	Mechanism	PGA (g)	SD* (Sec)
1	1.024	Gazli USSR	1976	Karakyr	6.8	Reverse	0.701	6.382
2	1.228	Imperial Valley-06	1979	Bonds Corner	6.53	strike slip	0.598	9.650
3	1.603	Loma Prieta	1989	Corralitos	6.93	Reverse Oblique	0.644	6.855
4	1.521	Erzican Turkey	1992	Erzincan	6.69	strike slip	0.386	8.405
5	0.905	Cape Mendocino	1992	Cape Mendocino	7.01	Reverse	1.493	6.200
6	0.971	Northridge-01	1994	Jensen Filter Plant	6.69	Reverse	0.571	6.900
7	1.105	Kobe Japan	1995	KJMA	6.9	strike slip	0.834	8.380
8	1.038	Chi-Chi Taiwan	1999	CHY028	7.62	Reverse Oblique	0.636	8.650
9	1.473	Duzce Turkey	1999	Duzce	7.14	strike slip	0.404	11.065
10	0.938	Tottori Japan	2000	TTRH02	6.61	strike slip	0.771	17.69
11	1.893	San Simeon CA	2003	Templeton	6.52	Reverse	0.435	9.550
12	1.027	Bam Iran	2003	Bam	6.6	strike slip	0.807	8.000
13	0.704	Niigata Japan	2004	NIG019	6.63	Reverse	1.166	10.590
14	1.895	Montenegro Yugoslavia	1979	Bar-Skupstina Opstine	7.1	Reverse	0.372	21.280
15	1.531	Iwate Japan	2008	IWTH24	6.9	Reverse	0.518	26.800
16	0.997	Darfield New Zealand	2010	GDLC	7	strike slip	0.764	16.005
17		Tohoku	1923		7.9	Subduction	0.427	83.340

SD: Significant Duration

The ground motions were scaled according to ASCE 7, using the maximum considered earthquake (MCE_R) as target response spectrum and a period range of $0.2T$ to $2.0T$, the results for original and matched ground motions are presented in Figure 5-10 and Figure 5-11. The original and matched acceleration (g), velocity (cm/sec), and displacement (cm) for the selected ground motions are presented in Appendices A5.1, A5.2, and A5.3.

Experimental Frame Original Accelerograms

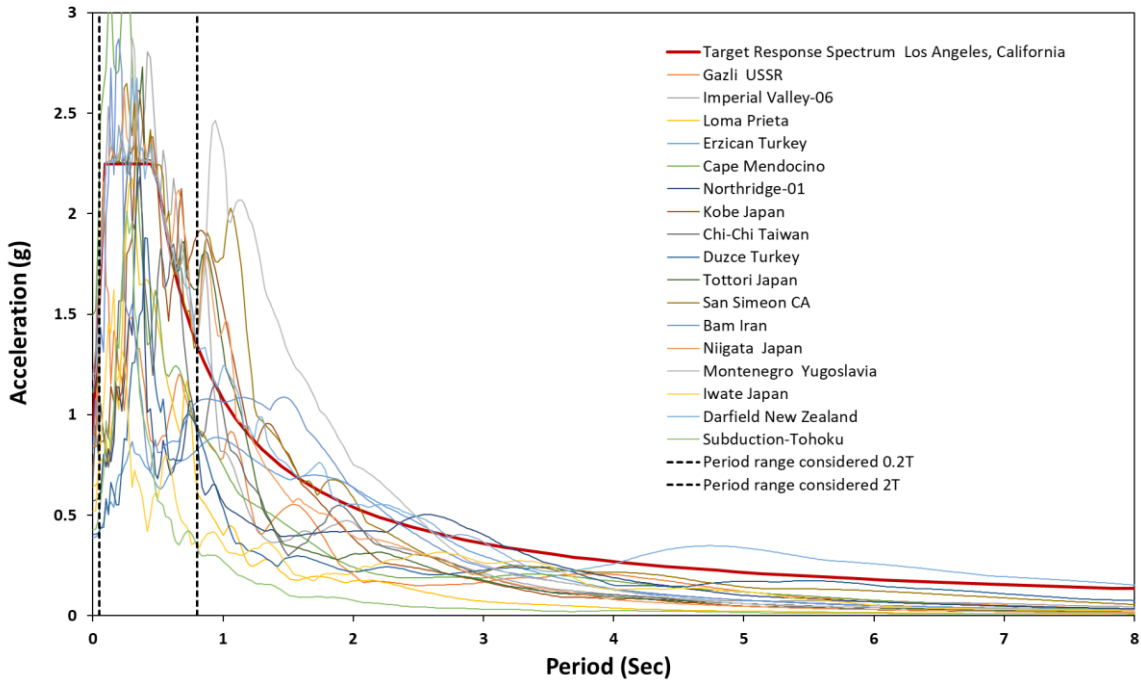


Figure 5-10. Original ground motions

Experimental Frame Matched Accelerograms

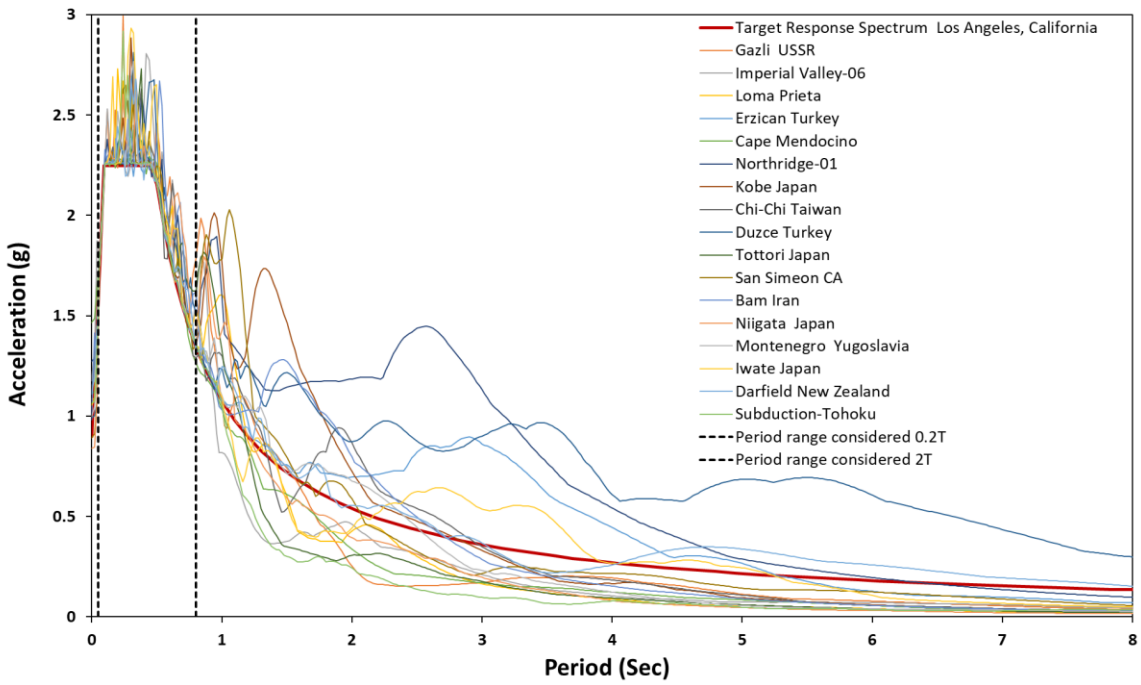


Figure 5-11. Scaled ground motions based on the target response spectrum (MCE_R)

5.4.1 History of displacement loading

The displacement of the shake table is limited to 10.16 cm in each direction, the pick displacement of each ground motion was scaled to match the limitation of the shake table. In order to scale the displacement and time steps of ground motions and keep them within the range of TRS (MCE_R), the target displacement of 10.16cm is divided by displacement of each ground motion to obtain the displacement scale factor. Then, to calculate the scaled time step, the square root of the original time step is multiplied by the displacement scale factor (Couch, 2020).

The frame was subjected to different scaled ground motions as shown in Figure 5-12 to Figure 5-15, as well as artificial motions such as sinusoidal, sweep and step loadings as presented in and Figure 5-16. The first sinusoidal is composed of five functions (A to E), with a maximum amplitude of 7.302cm (2.875in) and duration of 10.91 seconds. The functions A to E have equivalent cycles with a total of 18 cycles, function D has four cycles and function E has two cycles. The first 22 cycles (functions A to D) are derived in a way to disengage the friction damper, the damper slipped in the last two cycles. The second sinusoidal has a total duration of 150 seconds and a similar maximum amplitude of 7.302cm (2.875in). The number of cycles of each function A to E was multiplied by 15. This sinusoidal motion captured the generated heat in friction dampers caused by several slips cycled. The sweep function has a constant amplitude of 1.25cm (0.5in) with the duration of 192 seconds and the maximum acceleration of 0.64g and consists of eight frequencies with a range of 0.1, 0.2, 0.5 Hz, and 1 to 5 Hz with the adding step 1, each frequency used 10 cycles.

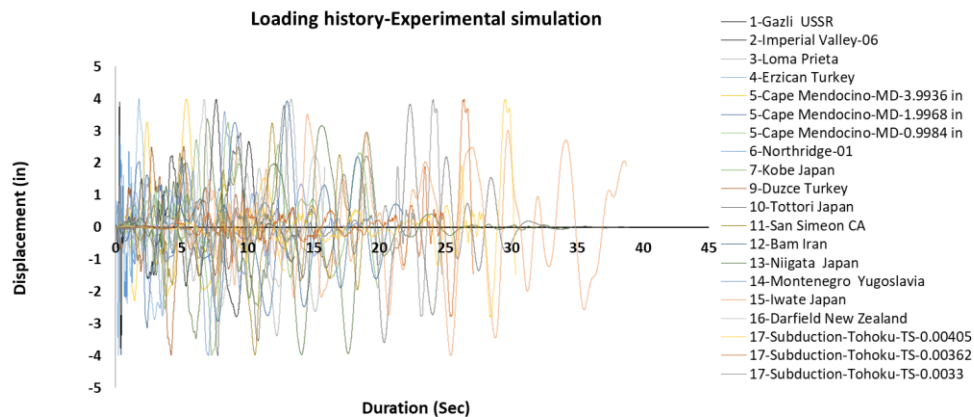


Figure 5-12. Displacement history of multiple ground motions

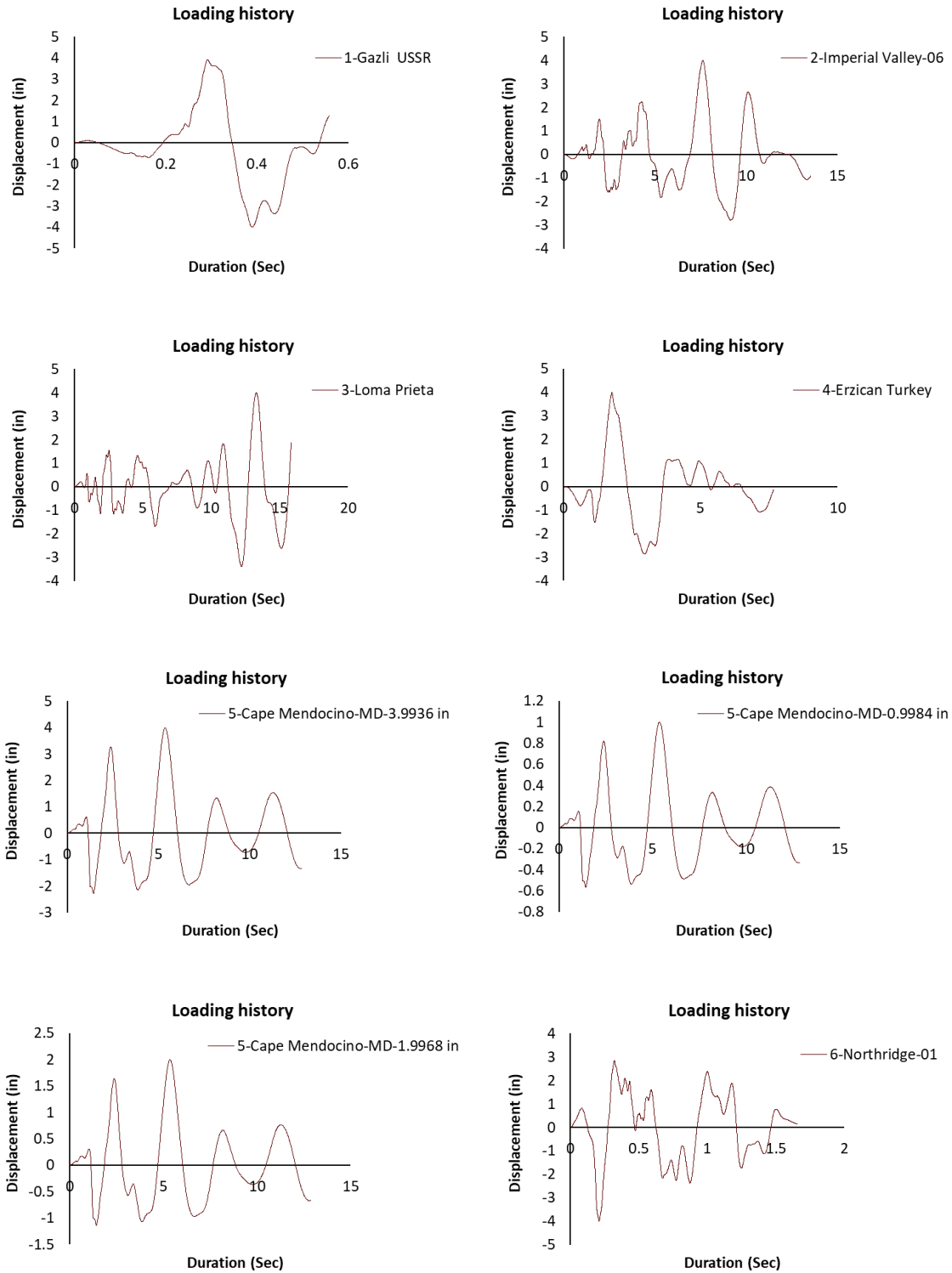


Figure 5-13. Individual displacement history of ground motions (Part-a)

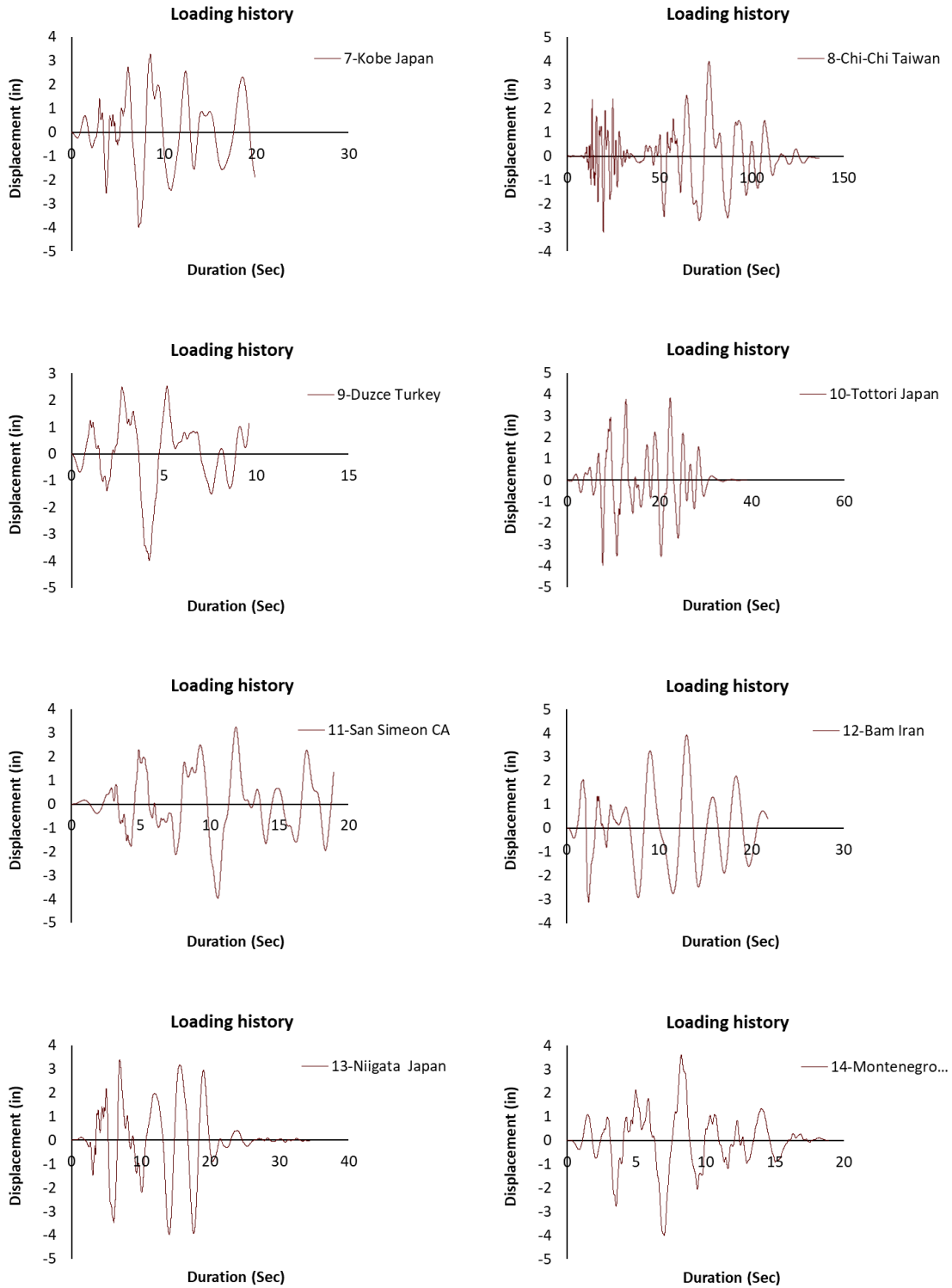


Figure 5-14. Individual displacement history of ground motions (Part-b)

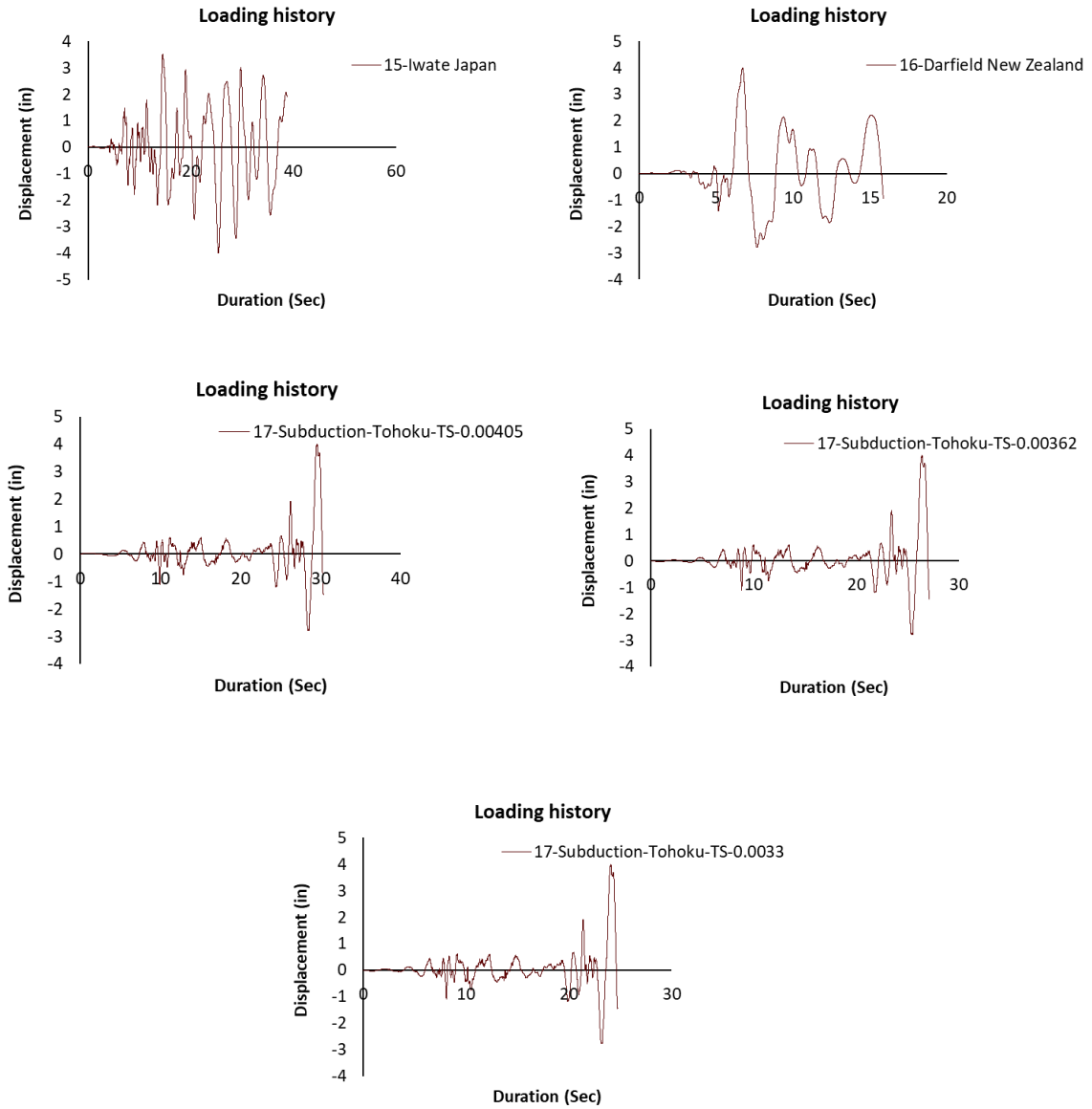


Figure 5-15. Individual displacement history of ground motions (Part-c)

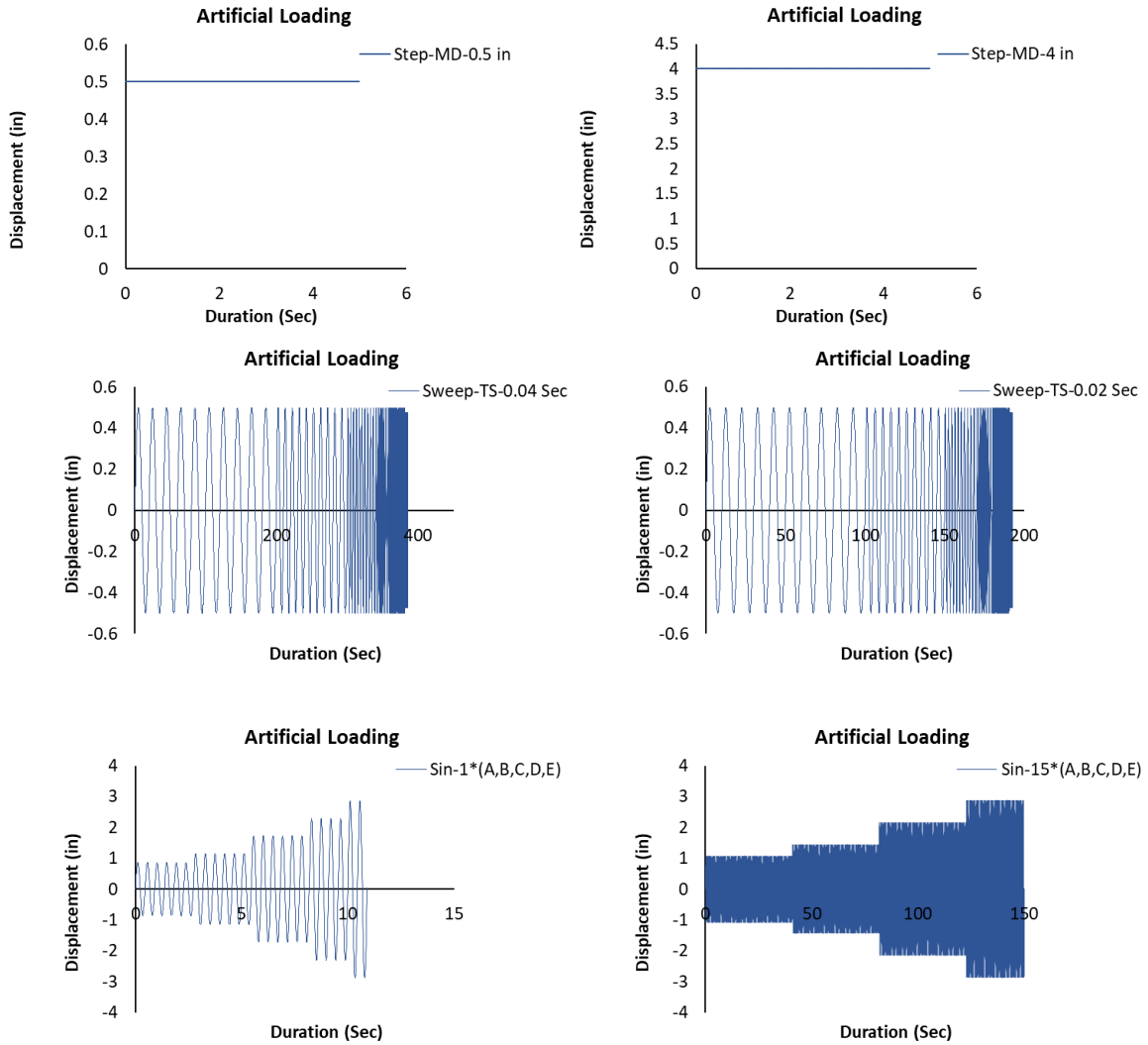


Figure 5-16. Displacement history of artificial motions

5.5 Phase 2: Numerical Work

In this section, six models are created based on the experimental tests using ETABS, OpenSees software. The frame consists of one bay with a length of 6'-7 1/2" (2.02 m) in X direction and two bays in the Y direction, the length of each bay is 2'-6 1/4" (0.77m). The design detail of the experimental frame, as well as the bracing sections, are presented in Table 5-3 and Table 5-4.

Table 5-3. Detail of the experimental frame sections

Story	Column sections				Beam sections			
	No.	Section	Material	Length (m)	No.	Section	Material	Length (m)
1	1	W6×9	A992 (MCS)	2.44	1	W6×15	A992 (MCS)	2.02
	1	W6×9	A992 (MCS)	2.44	1	W6×15	A992 (MCS)	2.02
	1	W6×9	A992 (MCS)	2.44	1	W6×15	A992 (MCS)	2.02
	1	W6×9	A992 (MCS)	2.44	4	W6×15	A992 (MCS)	0.77

MCS-Mild-carbon steel

Table 5-4. Detail of the bracing system

Story	Conventional Single leg brace				Yielding restrained brace			
	No.	Section	Material	Length (m)	No.	Section	Material	Length (m)
1	2	C6×10.5	A36	3.16	2	C6×10.5	A36	2.52
					1	IFD*	Quaketek	0.64

*IFD-0.64m×0.076m×0.165m, W=20kg

The total mass on the experimental frame is 19.57 KN (4400 lb), which includes two rigid blocks with the dimension of 1.22m×1.22m×0.31m (48in×48in×12in). The weight of the existing blocks is applied as two-point loads of 10.21 KN (2.3 Kip) each on the middle beam (2-L1&L2) and four-point loads of 5.1 KN (1.15 Kip) each on the outside beams (1&3-L1&L2) as demonstrated in Figure 5-17.

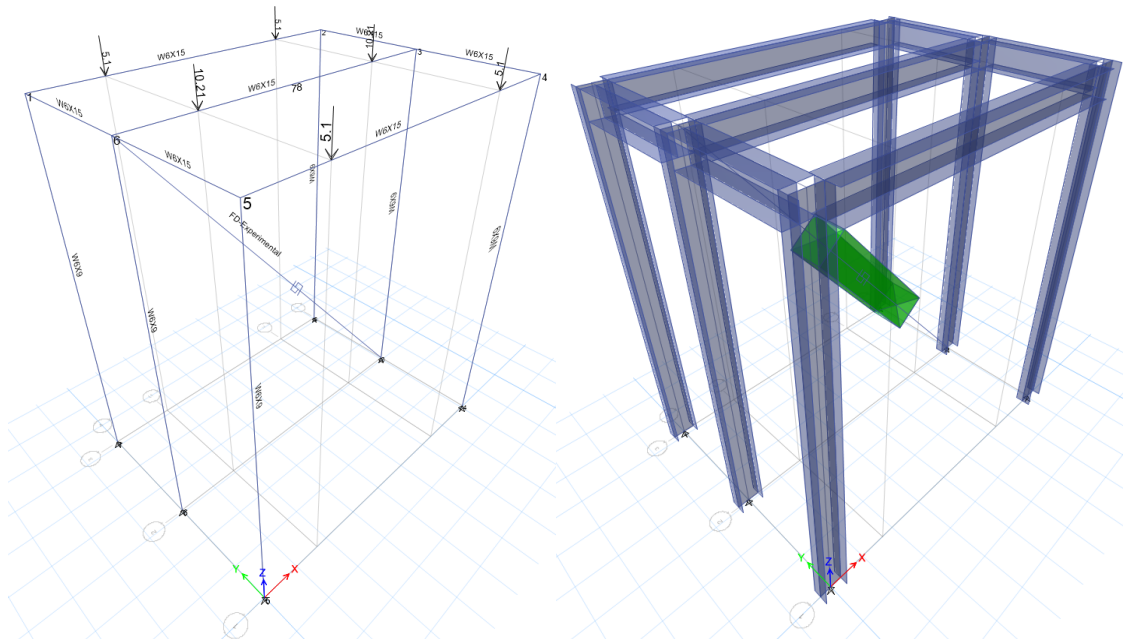


Figure 5-17. Simulation of the experimental frame using ETABS software (loads are in KN)

The moment resisting frame was designed to stay in the elastic region and re-centering the friction damper frame while carrying extra forces caused by the friction damper reaching the maximum slip distance. The OpenSees user is created for user documentation and can be found in the OpenSees command website indicated in the references, these procedures are presented in Appendix A5.4. Figure 5-18 demonstrates the modeling of the experimental frame using OpenSees software including steel moment-resisting frame using single leg brace (2C6×10.5) and yielding restrained brace. A schematic view of the Rayleigh Damping parameters is presented in Figure 5-19.

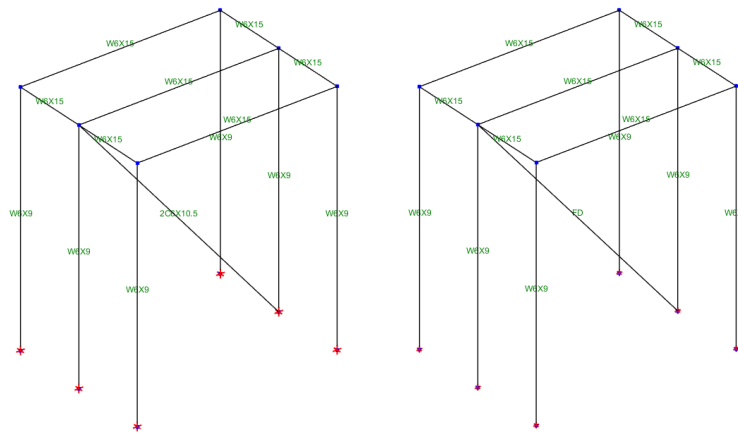


Figure 5-18. Simulation of experimental models in OpenSees

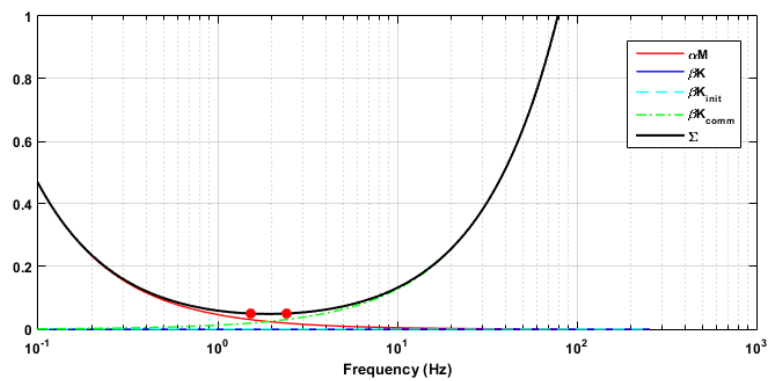


Figure 5-19. Rayleigh Damping parameters

5.6 Results and discussions

This part is a comparison between the experimental and numerical work of moment resisting frame with a single leg brace, and moment-resisting frame with friction damper.

5.6.1 Moment resisting frame with a single leg brace

The moment resisting frame is equipped with a single leg brace of mild carbon steel material, and a section of double channels C6×10.5 (A36). The experimental testing system of the conventional single leg brace, as well as its simulated model, are presented in Figure 5-20.

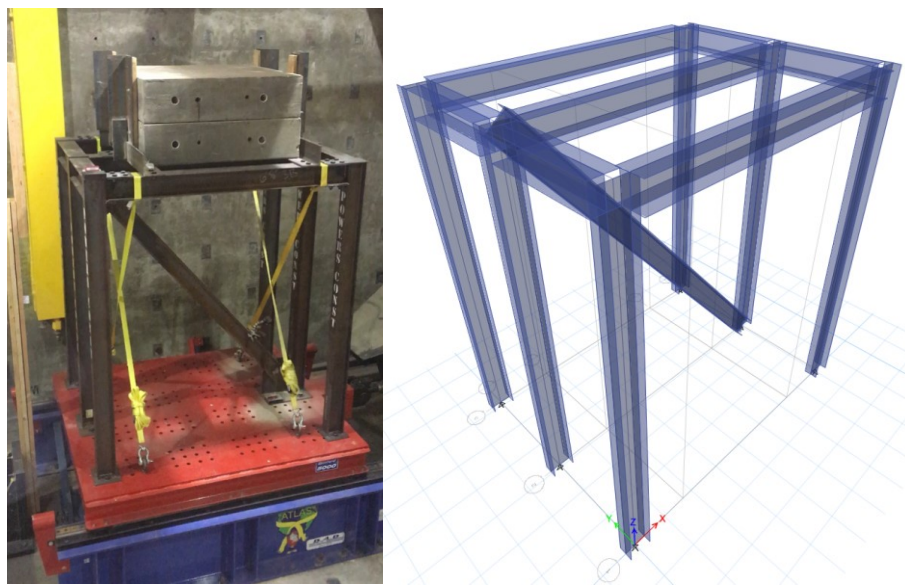


Figure 5-20. MRF with single leg brace (Couch et. al., 2020)

A comparison of roof acceleration for moment-resisting frame with ordinary single-leg brace of both experimental and analytical is presented in Figure 5-21. The experimental accelerations in both south-west and north-east locations were in the range of 1.21g to 2.00g. The analytical had a minimum and maximum acceleration of 1.25g and 1.90g. The roof history accelerations of different ground motions are presented in Figure 2-22 to Figure 2-26.

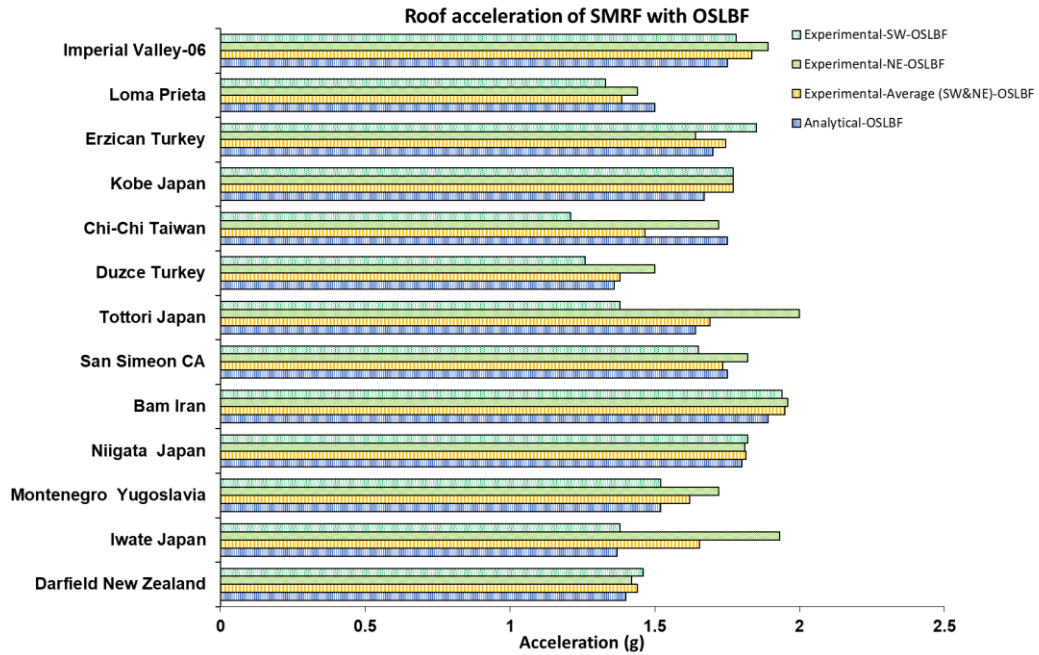


Figure 5-21. Comparison of roof acceleration of OSLBF subjected to different motions

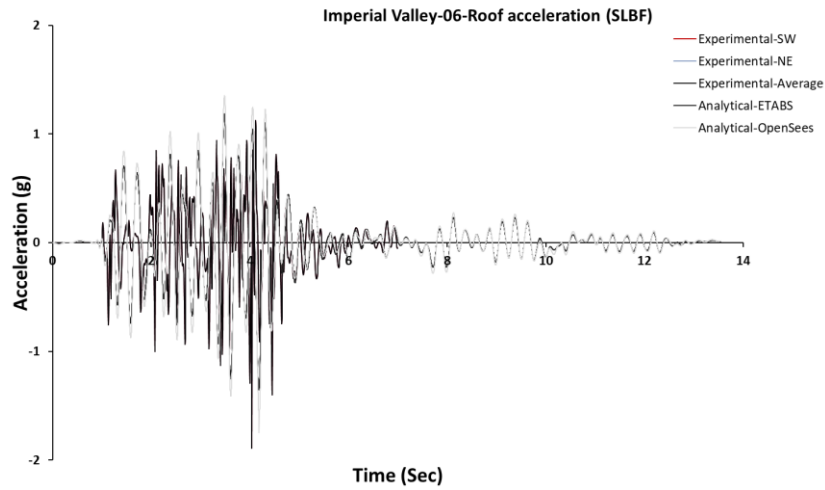


Figure 5-22. Comparison of roof history acceleration of OSLBF (Baseline Correction-Part-a)

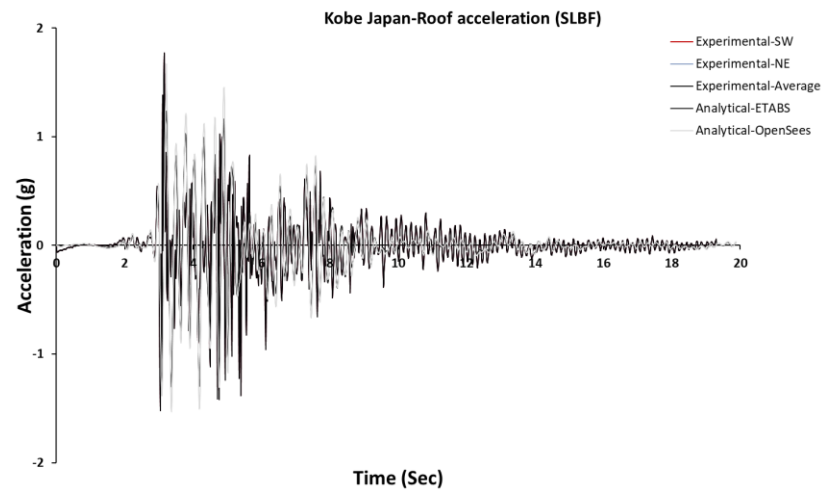
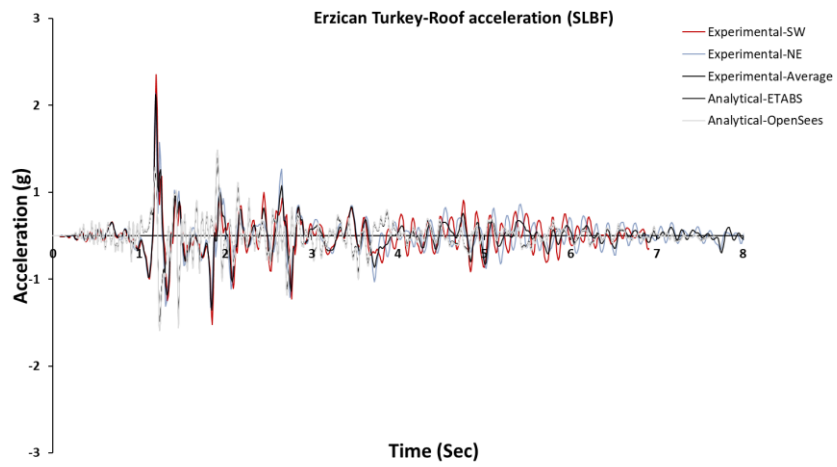
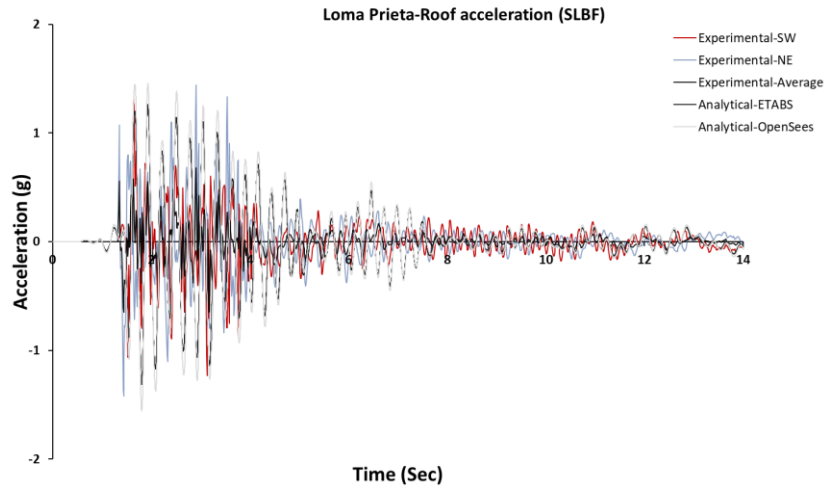


Figure 5-23. Comparison of roof history acceleration of OSLBF (Baseline Correction-Part-b)

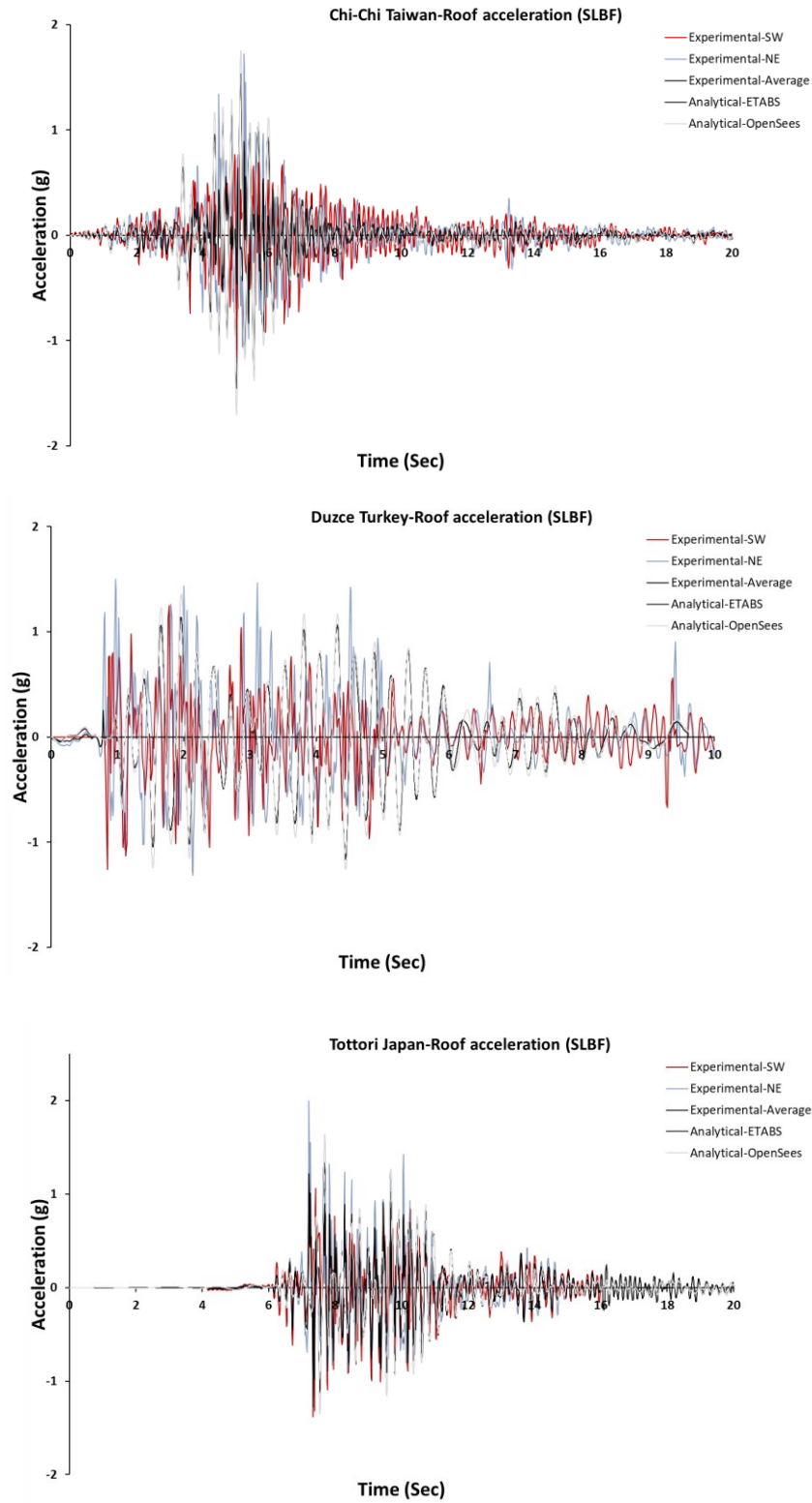


Figure 5-24. Comparison of roof history acceleration of OSLBF (Baseline Correction-Part-c)

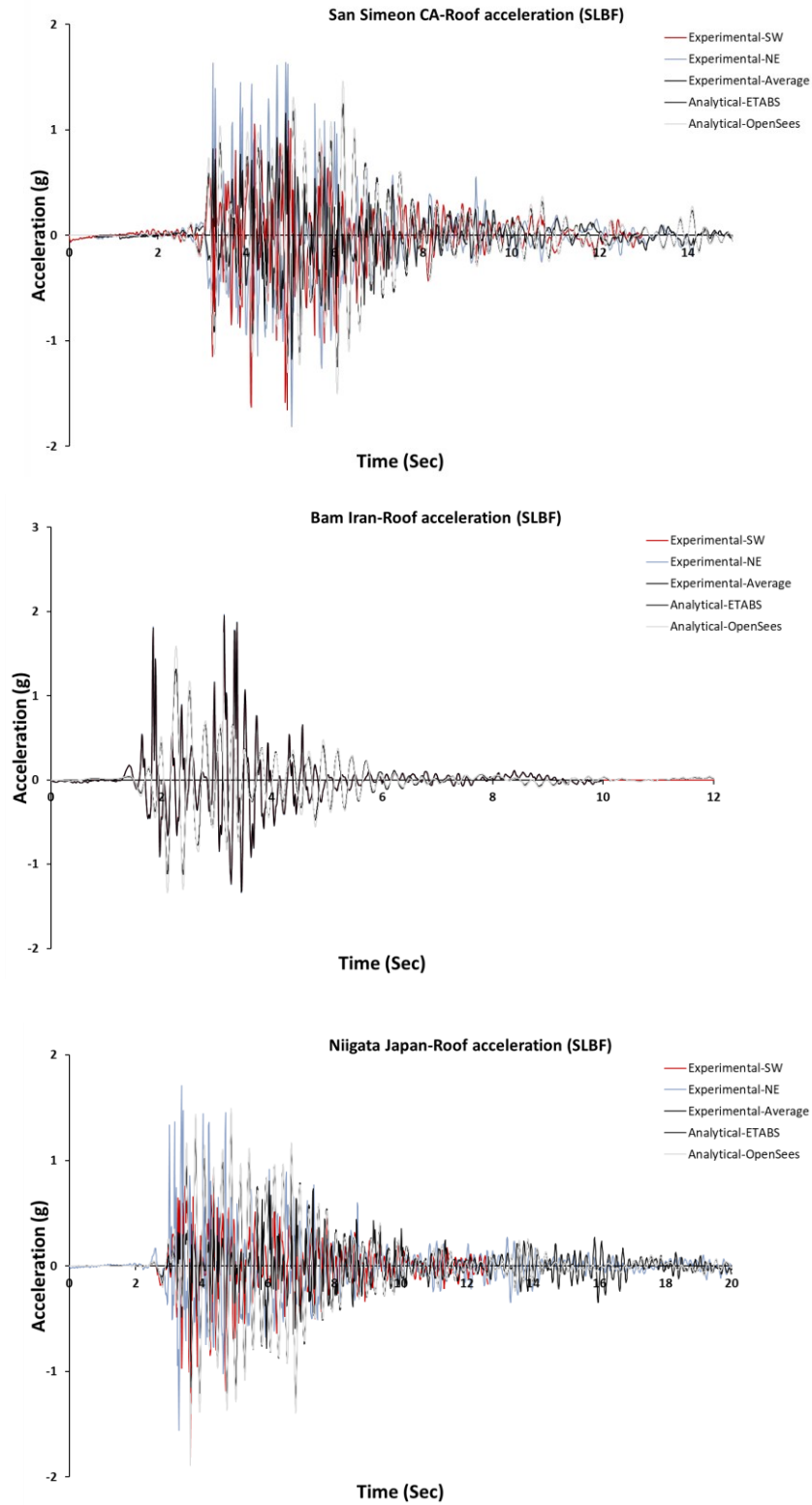


Figure 5-25. Comparison of roof history acceleration of OSLBF (Baseline Correction-Part-d)

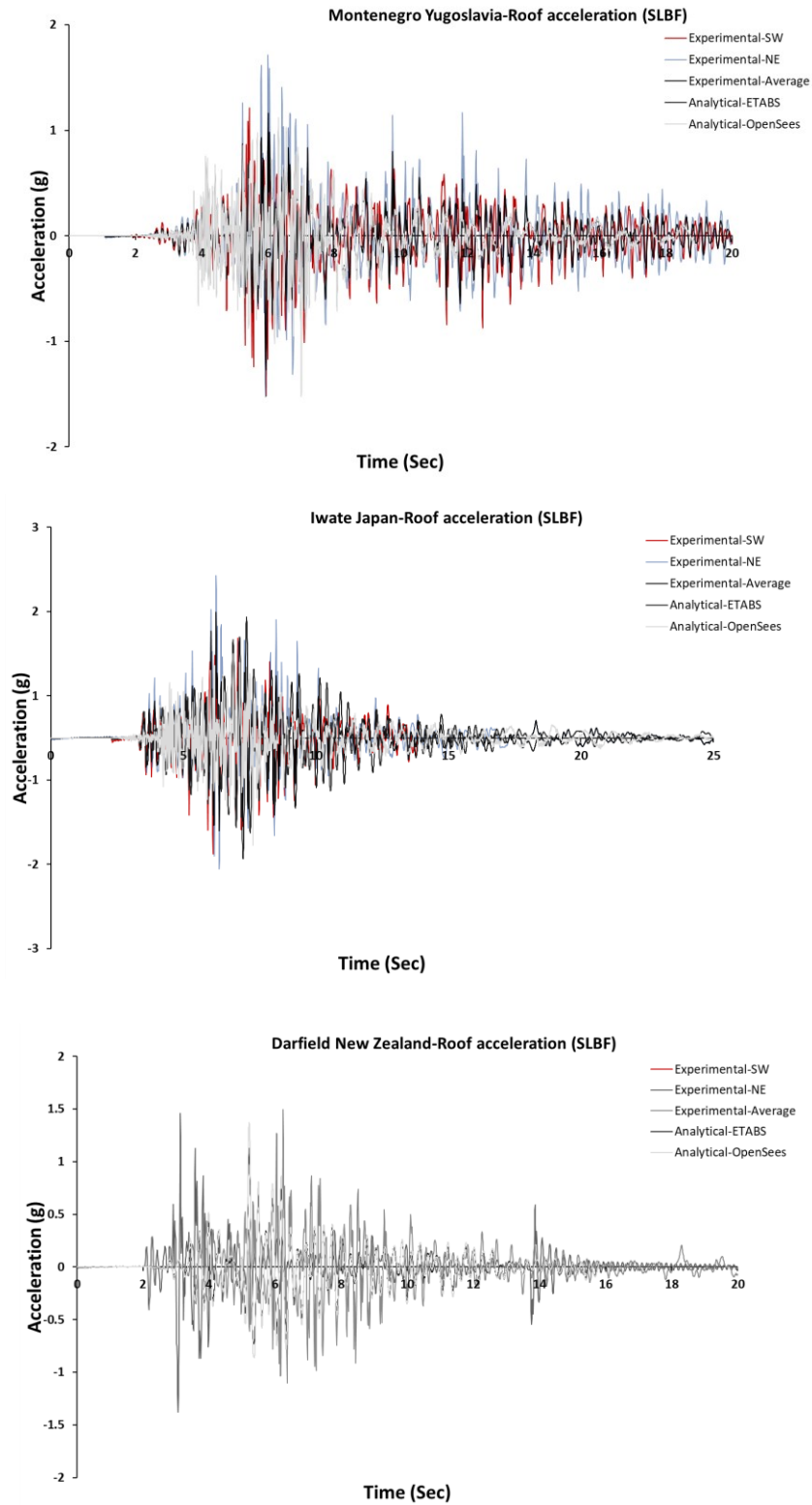


Figure 5-26. Comparison of roof history acceleration of OSLBF (Baseline Correction-Part-e)

The damping of the dual system (SMRF with conventional single leg brace) was calculated based on the different response spectrum curves, using the maximum response amplitude, $R_{d(max)}$, and resonant amplitude (Chopra, 2012). Figure 5-27 presents the comparison of different damping percentages of selected ground motions for experimental and analytical work. The damping percentage of MRF with a single-leg bracing system of experimental work in the south-west location was in the range of 14.47% to 26.09%, and in the north-east location was in the range of 13.67% to 23%. The results of the analytical had a minimum and maximum damping percentage of 16.2% and 22.6%.

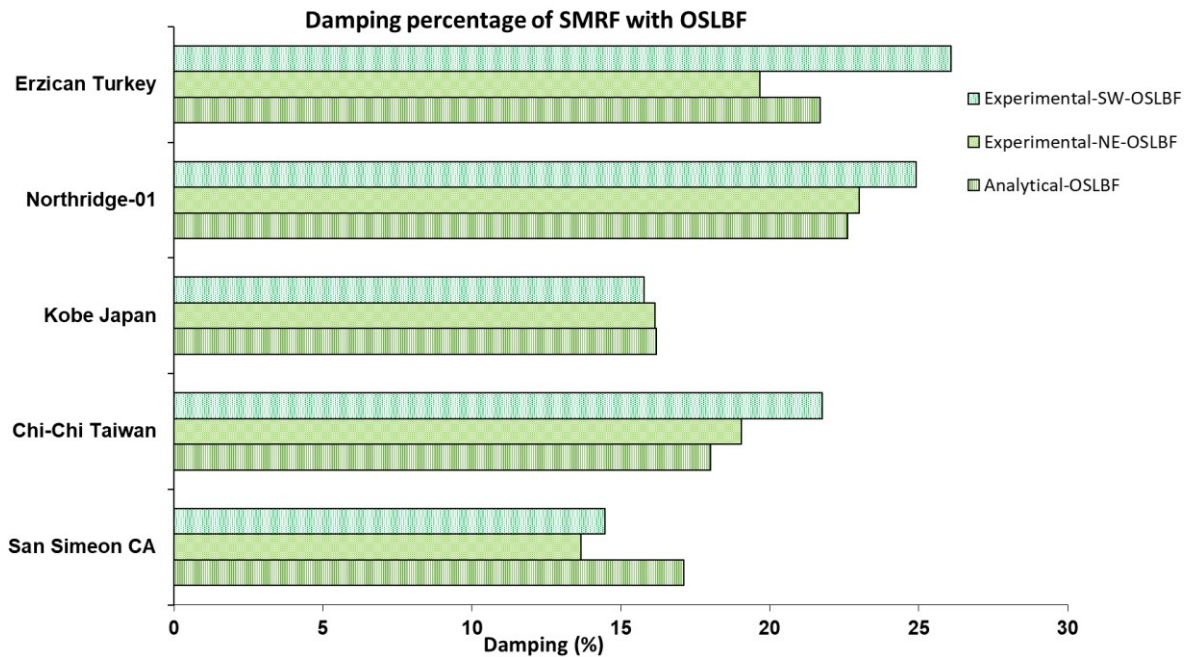


Figure 5-27. Comparison of damping property of the system in the percentage

5.6.2 Moment resisting frame with yielding restrained brace

The Ten-Co seismic brakes were provided by Quaketek company, had a dimension of 0.64m×0.076m×0.165m and the weight of 20kg, a schematic view of Ten-Co seismic brake is presented in Figure 5-28. These dampers had a slip load of 22 KN, with a maximum slip distance of 51 mm, the working slip distance of the experimental test was set to 3mm. Four 0.75-inch diameters of A390n bolts were used to connect the damper to the brace and one 0.75-inch diameter

of A490X bolt was utilized to connect the damper to the 0.625-inch-thick plate (Couch et. al., 2020).



Figure 5-28. Fabricated Ten-Co Seismic brake (Couch et. al., 2020)

The experimental simulation hysteresis behaviours of the frame utilizing a yielding restrained brace subjected to various types of scaled ground motions are presented in Figure 5-29 to Figure 5-32. The yielding restrained brace behaved elastically subjected to Cape Mendocino motion having the amplitude of 25mm (0.99 inches) and 50mm (1.99 inches), but when it increased to 100mm (3.99 inches), the hysteresis curve changed to the rectangular shape.

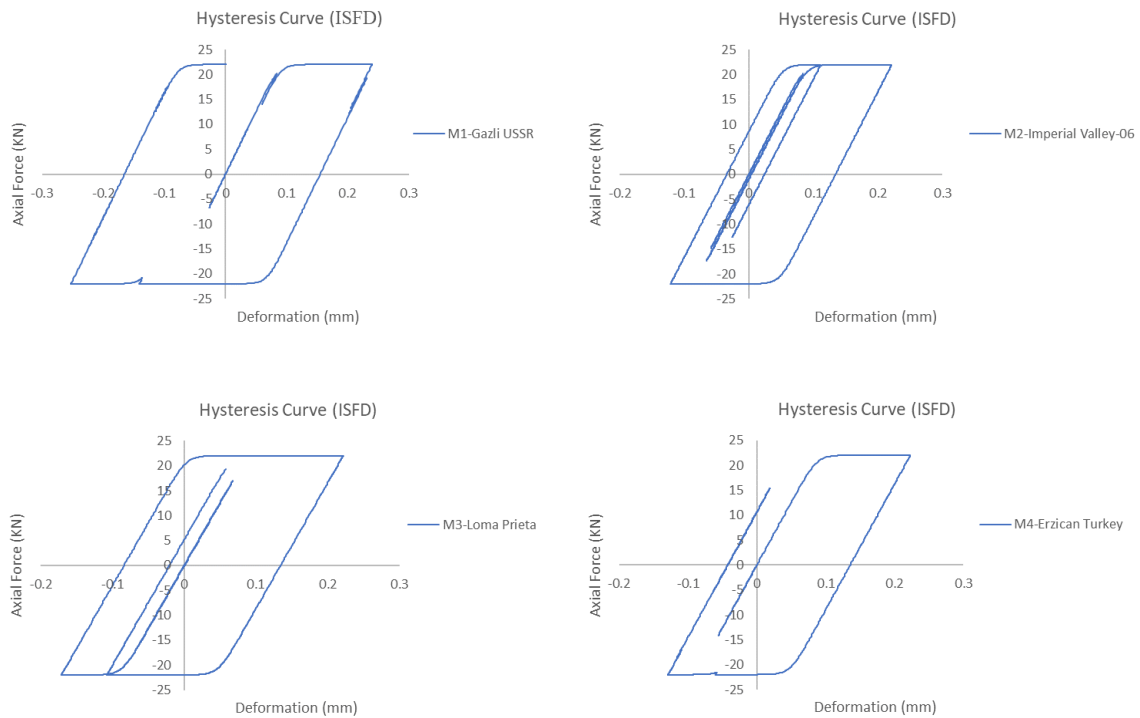


Figure 5-29. Hysteresis curves for ground/artificial motions (Part-a)

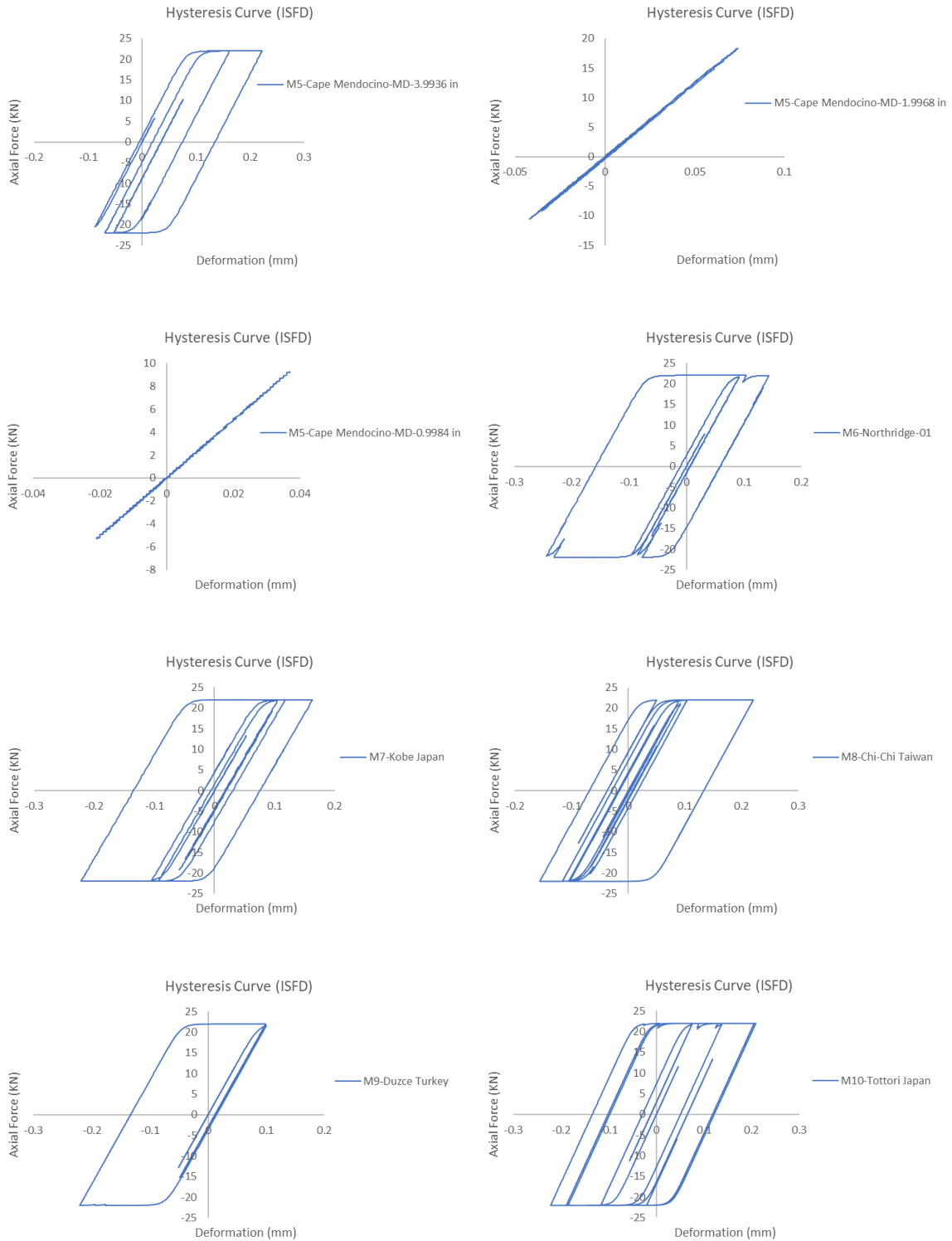


Figure 5-30. Hysteresis curves for ground/artificial motions (Part-b)

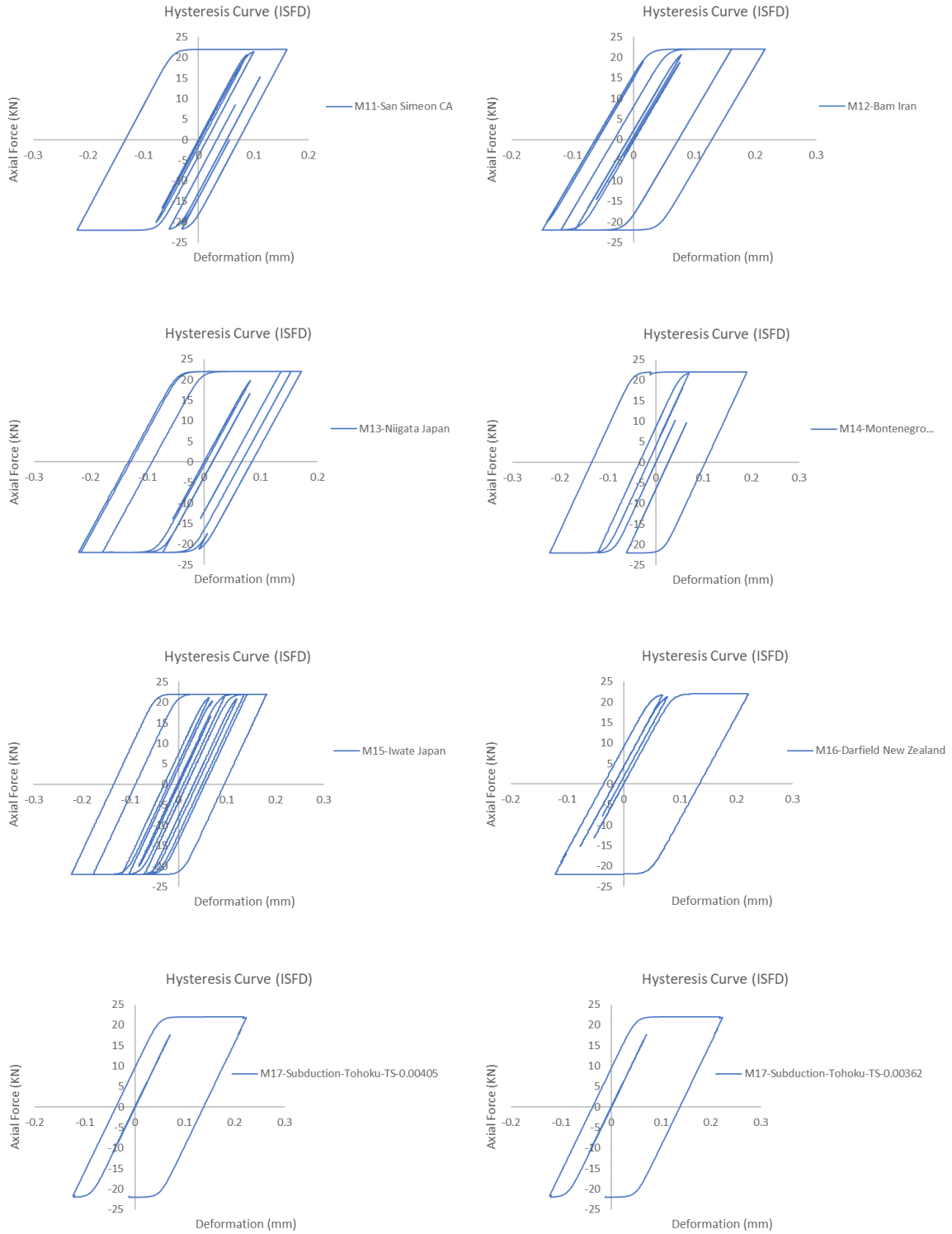


Figure 5-31. Hysteresis curves for ground/artificial motions (Part-c)

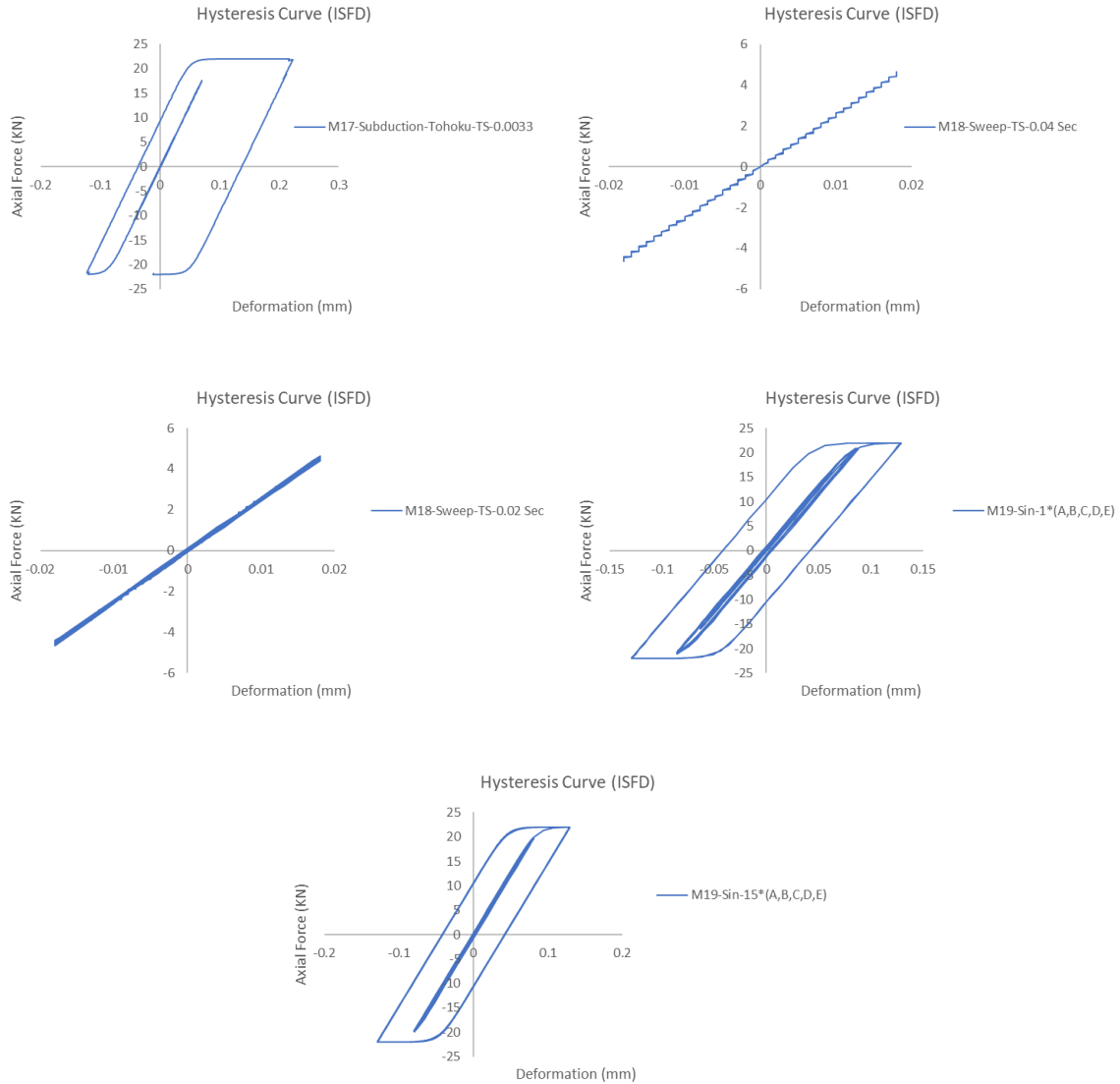


Figure 5-32. Hysteresis curves for ground/artificial motions (Part-d)

Figure 5-33 presents the roof acceleration of the dual system with a yielding restrained brace. The measured experimental accelerations in the southwest and northeast locations were in the range of 0.82g to 1.77g. The analytical accelerations were in the similar range of 0.87g and 1.71g with experimental work. Figure 5-34 to Figure 5-38 indicate the comparison of history accelerations for experimental in both locations (NE, SW) as well as OpenSees and ETABS software.

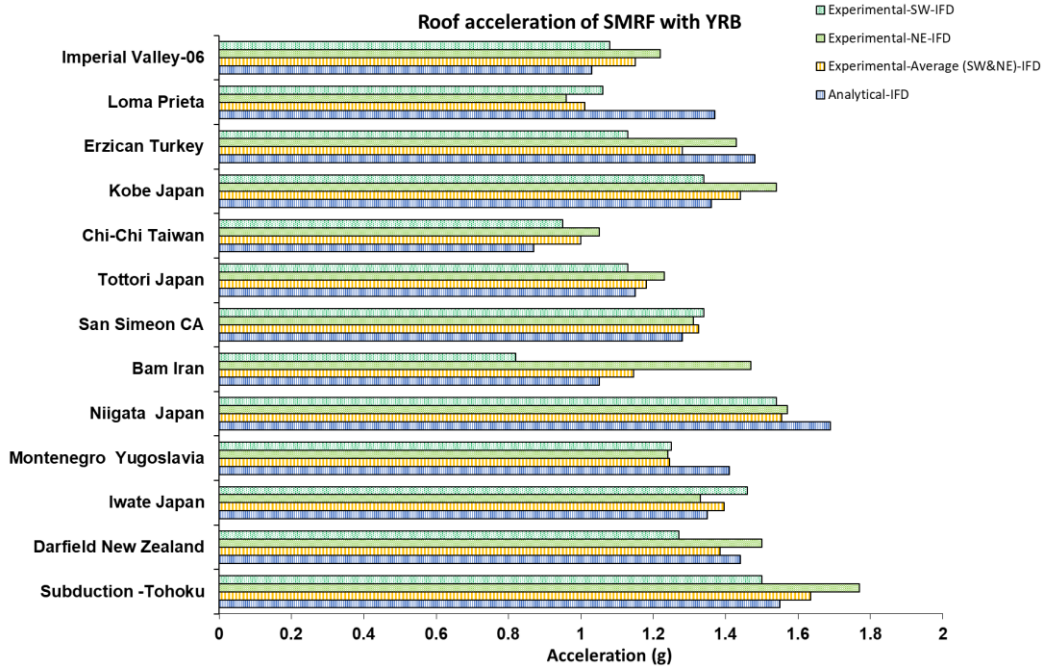


Figure 5-33. Comparison of roof acceleration of YRB subjected to different motions

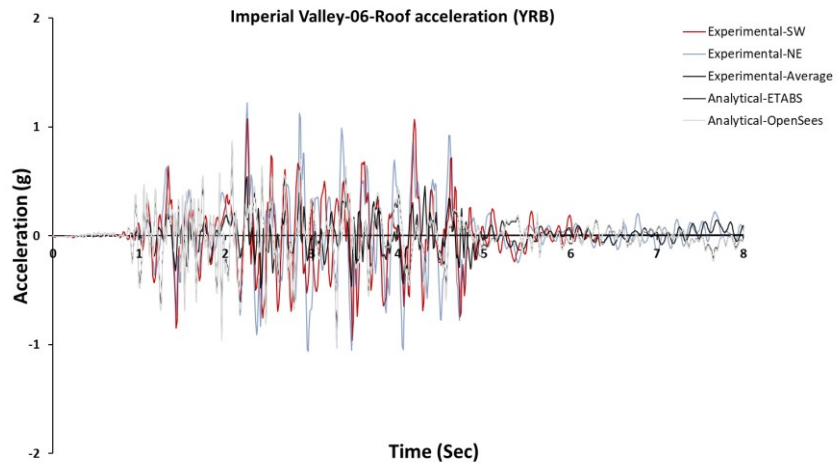


Figure 5-34. Comparison of roof history acceleration of YRB (Baseline Correction- Part-a)

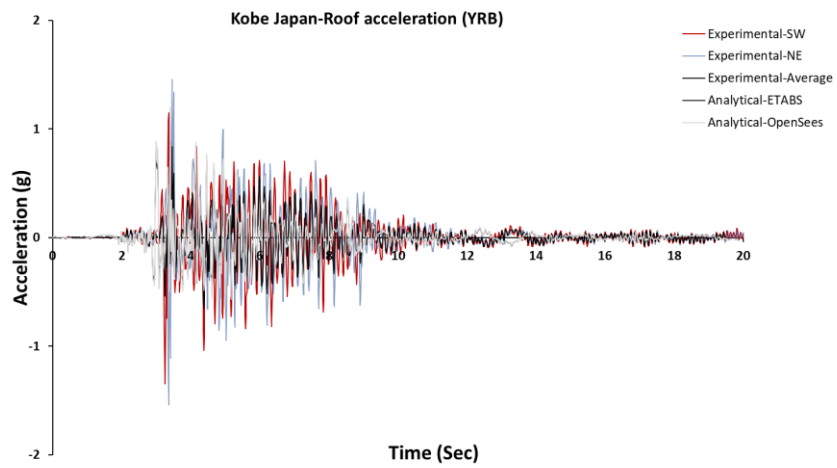
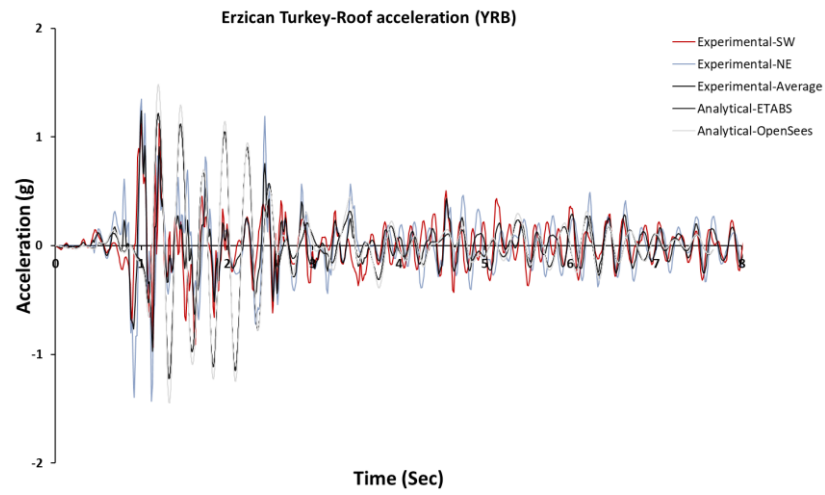
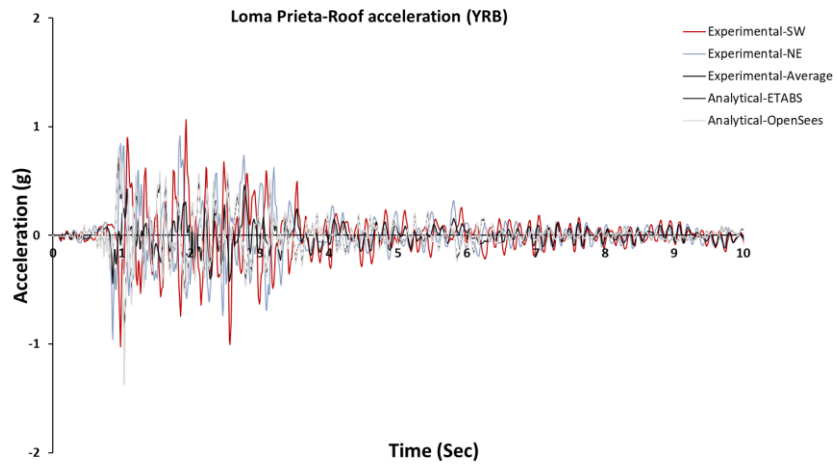


Figure 5-35. Comparison of roof history acceleration of YRB (Baseline Correction- Part-b)

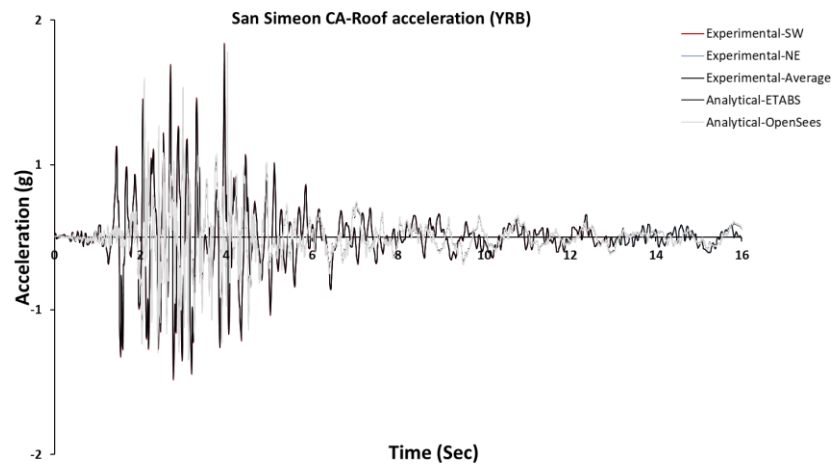
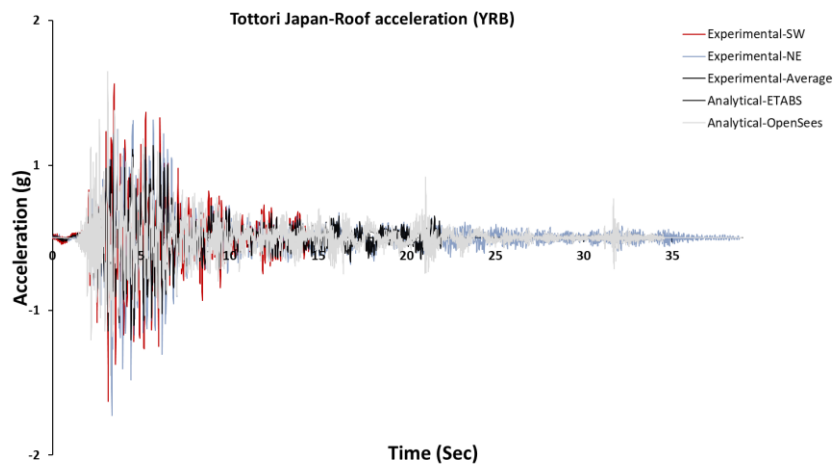
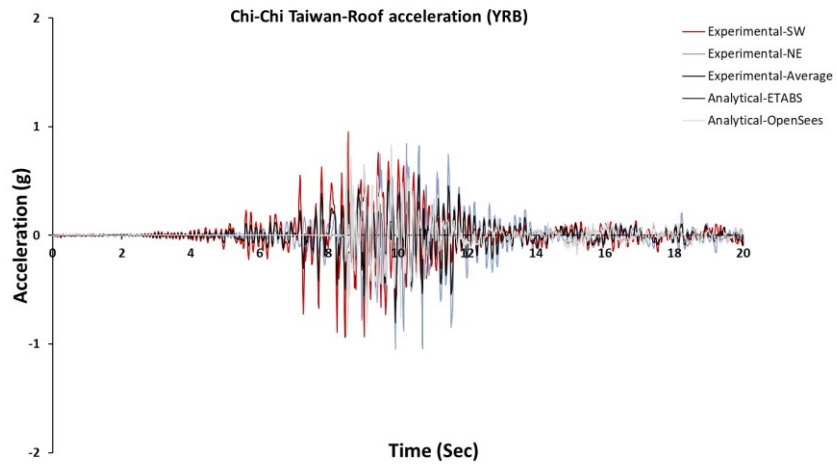


Figure 5-36. Comparison of roof history acceleration of YRB (Baseline Correction- Part-c)

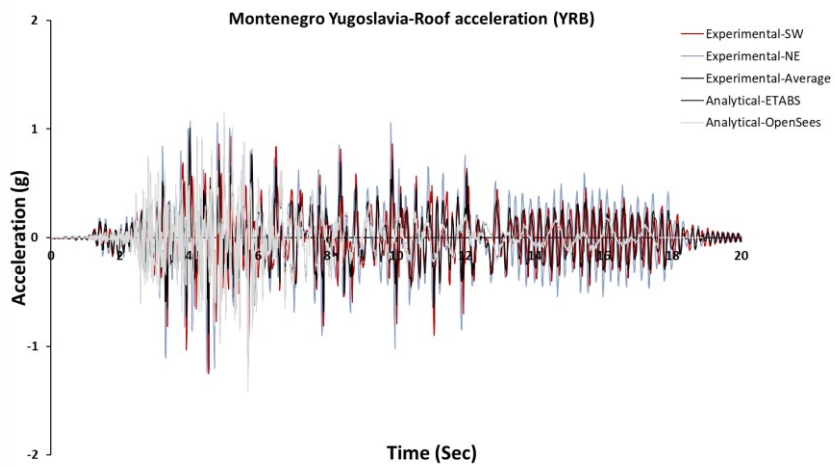
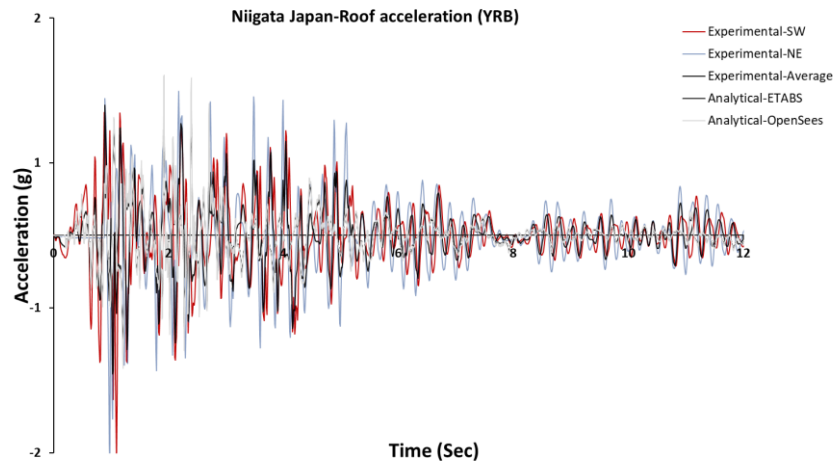
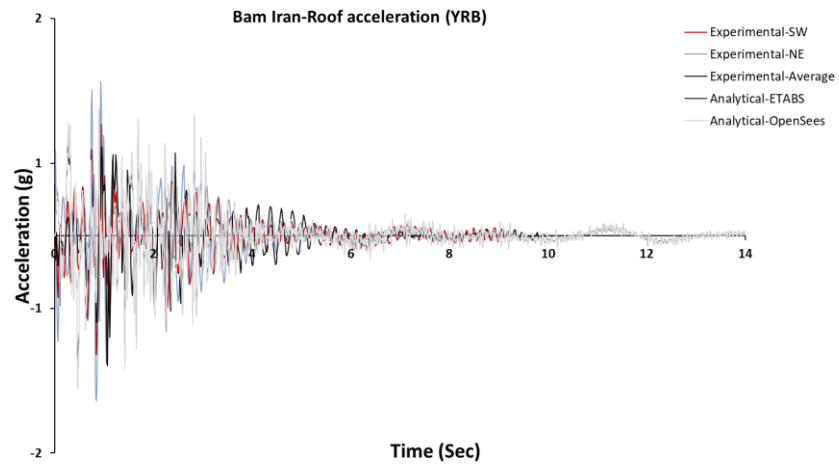


Figure 5-37. Comparison of roof history acceleration of YRB (Baseline Correction- Part-d)

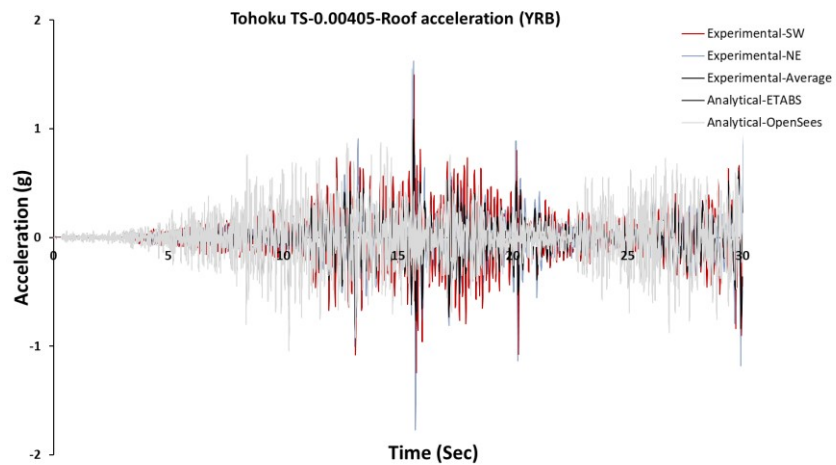
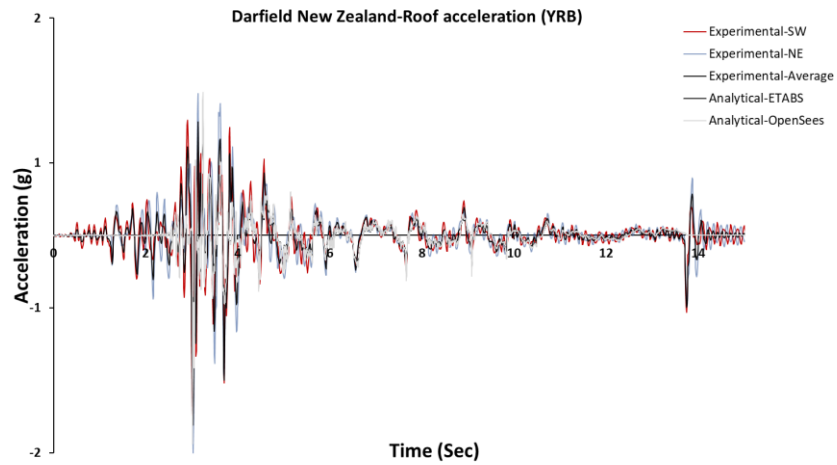
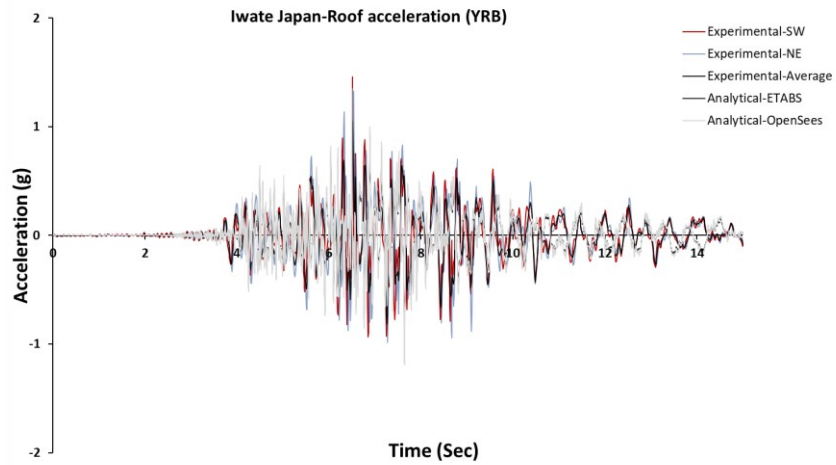


Figure 5-38. Comparison of roof history acceleration of YRB (Baseline Correction- Part-e)

Figure 5-39 indicates the damping percentage of experimental and analytical works under different selected ground motions. The minimum and maximum damping percentage of experimental tests in the southwest and northeast locations was 20.01% and 34.45%. The calculated damping properties of the system based on the analytical work were in the range of 25.96% and 34.38%.

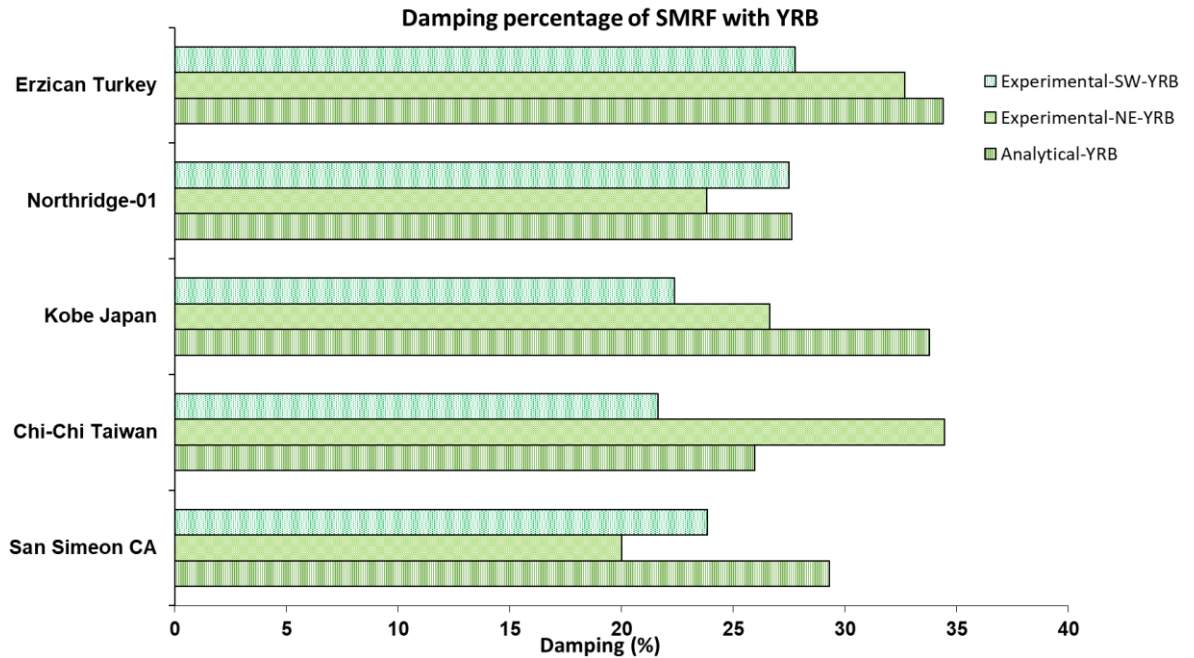


Figure 5-39. Comparison of damping properties of MRF with IFD

5.7 Summary and discussions

This study composed of two phases; the first phase covered the collaborating experimental tests of two full-scale steel moment-resisting frames with a single leg brace (2C6×10.5) as well as three yielding restrained braces. The frame consists of one bay in the X direction (2.019m) and two bays in the Y direction (0.768m), with a height of 2.44m. The tests were performed at the structural laboratory of the Lyles College of Engineering at California State University by an MSc student at CSU (Couch, 2020). The second phase was the verification of the results by simulating the experimental tests. The results covered a comparison of the conventional brace frame response (2C6×10.5) with the yielding restrained brace frame response of both experimental tests and

simulated work subjected to the scaled ground motions and artificial loadings. Different types of loading including Interim Protocol I and II are discussed. The frame is assumed to be located in Los Angeles, California in a high seismic zone. The ground motions are selected based on the site location from the “Pacific Earthquake Engineering Research Center (PEER) ground motion database”. Seventeen ground motions are selected and scaled based on the maximum target response spectrum and period of the frame according to ASCE 7. The following conclusions are withdrawn:

A comparison of roof acceleration of different ground motions for SMRF with OSLB and YRB is presented in Figure 5-40 and Figure 5-41. The ordinary single-leg brace frame had an average of 1.65g in both locations and 1.64g in analytical simulation. The average and standard deviation of OSLBF were 1.83g in southwest and northeast locations, and 1.81g in the simulated work. When the SMRF was equipped with YRB the average acceleration values were reduced to 1.28g in southwest and northeast locations and the analytically estimated value was 1.31g. The standard sum of average and standard deviation values was 1.48g of both locations and 1.53g in the analytical model. The results also indicated the friction damper reduces about 25%-27% of the acceleration when subjected to various types of scaled ground motions. Moreover, the combination of standard deviation and average of both experimental and analytical work had a difference of about 18% to 20% in OSLBF and YRB.

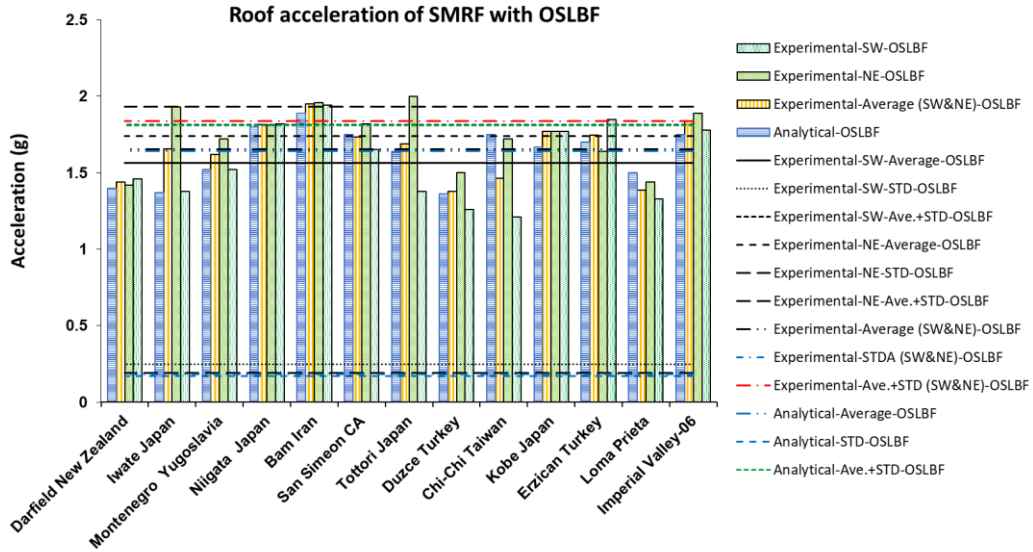


Figure 5-40. Average and standard deviation of roof acceleration of SMRF with OSLBF

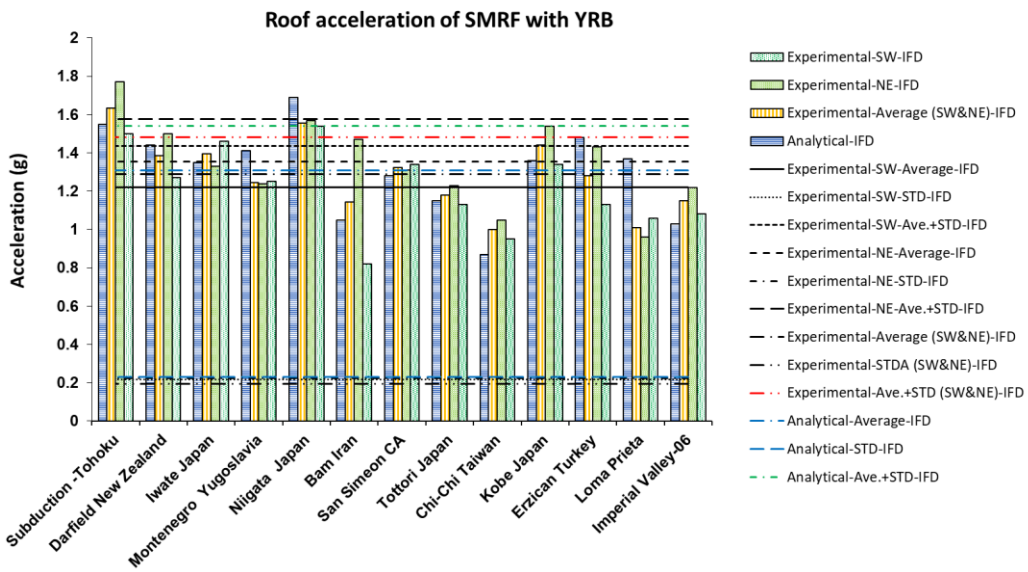


Figure 5-41. Average and standard deviation of roof acceleration of SMRF with YRB

The ordinary single-leg brace frame had average damping of 20.59% and 18.31% in the southwest and northeast locations and 19.12% based on the analytical calculation. The combination of standard deviation and average of SLBF was 25.86% in the southwest location, 21.86% in the Northeast location, and 21.97% from the simulated work. The SMRF with YRB had average damping of 24.6% and 27.54% in both locations and 30.20% in the analytical. The sum of standard deviation and average of the frame with YRB was 27.46% and 35.54% in southwest

and northeast locations, and 33.93% in the simulated frame. A comparison between analysis and experimental showed the YRB increased the damping of the system by about 7% in the simulated work, and 6.74% from the experimental test compared with conventional single leg brace as presented in Figure 5-42 and Figure 5-43.

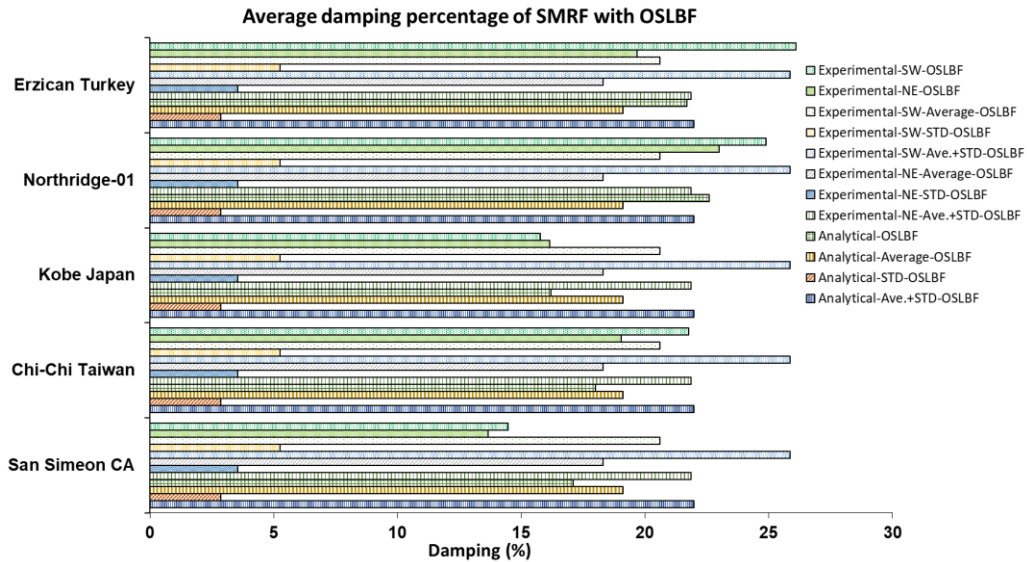


Figure 5-42. Damping percentage of MRF with OSLB

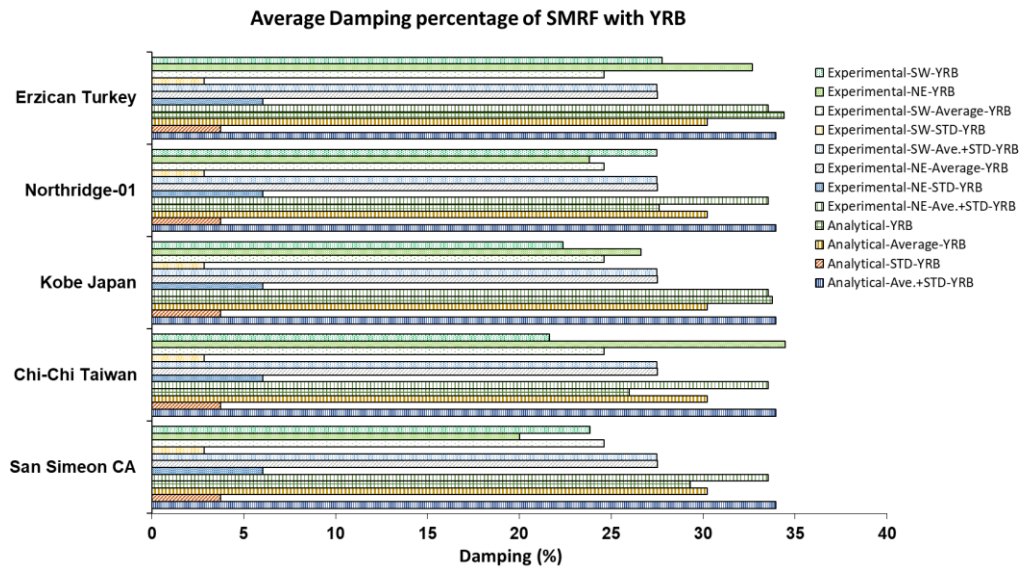


Figure 5-43. Damping percentage of MRF with IFD

The maximum displacement and drift of experimental and analytical studies are shown in Figure 5-44 and Figure 5-45. The sum of standard deviation and the average of displacement was 0.42 inch and 0.39 inch for the experimental and analytical respectively, the average drift values were 0.33% and 0.30% for the experimental test and simulated work. These values verified the fact that extra forces that occurred in the friction damper can be observed by SMRF while remaining in the elastic zone.

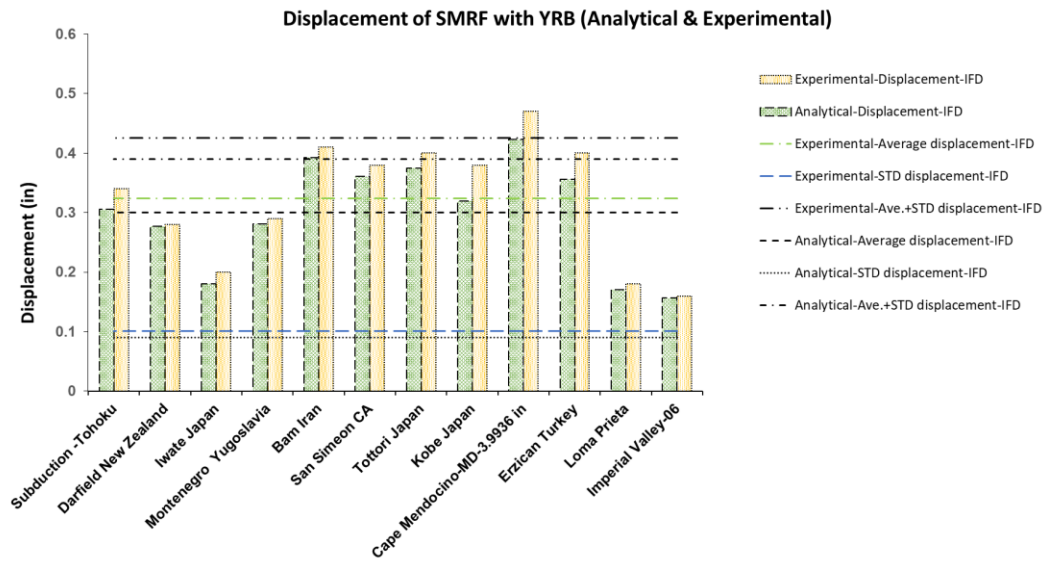


Figure 5-44. Maximum displacement of SMRF with YRB

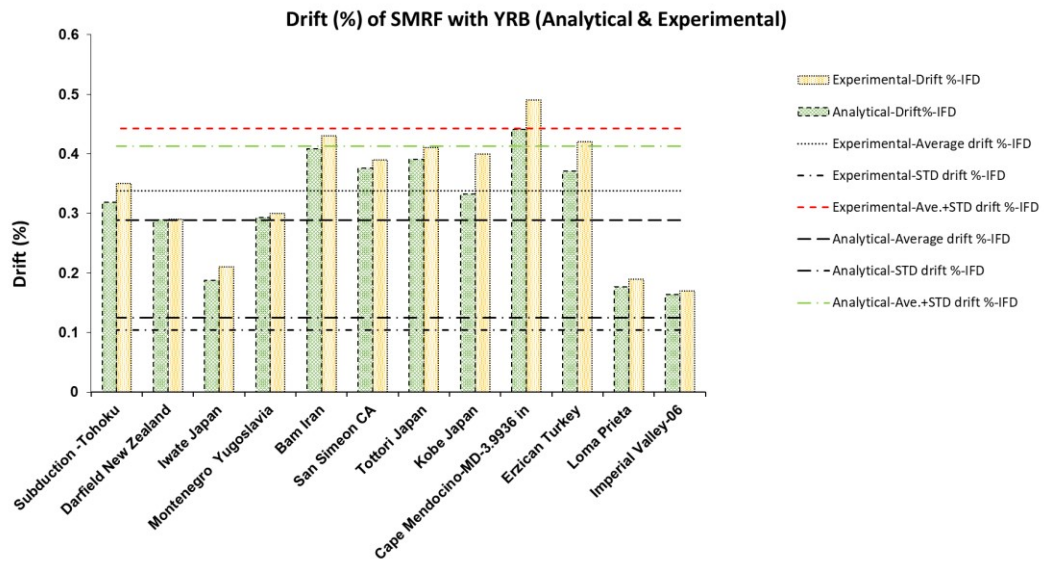


Figure 5-45. Maximum drift ratio of SMRF with YRB

The total weight on the frame was limited to the height of the crane 8ft from the shake table surface, also the shake table was limited to the maximum frequency of 10 Hz and maximum and minimum of ± 101.6 mm displacement. The experimental test was performed using ± 101.6 mm displacement and with a frequency of 2.5 Hz, which generate a maximum acceleration of 1.5g (Couch, 2020). This limitation resulted in a lower slip distance; however, the results verified the effectiveness of yielding restrained braces in structural performance compared with the conventional one. Moreover, the friction damper component with bolt connections can be replaced after a strong ground motion. Further investigations are required on the large-scale testing as well as its simulation on a multistory frame, including higher seismic weight and acceleration that produces higher slip distances and accounts for the higher mode effects.

CHAPTER 6

Summary, Conclusions, and Recommendations for Future Work

6.1 Summary

This study investigated the seismic response of concrete frame structures utilizing yielding restrained braces. Different types of control systems for seismic protection of structures including different types of friction devices and their modeling were discussed. Based on the literature most of the researchers focused on the retrofitting of steel structures using dissipation devices, or concrete structures with FRP, and the effects of supplementary devices i.e., friction dampers are not addressed properly on concrete structures. Moreover, a comparison of analytical with a full-scale experimental test is required to verify the behaviour of an inline friction damper subjected to real ground motions.

The thesis is composed of analytical and experimental investigations and is divided into three major parts. The first part is the analytical study to investigate the effects of different concrete moment resisting frames with supplemental damping. The second part is to evaluate the seismic performance and reduction factors of different energy dissipation systems on the concrete moment-resisting frame. The third part is the simulation of the collaborating experimental work of a full-scale steel frame with yielding restrained braces.

The following are the analytical and experimental studies:

- The seismic performance of four-, eight-, and the twelve-story ductile concrete moment-resisting frame was evaluated, also the effect of P- Δ was considered by the leaning column concept. A nonlinear model of structural components is calculated based on FENA 356 and ATC 72. The analysis covered modal, nonlinear static, Inelastic history analysis by the leaning column concept. It was observed the structural performance of SLE, DLE remained in the elastic part whereas, MCE due to the second-order elastic analysis the structure entered in the inelastic zone. Moreover, the higher mode effects shall be considered for

high-rise buildings and can be ignored for structures with a fundamental period of less than 0.8 seconds due to the use of load patterns.

- The effects of Inline Seismic Friction Dampers (ISFDs) on a 14-story with ductile, moderately ductile, and elastic concrete moment resisting frames (CMRFs) were investigated and compared with the moment resisting frames without dampers (bare frames) and their economic aspects were assessed. The detailed seismic performance of the building was investigated utilizing Pushover and nonlinear dynamic analysis. The results showed the building equipped with dampers had the desired performance level without any significant damage in the frame.
- A comparative study between conventional equivalent lateral force procedures, equivalent lateral force (ELF based on FEMA procedures), and response spectrum procedures (RSP) for buildings with damping devices were conducted. The seismic parameters of an eight-story building were evaluated using the above procedures. The seismic base shear, residual base shear, design, residual and maximum displacement, and their acceptance criteria, as well as design and maximum earthquake story velocities and a detailed calculation of damping properties of the structure, was determined based on ELF and RSP procedures and compared together. The conventional design is based on the reduced base shear, whereas the ELF and RS are based on the yield base shear. It was found the RS procedure is more conservative, which had effective damping of 54% compared with the ELF procedure with effective damping of 42%. Moreover, as the Canadian code does not recommend any integration of the damping properties, it is recommended to select the higher value of the initial design loads based on the ASCE 7 and NBCC.
- The seismic force reduction factors of four-, eight-, and fourteen-story ductile concrete frames with inline seismic friction dampers with different heights and span lengths were evaluated. Target displacement properties, as well as different hazard levels, were determined to calculate the overstrength, ductility, and response modification factors. The structural performance of the six models was verified by performing a nonlinear response history analysis using twenty-five ground motions. The results showed the calculated

overstrength factors are higher about 17% to 55% than the prescribed value in the NBCC 2015, the maximum ductility reduction factor was about 10% higher than the recommended value in the NBCC 2015.

- The design procedures of American and Canadian standards for a fourteen-story ductile concrete moment resisting frames were compared. One conventional Ductile Concrete Moment Resisting Frame (DCMRF), and five passive energy systems including Ten-Co Seismic Brake (TCSB), Fluid Viscous Damper (FVD), Triangular Metallic Yielding Dampers (TMYD), Lead Rubber Bearing Isolator (LRBI), and Triple Pendulum Isolator (TPI) were designed individually and their effects on the overall response of the structure were evaluated. The ASCE 7 was found to be more conservative than the NBCC 2015, the CMRF and TMYD had the maximum and minimum response modification factors. Moreover, using dissipation systems reduced the material quantity by about 15%.
- The collaborating experimental test was performed at the structural laboratory of the Lyles College of Engineering on a uniaxial shake table. The experimental tests were performed on one full-scale one-story steel moment-resisting frame with a traditional single-leg brace and yielding restrained brace. The frame was subjected to seventeen real ground motions and artificial loading including sinusoidal, sweep, and step function. The response of the frame was measured by three accelerometers, the results showed a significant reduction in roof acceleration of the SMRF with YRB in comparison to SMRF with OSLB, the reduction in accelerations was verified against similar results performed by Sarjou and Shabakty in 2017.
- The SMRF with OSLB and YRB was simulated using ETABS, OpenSees software, and their Acceleration, damping ratios, drift, and displacement were compared against one another. The moment resisting frame was equipped with a double channel (C6×10.5) and compared with YRB. The ordinary single-leg brace had an average acceleration of 1.65g, the average value from the software was 1.64g. The average acceleration was reduced to 1.28g and 1.31g in experimental and analytical simulation when the frame was equipped with YRB. The results showed the effectiveness of YRB which resulted in the reduction of

acceleration by about 25%-27%. A comparison of damping properties between SLBF and YRB of both experimental and analytical showed the YRB enhanced the damping of the system by about 7% more than the conventional frame.

6.2 Conclusions

The following conclusions are drawn based on the analytical and experimental results.

6.2.1 Conclusions based on the analytical results

The following conclusions are made based on the results of seismic performance of different concrete moment resisting frames:

- Structural performance based on hazard level obtained from the inelastic static analysis showed the SLE and DLE remained in the elastic zone, whereas due to second-order analysis the structure entered in the inelastic zone. The calculation of nonlinear hinges based on ATC 72 and FEMA 356 showed the same results, the FEMA 356 is based on the skeleton curve, whereas ATC 72 is based on the monotonic backbone curve.
- The higher mode effects can be neglected for buildings with a fundamental period of less than 0.8 seconds due to the condition of load pattern, however, for tall buildings, a dynamic procedure is required.

The seismic safety of a 14-story building with ductile, moderately ductile, and elastic concrete moment resisting frames (CMRFs) with and without inline friction dampers was evaluated with the following conclusions:

- The ductile frame with inline friction dampers had a reduction of about 75% in moment and shears compared to the bare frame.
- The moderately ductile frame with dampers experienced a reduction of about 69% in moment and shears compared with the frame without dampers.
- The elastic frame with inline friction dampers deducted the moment and shear by an average of 56% compared with the elastic frame without dampers, which was less than the moderately ductile and ductile frame.

- The cost analysis of the six different frames showed an average saving of 11.5% due to the integration of friction dampers. Therefore, the dampers can reduce the cost while improving the performance of the buildings.

The following are the results from a comparison between conventional equivalent lateral force procedures (ASCE 7 and NBCC 2015), new methods based on equivalent lateral force procedures (ELF), and response spectrum procedures (RSP) for buildings with damping devices:

- The response spectra for both design and maximum credible earthquake were developed in order to calculate the base shear based on ELF and RS procedures. The different types of the structural system define a reduction factor to reduce the base shear of conventional design, whereas the ELF and RS procedures are based on the yield base shear.
- The seismic response coefficient is not defined directly in the NBCC 2015, therefore the seismic coefficient, C_N , was defined and calculated for the Canadian code and compared with the seismic response coefficient, C_S , in the ASCE 7. The calculated base shear value with the NBCC 2015 was about 5% higher than the base shear value calculated with the ASCE 7. Since the NBCC 2015 does not recommend any integration of determining the damping properties, it is recommended to use the higher base shear value of the NBCC and ASCE 7 and establish calculating the damping properties of the system by either ELF or RS procedure.
- The seismic base shear for ELF and RS procedures should not be less than 75%V and the base shear is divided by the combination of inherent and supplemental damping. In the conventional design procedure, the base shear is related to the seismic response coefficient factor by considering the period of the system, design and maximum spectral response, response modification factor, and importance factor.
- Apart from general specifications of conventional design, the ELF and RS procedures need to be controlled based on the limitation defined in the acceptance criteria including roof displacement, story drift, and story velocity for the design and maximum considered earthquake.

- The maximum design and earthquake drift of ELF and RS procedures are dependent on damping systems. These values were similar for both procedures with a maximum average drift of 367mm for the design earthquake and 553mm for the maximum considered earthquake. The maximum velocity had about a 2% difference between ELF and RS procedures. The average maximum velocity for design and the maximum earthquake was 782 mm/s and 1165 mm/s for both procedures.
- The effective damping of ELF and RS procedures was determined based on the fundamental, residual, and higher modes. It was found RS procedure had effective damping of 54%, which is more conservative in comparison with the effective damping of 42% based on the ELF procedure.

The results of seismic performance and response modification factors of four-, eight-, and fourteen-story ductile concrete frames with inline seismic friction dampers are presented below:

- The recommended value for overstrength factor of an equivalent system is $R_0=1.2$ in the NBBC 2015 for buckling restrained braced frame. The calculated overstrength factors had a range from 1.41 to 3.06, which was higher than the prescribed value of 1.2 in the NBCC 2015. These values were found to be higher in the shorter span length and decreased with an increase in the height of the structure. The average value of overstrength factor was 2.06, the average minus standard deviation of overstrength factor was 1.50.
- The NBCC 2015 recommended the ductility factor of $R_d=4.0$ for an equivalent system (BRBF). The structures' ductility reduction factor was in the range of 2.55 to 4.43 compared to the ductility factor of 4.0 in the NBCC 2015. The average ductility factor was 3.34, and the average minus standard deviation was 1.94.
- The response modification factor decreased with the increase in the height and is greater in smaller span length. The response modification factor had a range of 5.53 to 8.01, with an average of 6.56 and an average minus standard deviation of 5.57, whereas the recommended value in the NBCC 2015 is 4.8 for BRBF. Therefore, it is recommended for

structures with a height of equal to or less than 50m to use the response modification factor of 5.5 which covers about 95% of the cases and is in the safe zone.

- The inline friction damper slip loads were determined based on the brace angle, shear deflection, lateral shear force, lateral stiffness of the bare frame, frame with dampers, and their combination. Hence, it can be recommended to model the system as a braced frame and consider the axial loads in the braces as equal or greater than the slip load of the inline friction dampers.
- The performance of the six models was verified subjected to twenty-five different ground motions. The results sum of standard deviation and mean values of inelastic response history analysis showed the reduction in the story drift of about 65% for three models equipped with inline friction dampers compare to the frames without dampers. The story drift demands concentrated in higher stories with an increase in the height.
- The base shear demand increased when the height increased and decreased with a smaller span length. The dissipated energy was higher in greater span length, inline friction dampers reduced the plastic hinges by an average of about 45%.

The results from a comparative investigation between design procedures of American and Canadian standard of a fourteen-story ductile concrete moment resisting frames as well as the effects of five different passive dissipation systems showed that:

- The material quantities based on the design procedure of ASCE 7 and ACE 318 were about 10% higher compared with the NBCC 2015 and CSA A23.3-19.
- The modal analysis of TCSB, FVD, and TMYD had an average value of 1.55 seconds, whereas the calculated value based on the empirical equation in the NBCC is 1.25 seconds and 1.37 seconds in the ASCE 7. The LRBI and TPI increased the period of the structure by about 60%.
- The values of the overstrength factors of CMRF, TCSB, FVD, TMYD were in the range of 1.44 to 1.97, the overstrength factors were reduced significantly in the structural system of LRBI and TPI.

- The lowest ductility value was for TMYD, which may result from its design and position, whereas CMRF had the highest value of ductility.
- The response modification factors had the highest value for CMRF and the lowest value for TMYD. The proposed value for CMRF by the ASCE 7 is 8 and the NBCC 2015 recommended the value of 6.8. The response modification factors of TCSB, FVD, TMYD for an equivalent system are recommended 4.8 and 8 in the NBCC 2015 and ASCE 7, these systems had an average value of 6.2.
- The most regular hysteresis curve was for TCSB compared to the other dissipation systems. Base isolators, however, were the most effective systems for the reduction of base shear as well as roof displacement.
- The results of nonlinear response history analysis showed the performance of life safety for all the models. The maximum sum of standard deviation and mean values for CMRF, TCSB, FVD, TMYD were in the range of 0.41% to 0.53%, and LRBI and TPI had a maximum drift at the base.
- The system equipped with TMYD is not replaceable, because the energy dissipated through the yielding of the plats and acts as a fuse in the structural system. The experimental tests in chapter 5 also verified the Ten-Co seismic brake can be categorized as “damage-free”, which dissipates energy through the slipping phase and can be replaced after a strong shock, this allows the primary member of the structure to remain in the elastic zone.

6.2.2 Conclusions based on the simulated of the experimental model

The following items were highlighted from the results of experimental and analytical works:

- The simulated response of the moment-resisting frame with an ordinary single-leg brace (2C6×10.5) was compared with the experimental test. The analytical acceleration results were in the range of 1.36g to 1.90g, and the experimental results were in the range of 1.38g to 1.95g. The average recorded acceleration value of south-west and north-east locations was 1.65g in the experimental work and 1.64g in the simulated work. The experimental

and analytical works had a mean value and standard deviation of 1.83g in both locations and 1.81g in the analytical work.

- The experimental recorded accelerations of the SMRF with yielding restrained brace were in the range of 1g to 1.63g, the analytical accelerations were 0.90g and 1.65g. The average values of acceleration were 1.28g in both locations and 1.31g for the analytical. The sum of standard deviation and mean value were 1.48g for both locations and 1.50g for analytical. The results indicated a significant reduction in the roof accelerations by about 25% to 27%.
- The damping percentage of SMRF with ordinary single-leg brace in the south-west and north-east locations were in the range of 13.67% to 26.09%, these values were limited to 16.2% and 22.6% in the analytical model. The experimental test had average damping of 20.59% and 18.31% in southwest and northeast locations, and the simulated model had an average of 19.12%. The southwest and northeast locations had a standard deviation plus a mean value of 25.86% and 21.86%, this value was 21.97% in the analytical model.
- The damping percentages of SMRF with yielding restrained brace were between 20.01% to 34.45% in the southwest and northeast locations, the analytical work had a maximum and minimum of 25.96% and 34.38%. The average damping percentages were in the range of 24.6% and 27.54% in the southwest and northeast locations and 30.20% from the analytical calculation. The combination of mean value and standard deviation showed the damping percentage of 27.46% and 35.54% in southwest and northeast locations, and 33.93% in the analytical frame. It was found the damping of the system was increased by about 7% in both analytical and experimental works compared with ordinary single-leg brace frame.
- The maximum displacements of SMRF with YRB were 0.47in and 0.42in for the experimental and analytical model and the average drift ratio was 0.33% for the experimental test and 0.30% for the simulated work. Both experimental tests and analytical

work showed the SMRF had a capacity to observe extra shock by dampers while remaining in the elastic zone.

- The data from yielding restrained braces through the experimental model can apply to verify the numerical models in the thesis.

6.3 Recommendations for Future Research

The analytical and experimental investigations explained in the thesis were limited to some criteria and parameters. Therefore, additional investigations in the evaluation of seismic dissipation systems are required in the following areas:

- Seismic characteristics assessment of concrete structures equipped with IFD considering various bracing configurations, different heights, and bracing angles.
- Sensitivity analysis and parametric study are required to validate the recommended value by the manufacturer of about 1/3rd of the story shear to the bare frame.
- Experimental tests on the effectiveness of different passive dissipation devices (i.e. TCSB, FVD, TMYD, LRBI, TPI) on the response of concrete structures. Moreover, additional research on CMRF with various types of dampers considering different heights and span lengths is necessary.
- Experimental tests on the large-scale multistory frame equipped with a conventional and yielding restrained brace, considering higher seismic weight and acceleration that produces higher slip distance and accounts for the higher mode effects.
- Further investigations on the generated heat in the yielding restrained brace to show the generated heat and friction have a direct effect on one another, for example, if the amount of generated heat does not correlate with the amount of observed energy by dampers, that means the deterioration in the damper is being occurred as the amount of heat is not increased.

References

- AASHTO (2002), American Association of State Highway and Transportation Officials.
- ACI 318-19. (2019). Building Code Requirements for Structural Concrete and Commentary, ACI Committee 318.
- Agrawal, A. K., and Yang, J. N. (2000). A semi-active electromagnetic friction damper for response control of structures, Structures Congress, 8-10, Philadelphia, PA. American Society of Civil Engineers, DOI: 10.1061/40492(2000)6.
- Aiken, L. D., and Kelly, J. M. (1990). Earthquake simulator testing and analytical studies of two energy-absorbing systems for multistory structures, UCB/EERC-90/03, Earthquake Engineering Research Center, Berkeley, CA.
- Aiken, L.D., Nims, D.K., and Kelly, J.M. (1992). Comparative study of four passive energy dissipation system, Bulletin of the New Zealand national society for earthquake engineering, Vol.25, No.3, PP.175-192.
- Akiyama, H. (2000). Evaluation of fractural mode of failure in steel structures following Kobe lessons, Journal of Constructional Research, No. 55, 211-227.
- Alam, M. S., Moni, M., and Tesfamariam, S. (2012). Seismic overstrength and ductility of concrete buildings reinforced with superelastic shape memory alloy rebar, Engineering Structures, 34, 8–20.
- ANSI/AISC 341-16. (2016). Seismic Provisions for Structural Steel Buildings, American Institute of Steel Construction, Chicago, Illinois 60601.
- ANSI/AISC 360-05. (2005). Specification for Structural Steel Buildings, American Institute of Steel Construction, Chicago, Illinois 60601.
- ASCE/SEI 41-17. (2017). Seismic evaluation and retrofit of existing buildings, American Society of Civil Engineers, Reston, Virginia.

- ASCE/SEI 7-05. (2005). Minimum Design Loads for Buildings and Other Structures, American Society of Civil Engineers.
- ASCE/SEI 7-10. (2010). Minimum Design Loads for Buildings and Other Structures, American Society of Civil Engineers.
- ASCE/SEI 7-16. (2016). Minimum design loads for buildings and other structures, Reston, VA: American Society of Civil Engineers.
- Asgarian, B., and Shokrgozar, H. R. (2009). BRBF response modification factor, *Journal of Constructional Steel Research*, 65(2), 290–298.
- ATC 3-06. (1978). Tentative provisions for the development of seismic regulations for buildings, ATC publication, V.Series, United States. National Bureau of Standards. Special publication, 510.
- ATC 58-1. (2003). Sponsored workshop on communicating earthquake risk, Applied Technology Council, www.ATCCouncil.org.
- ATC 72-1. (2019). Nonlinear modeling of tall buildings, Pacific Earthquake Engineering Research Center, <https://peer.berkeley.edu/peeratc-72-1-report-released-about-nonlinear-modeling-tall-buildings>.
- ATC. (1996). Seismic Evaluation and Retrofit of Concrete Buildings, Volume 1, ATC-40 Report, Applied Technology Council, Redwood City, California.
- ATC-19. (1995). Structural response modification factors, Applied Technology Council.
- ATC-34. (1995). A critical review of current approaches to earthquake-resistant design, Applied Technology Council, NCEER Project No. 92-4601.
- Atkinson, G.M., Adams J. (2013). Ground motion prediction equations for application to the 2015 Canadian national seismic hazard maps, *Can. J. Civ. Eng.*, 40, 988- 998.
- Baber, T. T., and Noori, M. N. (1986). Modeling general hysteresis behaviour and random vibration applications, *Journal of Vibration, Acoustics, Stress, and Reliability in Design*, 108 (4) pp. 411–420.

- Baber, T. T., Noori, M. N. (1985). Random Vibration of Degrading, Pinching Systems, *Journal of Engineering Mechanics*, 111, 1010–1026, [https://doi.org/10.1061/\(ASCE\)0733-9399\(1985\)111:8\(1010\)](https://doi.org/10.1061/(ASCE)0733-9399(1985)111:8(1010)).
- Baker J.W. (2007). Correlation of ground motion intensity parameters used for predicting structural and geotechnical response, *Applications of Statistics and Probability in Civil Engineering*, Taylor & Francis Group, London, ISBN 978-0-415-45134-5.
- Baker, J.W. (2011). Conditional Mean Spectrum: Tool for Ground-Motion Selection, *J. Struct. Eng.*, 137, 322–331, [https://doi.org/10.1061/\(ASCE\)ST.1943-541X.0000215](https://doi.org/10.1061/(ASCE)ST.1943-541X.0000215).
- Calvi, G., Priestley, M. J. N., Kowalsky, M. J. (2013). Displacement-Based Seismic Design of Bridges. *Structural Engineering International*, 23, 112-121. doi: 10.2749/101686613X13439149157399.
- Chang, C., Pall, A., Jason, J. C., and Louie, S. E. (2006). The Use of friction dampers for seismic retrofit of the Monterey County Government Center, In Proc., 8th US National Conference on Earthquake Engineering, San Francisco, Paper 951.
- Chen, C., and Chen, G. (2001). A High Efficiency Control Logic for Semi-Active Friction Dampers, *Structures 2001*, American Society of Civil Engineers, Washington, D.C., United States, 1–11.
- Chen, M. C. (2018). Enhanced Seismic Resiliency for Buildings via Base Isolation, PhD Dissertation, San Diego, CA: University of California, San Diego. <https://escholarship.org/uc/item/94v8d49h>.
- Chopra, A.K. (2012). *Dynamics of structures: theory and applications to earthquake engineering*, 4th ed. Prentice Hall, Upper Saddle River, N.J.
- Ciampi, V., De Angelis, M., and Paolacci, F. (1995). Design of yielding or friction-based dissipative bracings for seismic protection of buildings, *Engineering Structures*, 17(5), 381-391.

- Colajanni, P., and Papia, M. (1997). Hysteretic behaviour characterization of friction-damped braced frames, *Journal of structural engineering*, 123(8), PP.1020-1028.
- Constantinou M.C., Kalpakidis I., Filiatrault A., Lay R.A.E. (2011). LRFD-Based Analysis and Design Procedures for Bridge Bearings and Seismic Isolators, MCEER-11-0004, Multidisciplinary Center for Earthquake Engineering Research, University at Buffalo: NY.
- Constantinou, M., Mokha, A., Reinhorn, A. (1990). Teflon Bearings in Base Isolation II: Modeling, *Journal of Structural Engineering*, 116, 455–474, [https://doi.org/10.1061/\(ASCE\)0733-9445\(1990\)116:2\(455\)](https://doi.org/10.1061/(ASCE)0733-9445(1990)116:2(455)).
- Constantinou, M., Soong, T., Dargush, G. (1998). Passive Energy Dissipation Systems for Structural Design and Retrofit, MCEER Monograph No. 1, University at Buffalo, ISBN 0-9656682-1-5.
- Cordova, P. P., Deierlein, G. G., Mehanny, S. S. F., and Cornell, C. A. (2000). Development of a two-parameter seismic intensity measure and probabilistic assessment procedure, 2nd U.S.-Japan Workshop on Performance-based Earthquake Engineering Methodology for Reinforced Concrete Building Structures, Sapporo, Hokkaido, Japan, 187–206.
- CSA (2019). Design of concrete structures, CSA A23.3-19, Canadian Standards Association, Rexdale, Ontario.
- CSI, C. (2015). SAP2000 (version 20) Integrated Solution for Structural Analysis and Design – CSI Analysis Reference Manual, Computers and Structures, California, USA.
- CSI. (2016). Integrated Building Design Software, ETABS, CSI Analysis Reference Manual, Computers and Structures, Inc., California, USA, Retrieved from <https://www.csiamerica.com/products/etabs>.
- Davalos, J. F., Chen, A., Ray, I., and Levan, J. R. (2012). Comprehensive study on using externally bonded FRP composites for the rehabilitation of reinforced concrete t-beam bridges, *Journal of Infrastructure Systems (ASCE)*, Vol. 18, No. 2, pp. 89–102.

Deierlein, G.G., Reinhorn, A.M., Willford, M.R. (2010). Nonlinear structural analysis for seismic design, NEHRP seismic design technical brief, 4, 1–36.

Deierlein, G.G., Reinhorn, A.M., Willford, M.R. (2010). Nonlinear structural analysis for seismic design. NEHRP seismic design technical brief 4, 1–36.

Earthquake Engineering Research institute (EERI, 2020), www.eeri.org.

Elwood K.J., Eberhard M.O. (2006). Effective Stiffness of Reinforced Concrete Columns, Pacific Earthquake Engineering Research Center (PEER), Research Digest No.2006-1.

Elwood, K.J., Matamoros, A.B., Wallace, J.W., Lehman, D.E., Heintz, J.A., Mitchell, A.D., Moore, M.A., Valley, M.T., Lowes, L.N., Comartin, C.D., Moehle, J.P. (2007). Update to ASCE/SEI 41 Concrete Provisions, *Earthquake Spectra*, 23, 493–523.

FEMA 273. (1997). NEHRP Guidelines for the Seismic Rehabilitation of Buildings, Developed by the Building Seismic Safety Council for the Federal Emergency Management Agency (Report No. FEMA 273), Washington, D.C.

FEMA 302. (1997). NEHRP Recommended Provisions for Seismic Regulations for New Buildings and Other Structures, Building Seismic Safety Council, Washington.

FEMA 349. (2000). Action Plan for Performance Based Seismic Design, Earthquake engineering research institute.

FEMA 356. (2000). Prestandard and Commentary for the Seismic Rehabilitation of Buildings, Federal Emergency Management Agency.

FEMA 420. (2009). Engineering Guideline for Incremental Seismic Rehabilitation, Risk Management Series.

FEMA 450. (2000). Recommended provisions for seismic regulations for new buildings and other structures, NEHRP Federal Emergency Management Agency, Part 1: Provisions.

FEMA 451. (2006). Design methods, NEHRP Federal Emergency Management Agency, Building Seismic Safety Council.

- FEMA P-1050-1. (2015). Recommended Seismic Provisions for New Buildings and Other Structures, Volume I: Part 1 Provisions.
- FEMA P-2082. (2020). Recommended Seismic Provisions for New Buildings and Other Structures, Volume I: Part 1 Provisions.
- FEMA P58-1. (2012). Seismic performance assessment of buildings, Volume 1 - Methodology, Prepared by Applied Technology Council (ATC), Redwood City, USA.
- FEMA P695. (2009). Quantification of Building Seismic Performance Factors, Federal Emergency Management Agency, Washington, District of Columbia, USA.
- FEMA-440. (2005). Improvement of nonlinear static seismic analysis procedures, Federal Emergency Management Agency.
- FEMA-461. (2007). Interim Testing Protocols for Determining the Seismic Performance Characteristics of Structural and Non-structural Components, Federal Emergency Management Agency.
- Feng, M. Q., Shinozuka, M., Fujii, S. (1993). Friction controllable sliding isolation system, *J. Eng. Mechanics*. 9, 1845–1864.
- Fisco, N.R., and Adeli, H. (2011). Smart Structures: Part I-Active and Semi-Active Control, *Scientia Iranica* 18 (3): 275–284. doi:10.1016/j.scient.2011.05.034.
- Foliente, G. (1993). Stochastic dynamic response of wood structural systems, Ph.D. Thesis, Virginia Polytechnic Institute, Blacksburg, Virginia.
- Galindo, O., Frazao, R., Pastor, C., Coronado, G., and Gonzales, D. (2019a). Supplemental Damping for the seismic retrofit of 8-storey RC Hotel building in the Mexican Pacific using Yielding Restrained Braces – part A, Comparison of alternatives, 12th Canadian conference on earthquake engineering, 8.
- Galindo, O., Frazao, R., Pastor, C., Coronado, G., and Gonzales, D. (2019b). Supplemental Damping for the seismic retrofit of 8-storey RC Hotel building in the Mexican Pacific using

- Yielding Restrained Braces – part B, Methodology, 12th Canadian conference on earthquake engineering, 8.
- Gavin, H.P., Dickinson, B.W. (2011). Generation of Uniform-Hazard Earthquake Ground Motions, *J. Struct. Eng.*, 137, 423–432.
- Gordaninejad, F., Ray, A. D., Wang, H. (1994). Use of hybrid dampers for vibration control of structures, *Proceedings of the third US-Japan Workshop on Earthquake Protective Systems for Bridges*, 3-15, 3-29.
- Gupta, A.K. (1990). *Response spectrum method in seismic analysis and design of structures, New directions in civil engineering*, Blackwell Scientific Publications, Boston.
- Haider, J.R., & Kim, U. (2012). A parametric approach for the optimization of passive friction dampers, *Structure Congress*, ASCE, 1673-1684.
- Hamburger, R.O., and Holmes, W.T. (1998). *Vision Statement: EERI/FEMA Performance-based Seismic Engineering Project, Background Document for the EERI/FEMA Action Plan*, Earthquake Engineering Research Institute, Oakland, CA.
- Hamed, E., Chang, Z.T., Rabinovitch, O. (2014). Strengthening of Reinforced Concrete Arches with Externally Bonded Composite Materials: Testing and Analysis, *Journal of Composites for Construction*, ASCE, ISSN 1090-0268/04014031(15).
- Haselton, C.B., Liel, A.B., Lange, S.T., Deierlein, G.G. (2007). *Beam-Column Element Model Calibrated for Predicting Flexural Response Leading to Global Collapse of RC Frame Buildings*, PEER Report No. 2007, Pacific Earthquake Engineering Research Center College of Engineering, University of California, Berkeley.
- https://opensees.berkeley.edu/wiki/index.php/OpenSees_User
- Humar, J. (2015). Background to some of the seismic design provisions of the 2015 National Building Code of Canada, *Journal of civil engineering*, Vol.42, pp.940–952.
- Humar, J., and Mahgoub, M.A. (2003). Determination of seismic design forces by equivalent static load method, *Canadian Journal of Civil Engineering*, 30: 287–307.

- Ikhouane, F., Mañosa, V., Rodellar, J. (2007). Dynamic properties of the hysteretic Bouc-Wen model, *Systems & Control Letters*, 56, 197–205.
- ISIS Canada Educational Module. (2004), www.isiscanada.com.
- Kasai, K. (2013). Seismic Performance of Building Protective Systems: Evaluations from Full-Scale Lab Tests and Actual Earthquake Observations, Structural Engineering Research Center, Tokyo Institute of Technology, JAPAN.
- Kasai, K., Ooki, Y., Motoyui, S., Takeuchi, T., and Sato, E. (2007). E-Defense Tests on Full-Scale Steel Buildings: Part 1 – Experiments Using Dampers and Isolators, Research Frontiers at Structures Congress 2007 May 16-19, 2007, Long Beach, California: American Society of Civil Engineers.
- Kelly, J. M. (1999). The role of damping in seismic isolation, *Earthquake Engineering Structural Dynamic*, 28, 3-20.
- Kelly, J. M., Skinner, R. I., Heine, A. J., (1972). Mechanisms of energy absorption in special devices for use in earthquake resistant structures, *Bulletin of N.Z. Society for Earthquake Engineering*, Vol. 5 No. 3.
- Kiran, A. R., Agrawal, M. K., and Reddy, G. R. (2016). Seismic retrofitting of a process column using friction dampers, *Procedia Eng.*, 144, 1356-1363.
- Ko, E., and Field, C. (1988), *The Unbonded Brace™: From Research to Californian Practice, Technology*.
- Kobori, T., Takahashi, M., Nasu, T., Niwa, N., Ogasawara, K. (1993). Seismic response-controlled structure with active variable stiffness system, *Earthquake Engineering and Structural Dynamics*, 22, 925–941.
- Krawinkler, H. (1997). A framework for performance-based earthquake resistive design, EERC CUREe Symposium in Honor of Vitelmo V. Bertero, Berkeley, California.
- Krawinkler, H., and Seneviratna, G. D. P. K. (1998). Pros and cons of a pushover analysis of seismic performance evaluation, *Engineering Structures*, 20(4–6), 452–464.

- Krawinkler, H., Nassar, A. A. (1992). *Nonlinear Seismic Analysis and Design of Reinforced Concrete Buildings*, CRC Press, ISBN9780429176753.
- Law, S.S., Wu, Z.M., Chan, S.L. (2006). Analytical model of a slotted bolted connection element and its behaviour under dynamic load. *Journal of Sound and Vibration*, 292, 777–787, <https://doi.org/10.1016/j.jsv.2005.09.028>.
- Lawson, R. S., Vance, V. and Krawinkler, H. (1994). Nonlinear static pushover analysis - why, when and how? *Proc. 5th US Conf. Earthquake Engineering*, Vol. 1, Chicago, IL, 283-292.
- Lawsson, R. S., Vance, V., and Krawinkler, H. (1994). Nonlinear static pushover analysis- Why, When, and How, *Earthquake Engineering*, Chicago, 1, 283–292.
- Lignos, D. G., Krawinkler, H., and Whittaker, A. S. (2011). “Prediction and validation of sideway collapse of two scale models of a 4-storey steel moment frame.” *Earthquake Engineering and Structural Dynamics (EESD)*, 40(7), 807–825.
- Logan Anthony Couch. (2020). Resilience and response of the dual system moment frame and braced frame with friction damper, Master of Science in Civil Engineering in the Lyles College of Engineering California State University, Fresno.
- López-Almansa, F., Castro-Medina, J.C., Oller, S. (2012). A numerical model of the structural behaviour of buckling-restrained braces, *Engineering Structures* 41, 108–117, <https://doi.org/10.1016/j.engstruct.2012.03.045>.
- Lou, J. Y. K., Lutes, L. D., and Li, J. J. (1994). Active tuned liquid damper for structural control, *Proc. of the 1st World Conference on Structural Control*, Los Angeles, CA, TP1: 70-9.
- Lukkunaprasit, P., Wanitkorkul, A., and Filiatrault, A. (2004). Performance deterioration of slotted-bolted connection due to bolt impact and remedy by restrainers, *Thirteenth World Conference on Earthquake Engineering*, Vancouver, B.C., Canada.
- Makkar, C., Dixon, W.E., Sawyer, W.G., Hu, G. (2005). A new continuously differentiable friction model for control systems design, Presented at the 2005 IEEE/ASME International

- Conference on Advanced Intelligent Mechatronics, IEEE, Monterey, CA, pp. 600–605.
<https://doi.org/10.1109/AIM.2005.1511048>.
- Mazzoni, S., McKenna, F., Scott, M. H., Fenves, G. L. (2006). OpenSees command language manual, Pacific Earthquake Engineering Research (PEER) Center.
- McKenna, F. (1997). Object-oriented finite element programming: frameworks for analysis, algorithms and parallel computing, PhD thesis, Civil Engineering, University of California, Berkeley, Ca.
- McKenna, F., Fenves, G., Scott, M. (2013). Computer Program OpenSees: Open system for earthquake engineering simulation, Pacific Earthquake Engineering Center, University of California, Berkeley, CA.
- McMahon, S., and Makris, N. (1997). Large-scale ER-damper for seismic protection of bridges, Proc. Structures Congress, 1451–1455.
- Miranda, E. (1991). Evaluation of seismic performance of a ten story RC building during the whittier narrows earthquake, Ph.D. dissertation, Department of Civil Engineering, University of California, Berkeley, CA.
- Miranda, E., and Bertero, V. V. (1994). Evaluation of Strength Reduction Factors for Earthquake-Resistant Design, *Earthquake Spectra*, 10(2), 357–379.
- Moni, M., Moradi, S., and Alam, M. S. (2016). Response modification factors for steel buckling restrained braced frames designed as per the 2010 National Building Code of Canada, *Canadian Journal of Civil Engineering*, 43(8), 702–715.
- Morgan, T., A. (2007). “The use of innovative base isolation systems to achieve complex seismic performance objectives.” Ph.D. thesis, University of California, Berkeley.
- Mousavi Azad Kasmaei, S. (2011). Seismic performance evaluation of reinforced concrete shear wall seismic force resisting systems, Library and Archives Canada, Bibliothèque et Archives Canada, Ottawa.

- Mualla, I.H., Belev, B. (2002). Performance of steel frames with a new friction damper device under earthquake excitation, *Engineering Structures*, 24, 365–371, [https://doi.org/10.1016/S0141-0296\(01\)00102-X](https://doi.org/10.1016/S0141-0296(01)00102-X).
- Naghshineh, A., Kassem, A., Pilorge, A. G., Galindo, O. R., and Bagchi, A. (2018). Seismic Performance of Reinforced Concrete Frame Buildings Equipped with Friction Dampers, *Structures Congress 2018*, American Society of Civil Engineers, Fort Worth, Texas, 94–101.
- NBCC. (2015). National Research Council of Canada. National Building Code of Canada, Ottawa, ON.
- NBC. (2017). National Research Council of Canada, Structural Commentaries User’s Guide, Part 4 of Division B, Ottawa, ON.
- Newmark, N.M. and Hall, W.J. (1978). Development of criteria for earthquake resistant design, Report NUREGICR-0098, Nuclear Regulatory Commission, Washington, D.C., 49 pp.
- Newmark, N.M. and Hall, W.J. (1982). Earthquake Spectra and Design, EERI Monograph, Earthquake Engineering Research Institute, Berkeley, California.
- Newmark, N.M. and Hall, W.J. (1982). Earthquake Spectra and Design, EERI Monograph, Earthquake Engineering Research Institute, Berkeley, California, 103 pp.
- Newmark, N.M. and Rosenblueth, E. (1971). Fundamentals of Earthquake Engineering, Prentice Hall, Englewood Cliffs, New Jersey, 640 pp.
- Nikoukalam, M.T., Mirghaderi, S.R., Dolatshahi, K.M. (2017). Shear slotted bolted connection. *The Structural Design of Tall and Special Buildings*, 26, e1313, <https://doi.org/10.1002/tal.1313>.
- Nims, D. K., Richter, P.J., Bachman, R.E. (1993). Use of the energy dissipating restraint for seismic hazard mitigation, *Earthquake spectra*, Vol.9. No.3, 476-489.
- OSHPD and SEAOC (2020). Seismic design maps. Structural Engineers Association of California’s (SEAOC). <https://seismicmaps.org>.

- Pall, A. (1979). Limited slip bolted joints a device to control the seismic response of large panel structures, Ph.D. thesis, Concordia university, Montreal, Canada.
- Pall, A. S., and Pall, R. (1996). Friction dampers for seismic control of buildings a Canadian experience, 11WCEE, 497.
- Pall, S., & Marsh, C., (1982). Response of friction damped braced frames, Journal of structural engineering, ASCE, 108, ST6.
- Patil, C.S., Patil, V. B., Kharmale, S. B. (2015). Performance-based plastic design of a high-rise moment resisting frame with friction dampers, Earthquake Resistant Engineering Structures, 152, 73-82.
- Paulay T., and Priestley M. J. N. (1992). Seismic Design of Reinforced Concrete and Masonry Buildings, John Wiley and Sons, Inc.
- Paulay, T. (1988). Seismic Design in Reinforced Concrete- the State of the Art in New Zealand, Bulletin of the New Zealand National Society for Earthquake Engineering, 21(3), 208-232.
- PEER Ground Motion Database, PEER Center, <https://ngawest2.berkeley.edu>.
- Popov, E.P., Grigorian, C.E., Yang, T. S., (1995). Developments in seismic structural analysis and design. Engineering Structures, 17, 187–197. [https://doi.org/10.1016/0141-0296\(94\)00006-F](https://doi.org/10.1016/0141-0296(94)00006-F).
- Quaketek Inc. (2016). Seismic design, Available: <https://www.quaketek.com>.
- Risk and Resilience Measurement Committee (2019). Resilience-Based Performance: Next Generation Guidelines for Buildings and Lifeline Standards, American Society of Civil Engineers, Reston, VA. <https://doi.org/10.1061/9780784415276>.
- Roberts, J., and Spanos, P. (1990). Random vibration and statistical linearization, John Wiley & Sons Ltd.
- Roik, K., Dorka, U., Dechent, P. (1988). Vibration control of structures under earthquake loading by three-stage friction-grip elements, Earthquake Engng. Struct. Dyn., 16, 501–521, <https://doi.org/10.1002/eqe.4290160404>.

- Saatcioglu, M., Palermo, D., Ghobarah, A., Mitchell, D., Simpson, R., Adebar, P., Tremblay, R., Ventura, C., and Hong, H. (2013). Performance of reinforced concrete buildings during the 27 February 2010 Maule (Chile) earthquake, *Journal of civil Engineering, NRC*, 40: PP.693–710.
- Samani, H. R., Mirtaheri, M., and Zandi, A. P. (2015). Experimental and Numerical Study of a New Adjustable Frictional Damper, *Journal of Constructional Steel Research*, 112: 354–362. doi:10.1016/j.jcsr.2015.05.019.
- Santayana, G. (1917). *Those who cannot remember the past are condemned to repeat it, The Life of Reason or Phases of Human Progress*, New York.
- Sarjou, P.H., Shabakhty, N. (2017). Effect of the Improved Pall Friction Damper on the Seismic Response of Steel Frames, 7, 5.
- SEAOC. (1995). *Vision 2000, A framework for performance-based engineering*, Sacramento, CA, Structural Engineers Association of California.
- SeismoSoft. (2014). *SeismoStruct-User Manual For version 7.0*, www.seismosoft.com, Pavia, Italy.
- SENSRA (2021), Structural monitoring solutions, <https://sensr.com>.
- Sextro, W. (2007). *Dynamical contact problems with friction: models, methods, experiments and applications*, 2nd ed., Springer, Berlin, New York.
- Skinner, R. I., Kelly, J. M., Heine, A. J. (1975). Hysteretic dampers for earthquake-resistant structures. *Earthquake Engineering & Structural Dynamics*, 3, 287–296, <https://doi.org/10.1002/eqe.4290030307>.
- Soli, B., Baerwald, D., Krebs, P., and Pall, R. (2004). Friction dampers for seismic control of ambulatory care center, sharp memorial hospital, San Diego, CA, 13th World Conference on Earthquake Engineering, Vancouver, B.C., Canada, No. 1953.
- Soong, T. T., and Dargush, G. F. (1999). *Passive Energy Dissipation and Active Control*, Boca Raton: Structural Engineering Handbook, CRC Press LLC, 1–28.

- Soong, T. T., and G. F. Dargush. (1998). Passive energy dissipation systems for structural design and retrofit, Multidisciplinary Center for Earthquake Engineering Research (MCEER). <http://mceer.eng.buffalo.edu>.
- Soong, T. T., and Spencer, B. F. (2002). Supplemental Energy Dissipation: State-of-the-Art and State-of-the-Practice, *Engineering Structures* 24 (3): 243–259. doi:10.1016/S0141-0296(01)00092-X.
- Su, L., Ahmadi, G., Tadjbakhsh, I. G. (1989). Comparative Study of Base Isolation Systems, *Journal of Engineering Mechanics* 115, 1976–1992. [https://doi.org/10.1061/\(ASCE\)0733-9399\(1989\)115:9\(1976\)](https://doi.org/10.1061/(ASCE)0733-9399(1989)115:9(1976)).
- Sullivan, T., J. Calvi, G., M. (2013). Developments in the field of displacement-based seismic assessment, IUSS Press: Pavia, Italy, 2013.
- Sultana, P., and Youssef, M. A. (2016). Seismic performance of steel moment resisting frames utilizing superelastic shape memory alloys, *Journal of Constructional Steel Research*, 125, 239–251.
- Symans, M. D., and Constantinou, M. C. (1997). Semi-active control systems for seismic protection of structures: a state-of-the-art review, *Eng. Struct.* 21, 469-487.
- Taylor devices inc. (2020). *Damper-Design-Manual-ThirdEdition.pdf*.
- Tehrani, F. M. (1990). “Review of Manjil 1990 Earthquake damages of Buildings in Gilan and Zanjan.” [in Persian]. *Omran, Magazine of Civil Engineering Students of the Sharif University of Technology*. 2, 5-7.
- Tehrani, F.M., Nazari, M., Naghshineh, A., (2020). Role of Seismic Isolation and Protection Devices in Enhancing Structural Resilience, *EMI ORC MOP Part III Chapter 21*.
- Tena-Colunga, A. (1997). Mathematical modelling of the ADAS energy dissipation device, *Engineering Structures*, 19, 811–821. [https://doi.org/10.1016/S0141-0296\(97\)00165-X](https://doi.org/10.1016/S0141-0296(97)00165-X).
- Tirca, L. (2009). A simple approach for the seismic retrofit of buildings with staggered friction dampers, *Protection of Historical Buildings: Proceedings of the International Conference on*

- Protection of Historical Buildings, PROHITECH 09, Rome, Italy, 21-24 June 2009: PROHITECH 09, Vol. 1, 2009, ISBN 978-0-415-55804-4, p. 761-767, 761–767.
- Tirca, L., Serban, O., Tremblay, R., Jiang, Y., and Chen, L. (2018). Seismic Design, Analysis and Testing of a Friction Steel Braced Frame System for Multi-Storey Buildings in Vancouver, *Key Engineering Materials*, 763, 1077–1086.
- Tsai, K. C., Chen, H. W., Hong, C. P., and Su, Y. E. (1993). Design of steel triangular plate energy absorbers for seismic-resistant construction, *Earthquake Spectra*, 9(3), 505-528.
- Turek, M., Ventura, C.E., Thibert, K. (2008). Dynamic Characteristics of Tall Buildings in Vancouver, Canada, Presented at the Structures Congress 2008, American Society of Civil Engineers, Vancouver, British Columbia, Canada, pp. 1–10, [https://doi.org/10.1061/41016\(314\)116](https://doi.org/10.1061/41016(314)116).
- Uang, C.M., and Bertero, V. V., (1988). Use of Energy as a Design Criterion in Earthquake-Resistant Design, Technical Report UCB/EERC-88/18, University of California, Berkeley, CA.
- Vail, C., Hubbell, J. (2003). Structural Upgrade of the Boeing Commercial Airplane Factory at Everett, Washington, Proceedings, Structures Congress & Exposition, Seattle, WA, Paper # 000529.
- Wen, Y.K. (1980). Equivalent Linearization for Hysteretic Systems Under Random Excitation, *J. Appl. Mech.*, 47, 150, <https://doi.org/10.1115/1.3153594>.
- Whittaker, A. S., Bertero, V. V., Thompson, C. L., and Alonso, L. J. (1991). Seismic testing of steel plate energy dissipation devices, *Earthquake spectra*, vol.7, No.4.
- Whittaker, A., Hart, G., Rojahn, C. (1999). Seismic Response Modification Factors. *Journal of Structural Engineering*, 125, 438–444, [https://doi.org/10.1061/\(ASCE\)0733-9445\(1999\)125:4\(438\)](https://doi.org/10.1061/(ASCE)0733-9445(1999)125:4(438)).
- Whittaker, A.S., Uang, C.M., and Bertero V.V. (1987). Earthquake simulation tests and associated studies of a 0.3-scale model of a six-story eccentrically braced steel structure, *Earthquake*

engineering research center, Report No. UCB/EERC-87/02, University of California, Berkeley, California.

Yamamoto, M., Sone, T. (2014). Behaviour of active mass damper (AMD) installed in high-rise building during 2011 earthquake off Pacific coast of Tohoku and verification of regenerating system of AMD based on monitoring, *Structural Control and Health Monitoring* 21, 634–647. <https://doi.org/10.1002/stc.1590>.

Yanik, A., and Aldemir, U. (2019). A Short Review on the Active Control Approaches in Earthquake Engineering at the Last 10 Years (2008-2018). *International Journal of Engineering and Technology*, Oregon State University, Corvallis, OR 97331, USA 111–118, DOI: 10.7763/IJET. 2019.V11.1132.

Yousuf, M., and Bagchi, A. (2009). Seismic design and performance evaluation of steel-frame buildings designed using the 2005 National building code of Canada, *Journal of civil Engineering*, NRC, 36: PP.280–294.

Appendix A3.1: Beam-column joint

In order to avoid column plastic hinges, all beam-to-column joints in structural frames must satisfy the weak beam strong column criteria to ensure that the joint of the concrete moment resisting frames have adequate shear strength due to the maximum expected force in adjoining brace(s) in beam-column joints. This design procedure includes determining the effective area of the joint, determining the panel zone design shear force, and controlling the panel zone shear stress. The free-body stress condition of a beam-column joint is demonstrated in Figure 1(ACI 318-19).

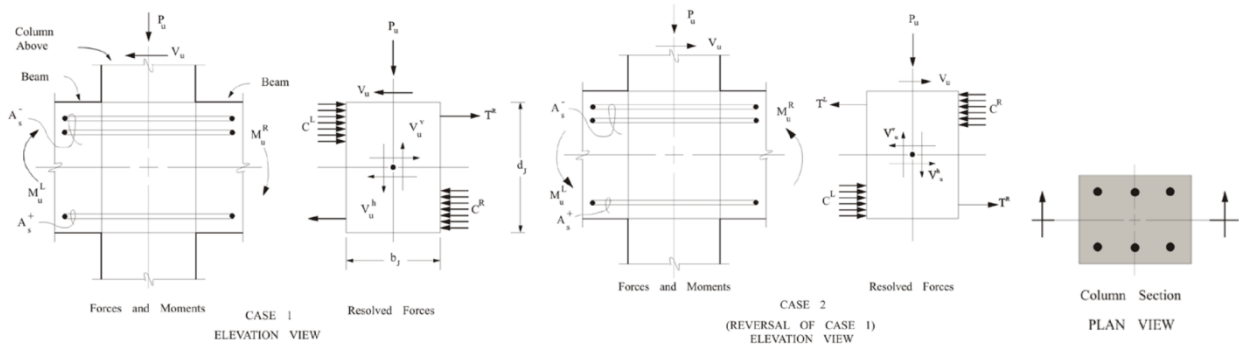


Figure 1. Beam-Column joint (ACI-318 & CSI, 2016)

Shear force, V_u , can be calculated from equation 1 from the moment capacities on the right and left sides of the panel zone considering the extra forces due to tension and compression of the bracing system as shown in Figure 2.

$$V_u = \frac{M_u^L + M_u^R}{H} \quad (1)$$

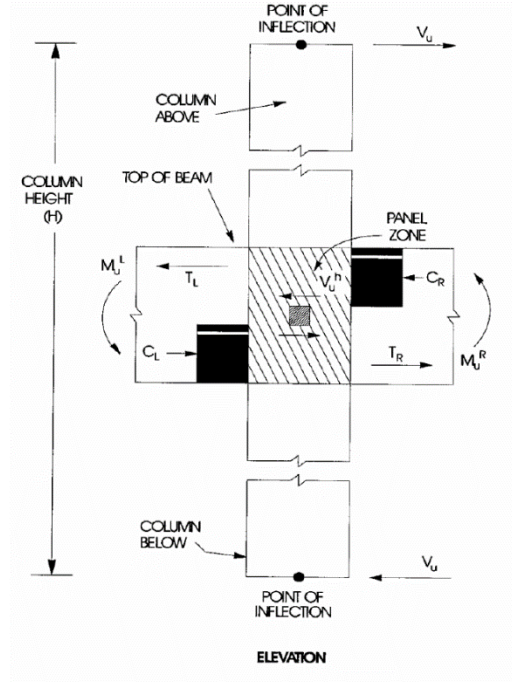


Figure 2. Column shear force (ACI 318 & CSI, 2016)

Sum of nominal flexural strengths of columns, M_{nc} , over the sum of nominal flexural strengths of beams, M_{nb} , framing into the joint shall be equal or greater than 1.2 from equation 2.

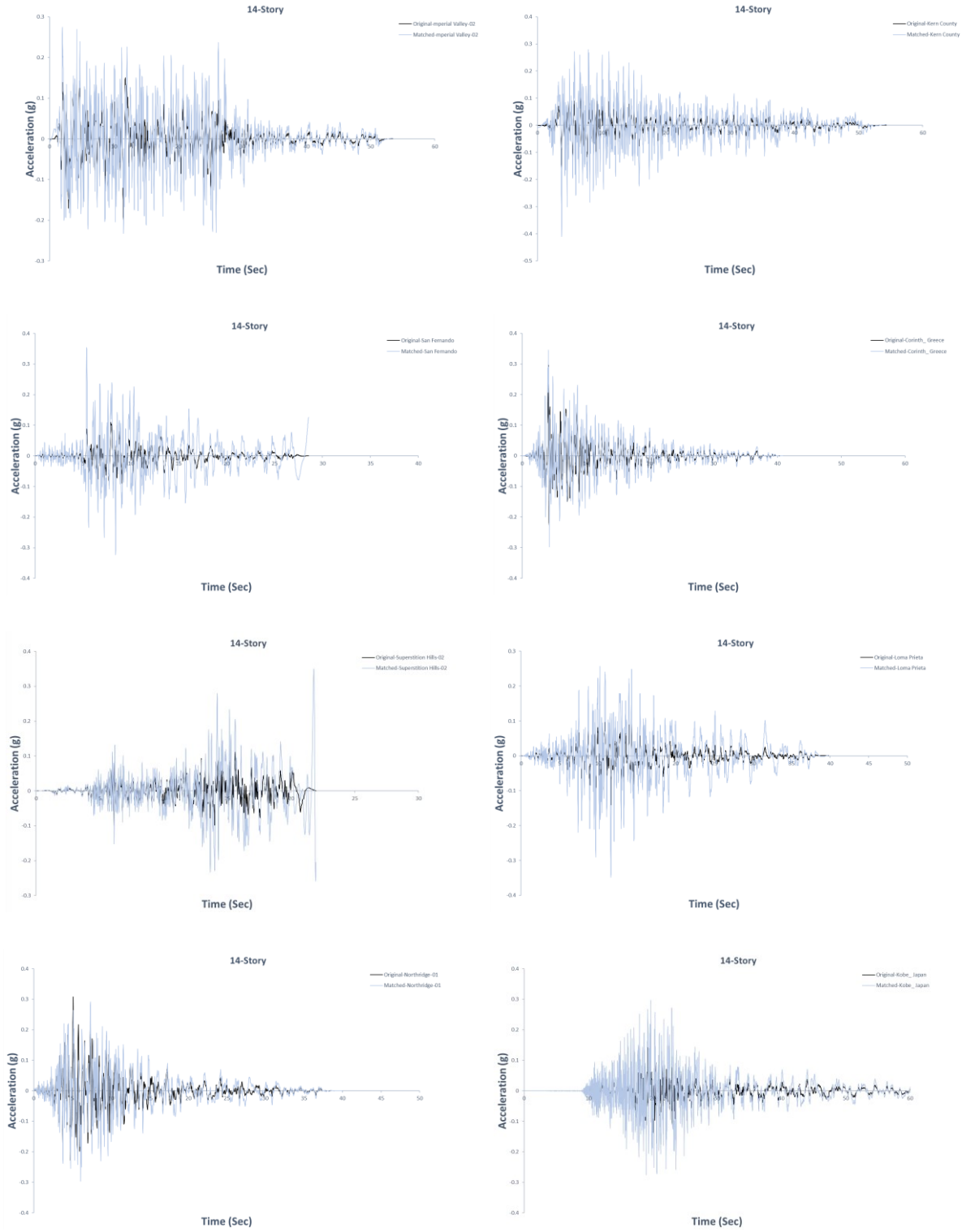
$$\frac{\sum M_{nc}}{\sum M_{nb}} \geq 1.2 \quad (2)$$

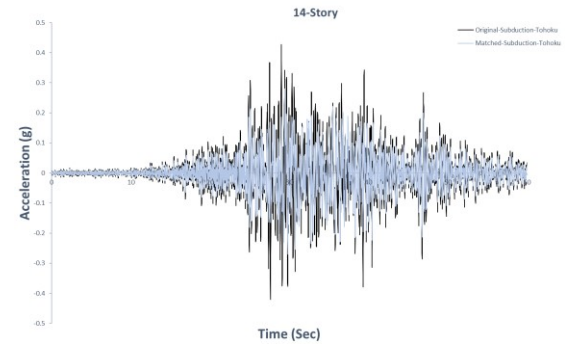
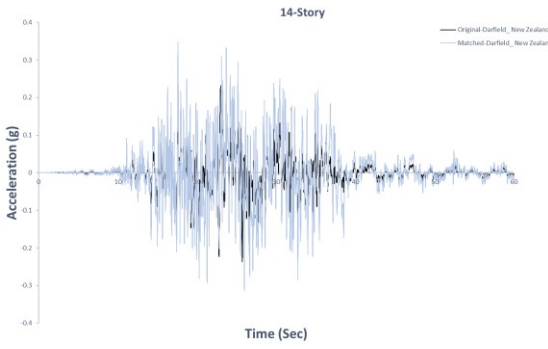
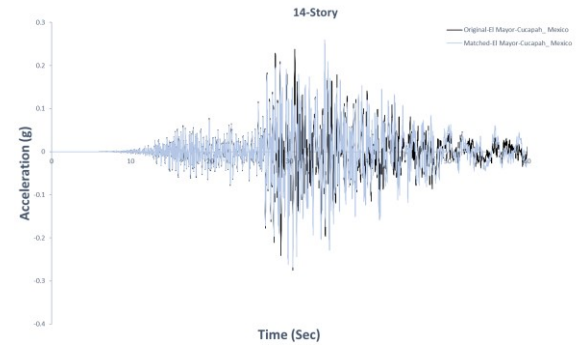
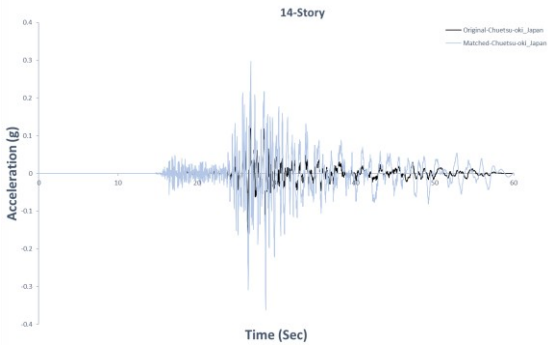
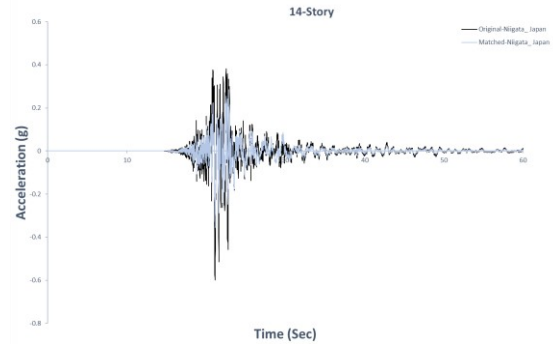
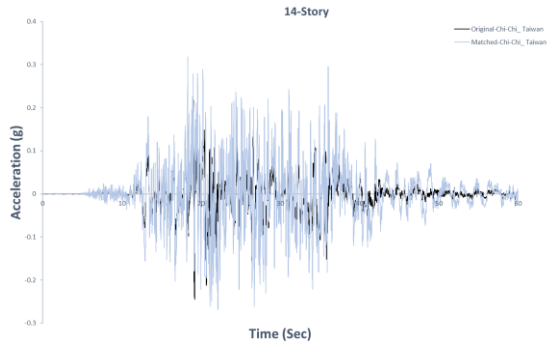
For calculating stiffness and strength of the structure when equation 34 is not satisfied, the lateral stiffness and strength of the column framing into the joint shall be ignored. Strengthening techniques of the panel zone are required for existing buildings to observe extra shock of the brace. Further details are provided in ACI 318-19.

Appendix A3.2 General important definitions based on ASCE 41-17

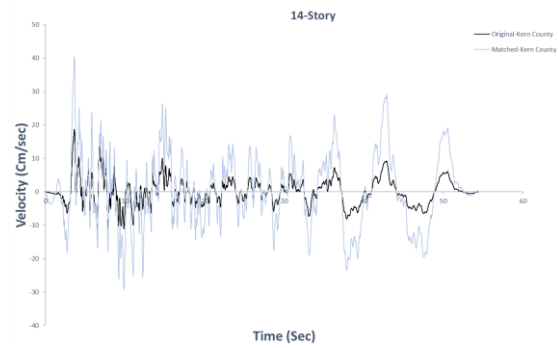
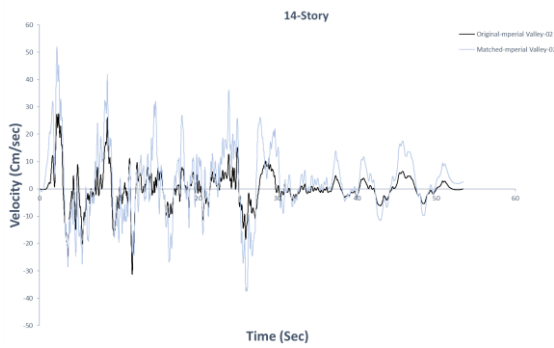
- BSE-1E: Basic Safety Earthquake-1 for basic performance objective for 20% in 50 years and not greater than BSE-1N at a site.
- BSE-1N: Basic Safety Earthquake-1 for basic performance objective equivalent to two-thirds of BSE-2N at a site.
- BSE-1X: Basic Safety Earthquake-1, either BSE-1E or BSE-1N
- BSE-2E: Basic Safety Earthquake-1 for basic performance objective for 5% in 50 years, and not greater than BSE-2N at a site.
- BSE-2N: Basic Safety Earthquake-1 for basic performance objective for ground shaking based on the Risk-Targeted Maximum Considered Earthquake (MCE_R) at a site.
- BSE-2X: Basic Safety Earthquake-2, either BSE-2E or BSE-2N
- Acceptance Criteria: Limiting values of properties, such as strength demand, drift, inelastic deformation.
- Action: An internal moment, shear, torque, axial force, deformation, displacement, or rotation corresponding to a displacement caused by a structural degree of freedom, each action shall be classified as deformation controlled (ductile) or force-controlled (nonductile).
- Component: A part of an architectural, mechanical, electrical, or structural system of a building, they are classified as primary and secondary.
- Primary Components: A structural component that is required to resist seismic forces for the desired performance level.
- Secondary Components: A structural component that is not required to resist seismic forces for the desired performance level (Non-structural component e.g. partitions or Structural component e.g. interior frames such as slab-column).

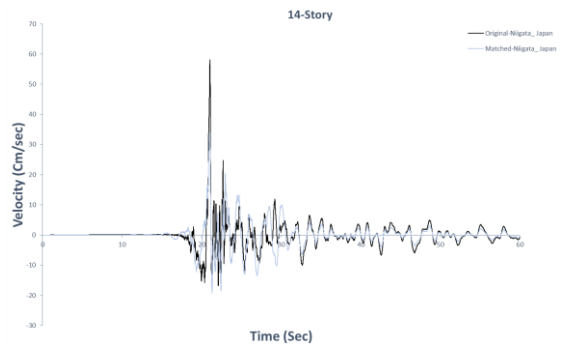
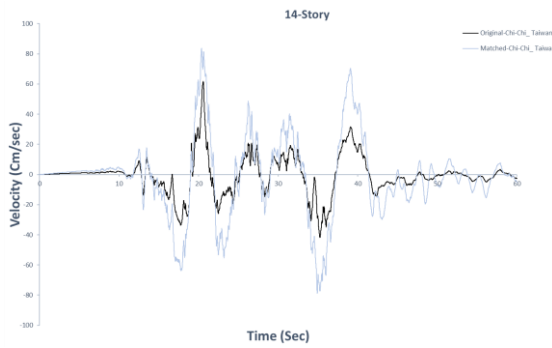
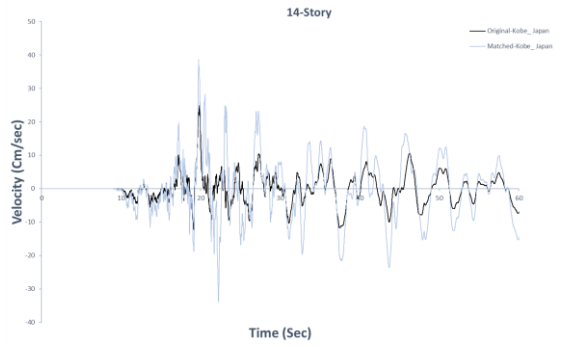
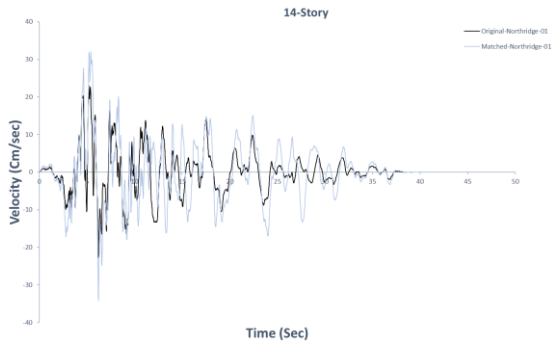
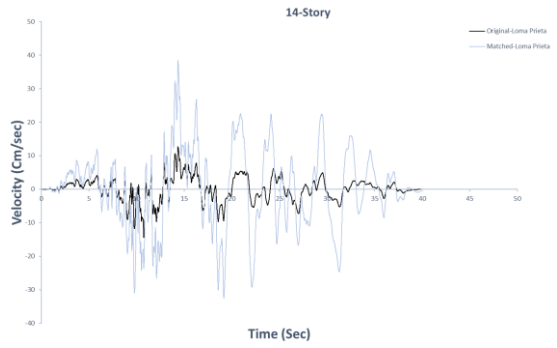
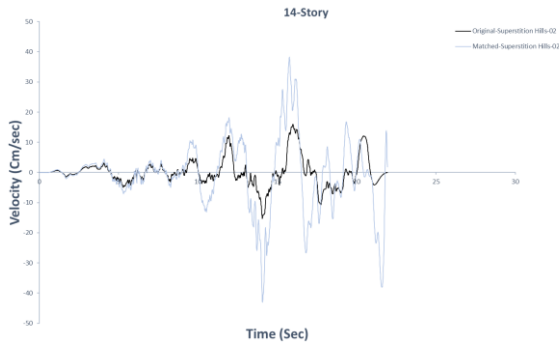
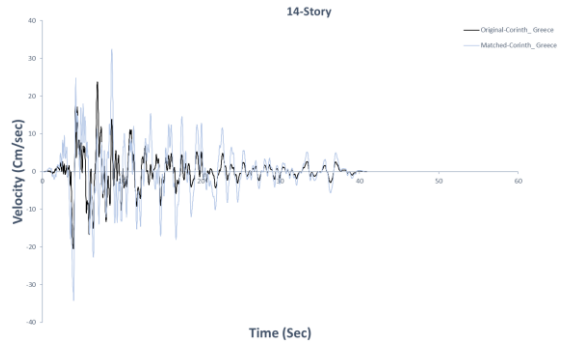
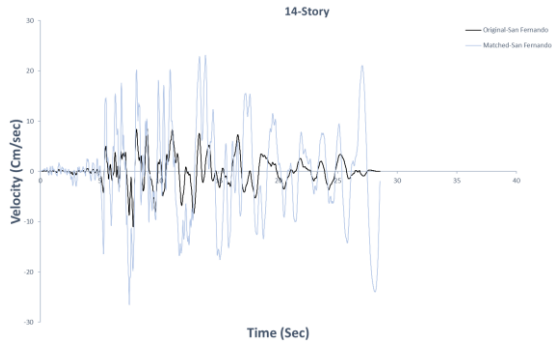
Appendix A4.1: Original and scaled Acceleration

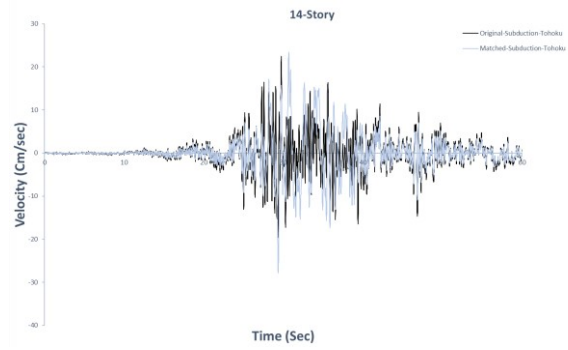
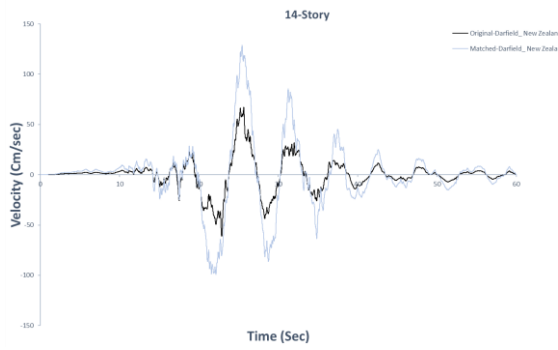
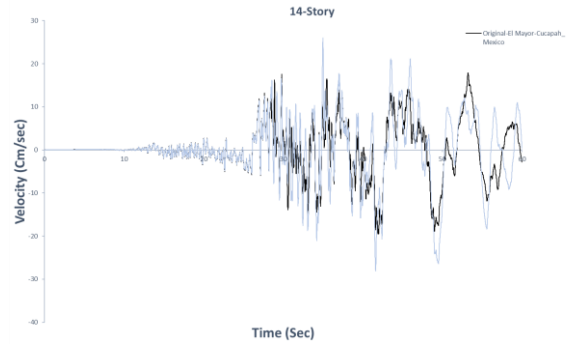
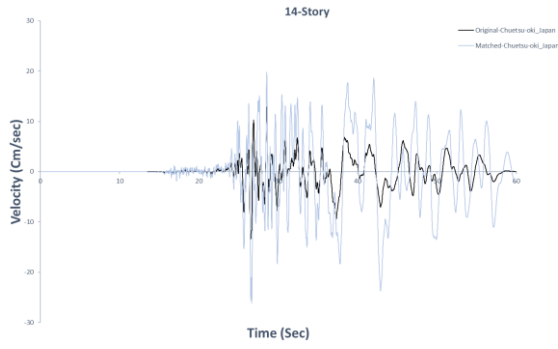




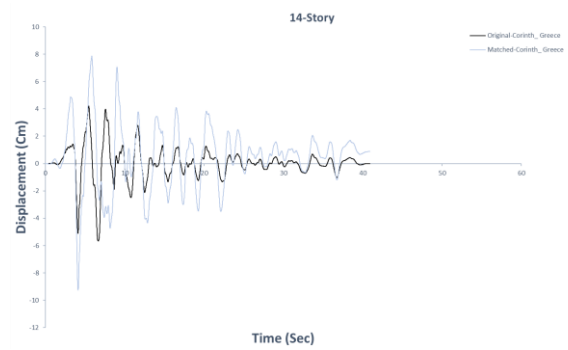
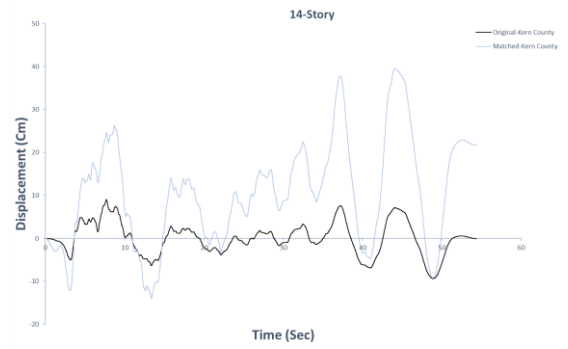
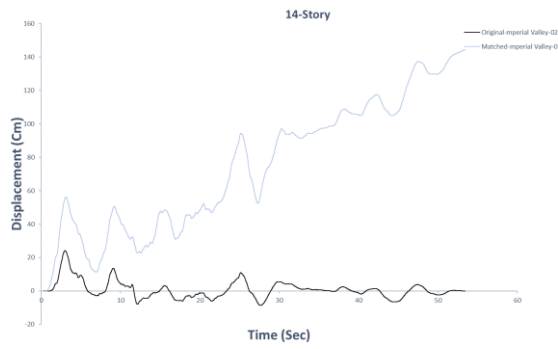
Appendix A4.2: Original and scaled Velocity

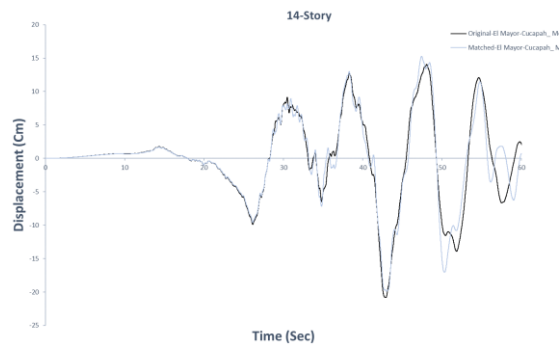
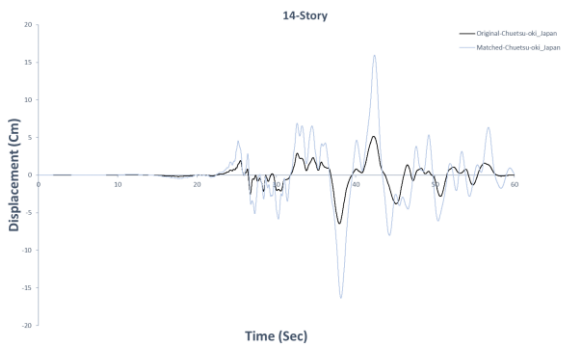
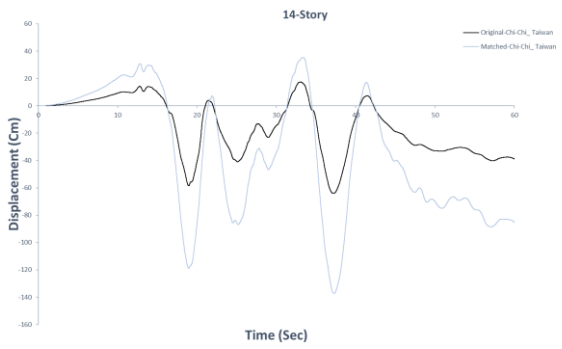
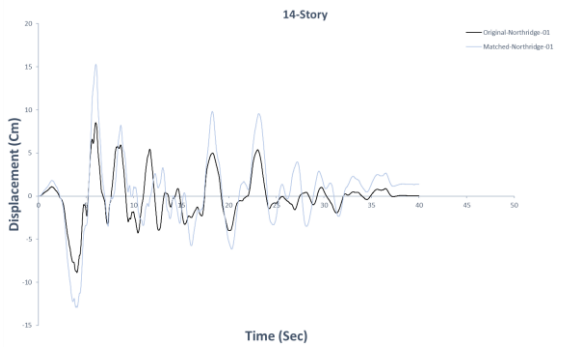
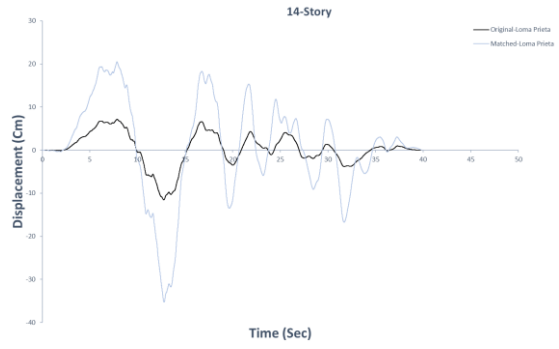
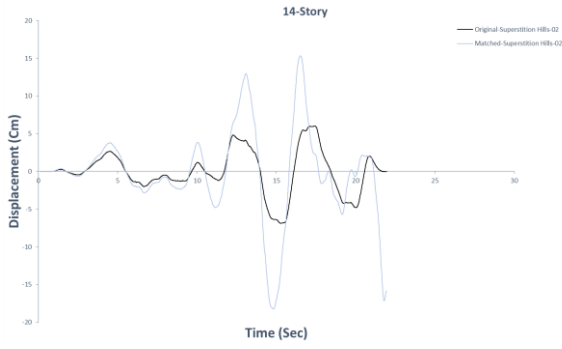


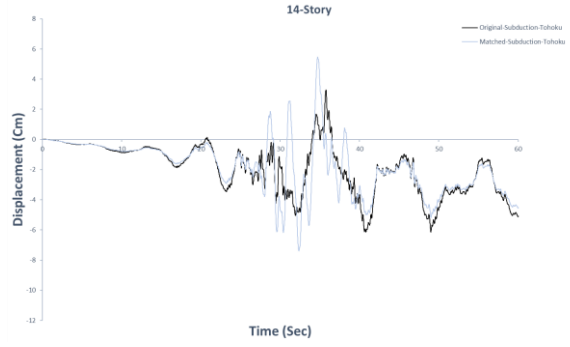
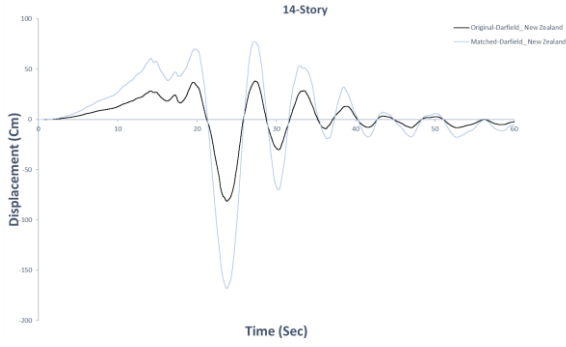




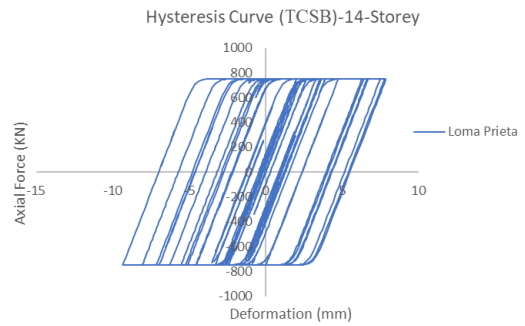
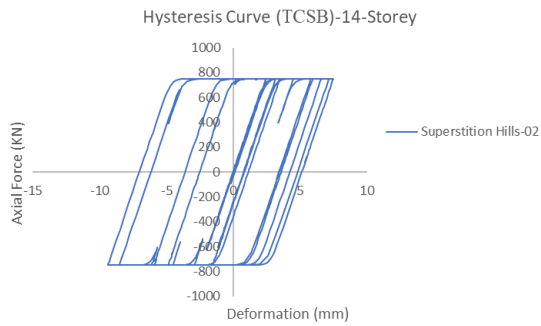
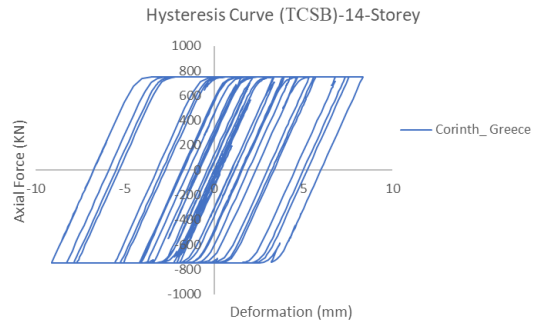
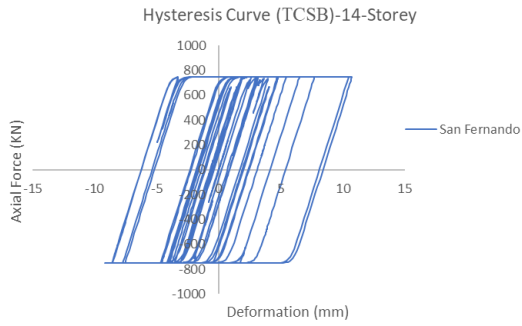
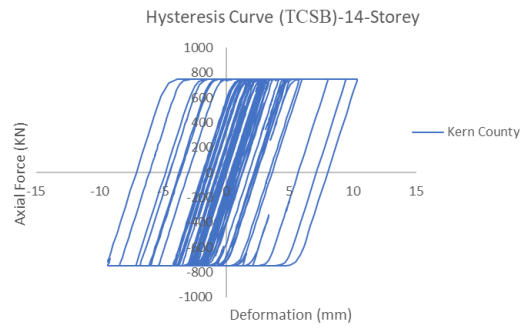
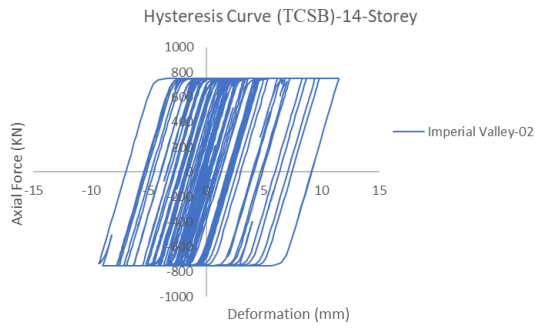
Appendix A4.3: Original and scaled displacement

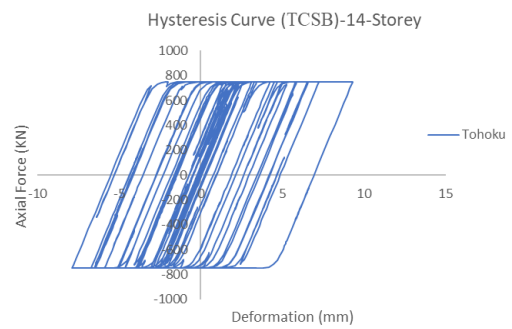
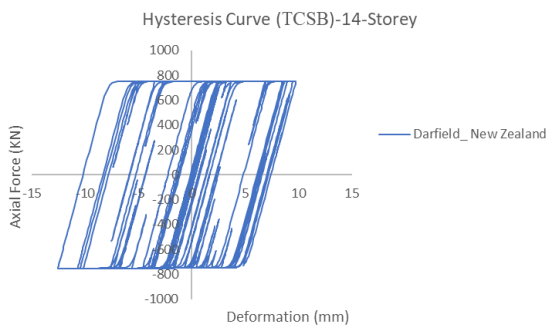
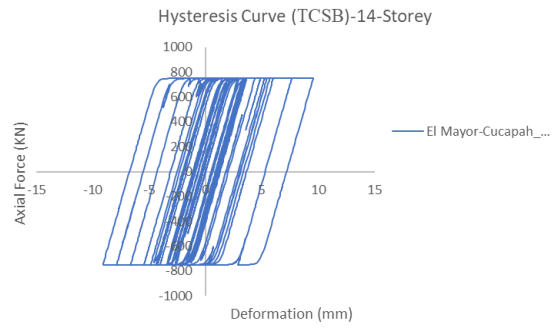
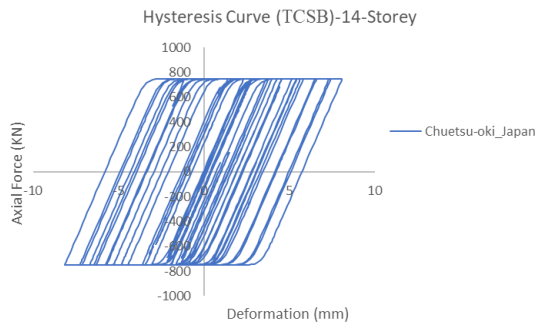
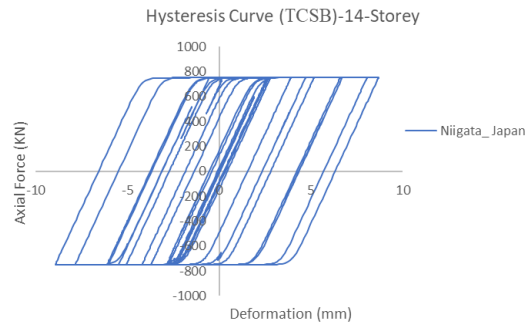
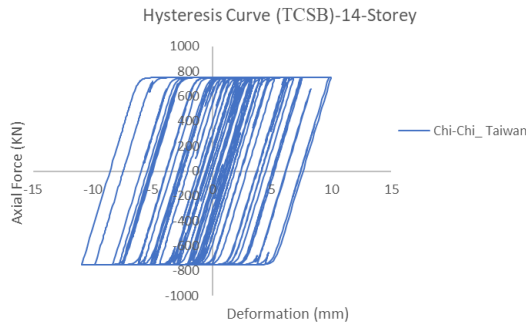
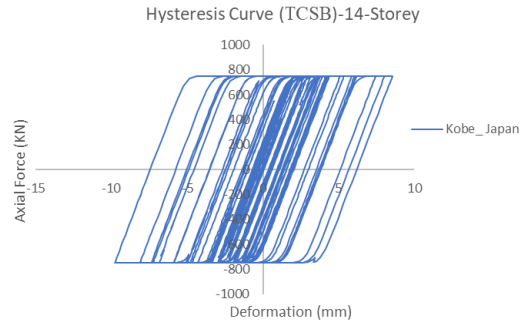
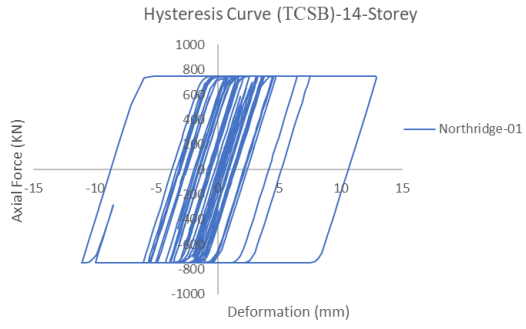




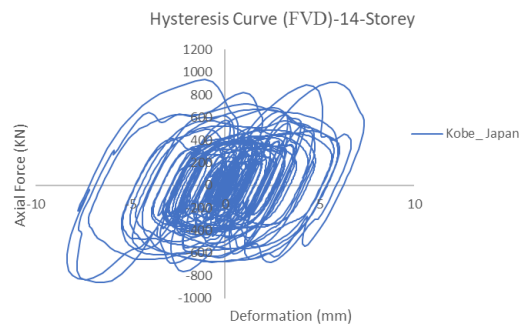
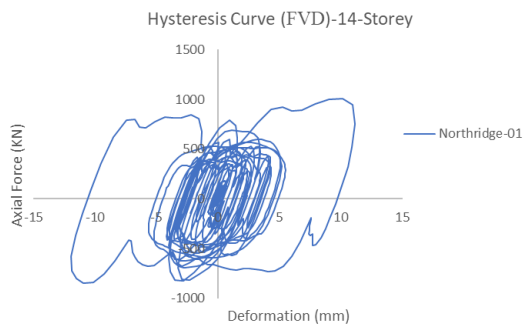
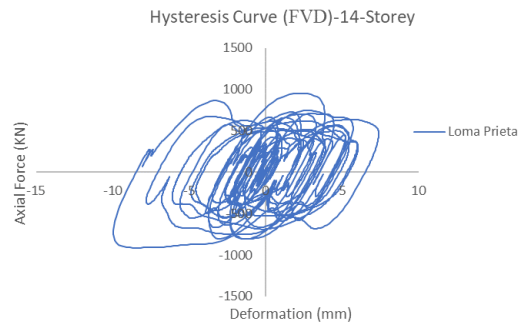
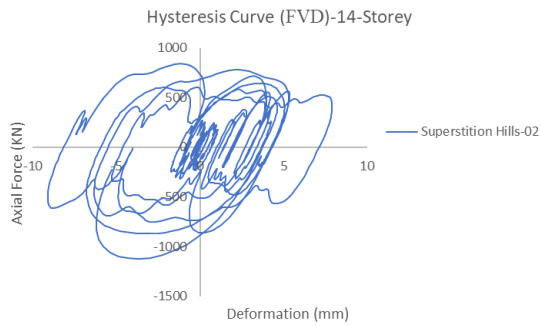
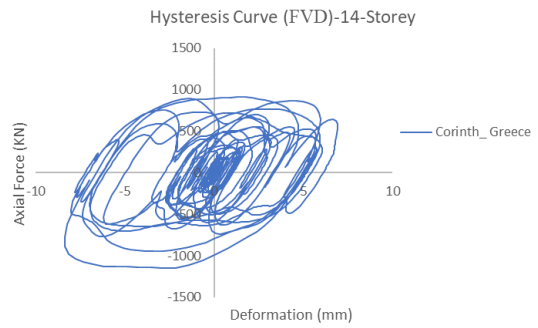
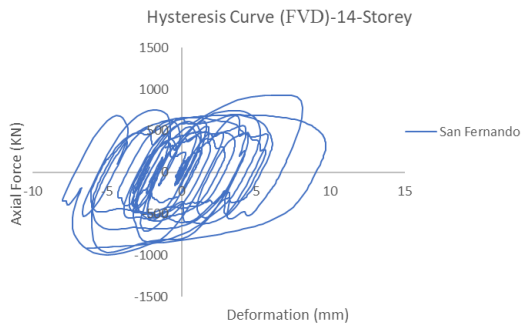
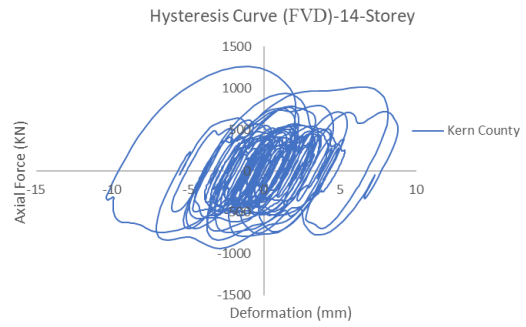
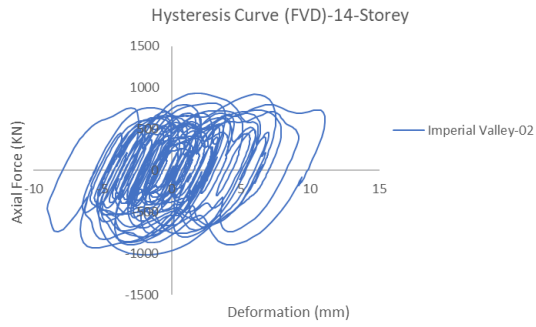


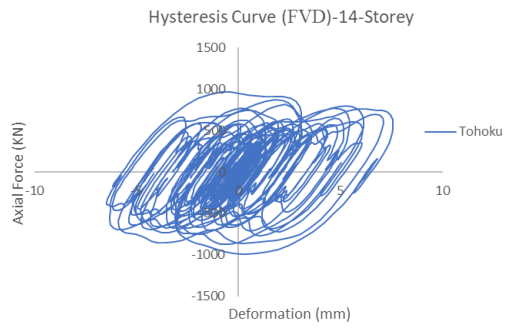
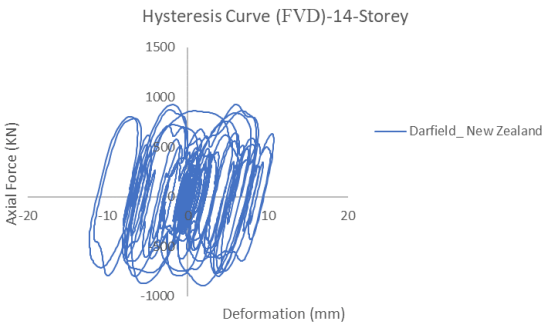
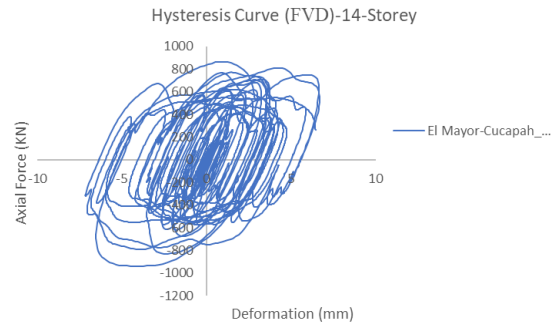
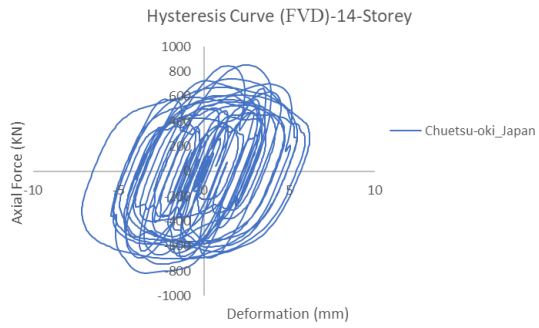
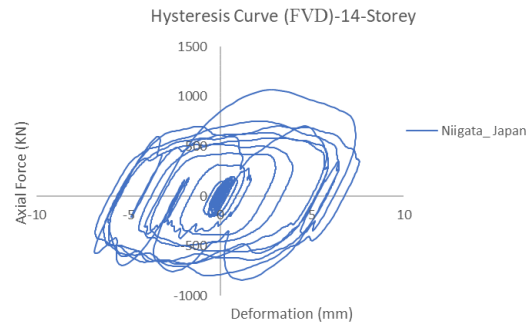
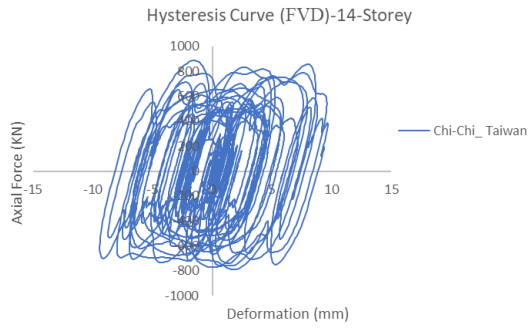
Appendix A4.4: Hysteresis Curves of TCSB



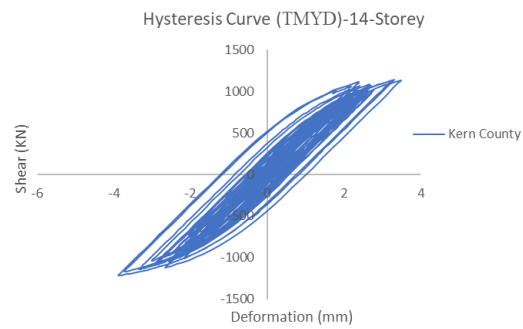
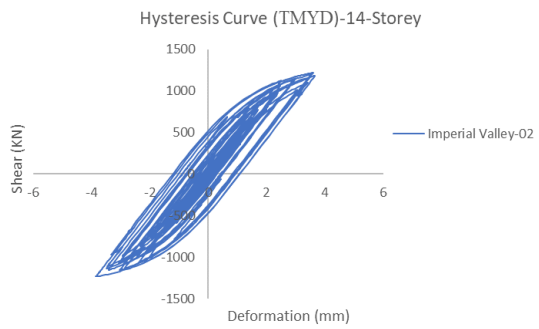


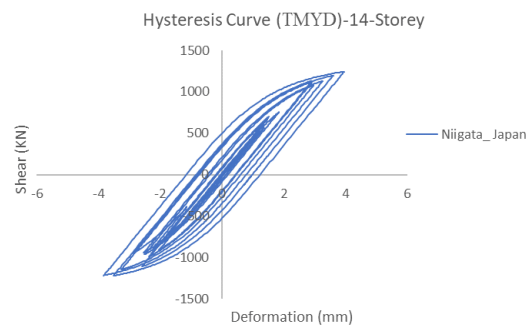
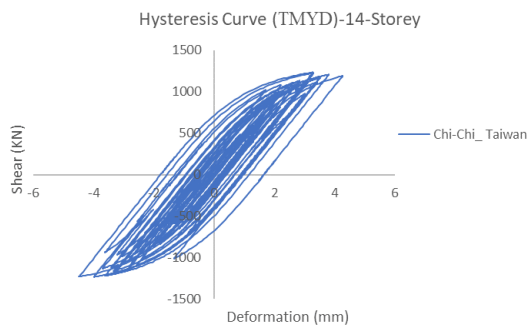
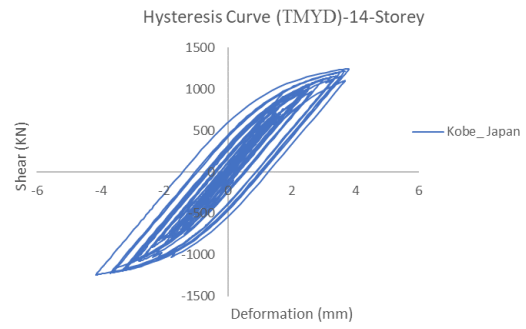
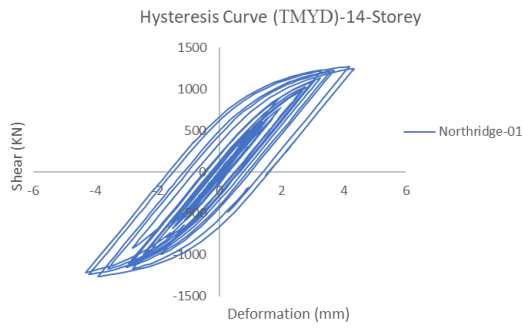
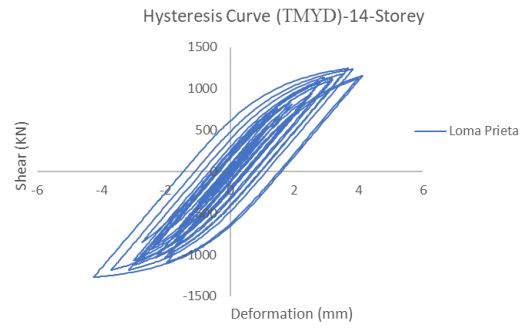
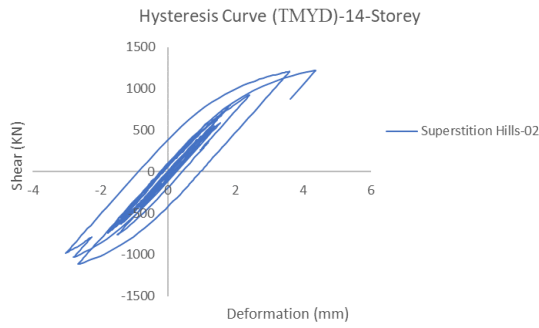
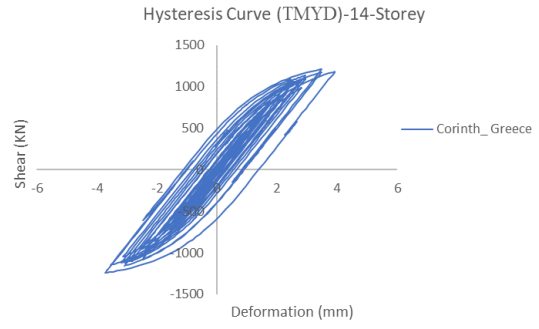
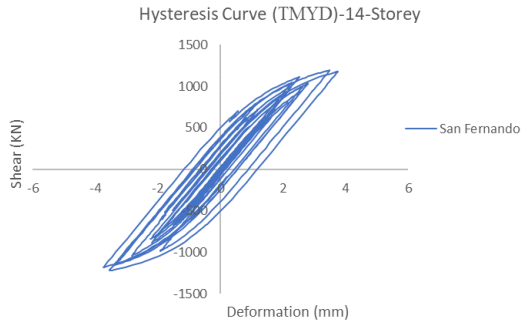
Appendix A4.5: Hysteresis Curves of FVD

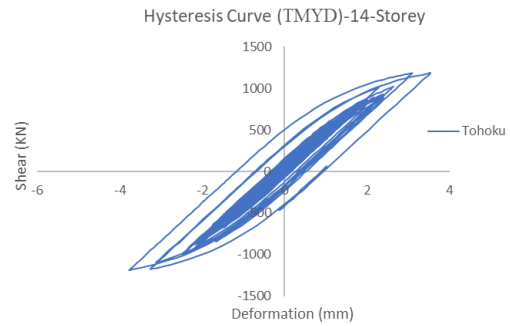
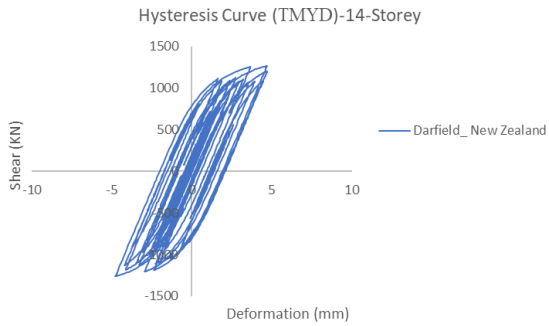
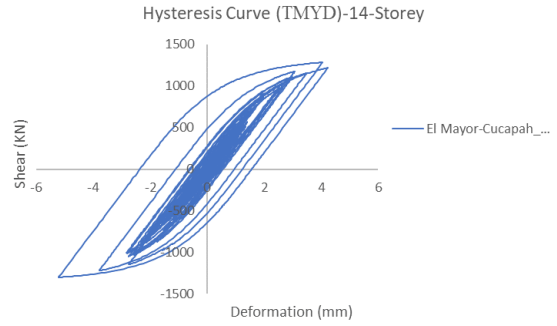
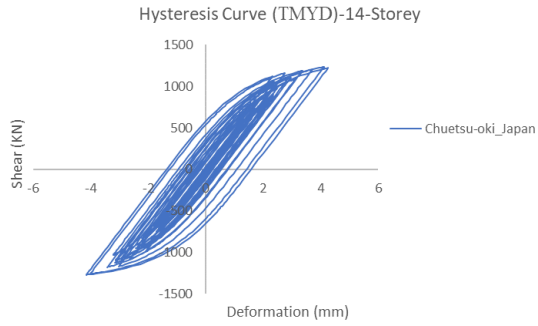




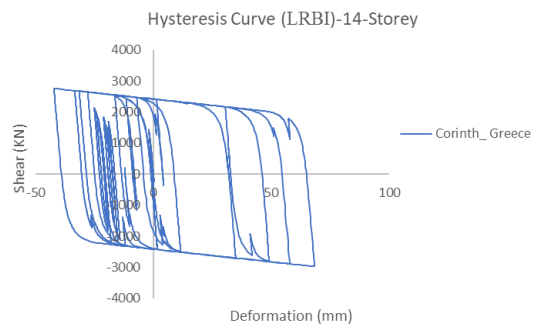
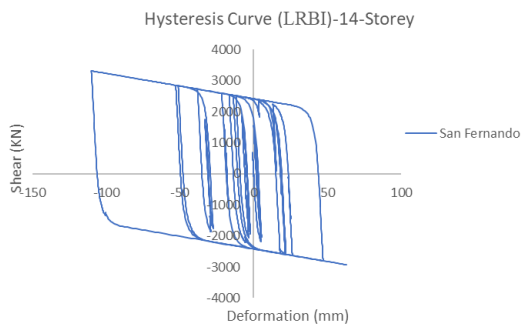
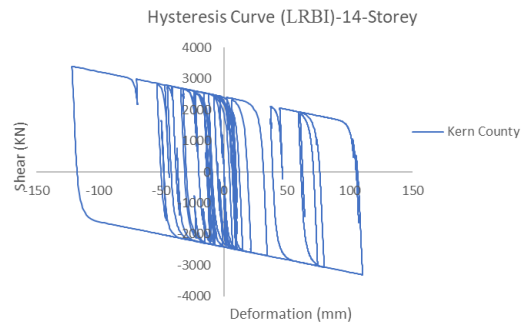
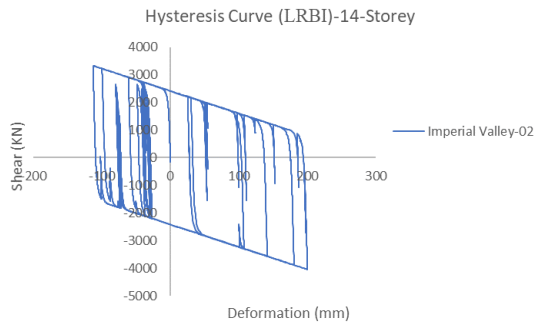
Appendix A4.6: Hysteresis Curves of TMYD

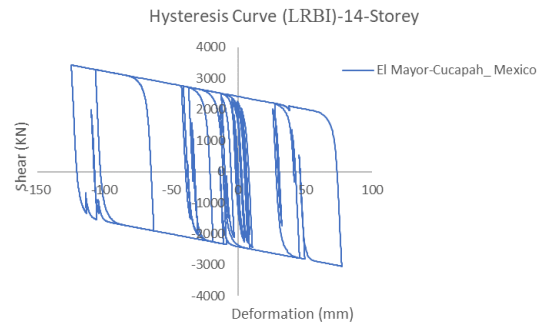
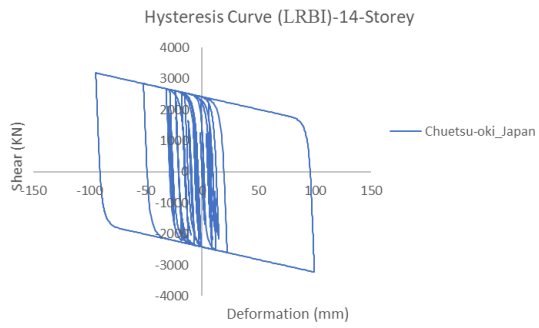
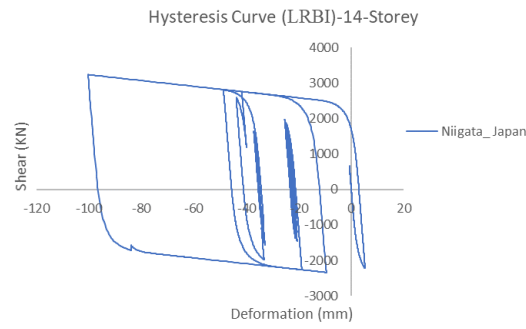
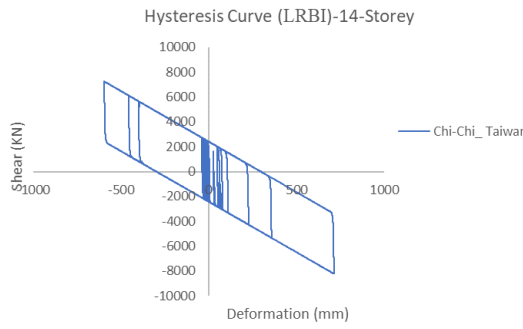
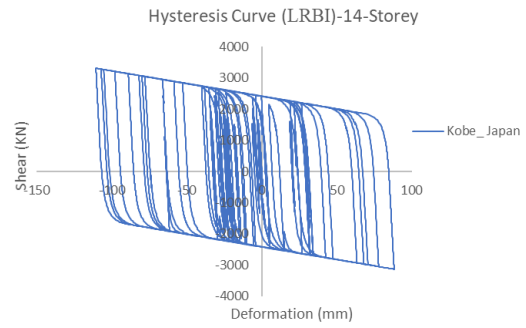
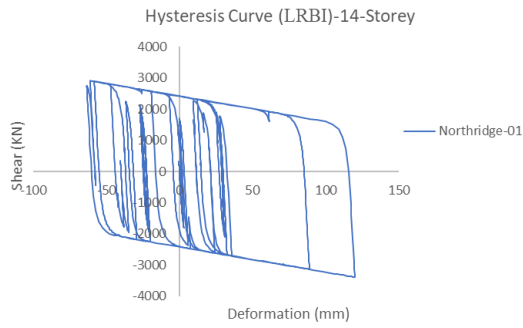
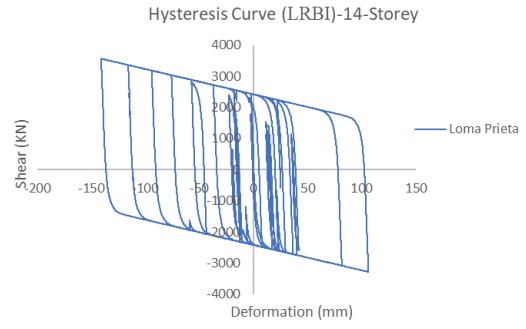
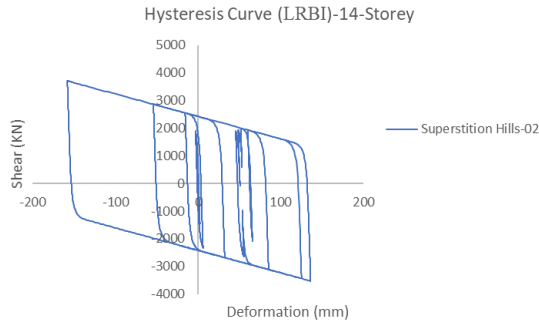


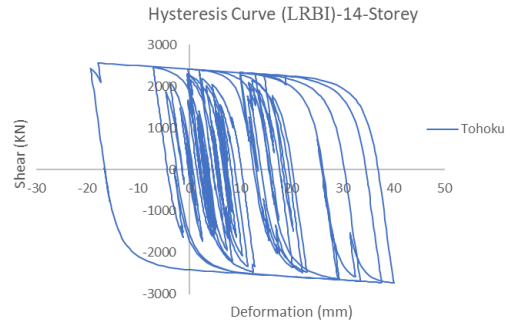
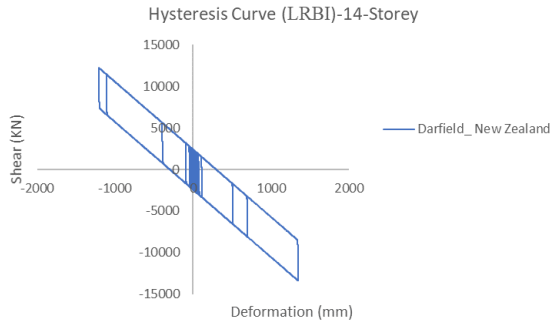




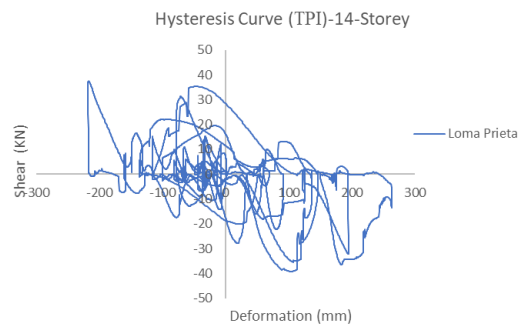
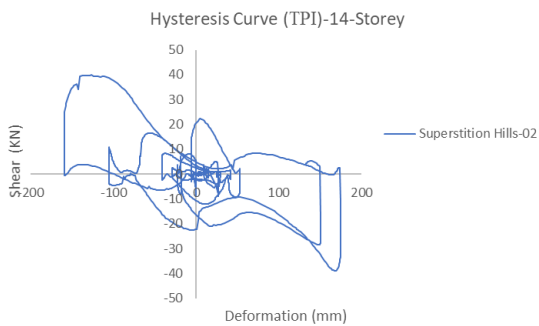
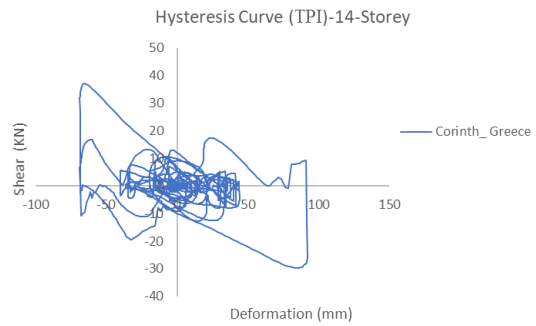
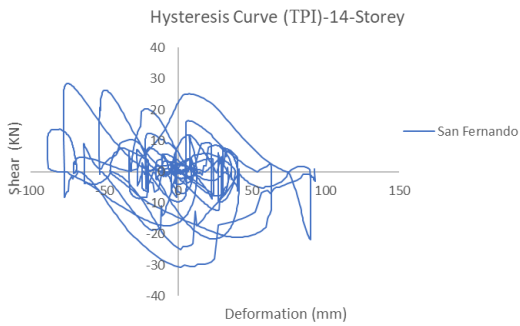
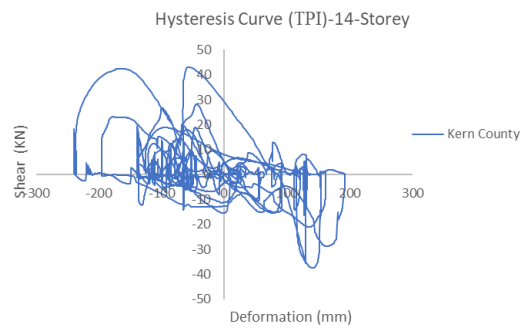
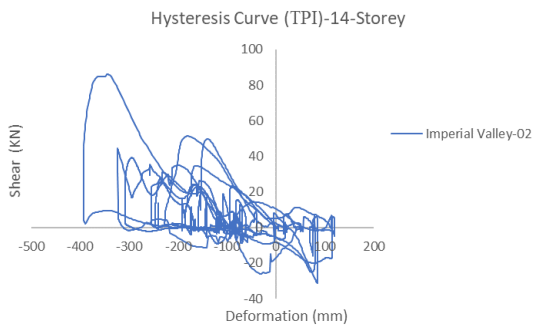
Appendix A4.7: Hysteresis Curves of LRBI

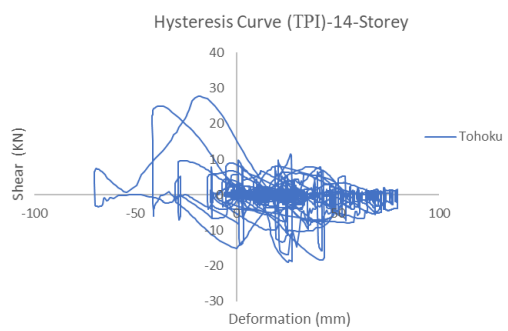
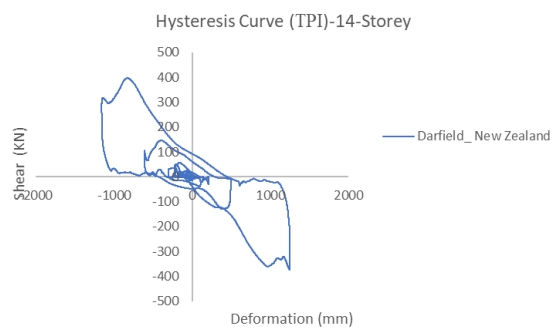
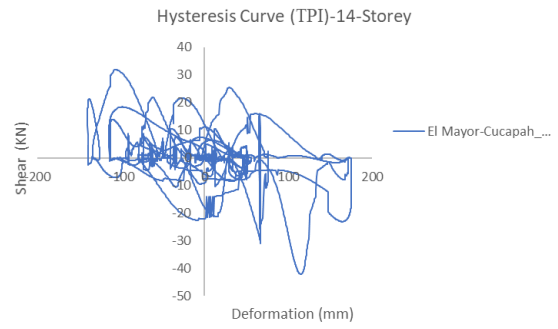
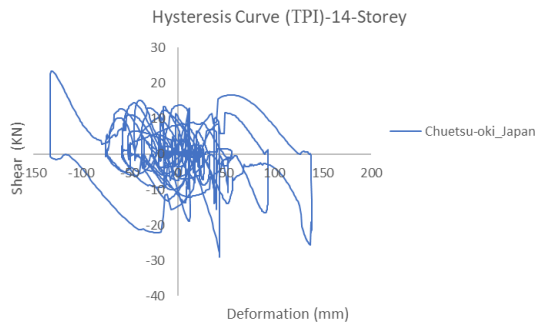
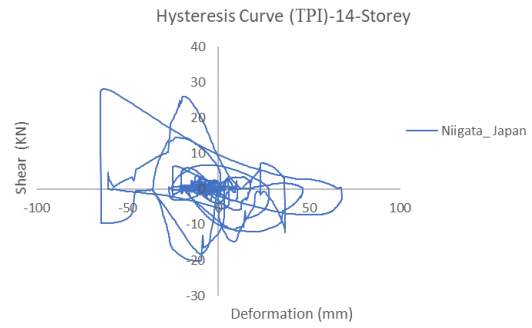
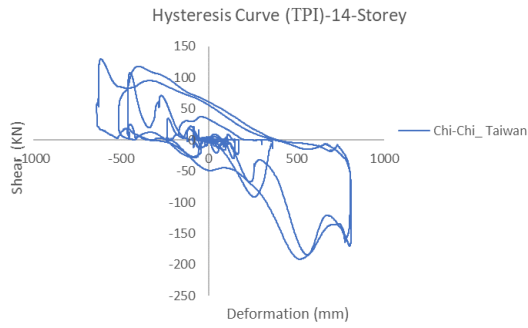
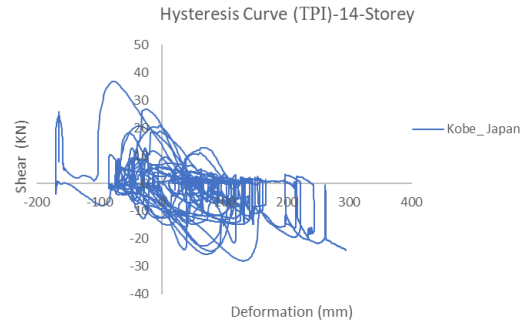
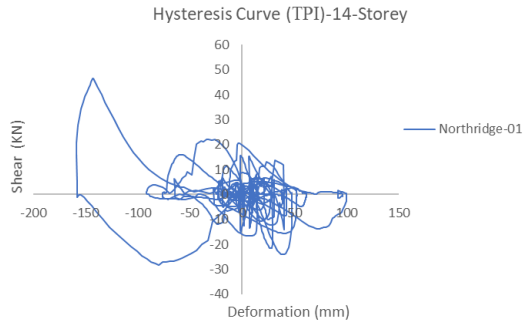




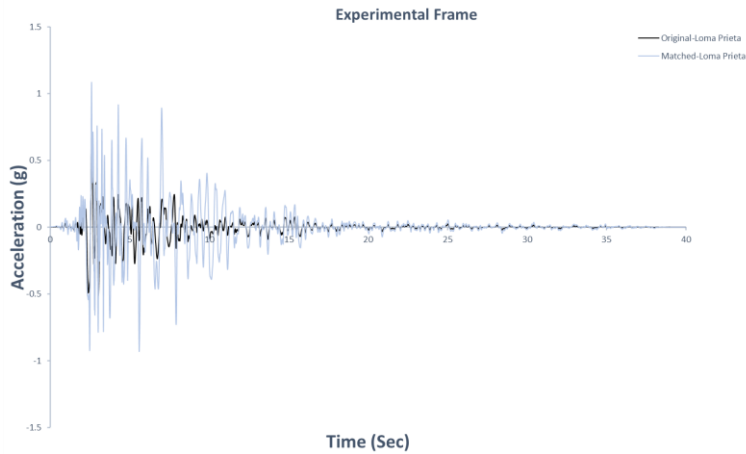
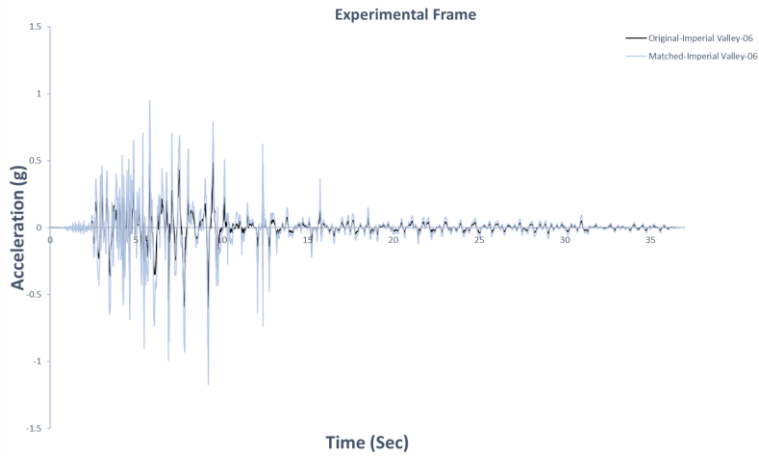
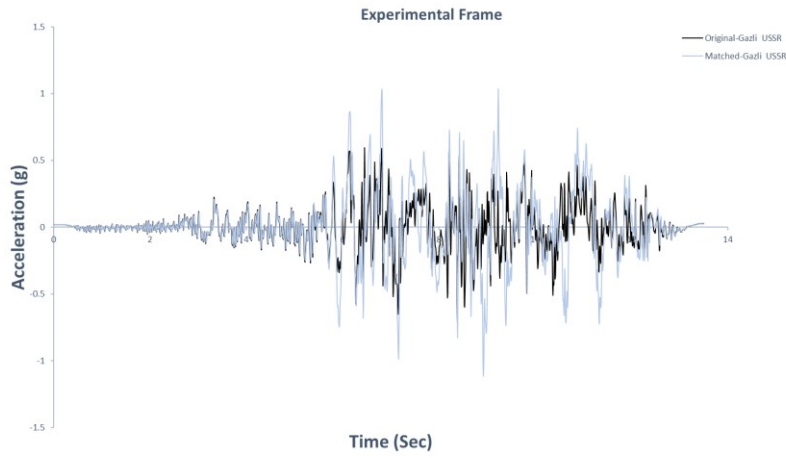


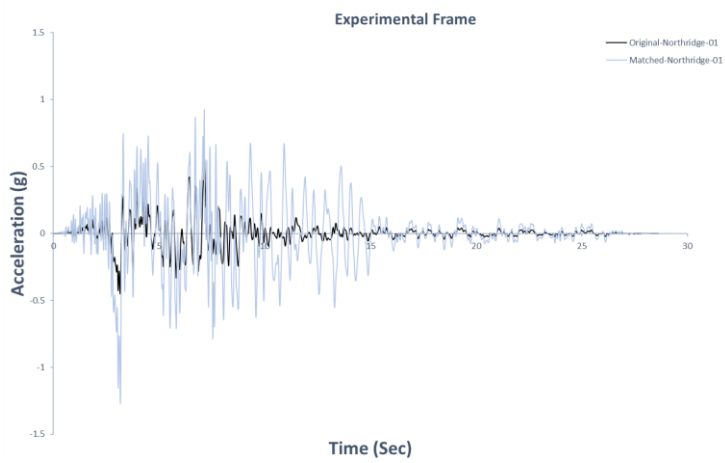
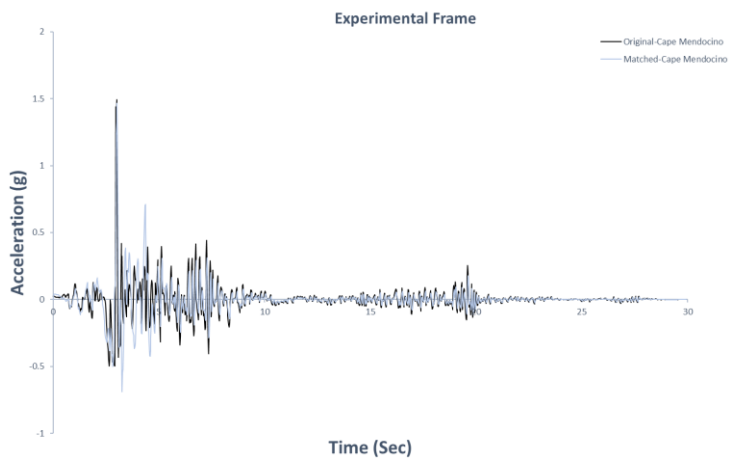
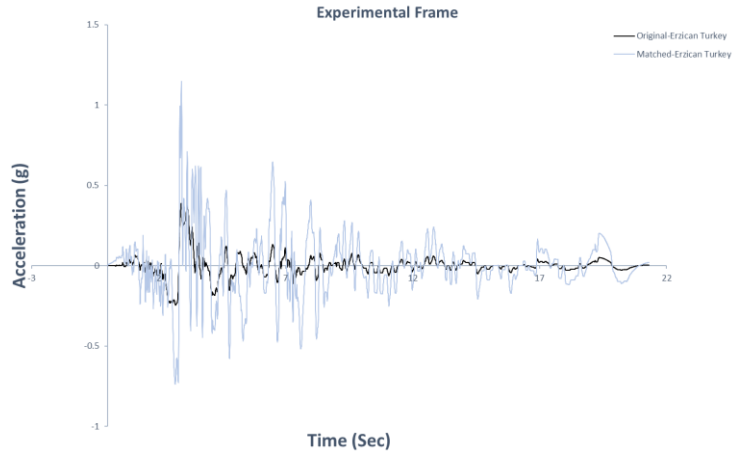
Appendix A4.8: Hysteresis Curves of TPI

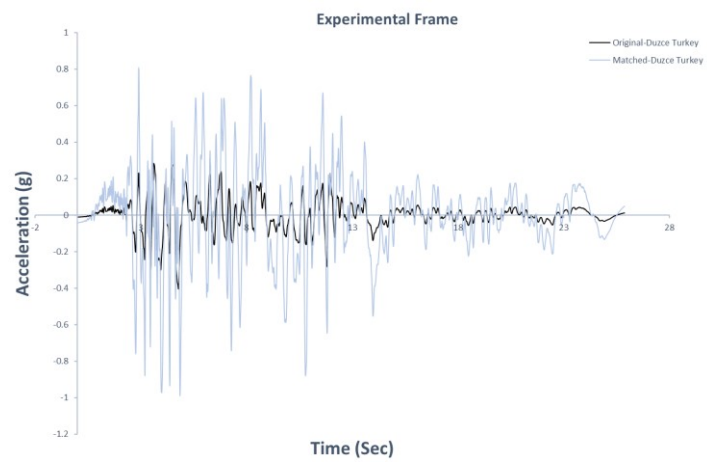
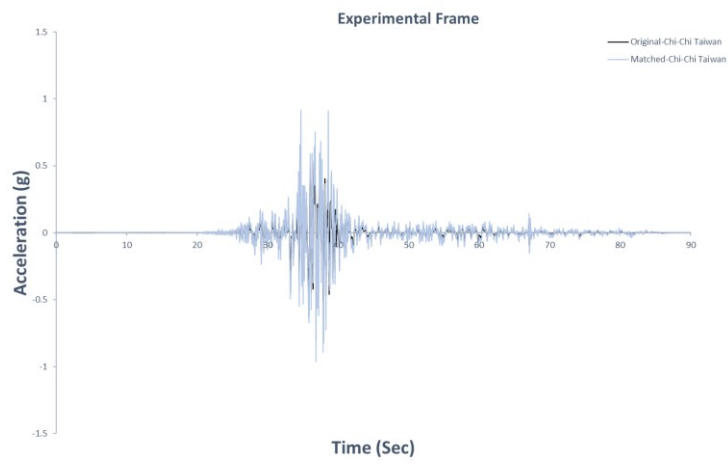
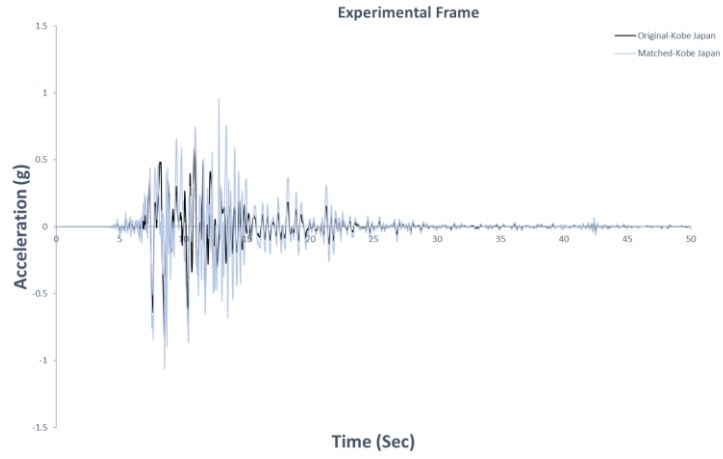


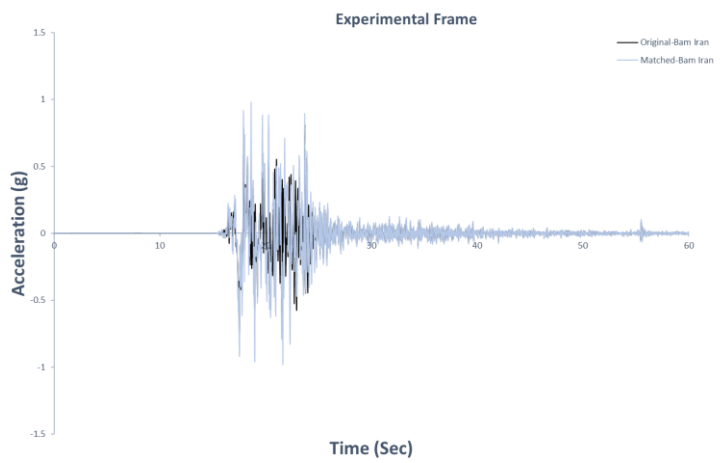
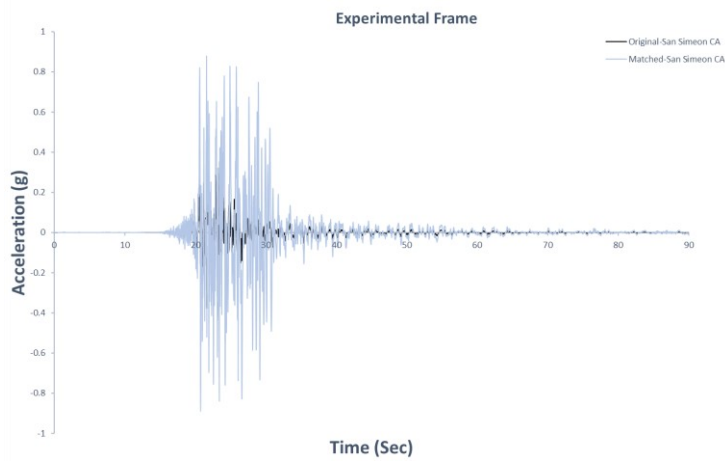
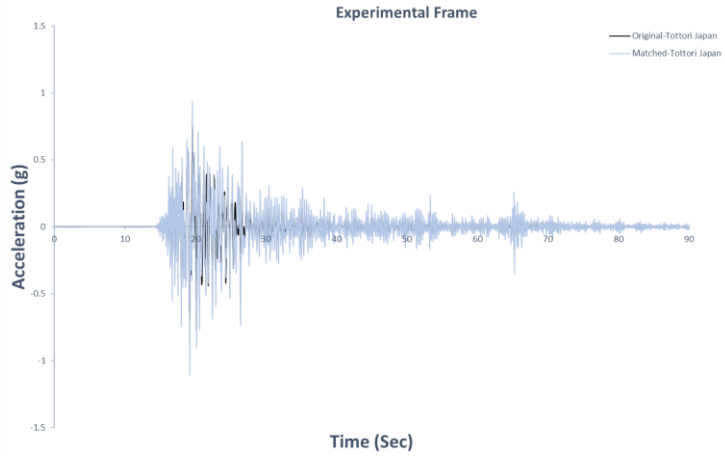


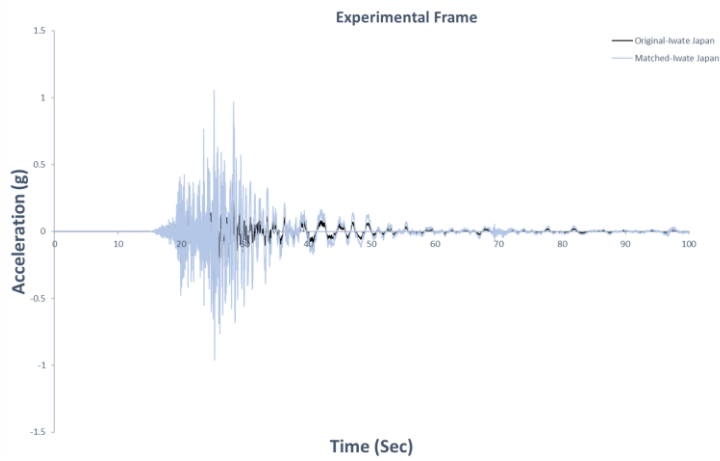
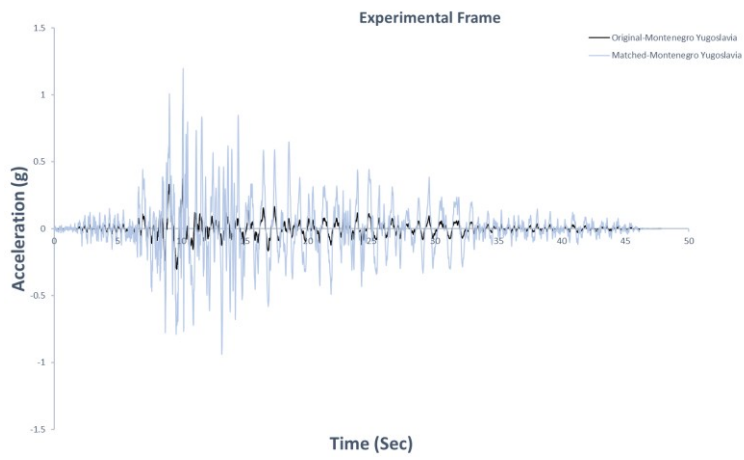
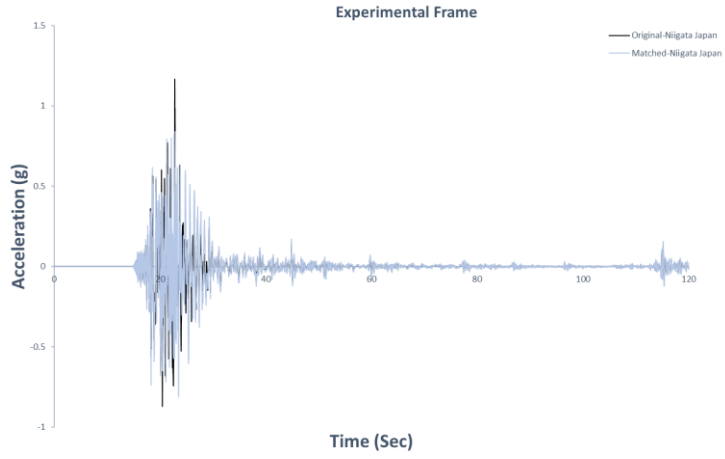
Appendix A5.1: Original and scaled Acceleration

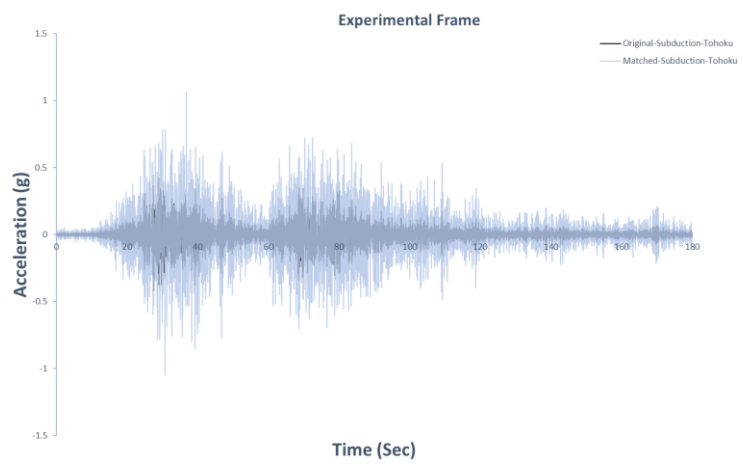
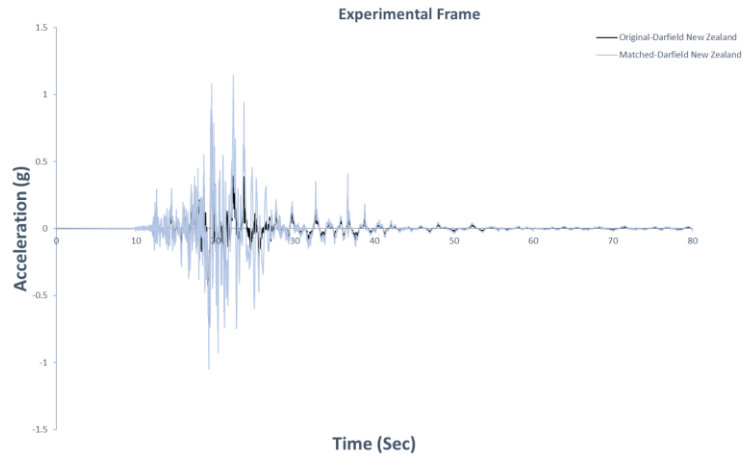




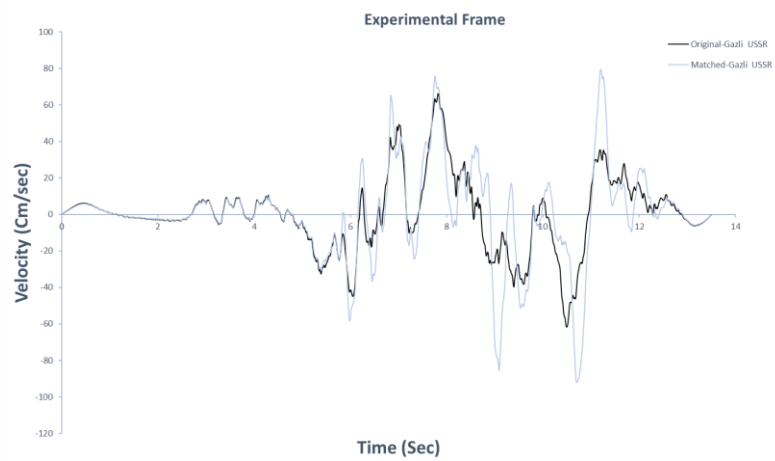


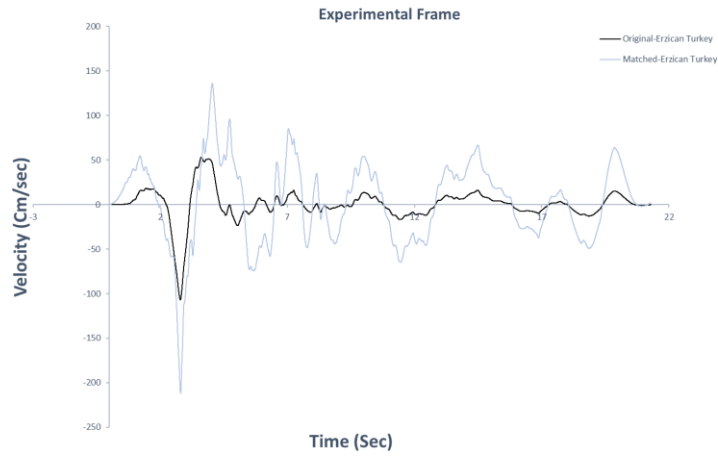
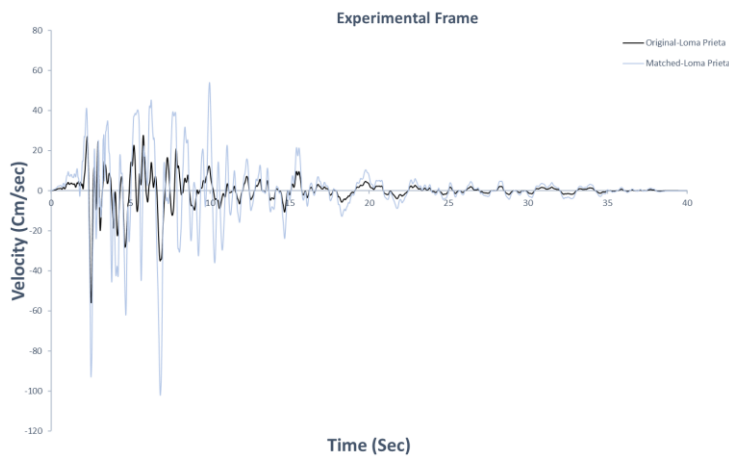
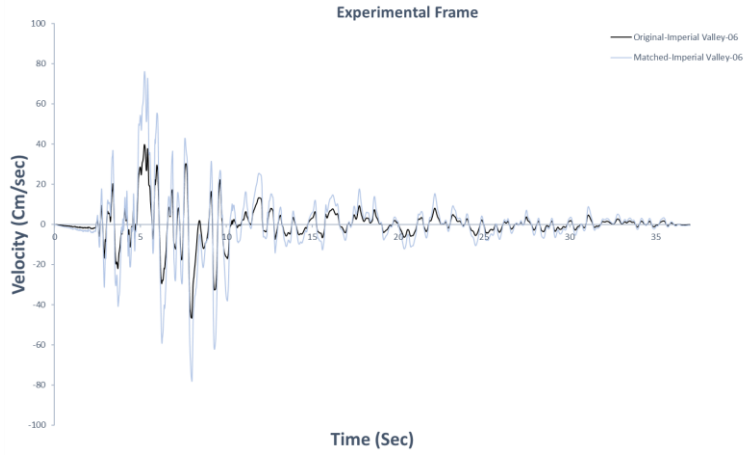


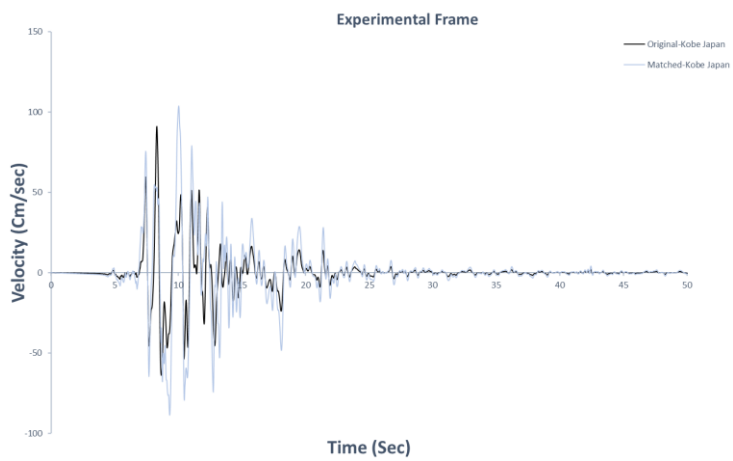
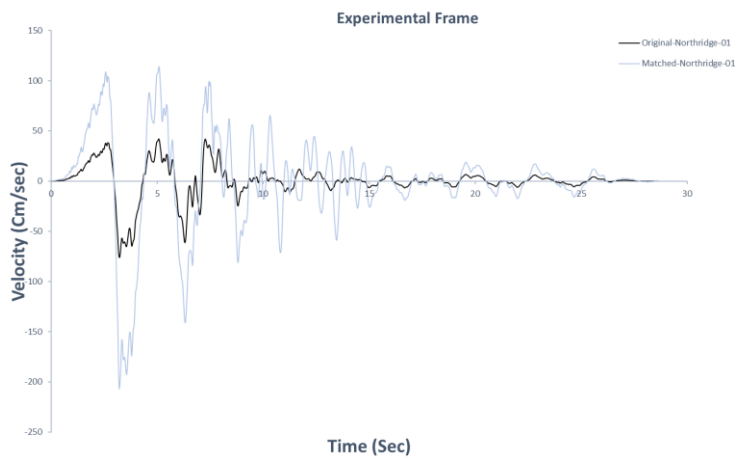
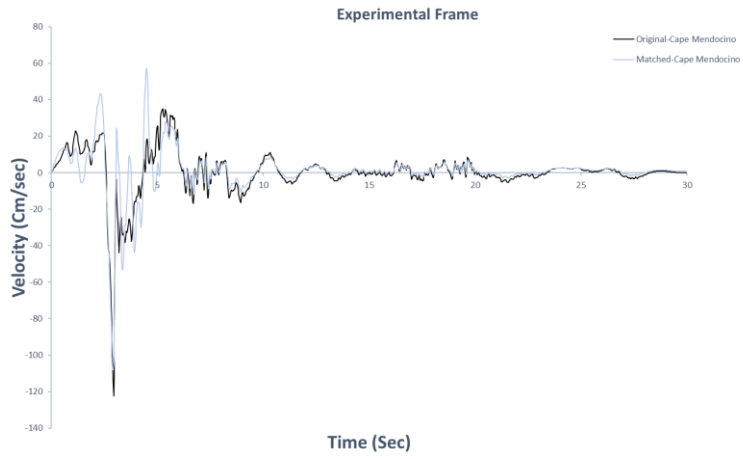


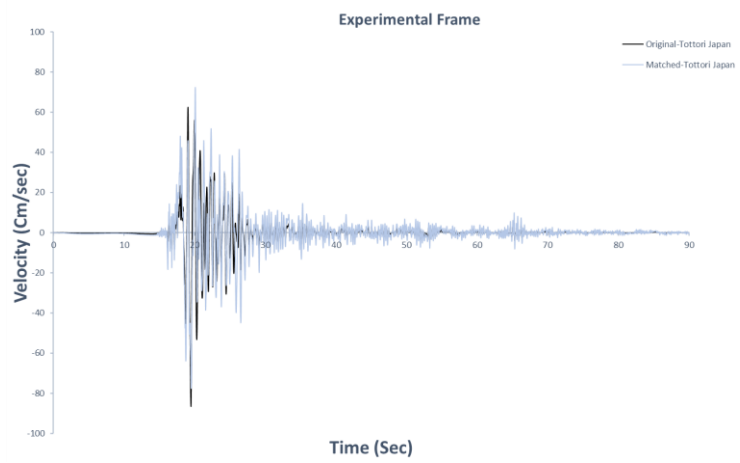
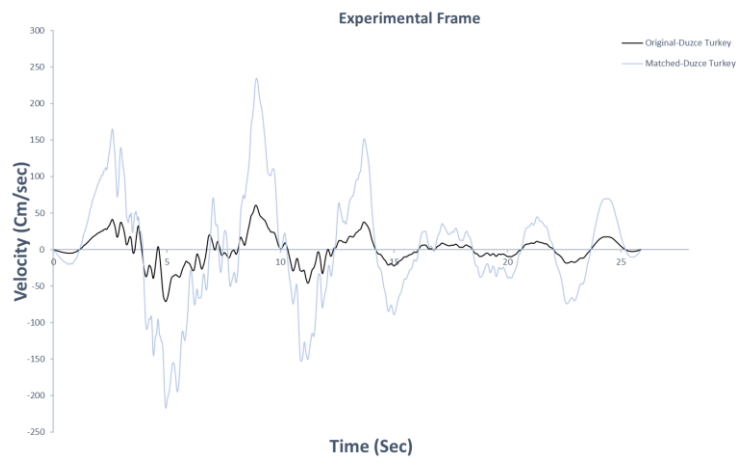
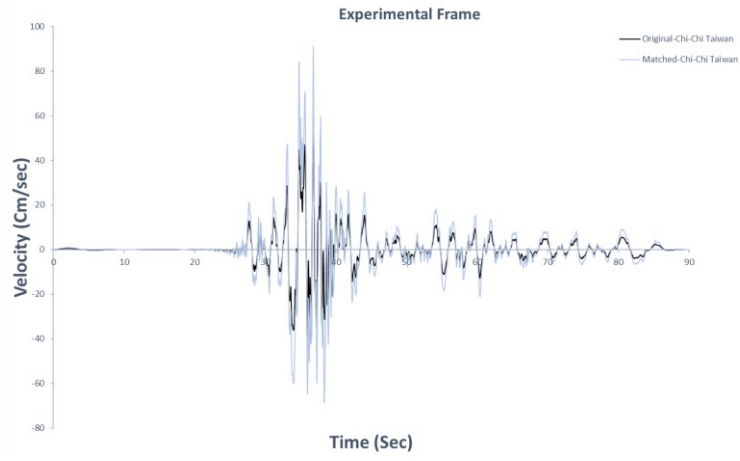


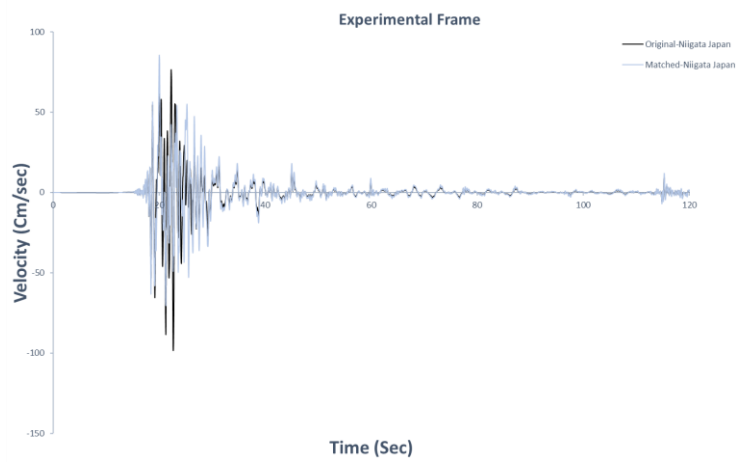
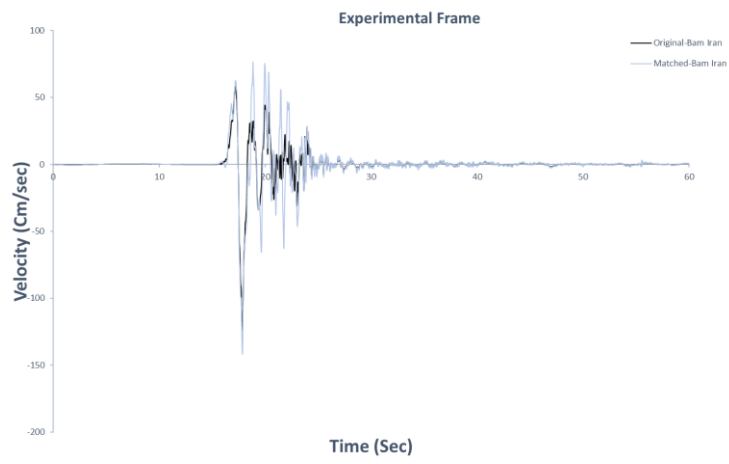
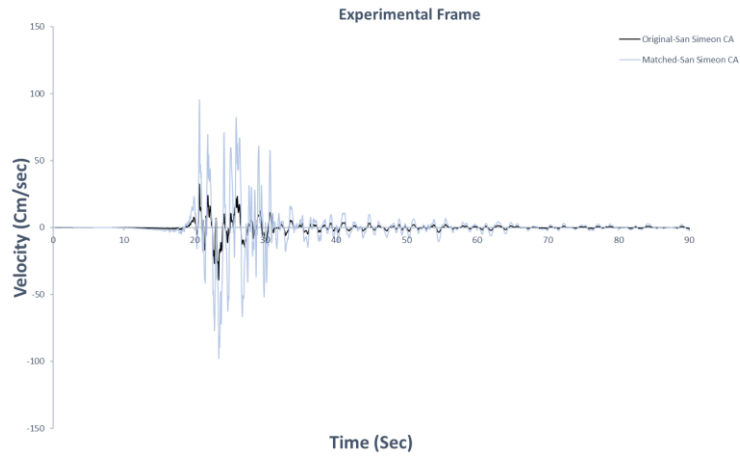
Appendix A5.2: Original and scaled Velocity

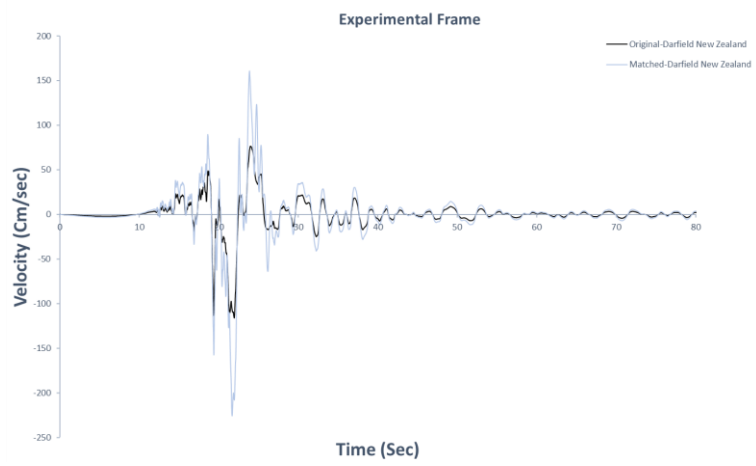
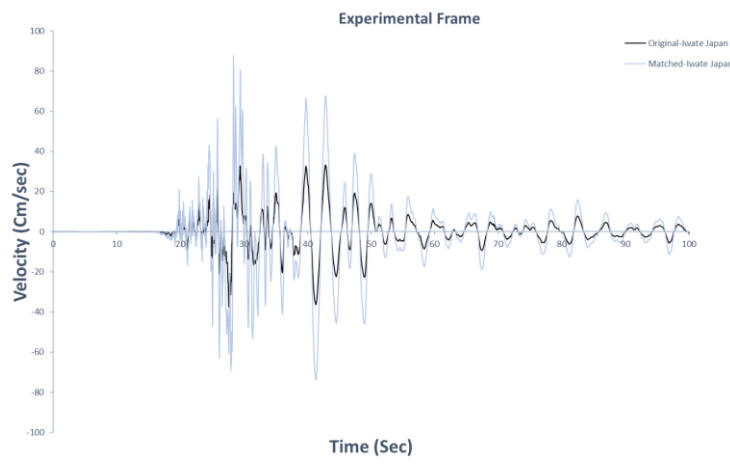
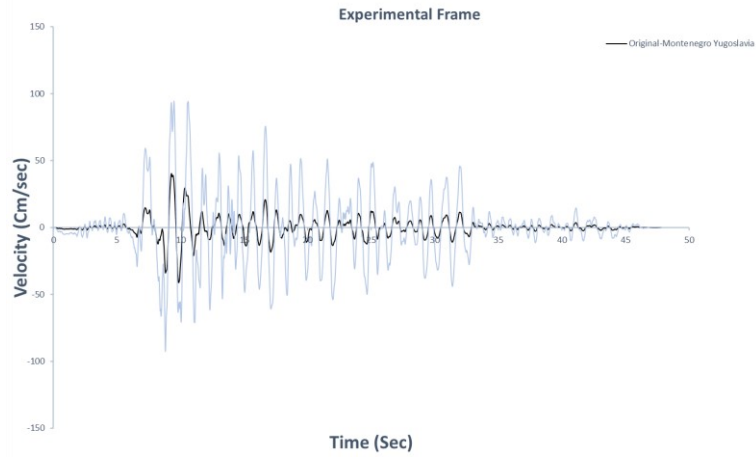


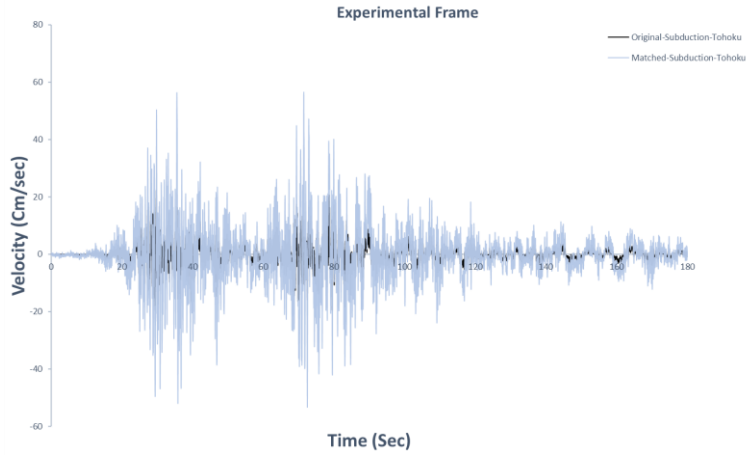




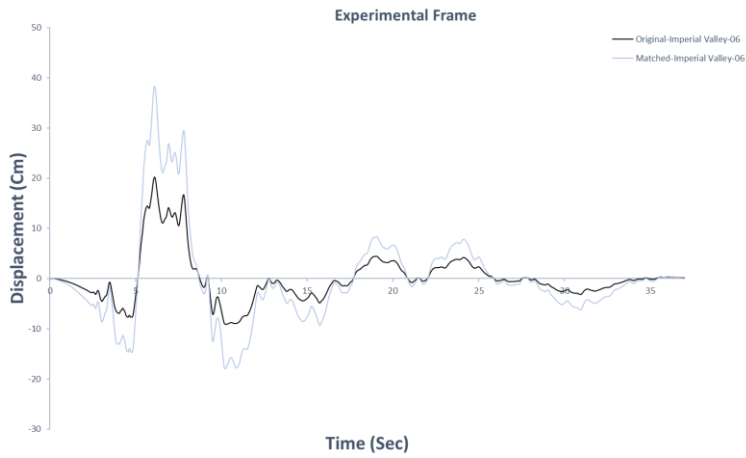
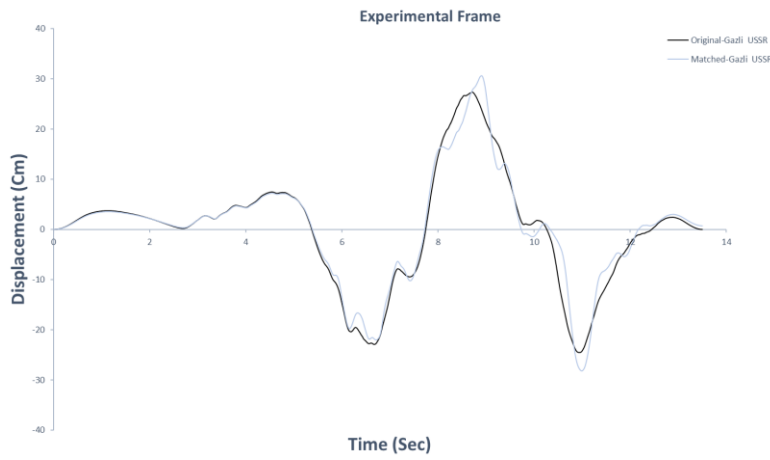


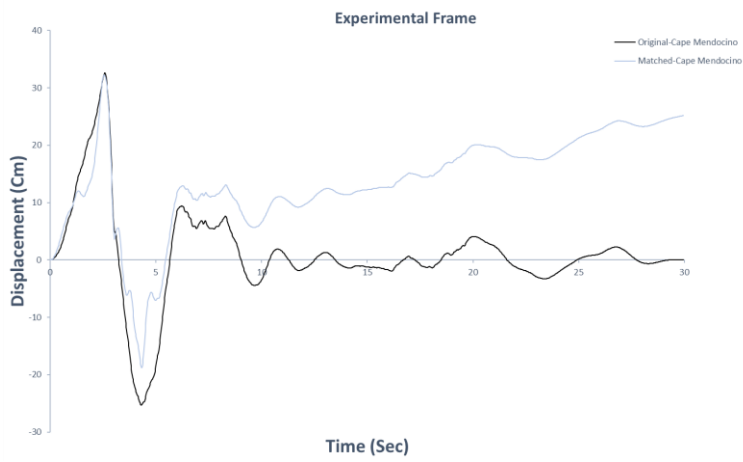
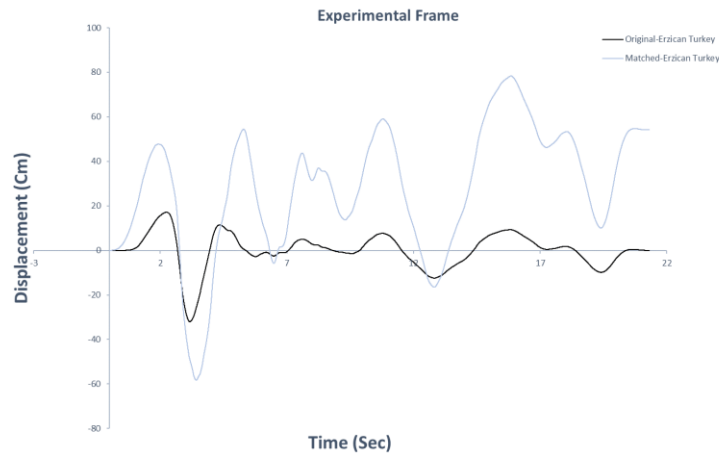
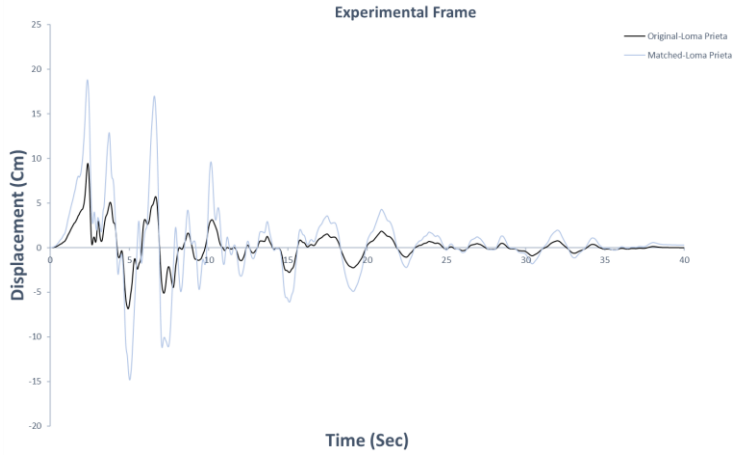


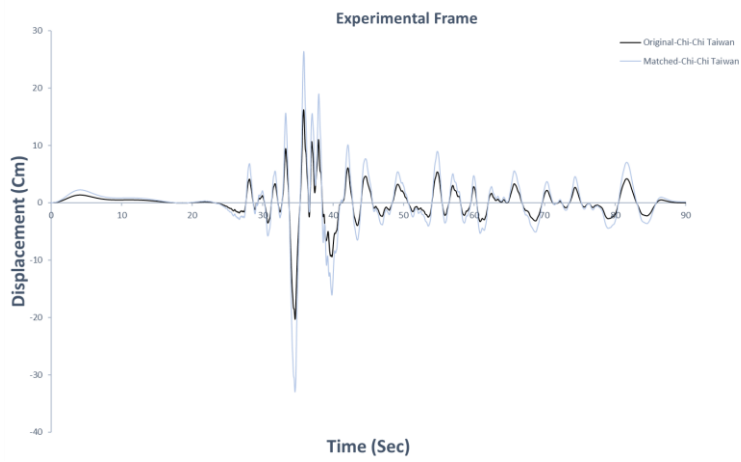
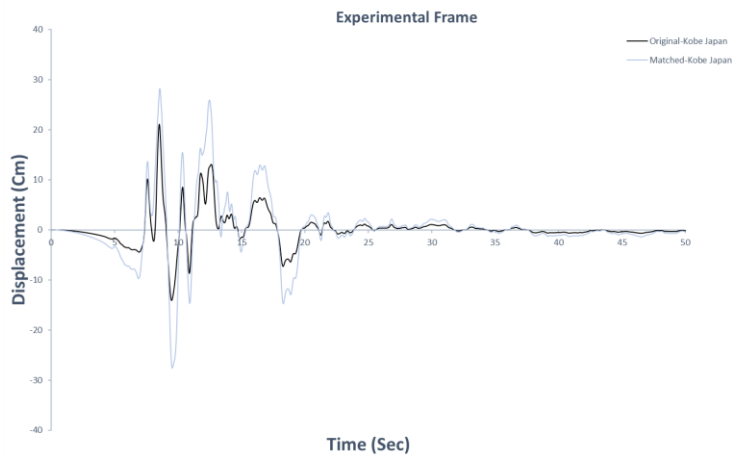
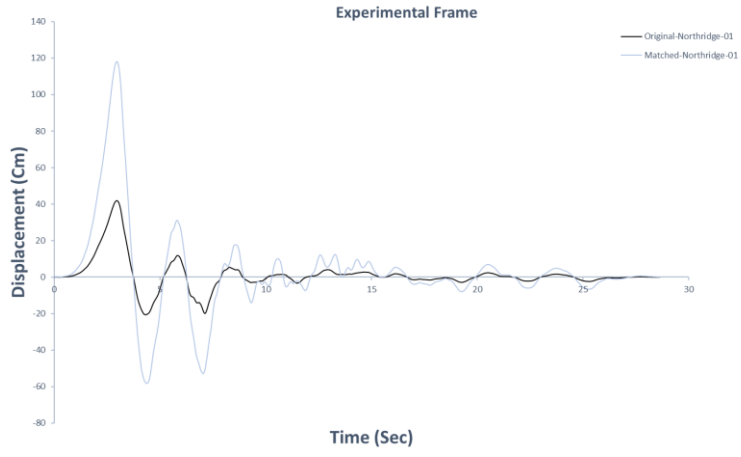


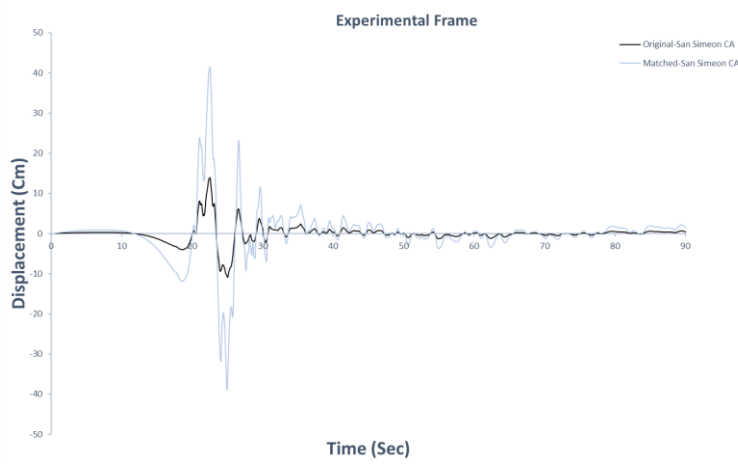
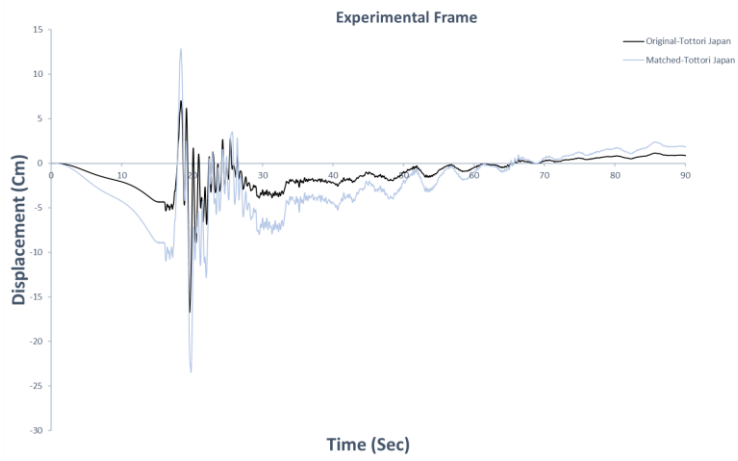
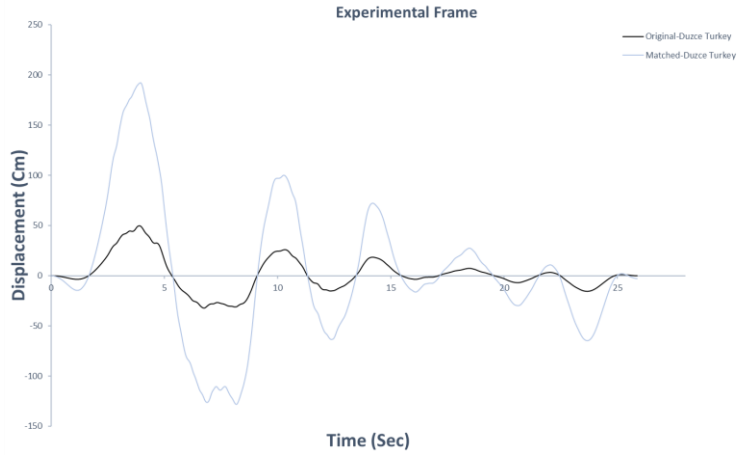


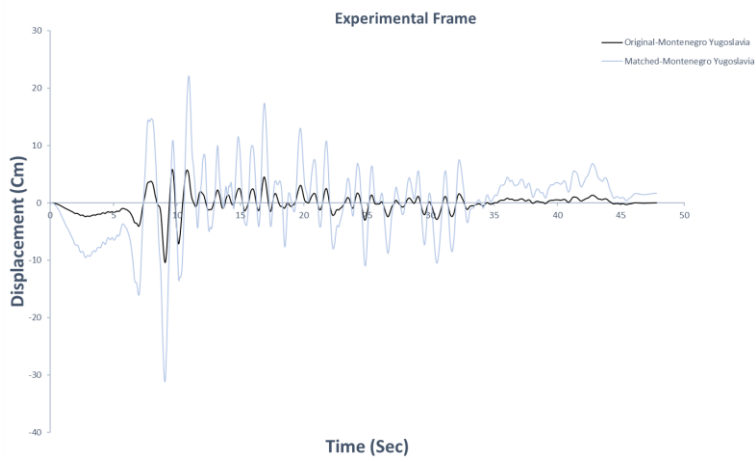
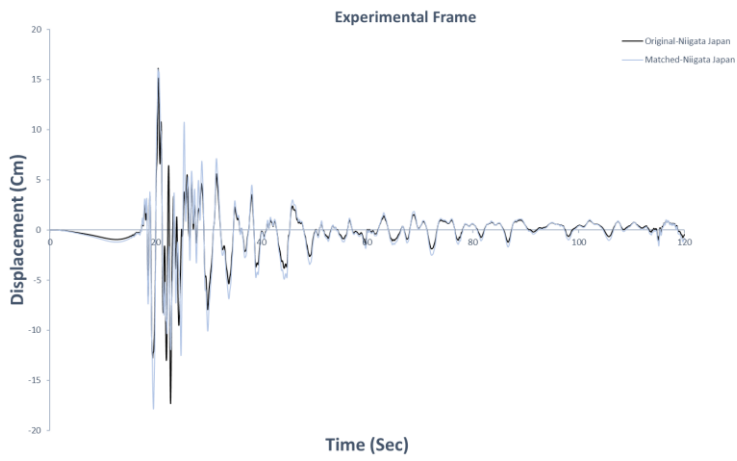
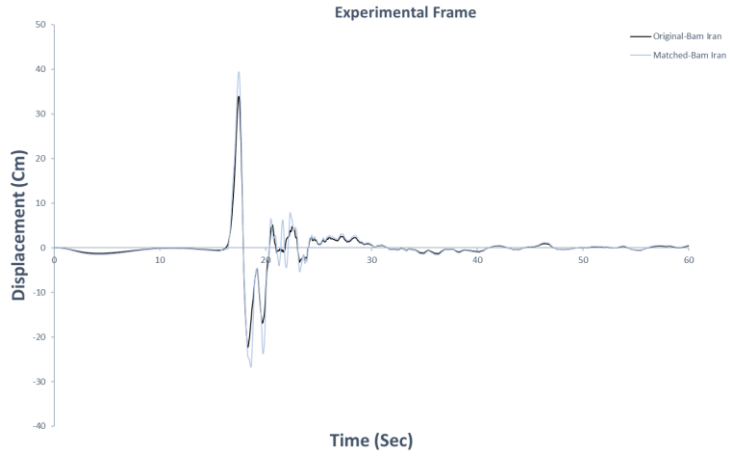
Appendix A5.3: Original and scaled Displacement

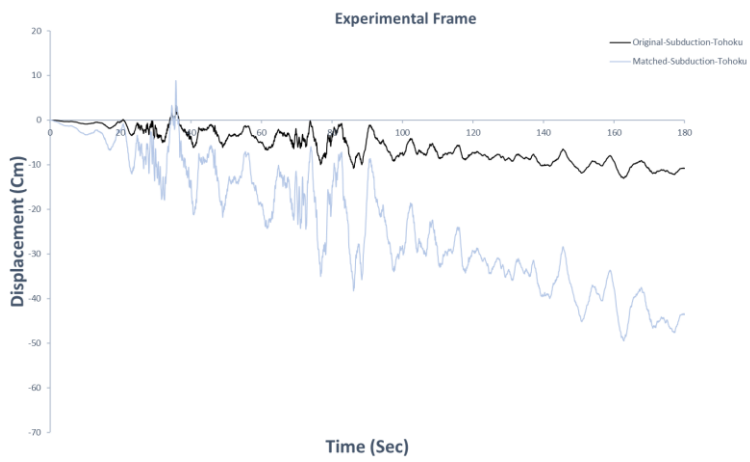
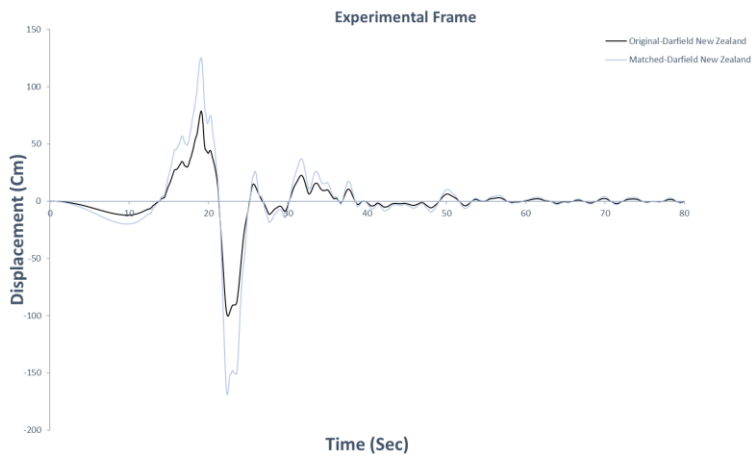
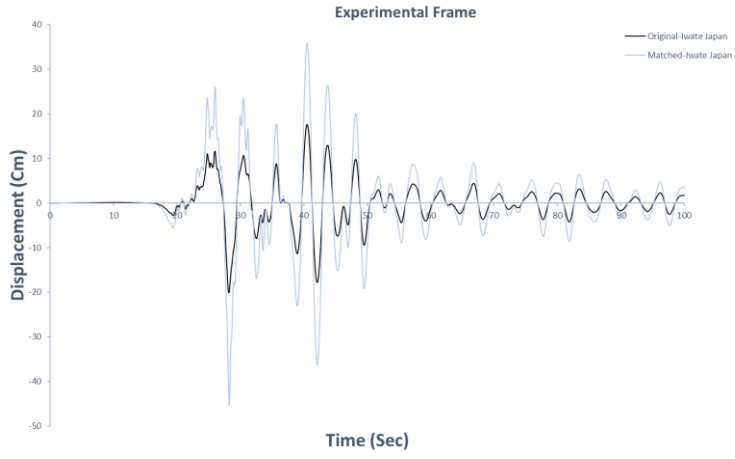












Appendix A5.4: OpenSees script

Based on the OpenSees manual the following commands for a 3D model have been used:

- Model
model BasicBuilder -ndm 3 -ndf 6
- Node
NodeCoord.tcl
Node tag xCrd yCrd zCrd ndf
node 1 +0.000000E+00 +0.000000E+00 +0.000000E+00 -ndf 6
node 2 +0.000000E+00 +0.000000E+00 +9.600000E+01 -ndf 6
node 3 +7.950000E+01 +0.000000E+00 +0.000000E+00 -ndf 6
node 4 +7.950000E+01 +0.000000E+00 +9.600000E+01 -ndf 6
node 5 +0.000000E+00 +3.025000E+01 +0.000000E+00 -ndf 6
node 6 +0.000000E+00 +3.025000E+01 +9.600000E+01 -ndf 6
node 7 +7.950000E+01 +3.025000E+01 +0.000000E+00 -ndf 6
node 8 +7.950000E+01 +3.025000E+01 +9.600000E+01 -ndf 6
node 9 +0.000000E+00 +6.050000E+01 +0.000000E+00 -ndf 6
node 10 +0.000000E+00 +6.050000E+01 +9.600000E+01 -ndf 6
node 11 +7.950000E+01 +6.050000E+01 +0.000000E+00 -ndf 6
node 12 +7.950000E+01 +6.050000E+01 +9.600000E+01 -ndf 6
- Mass
NodeMass.tcl
Node tag mx my mz mlx mly mlz
mass 2 +1.950000E-03 +1.950000E-03 +1.950000E-03 +0.000000E+00 +0.000000E+00
+0.000000E+00
mass 4 +1.950000E-03 +1.950000E-03 +1.950000E-03 +0.000000E+00 +0.000000E+00
+0.000000E+00
mass 6 +3.140000E-03 +3.140000E-03 +3.140000E-03 +0.000000E+00 +0.000000E+00
+0.000000E+00
mass 8 +3.140000E-03 +3.140000E-03 +3.140000E-03 +0.000000E+00 +0.000000E+00
+0.000000E+00
mass 10 +1.950000E-03 +1.950000E-03 +1.950000E-03 +0.000000E+00 +0.000000E+00
+0.000000E+00
mass 12 +1.950000E-03 +1.950000E-03 +1.950000E-03 +0.000000E+00 +0.000000E+00
+0.000000E+00
- sp/mp commands
SPCConstraint.tcl
SPC tag Dx Dy Dz Rx Ry Rz
fix 1 1 1 1 0 0 0
fix 3 1 1 1 0 0 0
fix 5 1 1 1 0 0 0
fix 7 1 1 1 0 0 0
fix 9 1 1 1 0 0 0
fix 11 1 1 1 0 0 0
MPConstraint.tcl
Rigid Diaphragm: Rigid Diaphragm joint: perpDir mNodeTag sNodeTags
rigidDiaphragm 3 6 2 10 4 8 12
- ndMaterial
Materials.tcl
Material "A36": matTag Fy E b R0 cR1 cR2 <a1 a2 a3 a4> <sig0>

```

uniaxialMaterial Steel02      1 +3.600000E+01 +2.900000E+04 +2.000000E-02 +1.850000E+01
+9.250000E-01 +1.500000E-01 +0.000000E+00 +1.000000E+00 +0.000000E+00 +1.000000E+00
+0.000000E+00
# Material "A992-Fy50": matTag Fy E b R0 cR1 cR2 <a1 a2 a3 a4> <sig0>
uniaxialMaterial Steel02      2 +5.000000E+01 +2.900000E+04 +1.500000E-02 +1.850000E+01
+9.250000E-01 +1.500000E-01 +0.000000E+00 +1.000000E+00 +0.000000E+00 +1.000000E+00
+0.000000E+00
# Material "ElasticDefault": matTag E <eta> <Eneg>
uniaxialMaterial Elastic      3 +2.900000E+04 +0.000000E+00

```

- Section

```

# Sections.tcl
# Section "2C6*10.5": secTag
section Fiber      1 {
  # PatchQuad "Top-Flange": matTag NSIJ NSJK ly lz Jy Jz Ky Kz Ly Lz
  patch quad      1 15 2 +2.657100E+00 +2.029900E+00 +2.657100E+00 -2.029900E+00
+3.000000E+00 -2.029900E+00 +3.000000E+00 +2.029900E+00
  # PatchQuad "Bot-Flange": matTag NSIJ NSJK ly lz Jy Jz Ky Kz Ly Lz
  patch quad      1 15 2 -3.000000E+00 +2.029900E+00 -3.000000E+00 -2.029900E+00 -
2.657100E+00 -2.029900E+00 -2.657100E+00 +2.029900E+00
  # PatchQuad "Web": matTag NSIJ NSJK ly lz Jy Jz Ky Kz Ly Lz
  patch quad      1 2 15 -2.657100E+00 +3.142000E-01 -2.657100E+00 -3.142000E-01
+2.657100E+00 -3.142000E-01 +2.657100E+00 +3.142000E-01
}
# Section "ElasticDefault": secTag E A lz ly G J <alphaY> <alphaZ>
section Elastic    2 +2.900000E+04 +1.800000E+02 +4.860000E+03 +1.500000E+03 +1.115400E+04
+3.916000E+03 +8.333333E-01 +8.333333E-01
# Section "W6X15": secTag
section Fiber      3 {
  # PatchAISC "Patch01": matTag NSIJ NSJK ly lz Jy Jz Ky Kz Ly Lz
  patch quad      2 15 2 +2.735000E+00 +2.995000E+00 +2.735000E+00 -2.995000E+00
+2.995000E+00 -2.995000E+00 +2.995000E+00 +2.995000E+00
  patch quad      2 2 15 -2.735000E+00 +1.150000E-01 -2.735000E+00 -1.150000E-01
+2.735000E+00 -1.150000E-01 +2.735000E+00 +1.150000E-01
  patch quad      2 15 2 -2.995000E+00 +2.995000E+00 -2.995000E+00 -2.995000E+00 -
2.735000E+00 -2.995000E+00 -2.735000E+00 +2.995000E+00 }
# Section "W6X9": secTag
section Fiber      4 {
  # PatchAISC "Patch01": matTag NSIJ NSJK ly lz Jy Jz Ky Kz Ly Lz
  patch quad      2 15 2 +2.735000E+00 +1.970000E+00 +2.735000E+00 -1.970000E+00
+2.950000E+00 -1.970000E+00 +2.950000E+00 +1.970000E+00
  patch quad      2 2 15 -2.735000E+00 +8.500000E-02 -2.735000E+00 -8.500000E-02
+2.735000E+00 -8.500000E-02 +2.735000E+00 +8.500000E-02
  patch quad      2 15 2 -2.950000E+00 +1.970000E+00 -2.950000E+00 -1.970000E+00 -
2.735000E+00 -1.970000E+00 -2.735000E+00 +1.970000E+00 }

```
- Geometric Transfer

```

# GeoTran type tag vec_xz
geomTransf PDelta  1 +1.000000E+00 +0.000000E+00 +0.000000E+00
# GeoTran type tag vec_xz
geomTransf PDelta  2 +0.000000E+00 +1.000000E+00 +0.000000E+00
# GeoTran type tag vec_xz
geomTransf PDelta  3 +0.000000E+00 -1.000000E+00 +0.000000E+00
# GeoTran type tag vec_xz

```

```

geomTransf PDelta 4 +0.000000E+00 -1.000000E+00 +0.000000E+00
# GeoTran type tag vec_xz
geomTransf PDelta 5 +0.000000E+00 -1.000000E+00 +0.000000E+00
• Element
# Elements.tcl
# Element "W6X9": eleTag Nodel NodeJ NIP secTag geoTranTag <-mass massDens> <-iter
maxlters tol>
element forceBeamColumn 1 1 2 6 4 2
# Element "W6X9": eleTag Nodel NodeJ NIP secTag geoTranTag <-mass massDens> <-iter
maxlters tol>
element forceBeamColumn 2 3 4 6 4 2
# Element "W6X15": eleTag Nodel NodeJ NIP secTag geoTranTag <-mass massDens> <-iter
maxlters tol>
element forceBeamColumn 3 2 4 6 3 3
# Element "W6X9": eleTag Nodel NodeJ NIP secTag geoTranTag <-mass massDens> <-iter
maxlters tol>
element forceBeamColumn 4 5 6 6 4 2
# Element "W6X9": eleTag Nodel NodeJ NIP secTag geoTranTag <-mass massDens> <-iter
maxlters tol>
element forceBeamColumn 5 7 8 6 4 2
# Element "W6X15": eleTag Nodel NodeJ NIP secTag geoTranTag <-mass massDens> <-iter
maxlters tol>
element forceBeamColumn 6 6 8 6 3 4
# Element "W6X9": eleTag Nodel NodeJ NIP secTag geoTranTag <-mass massDens> <-iter
maxlters tol>
element forceBeamColumn 7 9 10 6 4 2
# Element "W6X9": eleTag Nodel NodeJ NIP secTag geoTranTag <-mass massDens> <-iter
maxlters tol>
element forceBeamColumn 8 11 12 6 4 2
# Element "W6X15": eleTag Nodel NodeJ NIP secTag geoTranTag <-mass massDens> <-iter
maxlters tol>
element forceBeamColumn 9 10 12 6 3 5
# Element "W6X15": eleTag Nodel NodeJ NIP secTag geoTranTag <-mass massDens> <-iter
maxlters tol>
element forceBeamColumn 10 2 6 6 3 1
# Element "W6X15": eleTag Nodel NodeJ NIP secTag geoTranTag <-mass massDens> <-iter
maxlters tol>
element forceBeamColumn 11 6 10 6 3 1
# Element "W6X15": eleTag Nodel NodeJ NIP secTag geoTranTag <-mass massDens> <-iter
maxlters tol>
element forceBeamColumn 12 4 8 6 3 1
# Element "W6X15": eleTag Nodel NodeJ NIP secTag geoTranTag <-mass massDens> <-iter
maxlters tol>
element forceBeamColumn 13 8 12 6 3 1
• Static loading
eleLoad -range $eleTag1 $eleTag2 -type -beamPoint $Py $Pz $xL <$Px>
# LoadPattern "Dead
# Load nodeTag LoadValues
# eleLoad eleTags beamPoint Py Pz xL <Px>
eleLoad -ele 7 -type -beamPoint +0.000000E+00 -1.150000E+00 +2.080000E-01 +0.000000E+00
eleLoad -ele 7 -type -beamPoint +0.000000E+00 -1.150000E+00 +7.930000E-01 +0.000000E+00
eleLoad -ele 8 -type -beamPoint +0.000000E+00 -2.300000E+00 +2.080000E-01 +0.000000E+00

```

- ```

eleLoad -ele 8 -type -beamPoint +0.000000E+00 -2.300000E+00 +7.930000E-01 +0.000000E+00
eleLoad -ele 9 -type -beamPoint +0.000000E+00 -1.150000E+00 +2.080000E-01 +0.000000E+00
eleLoad -ele 9 -type -beamPoint +0.000000E+00 -1.150000E+00 +7.930000E-01 +0.000000E+00

```
- Dynamic loading

```

TimeSeries "1-Gazli_000": tsTag dt filePath cFactor
timeSeries Path 1 -dt +2.700000E-04 -filePath 1-Gazli_000.thf -factor +1.000000E+00
TimeSeries "2-Imp_Valley_BCR140": tsTag dt filePath cFactor
timeSeries Path 2 -dt +1.780000E-03 -filePath 2-Imp_Valley_BCR140.thf -factor +1.000000E+00
TimeSeries "3-Lomap_CLS000": tsTag dt filePath cFactor
timeSeries Path 3 -dt +1.981000E-03 -filePath 3-Lomap_CLS000.thf -factor +1.000000E+00
TimeSeries "4-Erzincan_ERZ_EW": tsTag dt filePath cFactor
timeSeries Path 4 -dt +1.844000E-03 -filePath 4-Erzincan_ERZ_EW.thf -factor +1.000000E+00
TimeSeries "5-Cape Mendocino-MD-0.9984 in-25%": tsTag dt filePath cFactor
timeSeries Path 5 -dt +8.250000E-03 -filePath 5-Cape Mendocino-MD-0.9984 in-25%.thf -factor
+1.000000E+00
TimeSeries "5-Cape Mendocino-MD-1.9968 in 50%": tsTag dt filePath cFactor
timeSeries Path 6 -dt +8.250000E-03 -filePath 5-Cape Mendocino-MD-1.9968 in 50%.thf -factor
+1.000000E+00
TimeSeries "5-Cape Mendocino-MD-3.9936 in": tsTag dt filePath cFactor
timeSeries Path 7 -dt +8.250000E-03 -filePath 5-Cape Mendocino-MD-3.9936 in.thf -factor
+1.000000E+00
TimeSeries "6-Northr_JGB022": tsTag dt filePath cFactor
timeSeries Path 8 -dt +2.900000E-04 -filePath 6-Northr_JGB022.thf -factor +1.000000E+00
TimeSeries "7-Kobe_KJM000": tsTag dt filePath cFactor
timeSeries Path 9 -dt +7.950000E-03 -filePath 7-Kobe_KJM000.thf -factor +1.000000E+00
TimeSeries "8-ChiChi_CHY028E": tsTag dt filePath cFactor
timeSeries Path 10 -dt +7.590000E-03 -filePath 8-ChiChi_CHY028E.thf -factor +1.000000E+00
TimeSeries "9-Duzce_DZC180": tsTag dt filePath cFactor
timeSeries Path 11 -dt +1.851000E-03 -filePath 9-Duzce_DZC180.thf -factor +1.000000E+00
TimeSeries "910-Tottori_TTRH02EW": tsTag dt filePath cFactor
timeSeries Path 12 -dt +1.949000E-03 -filePath 910-Tottori_TTRH02EW.thf -factor +1.000000E+00
TimeSeries "911-Sansimeo_36695090": tsTag dt filePath cFactor
timeSeries Path 13 -dt +1.891000E-03 -filePath 911-Sansimeo_36695090.thf -factor
+1.000000E+00
TimeSeries "912-Bam_L": tsTag dt filePath cFactor
timeSeries Path 14 -dt +2.012000E-03 -filePath 912-BamBam_L.thf -factor +1.000000E+00
TimeSeries "913-Niigata_NIG019EW": tsTag dt filePath cFactor
timeSeries Path 15 -dt +3.821000E-03 -filePath 913-Niigata_NIG019EW.thf -factor +1.000000E+00
TimeSeries "914-Montene_GRO_BSO000": tsTag dt filePath cFactor
timeSeries Path 16 -dt +3.950000E-03 -filePath 914-Montene_GRO_BSO000.thf -factor
+1.000000E+00
TimeSeries "915-Iwate_IWTH24EW": tsTag dt filePath cFactor
timeSeries Path 17 -dt +4.300000E-03 -filePath 915-Iwate_IWTH24EW.thf -factor +1.000000E+00
TimeSeries "916-Darfield_GDLCN55W": tsTag dt filePath cFactor
timeSeries Path 18 -dt +1.761000E-03 -filePath 916-Darfield_GDLCN55W.thf -factor
+1.000000E+00
TimeSeries "917-Subduction-Tohoku-TS-0.0033-150": tsTag dt filePath cFactor
timeSeries Path 19 -dt +3.302000E-03 -filePath 917-Subduction-Tohoku-TS-0.0033-150.thf -factor
+1.000000E+00
TimeSeries "917-Subduction-Tohoku-TS-0.00362-125": tsTag dt filePath cFactor
timeSeries Path 20 -dt +3.620000E-03 -filePath 917-Subduction-Tohoku-TS-0.00362-125.thf -factor
+1.000000E+00
TimeSeries "917-Subduction-Tohoku-TS-0.00405": tsTag dt filePath cFactor

```

```
timeSeries Path 21 -dt +4.050000E-03 -filePath 917-Subduction-Tohoku-TS-0.00405.thf -factor
+1.000000E+00
TimeSeries "AI0-Sin-1(A,B,C,D,E)": tsTag dt filePath cFactor
timeSeries Path 22 -dt +1.000000E-02 -filePath AI0-Sin-1(A,B,C,D,E).thf -factor +1.000000E+00
TimeSeries "AI0-Sin-15(A,B,C,D,E)": tsTag dt filePath cFactor
timeSeries Path 23 -dt +1.000000E-02 -filePath AI0-Sin-15(A,B,C,D,E).thf -factor +1.000000E+00
TimeSeries "AI1-Step-MD-0.5 in": tsTag dt filePath cFactor
timeSeries Path 24 -dt +1.000000E-02 -filePath AI1-Step-MD-0.5 in.thf -factor +1.000000E+00
TimeSeries "AI1-Step-MD-4 in": tsTag dt filePath cFactor
timeSeries Path 25 -dt +1.000000E-02 -filePath AI1-Step-MD-4 in.thf -factor +1.000000E+00
TimeSeries "AI2-Sweep-TS-0.02 Sec": tsTag dt filePath cFactor
timeSeries Path 26 -dt +2.000000E-02 -filePath AI2-Sweep-TS-0.02 Sec.thf -factor +1.000000E+00
TimeSeries "AI2-Sweep-TS-0.04 Sec": tsTag dt filePath cFactor
timeSeries Path 27 -dt +4.000000E-02 -filePath AI2-Sweep-TS-0.04 Sec.thf -factor +1.000000E+00
TimeSeries "LinearDefault": tsTag cFactor
timeSeries Linear 28 -factor +1.000000E+00
```

## **Appendix A6: Articles authored based on the present work**

### **- Conferences:**

Naghshineh, A., Tehrani, F.M., Galindo, O.R., and Bagchi, A. (2019). “Response modification factors for friction dampers as per the 2015 national building code of Canada”, ICAST2019: 30th International Conference on Adaptive Structures and Technologies, Montreal, QC, Canada.

Naghshineh, A. and Bagchi, A. (2019). “ Seismic performance of concrete moment resisting frames in western Canada”, ICAST2019: 30th International Conference on Adaptive Structures and Technologies, Montreal, QC, Canada.

Naghshineh, A., Kassem, A., Pilorge, A.-G., Galindo, O.R., and Bagchi, A. (2018). “Seismic Performance of Reinforced Concrete Frame Buildings Equipped with Friction Dampers”, Structures Congress 2018. American Society of Civil Engineers, Fort Worth, Texas. pp. 94–101.

### **- Journals:**

Naghshineh, A., and Bagchi, A. (2021). “A comparative study of the design procedures for buildings with damping devices in the Canadian and American contexts”, under review, Earthquake, and structures.

Naghshineh, A., and Bagchi, A., Tehrani, F. M. (2021). “Determining Seismic Performance and Response modification factors of inline seismic friction damper as per the 2015 national building code of Canada”, under review, Canadian Journal of Civil Engineering.

Naghshineh, A., and Bagchi, A. (2021). “Comparative study of six different passive energy dissipation systems”, under review, Earthquake Engineering and Engineering Vibration.